Long-acting Polymeric Nanospheres and Nanorods for Efficient Delivery of Antimalarial Drugs

THESIS

Submitted in partial fulfillment
of the requirements for the degree of

DOCTOR OF PHILOSOPHY

by

ATHARVA RAJENDRA BHIDE
ID. No. 2019PHXF0058P

Under the Supervision of

PROF. ANIL B. JINDAL

BIRLA INSTITUTE OF TECHNOLOGY AND SCIENCE, PILANI

2024

BIRLA INSTITUTE OF TECHNOLOGY AND SCIENCE, PILANI

DECLARATION

I hereby declare that the thesis work entitled **"Long-acting Polymeric Nanospheres and Nanorods for Efficient Delivery of Antimalarial Drugs"** is an original piece of work carried out under the guidance of Prof. Anil B. Jindal in the Department of Pharmacy, Birla Institute of Technology and Sciences (BITS PILANI), Pilani campus. This thesis has not been submitted by me for the award of any other degree of any other University/Institute.

Atharva Rajendra Bhide
2019PHXF0058P
Research Scholar
BITS PILANI, Pilani campus

BIRLA INSTITUTE OF TECHNOLOGY AND SCIENCE, PILANI

CERTIFICATE

This is to certify that the thesis entitled **"Long-acting Polymeric Nanospheres and Nanorods for Efficient Delivery of Antimalarial Drugs"** submitted by **Atharva Rajendra Bhide**, ID. No. **2019PHXF0058P** for award of Ph.D. degree of the institute, embodies original work done by him under my supervision.

PROF. ANIL B. JINDAL
Associate Professor
Date:

Table of contents

Acknowledgements

‘Feeling gratitude and not expressing it is like wrapping a present and not giving it’

- William Arthur Ward

I am thankful to Prof. V. Ramgopal Rao, Vice-Chancellor, BITS-Pilani, Prof. Sudhirkumar Barai, Director, BITS Pilani, Pilani Campus, Col. Soumyabrata Chakraborty (Retd), Registrar, BITS Pilani, Pilani Campus, Prof. Ajit Pratap Singh, Dean, AGSRD, BITS Pilani, for providing excellent work facilities and an absorbing research environment. I wish to express sincere thanks to Prof. Anil B. Gaikwad, Head, Department of Pharmacy, Prof. Hemant R. Jadhav & Prof. Atish T. Paul, former Head, for constant support in providing resources required during my research work.

I am immensely grateful to Prof. Anil B. Jindal, Associate Professor, Birla Institute of Technology Sciences - Pilani, Pilani Campus for their invaluable guidance, unwavering support, and boundless patience throughout my doctoral journey. His expertise, encouragement, and insightful feedback has been instrumental in shaping this research. I am deeply thankful for his mentorship, which has not only enriched this work but has also contributed significantly to my growth as a researcher.

I am indebted to my Doctoral Advisory Committee (DAC) members, Prof. Deepak Chitkara and Prof. Murali Manohar Pandey, for reviewing my thesis and helping in constructive criticism of my work. I would express my sincere thanks to Prof. Anil B. Jindal, Convener, Departmental Research Committee, for valuable guidance while compiling this thesis.

I am thankful to all my faculty members of the Department of Pharmacy, Prof. R. Mahesh, Prof. S. Murugesan, Prof. Rajeev Taliyan, Prof. Deepak Chitkara, Prof. Anupama Mittal, Dr. Gautam Singhvi, Dr. Murali Manohar Pandey, Dr. Sandeep Sundriyal and Dr. Richa Shrivastava, Dr. Pragyanshu Khare for their teachings. And I am thankful to Dr. Sushil Kumar Yadav for supporting in animal studies.

I would also like to extend my sincere thanks to my lab mates Dr. Dhanashree Surve, Dr. Kedar Prayag, Ms. Ila Sarode and Mr. Sanat K. Dash for their immense support, giving their precious time, patience in always listening to me and motivation.

All my seniors and colleagues Dr. Kowthavarapu Venkata Krishna, Dr. Saurabh Sharma, Dr. Kishan Italiya, Dr. Vajir Malek, Dr. Nisha Sharma, Dr. Ginson George, Dr. Pracheta Sengupta, Dr. Sudeep Pukale, Dr. Sarathlal K.C., Dr. Samrat Mazumdar, Ms. Geetika, Mrs. Paramita, Dr. Swetha, Dr. Violina, Dr. Swati, Dr. Karan, Dr. Rupesh, Dr. Himanshu, Mr. Rajesh, Dr. Amritansh, Mr. Arihant, Dr. Deepak Kumar, Ms. Moumita Basak, Ms. Nikita Hinge, Mr.

Mahipal, Mr. Imran, Ms. Kavyashree, Mr. N. Sai Bhargav, Ms. Reena, Ms. Sriravali, Ms. Nisha, Mr. Mukesh, Ms. Shreya, Ms. Sharyu, Mr. Amit, Mr. Shubham, Mr. Sai Pradyuth, Mr. Vishwadeep, Mr. Shivanshu, Mr. Jayant, Ms. Shobha, Mr. Abhay, Mr. Shrikant, Mr. Shailesh, Ms. Shikha, Mr. Ala Chandu, Ms. Neha, Mr. Giriprasad, Ms. Sonia, Ms. Sakshi, Mr. Muzaffar, Ms. Yashika, Mr. Mukul, Mr. Samarth, Mr. Vaghesh, Mr. Utkarsh, Ms. Shivangi, Mr. Animesh, Ms. Pranali, Ms. Shivangi, Mr. Pratik, Ms. Lavanya, Ms. Aarti, Mr. Yash, Ms. Jyotika, Mr. Bhupendra, Ms. Priyanka, Ms. Vaibhavi, Dr. Vivek and Dr. Yogeshvaran deserve special thanks for making the pleasant working environment in the lab, for all the fun and enjoyment, help and sarcasm.

I would like to thank Mr. Prakash P. Taur and Dr. Pramod Raichure for their invaluable assistance with the technical aspects.

Grateful for the generous assistance provided by Ms. Hansa Sehgal, Mr. Shreyas Iyer, Mr. Sumit Mandal, Mr. Yash Katakia and Mr. Prabhjeet Singh in navigating the laboratory equipment and support.

I want to thank graduates and postgraduates with whom I worked closely for exploring things. I thank Mr. Mani Famta, Ms. Rucha Bhangale, Ms. Bhakti, Mr. Himanshu and Mr. G. Pramoda, Ms. Dhanashree Patel and Ms. Bhakti Gagan.

I would also like to extend my sincere thanks to the entire non-teaching staff in the Department of pharmacy, Mr. Puran, Mr. Lakshman, Mr. Tarachand, Mr. Surendra, Mr. Vikas, Mr. Naveen, Mr. Abhishek, Mr. Sandeep, Mr. Ram Suthar, Mr. Vishal, Mr. Mukesh, Mr. Shyam Sunder and Mr. Shiv Kumar for their kind support during this work.

Deeply grateful to Ms. Manisha Choudhari, Mr. Ajinath Kale, Mr. Prashant Auti and Ms. Tejashree Waghule for their unwavering support and endless encouragement, making every challenge easier to conquer and every moment more memorable.

Thank you, Mr. Prashant, Mrs. Komal, Mstr. Keyur and Mstr. Atreya for being my unwavering support and the cornerstone of my strength. Your love and guidance have shaped my world in ways words can't express.

With a deep sense of adoration and gratitude. I dedicate all my work to my parents and my fiancée, Ms. Anuprita Lele and my family who were the constant source of moral support in my life; without their encouragement and blessings, no achievement would have been possible. My life would be incomplete without them. It is to them and the almighty that I owe all.

- Atharva Rajendra Bhide

Abstract

Malaria is a parasitic disease caused due to the infection of *Plasmodium*. It is transmitted to the humans by the bite of a *Plasmodium* infected female Anopheles mosquito. The symptoms include fever, headache, shaking chills etc. The severity of the infection depends upon the type of parasite contracted with *P. falciparum* being most lethal while *P. vivax* causing frequent relapses. The disease is amongst one of the leading causes of morbidity and mortality with around 249 million cases and 608,000 deaths in 2022. However, after years of research only one vaccine has been approved in 2023 and the burden of the disease lies on the available marketed chemotherapeutic agents. Amongst the various drugs available in the market, artemether-lumefantrine (Coartem®) is the first line treatment recommended by CDC. Artemether is highly effective against the erythrocytic stage and rapidly reduces the parasitic number of the parasite whereas lumefantrine eliminates the remaining parasites thus preventing recrudescence. However, in case of *P. vivax* infections, primaquine is the drug of choice for being able to eliminate the hepatic dormant stage of the parasite. While these drugs are effective against malaria, their therapy can be impeded by certain limitations. A pressing requirement exists for more innovative and effective strategies to alleviate the limitations associated with these existing drugs. Nanotechnological methods for delivering established drugs have demonstrated substantial enhancements in efficacy, often resulting in a considerable reduction in dosage by several folds.

In this dissertation, particle shape of the nanoformulation was explored for increasing the drug residence time in the body. By utilizing the unique characteristics presented by the non-spherical nanoparticles, we tried to increase the circulation time, decrease the macrophage uptake and improve the strength of the depot after its administration. Furthermore, a long-acting parenteral formulation utilizing biocompatible and non-toxic excipients was explored as a long-acting injectable formulation. The overall objective of the study was to prepare a formulation with a patient compliant dosage regimen.

This study addresses the limitations associated with artemether and primaquine. Both drugs are known for their strong antimalarial action and are used as the first line therapy in the treatment of malaria. However, their chemical properties present a significant challenge in their therapy. Artemether is known to have a very short half-life (2-4h) and hence is known to be administered along with a partner drug. Whereas, primaquine not only has a short half-life, but also has a long dosage regimen and dose dependent toxicity. Therefore, there was an urgent need to develop formulations that can mitigate these side effects. Nanoformulations are known to

reduce the drug dose and also present a long-term drug release. Hence, this work involves preparation of spherical and non-spherical nanoparticles of artemether and primaquine and evaluating them further for their long-acting ability.

A simple, robust and accurate RP-HPLC analytical method was developed to quantify artemether in nanoformulations whereas a precise LC-MS-MS bioanalytical method was developed to quantify artemether in plasma samples of rats. ART was transformed to α, β-unsaturated decalones by pre-column acid treatment to enhance the sensitivity of chromophoric group lacking ART for quantification by HPLC-UV. Waters Spherisorb® 5 µm ODS(C18) column (4.6 × 250 mm) with gradient elution by mobile phase comprising of ACN and PBS (10 mM; pH 6.0) was used to separate acid-treated ART. The analysis was carried at λ_{max} of - 253 nm with 20 min and 20 µL run time and injection volume respectively. The method was found to be linear in the concentration range of 0.5-10 µg/mL with 0.09 µg/mL and 0.27 µg/mL as LOD and LOQ respectively. Further, the method was also found to be specific for ART in presence of blank polymeric nanoparticles, accurate (% average recovery rate 101.7 ± 1.68 %), precise (RSD < 2 %), and robust. The method was successfully used to determine % entrapment efficiency and in vitro release of ART-loaded polymeric nanoparticles with HPLC using a UV-visible detector.

Further, artemether-loaded poly (lactic-co-glycolic acid) (PLGA) nanorods were prepared by mechanical stretching of nanospheres. Artemether-loaded PLGA nanospheres were prepared by the standard nanoprecipitation method. To prepare the nanorods, nanospheres (129nm) were embedded in polyvinyl alcohol (PVA) film. The film was stretched by using an *in-house* fabricated film stretching apparatus in one dimension at the rate of 10 mm/min in acetone or silicon oil. Nanorods were recovered by dissolving the film in Milli-Q-water after stretching. The effect of film thickness (100µm vs 150µm), the ratio of lactide to glycolide in PLGA (50:50 vs 75:25), extent of stretching (2x vs 4x), on the aspect ratio of the nanorods was studied. A sustained release of artemether was observed from both nanospheres and nanorods with almost 85% drug release at the end of 72h. In cytotoxicity study, almost 90% cell viability was found when THP-1 cells were treated with artemether, nanospheres, and nanorods equivalent to 0.001 to 100 µg/mL of artemether. At all the concentrations of artemether, nanorods showed less hemolysis of RBCs than the nanospheres.

Evaluation of nanospheres and nanorods using scanning electron microscopy with the rat erythrocytes revealed that the both nanospheres and nanorods were adsorbed onto the surface of rat erythrocytes after incubation of 10min. Whereas, in the pharmacokinetic study, after

intravenous administration to rats, artemether nanorods showed higher plasma concentration and lower elimination rate of artemether when compared with nanospheres. The biodistribution studies showed that, at 15min, the liver concentration of DiR loaded nanorods was higher than DiR loaded nanospheres after intravenous administration to BALB/c mice. The *in vitro* schizont inhibition study showed that both nanorods and nanospheres exhibited concentration-dependent parasitic inhibition, wherein at lower concentrations (2 ppm), nanorods were more effective than nanospheres. However, at higher concentration, nanospheres were formed to be more effective. Nanorods showed higher chemosuppression on day 5 and day 7 than nanospheres and free artemether when studied *P. berghei* mouse model. Moreover, the survival rate of *P. berghei* infected mice was also found to be higher after treatment with artemether nanoformulations when compared with free artemether. In conclusion, polymeric nanorods could be a promising next-generation delivery system for the treatment of malaria.

Furthermore, considering the hydrophilic nature of primaquine diphosphate a hydrophobic prodrug (PQ-PAL) (Molecular wt. 498.41g/mol) using primaquine diphosphate and palmitic acid was synthesized. An analytical RP-HPLC and a bioanalytical LC-MS-MS method for the quantification of PQ-PAL was developed and validated as per the ICH regulatory guidelines. The analytical method was found to be linear between a concentration range of 0.156–10µg/ml with a high correlation coefficient (R^2) of 1 and the equation y = 58447x + 606.47 at 266nm. The intraday and inter-day precision % relative standard deviation was less than 2%. Whereas, between a concentration range of 0.0.78–100ng/ml, the bioanalytical method was found to be linear with an (R^2) of 0.9974 and the equation y = 0.2068x - 0.0049. It was found that the total %recovery for the three different concentration levels fell between 80 and 120% of the acceptable range. The method development was followed by preparation of PQ-PAL loaded PLGA nanospheres (234.77±8.46nm) using the emulsion solvent evaporation method. The volume of organic phase and sonication time were found to be affecting the particle size. The particle size was found to be inversely proportional to the organic phase volume and sonication time. Whereas the PQ-PAL loaded nanorods were prepared by the mechanical stretching of nanospheres using *in-house* prepared film stretching apparatus. SEM analysis of the nanorods inferred that the nanorods were sufficiently stretched (AR - 6.73 ± 1.46) and of uniform shape. In the *in vitro* drug release study, both nanospheres and nanorods presented a sustained drug release action over a period of 7days. In the hemolysis study, nanospheres and nanorods were found to be non-haemolytic at all concentrations i.e. from 0.001 to 200µg/ml. In the pharmacokinetic study, after administration the nanorods showed lower C_{max} concentrations

and higher mean residence time thus ensuring a controlled release of the drug as compared to the nanospheres.

Long-acting gel formulations loaded with free PQ-PAL and PQ-PAL nanoparticles intended for the subcutaneous administration was prepared. The preparation of the gel phase involved formulation of 2 compositions. Composition 1 involved albumin dissolved in water, whereas composition 2 involved ethanol. The mixture of both the components resulted in the gel formation. Initially, the components of the formulation were varied in order to optimize the duration of gel formation. It was followed by the evaluation of the effect of formulation components on the viscosity and shear stress of the formed gel. It was observed that the viscosity and shear strength of the gel were directly proportional to the concentration of albumin in the aqueous phase. In the release study of the gel, it was observed that at the end of 7 days, the prodrug loaded gel and the prodrug nanoparticle loaded gel released less than 2% of the drug while the gel implant structure was intact during this duration. Finally, the pharmacokinetic study of PQ-PAL loaded long-acting gel formulation and the PQ-PAL nanoparticles loaded long-acting gel formulation revealed that the long-acting gel loaded with nanoparticles showed a protracted drug release for a period of 56 days, whereas, the free drug loaded long-acting gel formulation displayed an initial burst release followed by sustained drug release of PQ-PAL. Thus long-acting gel formulations prepared by a simple process, involving biodegradable components, capable of sustaining the drug release *in vivo* upto months were developed.

List of tables

List of Figures

List of abbreviations and symbols

ACN	Acetonitrile
API	Active pharmaceutical ingredient
AIC	Akaike Information Criteria
ANOVA	Analysis of variance
AR	Aspect ratio
ART	Artemether
AUC	Area under curve
BCS	Biological classification system
C_{max}	Maximum concentration
cm	Centimeter
°C	Degree Celsius
DiR	(DiIC18(7); 1,1′-dioctadecyl-3,3,3′,3′-tetramethylindotricarbocyanine iodide)-diamidino-2-phenylindole
DCM	Dichloromethane
DLS	Dynamic light scattering
%DL	% Drug loading
DS	Docusate sodium
DMSO	Dimethyl sulfoxide
%EE	% Entrapment efficiency
FESEM	Field Emission Scanning Electron Microscopy
FBS	Fetal bovine serum
HPLC	High-pressure liquid chromatography
ICH	The International Council for Harmonization of Technical

	Requirements for Pharmaceuticals for Human Use
IC_{50}	50% Inhibitory concentration
IV	Intravenous
LA	Long-acting
LC-MS-MS	Liquid chromatography-mass spectrometry
LOD	Limit of detection
LOQ	Limit of quantification
LLOQ	Lowest Limit of quantification
µg	Microgram
MTT	3-(4,5-dimethylthiazol-2-yl)-2,5-diphenyl tetrazolium bromide
mg	milligram
min	Minutes
mL	Milliliter
MRM	Multiple reaction monitoring
MRT	Mean residence time
ng	Nanogram
PDI	Poly dispersibility index
PMA	Phorbol 12-myristate 13-acetate
PQ-PAL	Primaquine prodrug
PQ	Primaquine diphosphate
SC	Subcutaneous
S/N	Signal to noise
K Da	Kilo Daltons
µL	Microliter

λ_{max}	Lambda max
RSD	Relative standard deviation
Vd	Volume of distribution
Tmax	Time taken to reach maximum concentration
THP-1	human monocytic cell line derived from an acute monocytic leukemia
$t_{1/2}$	Half-life

Chapter 1: Introduction

1.1 Background

Malaria is a serious parasitic infection caused by the *Plasmodium* parasite and transmitted to humans by an infected female Anopheles mosquito during a blood meal. According to the World Health Organization's 2019 statistics, malaria cases reached a staggering 229 million globally, with only a meagre 2% decline from 2015 to 2019 (*World Malaria Report 2020*, n.d.). Recognising the gravity of the situation, the Global Technical Strategy for Malaria 2016-2030 (GTS) has set ambitious targets to reduce the number of cases up to 75% by 2025 and at least 90% by 2030. To achieve this goal, various strategies have been introduced, including the country-led response "High Burden High Impact" (HBHI), mobilized by the World Health Organization and Rollback Malaria (RBM) (WHO, 2018). Malaria is caused by almost 200 different species of *Plasmodium*, of which *P. vivax*, *P. falciparum*, two species of *P. Ovale*, and *P. malariae* are the most common (Brasil et al., 2017; Nureye & Assefa, 2020; Singh & Daneshvar, 2013).

The *Plasmodium* parasite is present in two stages: the pre-erythrocytic stage and the erythrocytic stage. The erythrocytic invasion involves a series of events, including protein-protein interaction, protease cleavage, intracellular signaling, organelle release, and activation of the actin-myosin motor, making it a major target for drugs against malaria. Additionally, the clumping of red blood cells (RBCs) with *Plasmodium*-infected RBCs (pRBCs) can lead to death, further highlighting the importance of targeting the erythrocytic stage of malaria (Bell & Winstanley, 2004). While existing treatments against the erythrocytic stage of malaria have reduced malaria-related complications (as shown in Fig. 1.1), their efficacy is limited by factors such as increased drug resistance, toxicity, non-specific targets, poor bioavailability, short half-life, and poor solubility (Cui et al., 2015; Rai et al., 2017).

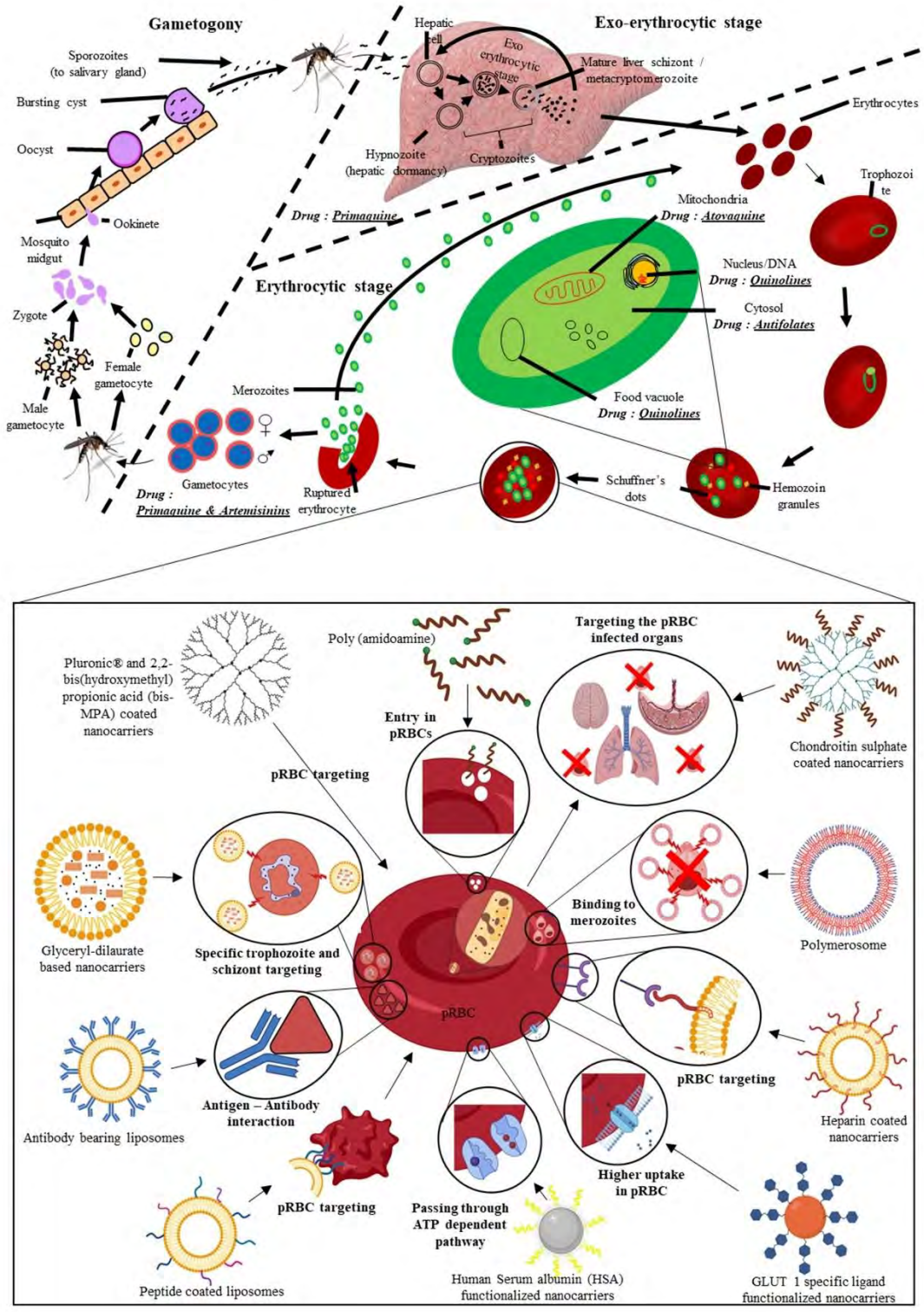

Fig. 1.1. Life cycle of malaria parasite and explored formulations for treatment against the erythrocytic stage of malaria

Nanotechnology has emerged as a promising field for improving conventional therapies by enhancing the bioavailability, pharmacokinetic profile, drug efficacy, reducing the dose,

frequency of administration, and toxicity (Walvekar et al., 2018). Several nanocarriers, such as liposomes (Fotoran et al., 2019), polymeric nanoparticles (Bhide et al., 2020, 2022; Bhide & Jindal, 2021; Hamelmann et al., 2023; Michels et al., 2019), solid lipid nanoparticles (Ogutu et al., 2014), nano lipid carriers (Prabhu, Suryavanshi, Pathak, Patra, et al., 2016; Prabhu, Suryavanshi, Pathak, Sharma, et al., 2016a; Yanan et al., 2019), and ligand-conjugated nanocarriers (Aditi et al., 2016a; Coma-cros et al., 2018; Moles et al., 2015), have been reported for delivering antimalarial drugs to target the *Plasmodium* cycle during the erythrocytic stage. pRBCs have shown structural modifications, including enhanced permeability and overexpression of surface receptors such as glucose transporter 1 (GLUT 1) (Heikham et al., 2015), glucosaminoglycan receptors (Bhadra et al., 2006; Ismail et al., 2019; Marques et al., 2014; Muga et al., 2018; Najer et al., 2014), and essential protein receptors (Aditi et al., 2016a; Alam et al., 2016; Rodriguez et al., 2008). Various ligands specific to overexpressed receptors, such as human serum albumin (HSA) (Aditi et al., 2016a), glucose (Heikham et al., 2015), heparin (Ismail et al., 2019; Marques et al., 2014; Muga et al., 2018; Najer et al., 2014), and chondroitin sulfate A (CSA) (Bhadra et al., 2006; Nash et al., 1992), have been conjugated onto the surface of nanocarriers to target pRBCs and enhance the drug concentration within infected erythrocytes (Fig. 1.1).

Several research groups have reviewed the application of nanocarriers for the delivery of antimalarial drugs, highlighting the challenges associated with anti-malarial drug delivery, non-functionalized nanocarriers for direct entry into erythrocytes, and membrane fusion of long-circulating nanocarriers with RBCs (Baruah et al., 2017; Gnanadesigan et al., 2019; Najer et al., 2014; Neves Borgheti-Cardoso et al., 2020; Puttappa et al., 2019). Moreover, nanocarriers for combination antimalarial therapy, prophylactic preloading of uninfected RBCs, and mosquito vector targeting have also been reviewed (Fernàndez-busquets, 2016). Some researchers have also reviewed various nanotechnology-based passive targeting strategies against malaria (Anamika et al., 2020). However, very few reports have focused on the development of ligands for specific pRBC targeting (Kirtane et al., 2021). The present review provides detailed insight into numerous receptors that are specific to pRBC, their interaction with the ligand during the erythrocytic and non-erythrocytic stages of malaria, and the adoption of the receptor-ligand interaction mechanism for effective antimalarial drug delivery within pRBC.

1.2 Lifecycle of malaria parasite

The fate of malarial parasite leaps between its mosquito and human vector involving sexual

and asexual reproduction, respectively. The mosquito vector, prominently the female Anopheles mosquito is responsible for exchange of parasite with the human vector(Rai et al., 2017). The parasite cycle can be classified in three stages, with respect to the growth phases of the *Plasmodium* which may slightly vary between the parasite species(Wells et al., 2010). Numerous protein interactions occur at each stage and are responsible for the completion of the life cycle. An insight into the specific interactions involved may embark novel active targeting strategies against malaria.

(i) Exo-erythrocytic stage: Around a hundred sporozoites present on the salivary glands enters the host dermis after the bite of an infected vector (Prudêncio et al., 2006a). These sporozoites traverse through the dermal cells to reach the circulation. Various proteins have been associated with traversal of the sporozoites. Sporozoite microneme protein essential for cell traversal (SPECT) (Ishino et al., 2004), SPECT2 (Ishino et al., 2005), cell-traversal protein for ookinetes and sporozoites (CelTOS) binding to phosphatidic acid (Kariu et al., 2006), TRAP-like protein (TLP) binding to aldolase (Moreira et al., 2008), surface phospholipase (Bhanot et al., 2005), are some of the prominent proteins experimentally identified, evaluated (Steel et al., 2018; Yang et al., 2017) and thoroughly reviewed for the mechanism of cell traversal (Ejigiri & Sinnis, 2009a; Yang & Boddey, 2017a) and are strongly involved in the membrane wounding, disruption, lysis and egress(Yang & Boddey, 2017b). Subsequent to the traversal, the sporozoites enter the circulatory system where they specifically target the liver through their exclusive surface proteins. The interaction is facilitated by circumsporozoite protein (CSP) – heparin sulphate proteoglycan (HSPGs) binding present on the surface of sporozoite and liver cells, respectively. The interaction is thought to be dependent on the degree of sulfonation of the HSPGs thus making stellate cells (with abundance in sulfate group) in the liver responsible for the primary arrest of sporozoites than the hepatocytes. After attachment to the Kupffer cells, the sporozoite traverses and invade hepatocytes. The sporozoite traversal and invasion again in this case is thought to be regulated by the degree of sulphonation. A series of proteins such as CSP, thrombospondin-related anonymous protein (TRAP), Apical membrane antigen 1 (AMA-1), P36/P36p, thrombospondin-related sporozoite protein (TRSP) are involved in various points of traversal and invasion(Ejigiri & Sinnis, 2009b). Once the sporozoite reaches the hepatocyte, it is tightly bound to the hepatocyte with the help of the protein TRAP which is followed by hepatocyte invasion and formation of the parasitophorous vacuole(Prudêncio et al., 2006a). The sporozoites then replicate into thousands of merozoites responsible for the further erythrocytic progression of the parasite(Zuzarte-Luis & Mota, 2020). Sporozoites in some cases

develop few intermediate stages (dormant hypnozoite stage, schizont stage) before becoming merozoites. These stages are termed as cryptozoites(Huff et al., 1943). The merozoites then are released from the parasitophorous vacuole and enter the host cell cytoplasm which is termed as merosome. These merosomes are then released into the bloodstream followed by erythrocyte infection(Prudêncio et al., 2006b).

(ii) Erythrocytic stage: The merozoites followed by the egress from the hepatocytes, enter the bloodstream. Once they come in contact with the erythrocytes, the specialized ligands present on the merozoites namely, the erythrocyte binding ligands (EBL) involved in the sialic acid (SA) dependent invasion and the reticulocyte binding like (RBL)/(PfRh) involved in SA independent invasion thus taking part in an active process of binding with the erythrocytes thus initiating the ingress (Jaskiewicz et al., 2019; Satchwell, 2016a). Conversely, SA dependent invasion receptors like the GPA/B/C/D while SA independent invasion receptors (Complement receptor 1, Basigin, Semaphorin 7a, Band 3/ GPA, Kx) of erythrocyte are involved in the binding with the merozoites and their ingress. A prominent pathway of the merozoite binding involves the erythrocyte binding antigen-175 (EBA-175) ligand interacting with Glycophorin A, the most abundant protein on the erythrocyte. This binding is believed to be responsible for the deformation of the erythrocyte membrane(Chasis et al., 1985). In a similar way, EBL-1 and EBA-140 are responsible for binding with GPB and C respectively. A similar type of behaviour is observed in the SA independent complement receptor (CR1). The receptor binding is involved in the phosphorylation of β spectrin resulting in Ca2+ influx leading to membrane deformability (Glodek et al., 2010; Satchwell, 2016b). PfRh4 is specific for CR1 involved in the parasite ingress while also provides binding site for PfEMP1 involved in the resetting of the erythrocytes. Another specific receptor known as the basigen is known to perform a very crucial part in merozoite invasion and its inhibition is also found to prevent all types of merozoite invasions. Additionally, the receptor is present in all the stages of erythrocyte development and thus can be targeted regardless of the stage (Satchwell, 2016b; Wright et al., 2014). Apart from these, literature has revealed the involvement of semaphoring 7a, band 3, Kx, cluster of differentiation 55 (CD55), CD44 and intercellular adhesion molecule 4 in erythrocyte binding thus targeting these receptors is presently a chief approach of modelling the nanocarriers(Satchwell, 2016b). The actin myosin motor of the parasite is responsible for its ingress in a specialized parasitophorous vacuole created by the parasite itself. Here, the merozoite is present in the rounded form and eventually becomes trophozoite. The trophozoite utilizes the erythrocytic hemoglobin as an amino acid source and its toxic metabolite heme is

polymerized into the nontoxic hemozoin. Once the invasion of the parasite is complete, the parasite remodels erythrocytic internal and external membranes for the proliferation in the host. The remodelling is also responsible for cytoadherence. Thereafter, trophozoite matures into schizonts leaving merozoites into the bloodstream. Some parasite differentiates into sexual erythrocytic stages (gametocytes)(Fujioka & Aikawa, 2002a).

(ii) Gametogony: The process is initiated in the mosquito midgut once the gametocytes are ingested by the mosquito. The male gametocyte produces eight haploid motile gametes by exflagellation. These male gametes fertilize the female gametes resulting in the formation of a diploid zygote which further forms motile ookinetes. The oocyte traverses through two barriers namely the peritrophic matrix (PM) and the midgut epithelium. Enzyme chitinase is thought to be responsible for PM traversal. Following traversal, the ookinetes become rounded to form oocysts. Once formed, oocyst grows which is characterized by nuclear division, vacuole formation. The oocyst cytoplasm is divided into sporoblasts by the vacuoles. Sporozoites emerge from these sporoblasts. Mature sporozoites egress the oocysts and reach the salivary glands of mosquito(Fujioka & Aikawa, 2002b).

1.3 Ligand-anchored nanocarriers for delivery of antimalarial drugs to *Plasmodium*-infected erythrocytes

Various ligands target RBC receptors, including glycosaminoglycans targeting GPA and band-3, inhibitory proteins targeting the microneme-secreted AMA1 and the rhoptry neck (RON 2/4/5) protein complex, as well as Cytochalasin and Latrunculin targeting the key step of actin polymerization dynamics involved in RBC invasion by the merozoites. Unexplored targets such as Myosin A, *P. falciparum* subtilisin protease, and Plasmepsin IX and X are also present (Burns et al., 2019). In this review, distinct ligands used for active targeting of pRBC have been categorized as proteins and peptides (A. K. Agrawal & Gupta, 2000; K. Agrawal, 1987; Chakrabarti et al., 2013; Chandra et al., 1991; Tagami et al., 2015; Urbán, Estelrich, Adeva, et al., 2011), polymers (Ismail et al., 2019; Rosen et al., 2009; Urbán et al., 2015), and lipids (S. A. Jain et al., 2014). The following section provides a brief overview of various examples belonging to each classification, surface-functionalized onto various nanocarriers, including liposomes (Date et al., 2007; Moles et al., 2015, 2016, 2017; Tagami et al., 2015; Urbán, Estelrich, Adeva, et al., 2011), solid lipid nanocarriers (Date et al., 2007; Muga et al., 2018), polymeric nanoparticles (Ismail et al., 2019; Najer et al., 2014; Shafi et al., 2017), and dendrimers (Bhadra et al., 2006; Rosen et al., 2009) (Table 1.1).

Table 1.1 Summary of receptor-specific ligand functionalized nanocarrier targeting *Plasmodium* infected RBC

Sr. No.	Receptor/internalization mechanism	Nanoformulation	Details	References
1	GPA (Complement receptor 1)	MAHRP121-40 (ADVPTEGMDVPFGFFDKNTL) peptide decorated liposomes DSPE-PEG-2000 liposomes encapsulating CQ and PQ	✓ 10-folds enhanced efficacy was observed in *in-vitro P. falciparum* 3D7 cultures compared with liposomes loaded with free CQ and PQ. The ring stage parasites were killed immediately while, when exposed to late stage parasite the parasite egressed and failed to infect new RBC or couldn't mature within newly infected RBC leaving the erythrocytic cycle incomplete when treated with MAHRRP121-40 CQ loaded liposomes. ✓ *In vivo* evaluation in mice grafted with human erythrocyte and infected with *P. falciparum* depicted diminished parasitemia upto 0.01% when treated with anti-Glycophorin A immunoliposomes compared with 0.4% in free CQ (1.75 mg/kg). 0.5 mg/kg CQ loaded non targeted immunoliposomes have much diminished effect compared with targeted immunoliposomes.	(Moles et al., 2015)
2		Anti-glycophorin-A half antibody (MBMI1232 and 1234) coated iLP	✓ 100% selectivity for RBC infected with late-form parasite mature trophozoite and schizont. While, 99% selectivity towards RBC infected with all forms. ✓ 26.7±1.8% *P. falciparum* growth inhibition was observed when pRBC were treated with half antibody iLP loaded with	(Urbán, Estelrich, Cortés, et al., 2011)

			CQ (equivalent to 2 nM chloroquine) (≥10 times its reported IC_{50} value)	
3		Anti-glycophorin A antibody coated PEG-DSPE iLP loaded with pyronaridine or atovaquone	✓ Optimal targeting to pRBC (99%) was obtained for iLP with lipid concentration of 0.05 μM ✓ 100% parasite inhibition was observed with Pyronaridine loaded anti-glycophorin A antibody iLP compared with 5% and 20% parasite inhibition with free Pyronaridine and pyronaridine loaded liposomes. ✓ Atovaquone and Pyronaridine co-loaded iLP cause 50% growth inhibition compared with only 1% growth inhibition when pRBC were treated with individual free drug.	(Biosca et al., 2019)
4	TER-199 and GPA	Aminoalcohol and aminoquinolone loaded TER-199 and anti-Glycophorin A antibody coated iLP	✓ >80% pRBC retentions efficacy was observed when treated with iLP. 2.3 to 26.5-folds decrease in IC50 of drugs was obtained when loaded within anti-GPA iLP compared with free drug. ✓ 45-55% decrease in blood *P. yeolli* 17XL mice model was observed when treated with drug loaded iLP. ✓ 7-8 fold units average daily parasite replication rate was found in free drug treated and drug loaded liposomal group whereas, ‹ 3.5 fold units average daily parasite replication rate was found in iLP.	(Moles et al., 2017)
5	PfEMP1	Lumefantrine loaded anti PfEMP1 anti-rosetting antibody (R29) coated iLP	✓ The R29-iLP were adsorbed onto the pRBC expressing PfEMP-1 receptors. Moreover, the R29-iLP prevented the	(Moles et al., 2016)

			rosetting of pRBC with RBC (equivalent to 0.75 µM Lumefantrine) and inhibited pRBC generation against their homologue R29 strains. Whereas, the anti-rosetting activity of R29-iLP without drug and free drug was observed at significantly higher concentration of 3.4µM and 4.8 µM, respectively. The R29 anti-body being polyclonal caused multiple binding onto the epitope, thereby depicting proficiency against rosetting. Once the R29-iLp adsorbed onto the pRBC, the hydrophobic lumefantrine penetrated through the lipid membrane thereby causing parasite inhibition. The LMP loaded R29-iLP reduced >60% ring form *Plasmodium* R29 strain while, >70% increase in ring form was observed when treated with free drug.	
6	HSA	Artemether-loaded HSA nanoparticles	✓ *In vitro* culture studies demonstrated 2.2-folds lower IC_{50} values of HSA nanoparticle (5.4 nM) than free ART (12.08 nM) ✓ I.V. administration of ART-HSA nanoparticles depicted increased plasma drug concentration and AUC (2-fold) than free ART ✓ Conventional and half of the dose demonstrated significant reduction in parasitaemia ✓ Parasitaemia was reduced to 13.21% and 13.71% at conventional and half of the	(Aditi et al., 2016b)

			dose of ART-HSA nanoparticles than 23.46% and 46.34% for conventional and half of the dose of marketed formulation	
7		Albumin bound artemisinin nanoparticles	✓ *In vitro* studies revealed 3.5-fold dose reduction for Albumin bound artemisinin nanoparticles than the reference standards for achieving 50% parasitaemia ✓ *In vivo* studies demonstrated 96% parasitaemia inhibition for nanoformulation (10mg/kg/day)	(Ibrahim et al., 2015)
8		HSA bound artemether nanoparticles	✓ *In vitro* studies demonstrated pronounced reduction in haemolysis for HSA bound artemether nanoparticles (7.16 % and 3.68 % for nanoformulation prepared by emulsification and desolvation respectively) than artemether (101%)	(Boateng-Marfo et al., 2018)
9		Indolone-N-oxides HSA nanoparticles	✓ HSA nanoparticles of indolone-N-oxides inhibited of 99. 1% parasitaemia at 25mg/kg/day where all mice survived for more than with mean survival time of greater than 34 days. ✓ In humanized mice, efficacy was observed by inhibition of 97.5% of parasitaemia at the same dose	(Ibrahim et al., 2014)
10	dehydrophenylalanine	-	✓ Curcumin loaded FΔF nanotubes (Ccm-FΔF) presented greater inhibition (IC_{50}, 3.0 µM) of *P. falciparum* as compared to free Ccm (IC_{50}, 13 µM) and 4.33-folds lesser IC50 compared with free Ccm ✓ While Ccm-FΔF treated mice survived throughout study (26 days) with significant parasitaemia reduction while	(Alam et al., 2016)

			the mice from the control group and treated with free drug died within 10 to 14 days and 18 days respectively due to high parasitaemia.	
11	GLUT-1	Chloroquine phosphate loaded Dehydroascorbic acid coated chitosan nanoparticles	✓ Preferential targeting to pRBC compared with normal RBC was observed. Significant reduction ($p<0.0004$) in IC_{50} of Chloroquine was observed during *in vitro* efficacy studies in *P. falciparum* infected 3D7 RBC culture.	(Shafi et al., 2017)
12		CDRI97/63 or quinine loaded starch nanoparticles	✓ 50% reduction in IC_{50} of CDRI 97/63 was observed when loaded into starch nanoparticles compared with free drug during *in vitro* efficacy studies in *P. falciparum* infected 3D7 RBC culture. The *in vitro* efficacy was increased by 63% and 20-22% for CDRI 97/63 and Quinine, respectively when loaded into starch nanoparticles.	(Heikham et al., 2015)
13	Heparin sulphate	CQ loaded heparin coated stearic acid-chitosan nanoparticles	✓ The IC50 value of CQ-heparin coated stearic acid-chitosan nanoparticles and CQ loaded uncoated nanoparticles was 2.41±0.27 ng/ml and 4.752±0.144 ng/ml, respectively against *in vitro* CQ-sensitive D6 strain. The efficacy of heparin coated CQ loaded nanoparticles was 50% more compared with heparin uncoated CQ loaded nanoparticles due to synergistic effect of heparin and CQ.	(Muga et al., 2018)
14		Artesunate-heparin conjugated nanocapsule	✓ *In vitro* efficacy studies in *P. falciparum* 3D7 erythrocyte cultures depicted slightly lower efficacy of the nanocapsule (10.16	(Ismail et al., 2019)

			nM) compared with free Artesunate (6.27 nM). However, the heparin-artesunate nanocapsule depicted pRBC selective targeting compared with free artesunate.	
15		PQ loaded heparin adsorbed 1,2-dioleoyl-3- trimethylammonium-propane liposomes	✓ The parasitemia in *P. falciparum* 3D7 cultures of heparin conjugated PQ loaded lipsoomes dropped from 77.8% to 13.8-19% compared with primaquine unconjugated liposomes.	(Ms et al., 2014)
16		PDMS-heparin block Copolymer polymerosome	✓ 2 order of magnitude reduction in IC_{50} value of nanomimics compared with free drug in *in vitro P. falciparum* (clone 3D7) suspension culture in 24-well pates.	
17	Electrostatic interaction with pRBC membrane lipid	Poly(N-vinylpyrrolidone) peptide conjugate	✓ *in vitro* assay depicted high potency and specific targeting of formulated nanoconjugates ✓ Nanoconjugates had 4-19 fold less toxicity than that of free peptide thus demonstrating its safety	(Jokonya et al., 2020)
18		PQ and CQ conjugated AGMA1, ISA1, and ISA23	✓ *In vitro* studies revealed AGMA1 preferentially bound to pRBCs ✓ CQ-AGMA1 and CQ-ISA23 (0.8mg/kg) i.p cured *P. yeolii* infected mice while *P. yeolii* infected mice treated with free drug (1.9mg/kg) did not survive	(Urbán et al., 2014)
19		PAA conjugated CQ nanoparticles	✓ CQ conjugated anionic and cationic PAA had preferential membrane permeability through intestinal epithelium ✓ (5mg/kg/day) ISA23-CQ cured 3 of 5, ARGO7-CQ cured 2 of 4 and AGMAI-CQ cured 2 of 5 thus depicting slight improvement than free drug.	(Coma-cros et al., 2018)

			✓ ISA23-CQ, ARGO7-CQ and AGMAI-CQ proved as potential vaccine candidates as they developed immunity in mice against *P. yeolli*	
20	Chondroitin-4-sulphate receptor	CSA coated CQ loaded dendrimer	✓ Haemolysis reduction was observed from 28.4±1.7 to 34.1±1.8% for CQ-CSA dendrimer ✓ CQ-CSA dendrimer had reduced macrophage uptake than uncoated dendrimers ✓ CQ-CSA and uncoated dendrimer in Albino rats led to an increase in AUC and MRT by 2-2.5 and 3.5-4 folds respectively	(Bhadra et al., 2006)
21	Erythrocyte Vesicle Protein 1	ART-clindamycin loaded GDL-NLC, lumefantrine-ART loaded GDL-NLC	✓ 5-20% dose of ART- clindamycin loaded GDL-NLC and lumefantrine-ART loaded GDL-NLC rendered complete parasitic clearance from the murine model.	(S. A. Jain et al., 2014)

2 CQ-chloroquine, PQ-Primaquine, iLP-immunoliposome, HSA-human serum albumin, PAA-polyamidoamine, CSA-chondroitin sulphate, EVP 1-Erythrocyte
3 vesicle protein 1, GPA-glycophorin A, GDL-glyceryl dilaurate, ART-artemether, NLC-nanostructured lipid carrier

1.3.1 Protein and peptide coated nanocarriers

1.3.1.1 Antibody bearing liposomes

Liposomes are versatile vesicles composed of phospholipids and cholesterol that can encapsulate both hydrophobic and hydrophilic drugs. They are widely studied for the treatment of malaria in infected animal models, with long-circulating PEGylated (Miatmoko et al., 2019) and negatively charged (F. Wang et al., 2020) liposomes being the focus of many investigations. The delivery of drugs within red blood cells (RBCs) has been established by membrane fusion (Neves Borgheti-Cardoso et al., 2020) or through the tubovesicular network observed in parasitized RBCs (pRBCs) (Anamika et al., 2020), which is influenced by the type and fluidity of phospholipids and particle size. However, passive targeting through membrane fusion can lead to non-targeted drug delivery to various cells (Neves Borgheti-Cardoso et al., 2020).

Monoclonal antibodies (Mabs) have been traditionally used as "magic bullets" against specific antigens. Combining Mabs with liposomes could lead to effective antimalarial drug delivery via both overexpressed antigen receptors and fusion with pRBCs (Di et al., 2020). IgG is the most commonly used immunoglobulin due to its presence in most body fluids, but antibody fragments that only include the complementarity-determining region are sufficient for targeting (Eloy et al., 2017). Mabs can be attached to liposomes via covalent and non-covalent linkages. Various reactions including thiolation, hydrazone linkage formation, and carboxyl-amine linkage aid in covalent linkage, while biotin-neutravidin/streptavidin leads to non-covalent Mab-liposomal linkage (Eloy et al., 2017).

The pharmacokinetics and pharmacodynamics of immunoliposomes depend on the structure, density, and affinity of the Mab on the liposomal surface, as well as the liposomal surface properties and drug-to-lipid ratio (Di et al., 2020). The development of immunoliposomes using antibodies targeting specific receptors on pRBCs could emerge as a successful pRBC targeting strategy against malaria. The CD47 receptor is overexpressed on RBCs and inhibits phagocytosis of infected cells, which can be blocked by CD47 receptor antibodies to eliminate pRBCs (Dulgeroff et al., 2021). Similarly, other receptors such as CR1 (Nichole & Niraj, 2016), GP-A and C, CD55 (Bikash et al., 2020), and basigin are involved in parasite binding and transmission, and blocking these receptors could inhibit infection.

Efforts to develop immunoliposomes for malaria treatment have focused on targeting specific receptors. For example, Moles et al. used anti-GPA immunoliposomes loaded with Chloroquine and Primaquine that accomplished >96% drug loading using pH-gradient methods

overcoming the drawback of insufficient drug efficacy in-vitro. Moreover, the immunoliposomes targeted both pRBC and RBC causing anti-malarial treatment and prophylaxis due to 100 % RBC and pRBC invasion through the GPA receptors (Moles et al., 2015). Additionally, the group elucidated specific targeting to pRBCs using NTS-DBL1αN-terminal domain anti-rosetting PfEMP1 antibody decorated liposomes that inhibited transmission of the parasite from pRBCs to healthy RBCs (Moles et al., 2016). For instance, lumefantrine-loaded immunoliposomes could specifically target pRBCs upon exposure to PfEMP1 and inhibit rosette formation. Administering drugs in the form of antibody-coated, drug-loaded liposomes has been shown to decrease the required dosage compared to administering free drugs. Moreover, the antibody-conjugated immunoliposome provided a dual effect of specific recognition of the PfEMP1 and elimination of the pRBC. In a study by Biosca et al., co-encapsulated pyronaridine and atovaquone in liposomes with HIR2 monoclonal antibodies targeting glycophorin A onto pRBC for anti-malarial effect (Biosca et al., 2019). Therefore, the immunoliposomes could be a viable option to deliver drugs with differential physicochemical properties or drugs and antigens for vaccine delivery with prophylaxis and treatment measures by targeting both RBC and RBC.

1.3.1.2 Human serum albumin-coated nanocarriers

Human serum albumin (HSA) is a highly abundant protein in blood plasma and plays a vital role in maintaining homeostasis in the human body (Merlot et al., 2014). Additionally, HSA has been shown to have a significant impact on the proliferation of *plasmodium* parasites, as it is abundantly available and accessible to the parasites within erythrocytes. pRBCs utilize various pathways for nutrient import and export, including the ATP-dependent pathway for the transport of HSA to the parasitic membrane (Tahir et al., 2003). HSA is responsible for interactions (Duranton et al., 2008), uptake (Tougan et al., 2020), proliferation (Lopez-Perez et al., 2020), and expansion (Somner et al., 2000) of the parasite within the human host, and due to its non-toxic, non-irritant, and rare adverse effects, it is widely used in parenteral formulations (Rowe et al., 2009). Researchers have formulated nanocarriers using HSA to specifically target pRBCs. For instance, Aditi et al. developed artemether (ART) loaded HSA nanoparticles that demonstrated a significant antimalarial effect when compared to blank HSA nanoparticles in vitro in *P. falciparum* cultures and in vivo in *P. berghei*-infected mice compared to marketed formulations, blank HSA nanoparticles, and control. The HSA nanoparticle provided an edge regarding uniform pharmacokinetic as against the erratic absorption and pharmacokinetics of Artemether from its presently available oil based marketed

formulation (Aditi et al., 2016a). Ibrahim et al. developed albumin nanoparticles loaded with artemisinin, intended for intravenous injection to allow for direct contact between the nanoparticles and erythrocytes. An efficacy study of the artemisinin-loaded albumin nanoparticles in humanized mice demonstrated their high effectiveness in treating the disease, resulting in an extended mean survival time and cessation of disease recrudescence (Ibrahim et al., 2015; Zwain et al., 2022). The HSA nanoparticles would be advantageous compared with another synthetic lipid- and polymer-based system due to their endogenous nature, long-circulation time, non-immunogenicity, and amenability to bind to varied drugs through hydrophobic or charged interaction. On the contrary, the encapsulation of macromolecules would be critical in a HSA-based nanocarrier considering it molecular size.

1.3.1.3 Short peptide nanotubes

The use of peptide-based nanoconstructs has shown promising results in enhancing the antimalarial activity of curcumin (Ccm), a compound derived from the rhizomes of Curcuma longa (turmeric) (Chakrabarti et al., 2013; Cui et al., 2007). Ccm has demonstrated antimalarial activity by causing microtubule disruption, inhibiting histone acylation, and generating reactive oxygen species (ROS) in parasitized red blood cells (pRBCs). However, Ccm has limitations due to its poor absorption, rapid metabolism, and fast elimination from the body (Ipar et al., 2019). Dipeptide-based self-assembled nanotubes (DNP) have shown to enhance the uptake of Ccm in pRBCs, specifically those consisting of α, β-dehydroamino acids (dehydrophenylalanine, ΔPhe) backbone. Four different dipeptides, namely phenylalanine-α,β-dehydrophenylalanine (FΔF), arginine-α,β-dehydrophenylalanine (RΔF), methionine-α,β-dehydrophenylalanine (MΔF), and valine-α,β-dehydrophenylalanine (VΔF) have been evaluated for their ability to enhance the antimalarial activity of Ccm (Chakrabarti et al., 2013). Among the dipeptides, FΔF DNP demonstrated 4.33-fold lesser IC50 compared with free Ccm in *P. falciparum* (indo), a chloroquine resistant antimalarial strain of *Plasmodium falciparum*. Furthermore, when administered in *P. berghei* (ANKA) infected BALB/c mice, Ccm loaded FΔF DNP showed the highest growth inhibition efficacy compared to control and free drugs. Mice treated with DNP survived until 26 days after treatment with a significant reduction in parasitemia, while the control group and free drug treatment group had a lower survival rate and higher parasitemia levels. These findings suggest that dipeptide-based nanoconstructs can potentially enhance the therapeutic efficacy of Ccm for the treatment of malaria (Alam et al., 2016).

1.3.1.4 Polymer peptide hybrid ligand coated nanocarrier

Jokonya and colleagues developed a novel approach to enhance the efficacy and specificity of antimicrobial peptides (AMPs) against pRBCs. The researchers synthesized polymer conjugates of the AMP tyrocidine coated with a pRBC-targeting ligand, GSRSKGT. They conjugated poly(N-vinylpyrrolidone) polymer with tyrocidine using reversible addition fragmentation chain transfer, followed by post-polymerization deprotection. In vitro assays demonstrated that the nanoconjugates exhibited high potency, with activity in the ng/mL concentration range. Additionally, the nanoconjugates demonstrated specific targeting of pRBCs and were 4-19 fold less toxic to erythrocytes compared to free peptide. These findings suggest that the polymer-peptide hybrid ligand has the potential to improve the delivery of AMPs to infected cells and enhance their therapeutic effectiveness against malaria(Jokonya et al., 2020).

1.3.2 Polymer-coated nanocarriers

1.3.2.1 GLUT 1 specific ligand functionalized nanocarriers

Blood-stage malaria parasites rely on glucose uptake through overexpressed GLUT-1 receptors to fuel glycolysis and ATP production. Deprivation of glucose impedes parasite replication by reducing ATP and depolarizing the plasma membrane (Slavic et al., 2011). Targeting the GLUT-1 receptor has emerged as a promising strategy to hinder parasite replication and improve drug efficacy. Various ligands, including glucose and glucosamine-bearing polymers (Najer et al., 2014), starch (Heikham et al., 2015), dehydroascorbic acid (DHA) (Shafi et al., 2017), heparin (Ismail et al., 2019; Muga et al., 2018; Najer et al., 2014), and chitosan (Shafi et al., 2017), have been investigated to block glucose uptake and increase antimalarial drug concentration in infected red blood cells (pRBCs). DHA, the most preferred GLUT-1 ligand, can compete out glucose (Sage & Carruthers, 2014). One study developed DHA functionalized CQ-chitosan nanoparticles, which showed enhanced uptake by pRBCs, increased efficacy, and reduced drug resistance (Shafi et al., 2017). Another study incorporated investigational drugs CDRI 97/63 and/or quinine in starch nanoparticles to target GLUT receptors, leading to improved efficacy compared with free drug (Heikham et al., 2015). Recently, a new GLUT receptor antagonist, WU-1, was synthesized, which specifically blocks 2-DG uptake through the PfRH receptor with minimal effect on human glucose receptors. Surface adsorption, functionalization, or co-encapsulation of WU-1 with other antimalarial drugs could pave the way for new anti-malarial treatment strategies (Heitmeier et al., 2019). Although several ligands have been investigated for GLUT receptor targeting, preferential targeting to pRBC

GLUT receptor and PfRH remains unexplored for effective anti-malarial therapy with minimal side effects and enhanced efficacy. GLUT1 transporters present on the blood-brain barrier have been utilized to target drug formulations to the cerebral region for the treatment of cerebral malaria. One such approach involved preparing brain-targeted liposomes conjugated with cholesterol-undecanoate-glucose. In a biodistribution study, these liposomes were found to accumulate more in the cerebral region compared to conventional control liposomes, demonstrating their targeting ability. The formulation was also effective in reducing infection and recurrence rates in a mouse model, demonstrating its efficacy (Tian et al., 2022). Therefore, the GLUT-1 targeting strategy rely upon the competitive inhibition of overexpressed GLUT receptors onto pRBC with glucose. In-vitro studies of starch nanoparticles depicted inefficient pRBC inhibition due to their inability to compete with dextrose (Shafi et al., 2017). Moreover, careful consideration is required in case of other disease causing GLUT receptor overexpression along with Malaria, despite their in vitro success. Moreover, due consideration shall be given to the cytotoxic effect of chitosan in vivo based on the dose and duration of administration.

1.3.2.2 Glucosaminoglycan functionalized nanocarriers

A. Heparin-coated nanocarriers

PfEMP1 is a key antigen that triggers the host's antibody response to clear the parasite *P. falciparum*. However, certain subpopulations of the parasite can switch expressions to different forms of PfEMP1, leading to immune evasion and re-infection (Pasternak & Dzikowski, 2009). PfEMP1 is a transmembrane protein that has 4 to 7 extracellular domains encoded by the var gene family. It can bind to various adhesion receptors, including CD36, intracellular adhesion molecule-1 (ICAM1), Vascular cell adhesion molecule-1 (VCAM1), CSA (Pasternak & Dzikowski, 2009), and non-infected RBCs, causing rosetting. Heparan sulphate (HS) receptors, blood group A antigen, and complement receptor 1 (CR1) present on the host cell surface initiate rosetting through the cysteine-rich domain of PfEMP1 (Albrecht et al., 2011). HS receptors are ubiquitous, while heparin is only found in mast cell granules within the connective tissue (Aláez-versón, 2017). When pRBCs bind to endothelial cells through PfEMP1, they can cause deep-seated parasite hubs that can complete their life cycle and multiply in various tissues, evading clearance via the spleen (Pasternak & Dzikowski, 2009). The N-terminal DBL1α domain of PfEMP1, known as a heparin-binding protein, binds to HS and is involved in the cytoadherence (Vogt et al., 2003). Highly sulfated heparin can inhibit sporozoites and merozoites of the malaria parasite by interacting with the surface of erythrocytic merozoite and

pRBC membrane, rupturing parasitophorous vacuoles, leaving the erythrocytic membrane intact, and preventing merozoite disaggregation into schizonts (Boyle et al., 2010; Marques et al., 2014; Vogt et al., 2003) (Glushakova et al., 2017). Recent studies have revealed that HS can be electrostatically adsorbed onto liposomes containing PQ, displaying potent anti-malarial activity at concentrations much lower than those needed for an anticoagulant effect (Lantero et al., 2020). Heparin may interact with amyloid-prone structures on the merozoite surface to inhibit *P. falciparum* growth. Heparin-functionalized solid lipid nanoparticles (SLN) have been shown to improve the anti-*plasmodium* activity of CQ against the D6 strain of *P. falciparum* (Muga et al., 2018). It display macrophage evading properties, enabling longer circulation half-life, and exhibit inherent antiplasmodial activity (Muga et al., 2018).

Polymersomes are unique 3D-membranous nanovesicles made of amphiphilic block copolymers that mimic the host cell membrane, allowing them to interact effectively with pathogens. These nanovesicles are more stable than liposomes and remain in circulation for a longer period of time (Najer et al., 2014). Researchers, including Najer et al., have developed nanomimics using different block copolymers, including Polydimethylsiloxane (PDMS)-heparin block copolymer and polymethyloxazoline) PMOXA-b-PDMS-b-PMOXA. These nanomimics specifically bind to merozoites of *P. falciparum* (3D7) culture, resulting in reduced RBC invasion potential. In contrast, polymersomes consisting of PMOXA-b-PDMS-b-PMOXA encapsulating tetrabutylammonium heparin without surface conjugation and free heparin showed no effect on parasites when compared to nanomimics (Najer et al., 2014). This study highlights the importance of heparin block co-polymer on the surface of polymersomes for effective pRBC targeting. Anselmo et al. used dendronized hyperbranched polymers to create nanostructures coated with heparin, which were shown to be a promising platform for targeted drug delivery. The nanostructures specifically targeted parasitized erythrocytes while also exhibiting their own antimalarial activity due to the presence of heparin. This suggests that the nanostructured formulation is a suitable technology for the drug delivery (San Anselmo et al., 2022). The heparin nanoparticles and surface-decorated heparin polymerosomes serve as suitable resort for specific pRBC or merozoite targeting, unlike the GLUT-1 targeting nanoparticles. Purification of heparin from the animal source and its development involves minimal cost. Despite the biocompatibility and biosafety aspect of heparin as a drug delivery vehicle, the faster elimination of heparin is a major cause of concern which might lead to lower efficacy(Lantero et al., 2020). Efforts should be directed towards the development of PEGylated heparin nanoparticles to counteract their quick elimination without losing their

efficacy and decreased anti-coagulation activity to transition them into the clinical pipeline.

B. Chondroitin sulphate-coated nanocarrier

Chondroitin sulphate (CS) has recently emerged as a crucial receptor for erythrocytes infected with *Plasmodium* falciparum, binding to the microvasculature of the lung (Rogerson & Brown, 1997) and placental syncytiotrophoblast. This binding leads to pregnancy-associated malaria and pulmonary edema. The interaction of *Plasmodium*-infected erythrocytes with the CS section of the Syndecan-1 receptor on the placental membrane is linked with the development of monocytes and macrophages, which results in increased autophagosome formation and decreased autophagosome and lysosome fusion, causing a reduced uptake of amino acids within the placenta (Clark, 2019; Zakama et al., 2020a). The pro-inflammatory state of the placenta caused by this interaction results in pathological changes and poor pregnancy outcomes (Zakama et al., 2020b). While pregnancy-associated malaria poses significant risks, including anaemia, maternal morbidity and mortality, low birth weight, preterm birth, and spontaneous abortion, the use of CS as a target for the prevention or treatment of malaria remains largely unexplored (Sharma & Shukla, 2017). One previous report showed that CQ-loaded CSA-coated PEGylated poly(L-lysine)-based dendrimers depicted in-vitro and antimalarial efficacy and efficient pharmacokinetic in-vivo (Bhadra et al., 2006). The CSA-coated CQ-loaded dendrimers masked a few hemotoxic functional groups of CQ upon encapsulation. CSA-coated dendrimers showed lower levels of hematological disturbances and adverse effects on organs compared to free CQ (Bhadra et al., 2006). Therefore, CSA-coated dendrimers have the potential to prolong drug delivery, escape reticuloendothelial system clearance, and increase safety compared to free CQ and uncoated dendrimers.

1.3.2.3 Poly (amidoamine)

Polyamidoamine (PAA) is a biodegradable and biocompatible polymer that has been studied for its ability to target erythrocytes. PAA has a structure resembling proteins and peptides (Barrand et al., 2012; Goodyer et al., 1997; Urbán et al., 2014), which allows it to permeate pRBCs, and has been explored for various applications such as tumor targeting (Kesharwani et al., 2015) and brain delivery (Gu et al., 2013; Huang et al., 2008). Researchers have found that PAA is compatible with erythrocytes and can interact with various charge groups with structures resembling biological membranes(Lombardo et al., 2016). pRBCs have been observed to possess new permeation pathways, leaky surfaces, and parasitic invasion pores, making them suitable for PAA to permeate (Bergmann-Leitner et al., 2009; Jevprasesphant et al., 2004). Studies have reported that pRBC has permeability to high molecular mass solutes

upto 70 nm diameter (Urbán et al., 2015).

The PAA have been widely used due to their cationic surface charge for complexation with nucleic acid and gene delivery(Zhong et al., 2008). The atomistic discrete molecular dynamic studies revealed strong electrostatic and hydrophobic interaction of PAA nanoparticles with serum HSA and Immunoglobulin G due to its surface properties and particle size (Marti et al., 2017; B. Wang et al., 2018). This depicts the affinity of the PAA towards proteins. On the contrary, the interaction with serum proteins decreased when the surface amino groups were conjugated with neutral functional groups(B. Wang et al., 2018). The pRBC are characterized by their expression of adhesive proteins (PfEMP1) which are exported by the *Plasmodium* during infection to an erythrocyte(Smith D, 2014). Increased PfEMP1 facilitate the adherence to the over expressed normal cell surface receptors including ICAM-1, VCAM-1, thrombospondin, CD36, E-selectin, endothelial protein C receptor (EPCR), and PECAM-1 to facilitate the transfer of *Plasmodium* infection(Marin et al., 2023; Viebig et al., 2005; Wassmer et al., 2005). The free amino group incase of AGMA-1 would lead to quick elimination due to the formation of protein corona activating the immune system. However, the ISA-1 and ISA-2 would lead to longer circulation. Since the PAA structurally mimick the β-structure of protein(Gajbhiye et al., 2009), we hypothesize that the hydrophobic and electrostatic interaction arising from the peptide mimicking amides and other hydrophobic groups in PAA, would make it structurally similar to the ICAM-1/VCAM-1or other proteins facilitating specific interaction with the PfEMP1 onto the pRBC. To conclude, the PAA elicit specific targeting to pRBC due to their particle size, peptide mimicking structure PfEMP1 targeting, and surface charge. On contrary, the normal RBC do not possess PfEMP1, the tubovesicular network and and are non-permeable making their affinity to PAA a rare phenomenon.

Due to its polyelectrolyte nature and the presence of amido groups in its structure, PAA can be used to target antimalarial drugs within infected RBCs (Urbán et al., 2014). Various PAA, including AGMA1, ISA1, and ISA23, have been explored for their anti-malarial activity (Fig. 1.2) (Urbán et al., 2015). In vitro studies have revealed that AGMA1 has preferential binding affinity towards pRBCs and interacts with normal RBCs depending on the molecular size of AGMA1, while ISA1 and ISA23 have specific selectivity towards pRBCs. The non-specific distribution towards RBC and pRBC incase of AGMA1 could be attributed to the free amino end groups. PAA polymers were never internalized into normal RBCs due to the absence of endocytic uptake routes in RBCs. In vivo administration of PAA-loaded drugs revealed a rapid biodistribution of AGMA1, which was attributed to its resemblance with the extracellular

binding protein tripeptide arginine-glycine-aspartic acid (RGD) (Urbán et al., 2014). In vivo efficacy studies of PAA conjugated CQ nanoparticles revealed only slight improvement compared to free CQ when administered orally. However, the mice that were treated with PAA-conjugated drugs and then reinfected with *P. yoelli* did not develop malarial symptoms, indicating the potential of PAA as a vaccine adjuvant. Modifications to PAA, such as PEGylation or functionalization with targeting moieties, could further improve its potential as a carrier for oral delivery (Coma-cros et al., 2018).

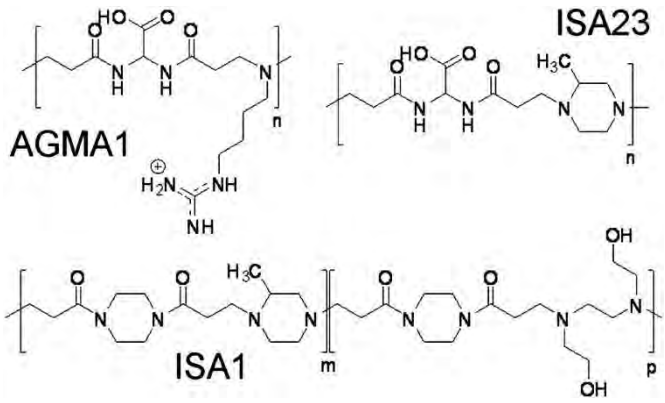

Fig. 1.2. Structure of poly(amidoamine) including AGMA1, ISA23 and ISA1

1.3.3 Lipid-based nanocarriers

Lipid nanocarriers have shown promising potential for the delivery of antimalarial drugs with high specificity towards the ring stage, trophozoite stage, and schizont stage of the malaria parasite (S. A. Jain et al., 2014; Maier et al., 2009). These stages of the parasite can create nutrient uptake channels, such as new permeation pathways and the tubulovesicular network, in red blood cells (RBCs) during their growth (Hagai et al., 1985; Kirk, 2001; Rathod et al., 1997). Lipid molecules can be transported through the TVN into the RBCs with the help of the ATP (Tamez et al., 2008). Glyceryl-dilaurate nanostructured lipid carriers (GDL-NLC) have been reported to effectively enter the parasitized RBCs by disrupting the tubulovesicular network. When administered intravenously in mice, GDL-NLC enhances the mitochondrial membrane potential, leading to the release of ROS and externalization of phosphatidylserine, ultimately causing the lysis of parasitized RBCs (Mandal et al., 2002; Rotmann et al., 2010). However, the non-specific binding potential of GDL could lead to higher dosages and side effects, which need to be addressed through further exploration.

1.3.4 Extracellular vesicles

Extracellular vesicles (EVs) are small spherical carrier bodies composed of phospholipid bilayers, mainly transporting lipids, DNAs, RNAs, and proteins between cells. They can be

roughly categorized as exosomes, microvesicles, and apoptotic bodies depending on the process of their genesis (Elsharkasy et al., 2020). Once considered mere garbage bags, recent studies have unveiled the significant role of EVs in facilitating the transfer of crucial biological information. Cells efficiently sort and package desired biomolecules into these EVs, which are then released into the extracellular environment. Interestingly, these vesicles, composed of endogenous materials, seamlessly penetrate target cells, triggering the transfer of biomolecules and evoking the desired biological responses (Chavda et al., 2023; Vader et al., 2016). EVs play a crucial role in transporting materials to specific target cells, and researchers have recently explored it as drug delivery carriers (Borgheti-Cardoso et al., 2020a; Pandya et al., 2022).

EVs are believed to be responsible for facilitating communication between host and parasite cells. Researchers have observed an elevated production of EVs during Plasmodium infection, implying their potential pathological role in disease progression (Avalos-Padilla et al., 2021). The EVs secreted by the parasitized red blood cells (pRBCs) are recognized for their role in orchestrating various essential processes, including population changes, gametocyte differentiation, alterations in the infection's severity, and immune suppression or activation (Babatunde et al., 2020). In addition, these imbalanced levels of EVs could serve as a potential biomarker for the disease, providing valuable diagnostic information and aiding in the monitoring of the infection's progression (Opadokun & Rohrbach, 2021).

EVs have emerged as crucial elements in vaccine development as well. Herraiz et al. conducted proteomics analysis on EVs derived from P. vivax-infected patients, aiming to identify antigens that could serve as promising vaccine candidates (Aparici-Herraiz et al., 2022). On the other hand, De Sousa et.al. successfully characterized the protein cargo in the plasma of P. yoelii-infected mice. Through their work, they were able to identify specific proteins of interest while excluding essential metabolic proteins (De Sousa et al., 2022). In recent studies, EVs, particularly exosomes, have been assessed for their protective capabilities. Researchers observed that mice immunized with purified exosomes developed IgG antibodies capable of recognizing parasitized red blood cells (pRBCs). Moreover, these immunized animals exhibited reduced parasitemia and increased survival time, highlighting the potential of exosomes as carriers for antigens and adjuvants in the vaccine development (Martin-jaular et al., 2011).

Indeed, EVs have been explored as potential drug carriers for delivering therapeutics to parasitized red blood cells (pRBCs). In a study by Cardoso et al., EVs were isolated from both

healthy and pRBCs, and their lipidomic profiles were found to be similar with no significant differences. Despite this, EVs derived from infected erythrocytes demonstrated more efficient internalization compared to EVs from non-infected erythrocytes (Borgheti-Cardoso et al., 2020b). EVs secreted by infected and healthy erythrocytes exhibit differential interactions with the erythrocytic cell membrane. This presents an interesting avenue of research. Exploring EVs further can lead to the development of biomarkers and better treatment strategies, including vaccines and drug delivery carriers.

1.4 Conclusion and Future Perspective

To achieve the target of eradicating 90% of malaria globally by 2030, a deep understanding of the interaction between the malaria parasite and host cells is crucial. Targeting the erythrocytic stage of malaria through drug delivery can eliminate the risk of transmission to other tissues and prevent recurrence. This review summarizes current strategies for erythrocytic targeting and highlights the receptor-ligand interactions that can aid future developments in malaria therapy. Although the literature reports a complex mechanism for parasite entry and transmission, only a few receptors have been explored for ligand-based nanocarrier targeting. The review identifies unexplored receptors that offer potential avenues for erythrocytic stage malaria treatment. Existing erythrocyte targeting strategies involve either inhibiting parasite entry and transmission or having a static effect on parasite growth within RBC. While some strategies, such as immunoliposomes targeting glycophorin A, restrict parasite entry, others, like anti-rosetting PfEMP1 antibody-decorated liposomes, HSA, and heparin sulphate decorated nanoparticles, inhibit parasite transmission from pRBC to normal RBC. However, a comprehensive approach targeting multiple receptors to inhibit the erythrocytic stage of malaria has not been established. Key concerns related to established active targeting strategies include evaluating clinical efficacy, scaling up developed surface-functionalized nanocarriers, the total cost of therapy, pharmacokinetics of surface-functionalized nanocarriers in erythrocytes, and toxicity studies, which are still gaps in current reports related to various ligand-anchored nanocarriers for malaria.

1.5 Rationale of the present work

Artesunate for injection has been approved by the United States Food and Drug Administration for the initial treatment of severe malaria in adults and pediatric patients. It is administered intravenously at 0 h, 12 h and 24 h and thereafter once daily until the patient is able to tolerate oral antimalarial therapy (*Artesunate*, 2023). The major limitations of artesunate therapy are poor patient compliance due to high dosing frequency and the pain associated with parenteral

administration. In the absence of artesunate, artemether is recommended for the treatment of severe malaria (*Guidelines for the Treatment of Malaria - 3rd Edition World Health Organization (14/06/2022)*, n.d.). It is available in the market as an oily injection for intramuscular use which showed erratic absorption of artemether from the injection site, probably due to poor solubility of the drug. Moreover, artemether exhibits a very short elimination half-life (2-3 h) which demands high dosing frequency to maintain the plasma concentration of the drug within the therapeutic range (Bhandari et al., 2017). Therefore, an alternative delivery strategy is needed to overcome the limitations associated with the current antimalarial therapy.

Different advanced drug delivery systems including polymeric micro and nanoparticles (Gérard Yaméogo et al., 2020; Mangrio et al., 2017; Sidhaye et al., 2016; Yaméogo et al., 2012), lipidic nanoparticles (K. Jain et al., 2015; Nnamani et al., 2014; Parashar et al., 2016; Patil et al., 2020; Prabhu, Suryavanshi, Pathak, Patra, et al., 2016; Prabhu, Suryavanshi, Pathak, Sharma, et al., 2016b), liposomes (Isacchi et al., 2011) and micro and nanoemulsions (Ma et al., 2014) have been exploited for the delivery of artemether with the aim to improve the present malaria therapy. The major limitations of the above formulations are rapid clearance of nanocarriers from blood circulation due to phagocytosis and the inability to maintain drug concentration within the therapeutic range inside infected erythrocytes. It has been reported that nonspherical nanoparticles could evade phagocytosis after parenteral administration (Devarajan et al., 2010; Jindal, 2017) and showed significant influence on margination and wall adhesion in blood flow (Guha & Jindal, 2020; Jurney et al., 2017). However, the role of particle shape in the improvement of antimalarial efficacy of the drugs has remained unexplored yet.

Primaquine phosphate is indicated for the radical cure (prevention of relapse) of vivax malaria. A 14-day course is found to be effective for the prevention of vivax malaria relapse (Castelli et al., 2010; Rodrigues et al., 2012). Patients suffering from an attack of vivax malaria or having parasitized red blood cells should receive a course of chloroquine phosphate, which quickly destroys the erythrocytic parasites and terminates the paroxysm. Primaquine phosphate should be administered concurrently in order to eradicate the exoerythrocytic parasites in a dosage of 1 tablet (equivalent to 15 mg base) daily for 14 days (Kevin Baird et al., 2003).

Adherence to the 14-day regimen of primaquine is a major challenge for the prevention of relapse which was varied from 25-85% (Brown, 1993; Mazier et al., 2009). Although direct observation of dosing intake has improved the adherence to the therapy, it is practically difficult

and time-consuming. To meet the WHO mission of 90% reduction of malaria cases by 2030, there is an urgent need for either a new antimalarial drug that can remain in the blood in the therapeutic range for weeks after single-dose administration or an innovative drug delivery strategy that could enable long-acting release of antimalarial drugs for few days and plasma concentration of the drug can be maintained within the therapeutic range. The discovery of the new antimalarial drug is a time-consuming process and demands huge investments. On the other hand, exploration of new drug delivery technology which could meet the requirements of maintenance of plasma concentration of the drug for a few days after single-dose administration is a significantly fast process and can be completed by low investment than the amount required for the discovery of a new drug.

The objective of the project was to increase the efficiency of artemether and primaquine by preparing their long-acting formulation. Initially, leveraging the concept of particle shape, we prepared antimalarial drug loaded polymeric nanorods using the film stretching technique. It has been reported that nonspherical nanoparticles could evade phagocytosis after parenteral administration (Devarajan et al., 2010; Jindal, 2017) and showed significant influence on margination and wall adhesion in blood flow (Guha & Jindal, 2020; Jurney et al., 2017).
Whereas, the second approach involves the development of long-acting injectable implant using albumin. The initial step involves exposing the albumin solution to an ethanol solution, triggering the formation of insoluble aggregates within a specified timeframe, dependent on the quantity of ethanol used. These insoluble aggregates contribute to the viscosity of the solution mixture. Consequently, when administered parenterally, this solution serves as a depot for sustained drug release. Unlike in situ forming depots, the formation of this depot is not contingent on the physiological conditions of the injection site but is solely determined by the quantity of ethanol employed to induce albumin denaturation.

1.6 The objectives of the present work

The following are the specific objectives of the thesis work

Objective i: Development and validation of HPLC-based analytical method and LC-MS-MS based bioanalytical method for quantification of artemether and primaquine prodrug.

Objective ii: Development and evaluation of artemether loaded polymeric nanorods for enhanced antimalarial effect.

Objective iii: Development and evaluation of long-acting primaquine prodrug loaded nanorods for prolong plasma drug concentration.

Objective iv: Development and evaluation of long-acting biodegradable nanoparticle loaded implant for prolong plasma drug concentration of primaquine prodrug.

References

Aditi, S., Kanchan, B., Sneha, Za., Munna, A., Niroshini, N., & Kamalinder, S. (2016a). serum albumin nanoparticles for effective control of malaria-infected erythrocytes. *Nanomedicine(Lond.)*, *11*(21), 2809–2828.

Aditi, S., Kanchan, B., Sneha, Za., Munna, A., Niroshini, N., & Kamalinder, S. (2016b). serum albumin nanoparticles for effective control of malaria-infected erythrocytes. *Nanomedicine(Lond.)*, *11*(21), 2809–2828.

Agrawal, A. K., & Gupta, C. M. (2000). Tuftsin-bearing liposomes in treatment of macrophage-based infections. *Advanced Drug Delivery Reviews*, *41*, 135–146.

Agrawal, K. (1987). Functional Drug Targeting to Erythrocytes In Vivo Using Antibody Bearing Liposomes As Drug Vehicles. *Biochemical and Biophysical Research Communications*, *148*(1), 357–361.

Aláez-versón, C. R. (2017). *Heparin : new life for an old drug*.

Alam, S., Panda, J. J., Mukherjee, T. K., & Chauhan, V. S. (2016). Short peptide based nanotubes capable of effective curcumin delivery for treating drug resistant malaria. *Journal of Nanobiotechnology*, *14*(26), 1–14. https://doi.org/10.1186/s12951-016-0179-8

Albrecht, L., Moll, K., Blomqvist, K., Normark, J., Chen, Q., & Wahlgren, M. (2011). var gene transcription and PfEMP1 expression in the rosetting and cytoadhesive Plasmodium falciparum clone FCR3S1 . 2. *Malaria Journal*, *10*(17), 1–9.

Anamika, J., Nikhar, V., Laxmikant, G., Priya, S., Sonal, V., & Vyas, S. P. (2020). Nanobiotechnological modules as molecular target tracker for the treatment and prevention of malaria: options and opportunity. *Drug Delivery and Translational Research*, *10*(4), 1095–1110. https://doi.org/10.1007/s13346-020-00770-z

Aparici-Herraiz, I., Gualdrón-López, M., Castro-Cavadía, C. J., Carmona-Fonseca, J., Yasnot, M. F., Fernandez-Becerra, C., & del Portillo, H. A. (2022). Antigen Discovery in Circulating Extracellular Vesicles From Plasmodium vivax Patients. *Frontiers in Cellular and Infection Microbiology*, *11*(January), 1–12. https://doi.org/10.3389/fcimb.2021.811390

Artesunate. (2023). Https://Www.Accessdata.Fda.Gov/Drugsatfda_docs/Label/2022/213036Orig1s001lbl.Pdf.

Avalos-Padilla, Y., Georgiev, V. N., Lantero, E., Pujals, S., Verhoef, R., Borgheti-Cardoso, L. N., Albertazzi, L., Dimova, R., & Fernàndez-Busquets, X. (2021). The ESCRT-III machinery participates in the production of extracellular vesicles and protein export during Plasmodium falciparum infection. *PLoS Pathogens*, *17*(4), 1–24. https://doi.org/10.1371/JOURNAL.PPAT.1009455

Babatunde, K. A., Yesodha Subramanian, B., Ahouidi, A. D., Martinez Murillo, P., Walch, M., & Mantel, P. Y. (2020). Role of Extracellular Vesicles in Cellular Cross Talk in Malaria. *Frontiers in Immunology*, *11*(January), 1–13. https://doi.org/10.3389/fimmu.2020.00022

Barrand, M. A., Winterberg, M., Ng, F., Nguyen, M., Kirk, K., & Hladky, S. B. (2012). Glutathione export from human erythrocytes and Plasmodium falciparum malaria parasites. *Biochem. J.*, *448*, 389–400. https://doi.org/10.1042/BJ20121050

Baruah, U. K., Gowthamarajan, K., Vanka, R., Venkata, V., Reddy, S., Selvaraj, K., Jojo, G. M., Ã, U. K. B., Gowthamarajan, K., Ã, R. V., Venkata, V., Reddy, S., Selvaraj, K., & Jojo, G. M. (2017). Malaria treatment using novel nano-based drug delivery systems Malaria treatment using novel nano-based drug delivery systems. *Journal of Drug Targeting*, *25*(7), 567–581. https://doi.org/10.1080/1061186X.2017.1291645

Bell, D., & Winstanley, P. (2004). Current issues in the treatment of uncomplicated malaria in

Africa. *British Medical Bulletin*, *71*, 29–43. https://doi.org/10.1093/bmb/ldh031
Bergmann-Leitner, E. S., Duncan, E. H., & Angov, E. (2009). MSP-1p42-specific antibodies affect growth and development of intra-erythrocytic parasites of Plasmodium falciparum. *Malaria Journal*, *8*(1), 1–12. https://doi.org/10.1186/1475-2875-8-183
Bhadra, D., Bhadra, S., & Jain, N. K. (2006). PEGylated Peptide Dendrimeric Carriers for the Delivery of Antimalarial Drug Chloroquine Phosphate. *Pharamceutical Research*, *23*(3), 623–633. https://doi.org/10.1007/s11095-005-9396-9
Bhandari, S., Bhandari, V., Sood, J., Jaswal, S., Rana, V., Bedi, N., Sehgal, R., & Tiwary, A. K. (2017). Improved pharmacokinetic and pharmacodynamic attributes of artemether–lumefantrine-loaded solid SMEDDS for oral administration. *Journal of Pharmacy and Pharmacology*, *69*(11), 1437–1446. https://doi.org/10.1111/jphp.12795
Bhanot, P., Schauer, K., Coppens, I., & Nussenzweig, V. (2005). A surface phospholipase is involved in the migration of Plasmodium sporozoites through cells. *Journal of Biological Chemistry*. https://doi.org/10.1074/jbc.M411465200
Bhide, A. R., & Jindal, A. B. (2021). Fabrication and evaluation of artemether loaded polymeric nanorods obtained by mechanical stretching of nanospheres. *International Journal of Pharmaceutics*, *605*(June), 120820. https://doi.org/10.1016/j.ijpharm.2021.120820
Bhide, A. R., Suri, M., Katnoria, S., Kaur, S., Jirwankar, Y. B., Dighe, V. D., & Jindal, A. B. (2022). *Evaluation of Pharmacokinetics, Biodistribution, and Antimalarial Efficacy of Artemether-Loaded Polymeric Nanorods*. https://doi.org/10.1021/acs.molpharmaceut.2c00507
Bhide, A. R., Surve, D. H., Guha, S., & Jindal, A. B. (2020). A sensitive RP-HPLC method for estimation of artemether from polymeric nanoparticles after pre-column acid treatment using UV-visible detector. *Journal of Liquid Chromatography and Related Technologies*. https://doi.org/10.1080/10826076.2020.1777564
Bikash, S., Saurabh, P. D., Tani, Y., & Egan, E. (2020). *Erythrocyte CD55 facilitates the internalization of Plasmodium falciparum parasites*. https://doi.org/10.32388/skxewk
Biosca, A., Dirscherl, L., Moles, E., & Imperial, S. (2019). An ImmunoPEGliposome for Targeted Antimalarial Combination Therapy at the Nanoscale. *Pharmaceutics*, *11*(341), 1–19.
Boateng-Marfo, Y., Dong, Y., Loh, Z. H., Lin, H., & Ng, W. K. (2018). Intravenous human serum albumin (HSA)-bound artemether nanoparticles for treatment of severe malaria. *Colloids and Surfaces A: Physicochemical and Engineering Aspects*. https://doi.org/10.1016/j.colsurfa.2017.08.016
Borgheti-Cardoso, L. N., Kooijmans, S. A. A., Chamorro, L. G., Biosca, A., Lantero, E., Ramírez, M., Avalos-Padilla, Y., Crespo, I., Fernández, I., Fernandez-Becerra, C., del Portillo, H. A., & Fernàndez-Busquets, X. (2020a). Extracellular vesicles derived from Plasmodium-infected and non-infected red blood cells as targeted drug delivery vehicles. *International Journal of Pharmaceutics*, *587*(January), 119627. https://doi.org/10.1016/j.ijpharm.2020.119627
Borgheti-Cardoso, L. N., Kooijmans, S. A. A., Chamorro, L. G., Biosca, A., Lantero, E., Ramírez, M., Avalos-Padilla, Y., Crespo, I., Fernández, I., Fernandez-Becerra, C., del Portillo, H. A., & Fernàndez-Busquets, X. (2020b). Extracellular vesicles derived from Plasmodium-infected and non-infected red blood cells as targeted drug delivery vehicles. *International Journal of Pharmaceutics*, *587*(January), 119627. https://doi.org/10.1016/j.ijpharm.2020.119627
Boyle, M. J., Richards, J. S., Gilson, P. R., Chai, W., & Beeson, J. G. (2010). Interactions with heparin-like molecules during erythrocyte invasion by Plasmodium falciparum

merozoites. *Blood*, *115*(22), 4559–4568. https://doi.org/10.1182/blood-2009-09-243725.The

Brasil, P., Zalis, M. G., Pina-costa, A. De, Siqueira, A. M., Júnior, C. B., & Silva, S. (2017). Outbreak of human malaria caused by Plasmodium simium in the Atlantic Forest in Rio de Janeiro : a molecular epidemiological investigation. *Lancet Gob Health*, *5*, e1038–e1046. https://doi.org/10.1016/S2214-109X(17)30333-9

Brown, G. V. (1993). Chemoprophylaxis of malaria. *Medical Journal of Australia*, *159*(3), 187–196. https://doi.org/10.5694/j.1326-5377.1993.tb137787.x

Burns, A. L., Dans, M. G., Balbin, J. M., De, T. F., Gilson, P. R., Beeson, J. G., Boyle, M. J., & Wilson, D. W. (2019). Targeting malaria parasite invasion of red blood cells as an antimalarial strategy. *FEMS Microbiology Reviews*, *43*, 223–238. https://doi.org/10.1093/femsre/fuz005

Castelli, F., Odolini, S., Autino, B., Foca, E., & Russo, R. (2010). Malaria Prophylaxis: A Comprehensive Review. *Pharmaceuticals*, *3*(10), 3212–3239. https://doi.org/10.3390/ph3103212

Chakrabarti, R., Rawat, P. S., Cooke, B. M., Coppel, R. L., & Patankar, S. (2013). Cellular Effects of Curcumin on Plasmodium falciparum Include Disruption of Microtubules. *PLOS ONE*, *8*(3), 1–14. https://doi.org/10.1371/journal.pone.0057302

Chandra, S., Agrawal, A. K., & Gupta, C. M. (1991). Chloroquine delivery to erythrocytes in Plasmodium berghei- infected mice using antibody-bearing liposomes as drug vehicles *. *J. Biosci.*, *16*(3), 137–144.

Chasis, J. A., Mohandas, N., & Shohet, S. B. (1985). Erythrocyte membrane rigidity induced by glycophorin A-ligand interaction. Evidence for a ligand-induced association between glycophorin A and skeletal proteins. *Journal of Clinical Investigation*. https://doi.org/10.1172/JCI111907

Chavda, V. P., Pandya, A., Kumar, L., Raval, N., Vora, L. K., Pulakkat, S., Patravale, V., Salwa, Duo, Y., & Tang, B. Z. (2023). Exosome nanovesicles: A potential carrier for therapeutic delivery. *Nano Today*, *49*, 101771. https://doi.org/10.1016/j.nantod.2023.101771

Clark, R. L. (2019). Genesis of placental sequestration in malaria and possible targets for drugs for placental malaria. *Birth Defects Research*, *111*(10), 569–583. https://doi.org/10.1002/bdr2.1496

Coma-cros, E. M., Biosca, A., Marques, J., Carol, L., Urb, P., Berenguer, D., Riera, M. C., Delves, M., Sinden, R. E., Valle-delgado, J. J., Spanos, L., Siden-kiamos, I., Paula, P., Paaijmans, K., Rottmann, M., Manfredi, A., Ferruti, P., Ranucci, E., & Fern, X. (2018). Polyamidoamine Nanoparticles for the Oral Administration of Antimalarial Drugs. *Pharmaceutics*, *10*(225), 1–20. https://doi.org/10.3390/pharmaceutics10040225

Cui, L., Mharakurwa, S., Ndiaye, D., Rathod, P. K., & Rosenthal, P. J. (2015). Antimalarial Drug Resistance : Literature Review and Activities and Findings of the ICEMR Network. *Am. J. Trop. Med. Hyg*, *93*(Suppl 3), 57–68. https://doi.org/10.4269/ajtmh.15-0007

Cui, L., Miao, J., & Cui, L. (2007). Cytotoxic Effect of Curcumin on Malaria Parasite Plasmodium falciparum : Inhibition of Histone Acetylation and Generation of Reactive Oxygen Species ☋. *Antimicrobial Agents and Chemotherapy*, *51*(2), 488–494. https://doi.org/10.1128/AAC.01238-06

Date, A. A., Joshi, M. D., & Patravale, V. B. (2007). Parasitic diseases: Liposomes and polymeric nanoparticles versus lipid nanoparticles. *Advanced Drug Delivery Reviews*, *59*(6), 505–521. https://doi.org/10.1016/j.addr.2007.04.009

De Sousa, K. P., Potriquet, J., Mulvenna, J., Sotillo, J., Groves, P. L., Loukas, A., Apte, S. H.,

& Doolan, D. L. (2022). Proteomic identification of the contents of small extracellular vesicles from in vivo Plasmodium yoelii infection. *International Journal for Parasitology*, *52*(1), 35–45. https://doi.org/10.1016/j.ijpara.2021.06.001

Devarajan, P. v., Jindal, A. B., Patil, R. R., Mulla, F., Gaikwad, R. v., & Samad, A. (2010). Particle Shape: A New Design Parameter for Passive Targeting In Splenotropic Drug Delivery. *Journal of Pharmaceutical Sciences*, *99*(6), 2576–2581. https://doi.org/10.1002/jps.22052

Di, J., Xie, F., & Xu, Y. (2020). When liposomes met antibodies: Drug delivery and beyond. *Advanced Drug Delivery Reviews*, *154–155*, 151–162. https://doi.org/10.1016/j.addr.2020.09.003

Dulgeroff, L. B. T., Oakley, M. S., Tal, M. C., Yiu, Y. Y., He, J. Q., Shoham, M., Majam, V., Okoth, W. A., Malla, P., Kumar, S., & Weissman, I. L. (2021). CD47 blockade reduces the pathologic features of experimental cerebral malaria and promotes survival of hosts with Plasmodium infection. *Proceedings of the National Academy of Sciences of the United States of America*, *118*(11). https://doi.org/10.1073/pnas.1907653118

Duranton, C., Tanneur, V., Lang, C., Brand, V. B., Koka, S., Kasinathan, R. S., Dorsch, M., Hedrich, H. J., Baumeister, S., Lingelbach, K., Lang, F., & Huber, S. M. (2008). A high specificity and affinity interaction with serum albumin stimulates an anion conductance in malaria-infected erythrocytes. *Cellular Physiology and Biochemistry*. https://doi.org/10.1159/000185483

Ejigiri, I., & Sinnis, P. (2009a). Plasmodium sporozoite-host interactions from the dermis to the hepatocyte. *Current Opinion in Microbiology*, *12*(4), 401–407. https://doi.org/10.1016/j.mib.2009.06.006

Ejigiri, I., & Sinnis, P. (2009b). Plasmodium sporozoite-host interactions from the dermis to the hepatocyte. *Current Opinion in Microbiology*, *12*(4), 401–407. https://doi.org/10.1016/j.mib.2009.06.006

Eloy, J. O., Petrilli, R., Noboru, L., Trevizan, F., & Chorilli, M. (2017). Immunoliposomes: A review on functionalization strategies and targets for drug delivery. *Colloids and Surfaces B: Biointerfaces*, *159*, 454–467. https://doi.org/10.1016/j.colsurfb.2017.07.085

Elsharkasy, O. M., Nordin, J. Z., Hagey, D. W., de Jong, O. G., Schiffelers, R. M., Andaloussi, S. EL, & Vader, P. (2020). Extracellular vesicles as drug delivery systems: Why and how? *Advanced Drug Delivery Reviews*, *159*, 332–343. https://doi.org/10.1016/j.addr.2020.04.004

Fernàndez-busquets, X. (2016). Novel strategies for Plasmodium-targeted drug delivery. *Expert Opin. Drug Deliv.*, *13*(March), 919–932. https://doi.org/10.1517/17425247.2016.1167038

Fotoran, W. L., Müntefering, T., Kleiber, N., Miranda, B. N. M., Liebau, E., Irvine, D. J., & Wunderlich, G. (2019). A multilamellar nanoliposome stabilized by interlayer hydrogen bonds increases antimalarial drug efficacy. *Nanomedicine: Nanotechnology, Biology, and Medicine*, *22*. https://doi.org/10.1016/j.nano.2019.102099

Fujioka, H., & Aikawa, M. (2002a). Structure and life cycle. In *Chemical Immunology*. https://doi.org/10.1159/000058837

Fujioka, H., & Aikawa, M. (2002b). Structure and life cycle. In *Chemical Immunology*. https://doi.org/10.1159/000058837

Gajbhiye, V., Palanirajan, V. K., Tekade, R. K., & Jain, N. K. (2009). Dendrimers as therapeutic agents: a systematic review. *Journal of Pharmacy and Pharmacology*, *61*(8), 989–1003. https://doi.org/10.1211/jpp/61.08.0002

Gérard Yaméogo, J. B., Mazet, R., Wouessidjewe, D., Choisnard, L., Godin-Ribuot, D., Putaux, J. L., Semdé, R., & Gèze, A. (2020). Pharmacokinetic study of intravenously

administered artemisinin-loaded surface-decorated amphiphilic γ-cyclodextrin nanoparticles. *Materials Science and Engineering C*, *106*(April 2019), 110281. https://doi.org/10.1016/j.msec.2019.110281

Glodek, A. M., Mirchev, R., Golan, D. E., Khoory, J. A., Burns, J. M., Shevkoplyas, S. S., Nicholson-Weller, A., & Ghiran, I. C. (2010). Ligation of complement receptor 1 increases erythrocyte membrane deformability. *Blood*. https://doi.org/10.1182/blood-2010-04-273904

Glushakova, S., Busse, B. L., Garten, M., Beck, J. R., Fairhurst, R. M., Goldberg, D. E., & Zimmerberg, J. (2017). Exploitation of a newly-identified entry pathway into the malaria parasite-infected erythrocyte to inhibit parasite egress. *Scientific Reports*, *September*, 1–13. https://doi.org/10.1038/s41598-017-12258-x

Gnanadesigan, M., Nanadagopalan, V., Kapildev, G., & Gundappa, M. (2019). Chapter 16 - Nano Drugs for Curing Malaria: The Plausibility. In *Applications of Targeted Nano Drugs and Delivery Systems*. Elsevier Inc. https://doi.org/10.1016/B978-0-12-814029-1.00016-8

Goodyer, I. D., Pouvelle, B., Schneider, T. G., Trelka, D. P., & Taraschi, T. F. (1997). Characterization of macromolecular transport pathways in malaria-infected erythrocytes. *Molecular and Biochemical Parasitology*, *87*, 13–28.

Gu, L., Wu, Z. H., Qi, X., He, H., Ma, X., Chou, X., Wen, X., Zhang, M., & Jiao, F. (2013). Polyamidomine dendrimers: An excellent drug carrier for improving the solubility and bioavailability of puerarin. *Pharmaceutical Development and Technology*, *18*(5), 1051–1057. https://doi.org/10.3109/10837450.2011.653822

Guha, S., & Jindal, A. B. (2020). An insight into obtaining of non-spherical particles by mechanical stretching of micro- and nanospheres. In *Journal of Drug Delivery Science and Technology*. https://doi.org/10.1016/j.jddst.2020.101860

Guidelines for the treatment of malaria - 3rd edition World Health Organization (14/06/2022). (n.d.).

Hagai, G., Kutner, S., Krugliak, M., & Cabantchik, I. (1985). Charactierzation of permeation pathways appearing in the host membrane of Plasmodium falciparum infected red blood cells. *Molecular and Biochemical Parasitology*, *14*, 313–322.

Hamelmann, N. M., Paats, J. W. D., Avalos-Padilla, Y., Lantero, E., Spanos, L., Siden-Kiamos, I., Fernàndez-Busquets, X., & Paulusse, J. M. J. (2023). Single-Chain Polymer Nanoparticles Targeting the Ookinete Stage of Malaria Parasites. *ACS Infectious Diseases*, *9*(1), 56–64. https://doi.org/10.1021/acsinfecdis.2c00336

Heikham, K. D., Gupta, A., Kumar, A., Singh, C., Saxena, J., Srivastava, K., Puri, S. K., Dwivedi, A. K., Habib, S., & Misra, A. (2015). Preferential targeting of human erythrocytes infected with the malaria parasite Plasmodium falciparum via hexose transporter surface proteins. *International Journal of Pharmaceutics*, *483*(1–2), 57–62. https://doi.org/10.1016/j.ijpharm.2015.02.011

Heitmeier, M. R., Hresko, R. C., Edwards, R. L., Prinsen, M. J., Ilagan, M. X. G., Odom John, A. R., & Hruz, P. W. (2019). Identification of druggable small molecule antagonists of the Plasmodium falciparum hexose transporter PfHT and assessment of ligand access to the glucose permeation pathway via FLAG-mediated protein engineering. *PLoS ONE*, *14*(5), 1–20. https://doi.org/10.1371/journal.pone.0216457

Huang, R., Ke, W., Liu, Y., Jiang, C., & Pei, Y. (2008). The use of lactoferrin as a ligand for targeting the polyamidoamine-based gene delivery system to the brain. *Biomaterials*, *29*(2), 238–246. https://doi.org/10.1016/j.biomaterials.2007.09.024

Huff, C. G., Coulston, F., & Cantrell, W. (1943). Malarial cryptozoites. In *Science*. https://doi.org/10.1126/science.97.2517.286

Ibrahim, N., Ibrahim, H., Dormoi, J., Briolant, S., Pradines, B., Moreno, A., Mazier, D., Legrand, P., & Nepveu, F. (2014). Albumin-bound nanoparticles of practically water-insoluble antimalarial lead greatly enhance its efficacy. *International Journal of Pharmaceutics*. https://doi.org/10.1016/j.ijpharm.2014.01.001

Ibrahim, N., Ibrahim, H., Sabater, A. M., Mazier, D., Valentin, A., & Nepveu, F. (2015). Artemisinin nanoformulation suitable for intravenous injection: Preparation, characterization and antimalarial activities. *International Journal of Pharmaceutics*. https://doi.org/10.1016/j.ijpharm.2015.09.020

Ipar, V. S., Dsouza, A., & Devarajan, P. V. (2019). Enhancing Curcumin Oral Bioavailability Through Nanoformulations. *European Journal of Drug Metabolism and Pharmacokinetics*, *44*, 459–480. https://doi.org/10.1007/s13318-019-00545-z

Isacchi, B., Arrigucci, S., Marca, G. la, Bergonzi, M. C., Vannucchi, M. G., Novelli, A., & Bilia, A. R. (2011). Conventional and long-circulating liposomes of artemisinin: Preparation, characterization, and pharmacokinetic profile in mice. *Journal of Liposome Research*. https://doi.org/10.3109/08982104.2010.539185

Ishino, T., Chinzei, Y., & Yuda, M. (2005). A Plasmodium sporozoite protein with a membrane attack complex domain is required for breaching the liver sinusoidal cell layer prior to hepatocyte infection. *Cellular Microbiology*. https://doi.org/10.1111/j.1462-5822.2004.00447.x

Ishino, T., Yano, K., Chinzei, Y., & Yuda, M. (2004). Cell-passage activity is required for the malarial parasite to cross the liver sinusoidal cell layer. *PLoS Biology*. https://doi.org/10.1371/journal.pbio.0020004

Ismail, M., Du, Y., Ling, L., & Li, X. (2019). Artesunate-heparin conjugate based nanocapsules with improved pharmacokinetics to combat malaria. *International Journal of Pharmaceutics*, *562*, 162–171. https://doi.org/10.1016/j.ijpharm.2019.03.031

Jain, K., Sood, S., & Gowthamarajan, K. (2015). Optimization of artemether-loaded NLC for intranasal delivery using central composite design. *Drug Delivery*, *22*(7), 940–954. https://doi.org/10.3109/10717544.2014.885999

Jain, S. A., Basu, H., Prabhu, P. S., Soni, U., Joshi, M. D., Mathur, D., Patravale, V. B., & Pathak, S. (2014). Parasite impairment by targeting Plasmodium -infected RBCs using glyceryl-dilaurate nanostructured lipid carriers. *Biomaterials*, *35*(24), 6636–6645. https://doi.org/10.1016/j.biomaterials.2014.04.058

Jaskiewicz, E., Jodłowska, M., Kaczmarek, R., & Zerka, A. (2019). Erythrocyte glycophorins as receptors for Plasmodium merozoites. In *Parasites and Vectors*. https://doi.org/10.1186/s13071-019-3575-8

Jevprasesphant, R., Penny, J., Attwood, D., & D'Emanuele, A. (2004). Transport of dendrimer nanocarriers through epithelial cells via the transcellular route. *Journal of Controlled Release*, *97*(2), 259–267. https://doi.org/10.1016/j.jconrel.2004.03.022

Jindal, A. B. (2017). The effect of particle shape on cellular interaction and drug delivery applications of micro- and nanoparticles. In *International Journal of Pharmaceutics*. https://doi.org/10.1016/j.ijpharm.2017.09.028

Jokonya, S., Langlais, M., Leshabane, M., Reader, P. W., Vosloo, J. A., Pfukwa, R., Coertzen, D., Birkholtz, L. M., Rautenbach, M., & Klumperman, B. (2020). Poly(N-vinylpyrrolidone) Antimalaria Conjugates of Membrane-Disruptive Peptides. *Biomacromolecules*. https://doi.org/10.1021/acs.biomac.0c01202

Jurney, P., Agarwal, R., Singh, V., Choi, D., Roy, K., Sreenivasan, S. v., & Shi, L. (2017). Unique size and shape-dependent uptake behaviors of non-spherical nanoparticles by endothelial cells due to a shearing flow. *Journal of Controlled Release*. https://doi.org/10.1016/j.jconrel.2016.11.033

Kariu, T., Ishino, T., Yano, K., Chinzei, Y., & Yuda, M. (2006). CelTOS, a novel malarial protein that mediates transmission to mosquito and vertebrate hosts. *Molecular Microbiology*. https://doi.org/10.1111/j.1365-2958.2005.05024.x

Kesharwani, P., Xie, L., Mao, G., Padhye, S., & Iyer, A. K. (2015). Hyaluronic acid-conjugated polyamidoamine dendrimers for targeted delivery of 3,4-difluorobenzylidene curcumin to CD44 overexpressing pancreatic cancer cells. *Colloids and Surfaces B: Biointerfaces*, *136*, 413–423. https://doi.org/10.1016/j.colsurfb.2015.09.043

Kevin Baird, J., Fryauff, D. J., & Hoffman, S. L. (2003). Primaquine for Prevention of Malaria in Travelers. *Clinical Infectious Diseases*, *37*(12), 1659–1667. https://doi.org/10.1086/379714

Kirk, K. (2001). Membrane Transport in the Malaria-Infected Erythrocyte. *Phyiological Reviews*, *81*(2), 495–537.

Kirtane, A. R., Verma, M., Karandikar, P., Furin, J., Langer, R., & Traverso, G. (2021). Nanotechnology approaches for global infectious diseases. *Nature Nanotechnology*, *16*(4), 369–384. https://doi.org/10.1038/s41565-021-00866-8

Lantero, E., Ra, C., Romero, P., & Sierra, T. (2020). Repurposing Heparin as Antimalarial : Evaluation of Multiple Modifications Toward In Vivo Application. *Pharmaceutics*, *12*(825), 1–18.

Lombardo, D., Calandra, P., Bellocco, E., Laganà, G., Barreca, D., Magazù, S., Wanderlingh, U., & Kiselev, M. A. (2016). Effect of anionic and cationic polyamidoamine (PAMAM) dendrimers on a model lipid membrane. *Biochimica et Biophysica Acta - Biomembranes*, *1858*(11), 2769–2777. https://doi.org/10.1016/j.bbamem.2016.08.001

Lopez-Perez, M., Van Der Puije, W., Castberg, F. C., Ofori, M. F., & Hviid, L. (2020). Binding of human serum proteins to Plasmodium falciparum-infected erythrocytes and its association with malaria clinical presentation. *Malaria Journal*. https://doi.org/10.1186/s12936-020-03438-8

Ma, Y., Lu, T., Zhao, W., Wang, Y., Chen, T., Mei, Q., & Chen, T. (2014). Enhanced antimalarial activity by a novel artemether-lumefantrine lipid emulsion for parenteral administration. *Antimicrobial Agents and Chemotherapy*. https://doi.org/10.1128/AAC.01428-13

Maier, A. G., Cooke, B. M., Cowman, A. F., & Tilley, L. (2009). Malaria parasite proteins that remodel the host erythrocyte. *Microbiology*, *7*(may), 341–354. https://doi.org/10.1038/nrmicro2110

Mandal, D., Moitra, P. K., Saha, S., & Ã, J. B. (2002). Caspase 3 regulates phosphatidylserine externalization and phagocytosis of oxidatively stressed erythrocytes. *FEBS Letters*, *513*, 184–188.

Mangrio, F. A., Dwivedi, P., Han, S., Zhao, G., Gao, D., Si, T., & Xu, R. X. (2017). Characteristics of Artemether-Loaded Poly(lactic-co-glycolic) Acid Microparticles Fabricated by Coaxial Electrospray: Validation of Enhanced Encapsulation Efficiency and Bioavailability. *Molecular Pharmaceutics*. https://doi.org/10.1021/acs.molpharmaceut.7b00862

Marin, A. A., Juillard, A., Katzin, A. M., Carvalho, L. J. M., & Grau, G. E. R. (2023). Perillyl alcohol modulates activation, permeability and integrity of human brain endothelial cells induced by Plasmodium falciparum. *Memorias Do Instituto Oswaldo Cruz*, *118*(18), 1–9. https://doi.org/10.1590/0074-02760230033

Marques, J., Moles, E., Urbán, P., Prohens, R., Busquets, M. A., Sevrin, C., Grandfils, C., & Fernàndez-busquets, X. (2014). Application of heparin as a dual agent with antimalarial and liposome targeting activities toward Plasmodium -infected red blood cells. *Nanomedicine: Nanotechnology, Biology, and Medicine*, *10*(8), 1719–1728.

https://doi.org/10.1016/j.nano.2014.06.002
Marti, E., Paajimans, K., Urban, P., Manfredi, A., Biosca, A., Lantero, E., Moles, E., Ranucci, E., Ferruti, P., & Xaviers, F.-B. (2017). Amphoteric polyamidoamines as innovative tools to selectively direct antimalarial drugs towards Plasmodium-infected red blood cells. *The Milan Polymer Days Conference-MIPOL2017*, 76.
Martin-jaular, L., Nakayasu, E. S., Ferrer, M., Almeida, I. C., & Hernando, A. (2011). *Exosomes from Plasmodium yoelii-Infected Reticulocytes Protect Mice from Lethal Infections*. *6*(10), 1–10. https://doi.org/10.1371/journal.pone.0026588
Mazier, D., Rénia, L., & Snounou, G. (2009). A pre-emptive strike against malaria's stealthy hepatic forms. *Nature Reviews Drug Discovery*, *8*(11), 854–864. https://doi.org/10.1038/nrd2960
Merlot, A. M., Kalinowski, D. S., & Richardson, D. R. (2014). Unraveling the mysteries of serum albumin-more than just a serum protein. *Frontiers in Physiology*. https://doi.org/10.3389/fphys.2014.00299
Miatmoko, A., Annuryanti, F., Sari, R., & Hendradi, E. (2019). Dual Loading Of Primaquine And Chloroquine Into Liposome. *European Pharamceutical Journal*, *66*(2), 18–25. https://doi.org/10.2478/afpuc-2019-0009
Michels, L. R., Maciel, T. R., Nakama, K. A., & Haas, S. E. (2019). Effects of Surface Characteristics of Polymeric Nanocapsules on the Pharmacokinetics and Ef fi cacy of Antimalarial Quinine. *International Journal of Nanomedicine*, *14*, 10165–10178.
Moles, E., Galiano, S., Gomes, A., Quiliano, M., Teixeira, C., Gomes, P., & Fernàndez-busquets, X. (2017). ImmunoPEGliposomes for the targeted delivery of novel lipophilic drugs to red blood cells in a falciparum malaria murine model. *Biomaterials*, *145*, 178–191. https://doi.org/10.1016/j.biomaterials.2017.08.020
Moles, E., Moll, K., Ch, J., Parini, P., Wahlgren, M., & Fern, X. (2016). Development of drug-loaded immunoliposomes for the selective targeting and elimination of rosetting Plasmodium falciparum-infected red blood cells. *Journal of Controlled Release*, *241*, 57–67. https://doi.org/10.1016/j.jconrel.2016.09.006
Moles, E., Urbán, P., Jiménez-díaz, M. B., Viera-morilla, S., Angulo-barturen, I., Busquets, M. A., & Fernàndez-busquets, X. (2015). Immunoliposome-mediated drug delivery to Plasmodium-infected and non- infected red blood cells as a dual therapeutic/prophylactic antimalarial strategy. *Journal of Controlled Release*, *210*, 217–229. https://doi.org/10.1016/j.jconrel.2015.05.284
Moreira, C. K., Templeton, T. J., Lavazec, C., Hayward, R. E., Hobbs, C. V., Kroeze, H., Janse, C. J., Waters, A. P., Sinnis, P., & Coppi, A. (2008). The Plasmodium TRAP/MIC2 family member, TRAP-Like Protein (TLP), is involved in tissue traversal by sporozoites. *Cellular Microbiology*. https://doi.org/10.1111/j.1462-5822.2008.01143.x
Ms, J. M., Ms, E. M., Urbán, P., Prohens, R., Busquets, M. A., Sevrin, C., Grandfils, C., & Fernàndez-busquets, X. (2014). Application of heparin as a dual agent with antimalarial and liposome targeting activities towards Plasmodium-infected red blood cells. *Nanomedicine: Nanotechnology, Biology, and Medicine*. https://doi.org/10.1016/j.nano.2014.06.002
Muga, J. O., Gathirwa, J. W., Tukulula, M., & Jura, W. G. Z. O. (2018). In vitro evaluation of chloroquine - loaded and heparin surface - functionalized solid lipid nanoparticles. *Malaria Journal*, 1–7. https://doi.org/10.1186/s12936-018-2302-9
Najer, A., Wu, D., Bieri, A., Palivan, C. G., Beck, H., & Meier, W. (2014). Nanomimics of Host Cell Membranes Block Invasion and Expose Invasive Malaria Parasites. *ACS Nano*, *8*(12), 12560–12571. https://doi.org/10.1021/nn5054206
Nash, G. B., Marsh, K., & Newbold, C. (1992). Rheological analysis of the adhesive

interactions of red blood cells parasitized b Plasmodium falciparum Rheological analysis of the adhesive interactions of red blood cells parasitized by Plasmodium falciparum. *Blood*, *79*(March), 798–807. https://doi.org/10.1182/blood.V79.3.798.bloodjournal793798

Neves Borgheti-Cardoso, L., San Anselmo, M., Lantero, E., Lancelot, A., Serrano, J. L., Hernández-Ainsa, S., Fernàndez-Busquets, X., & Sierra, T. (2020). Promising nanomaterials in the fight against malaria. *Journal of Materials Chemistry B*, *8*(41), 9428–9448. https://doi.org/10.1039/d0tb01398f

Nichole, S. D., & Niraj, T. H. (2016). Red cell receptors as access points for malaria infection. *Curr Opin Hematol*, *23*(3), 215–223. https://doi.org/10.1097/MOH.0000000000000219.Red

Nnamani, P. O., Hansen, S., Windbergs, M., & Lehr, C. M. (2014). Development of artemether-loaded nanostructured lipid carrier (NLC) formulation for topical application. *International Journal of Pharmaceutics*. https://doi.org/10.1016/j.ijpharm.2014.10.004

Nureye, D., & Assefa, S. (2020). Old and Recent Advances in Life Cycle , Pathogenesis , Diagnosis , Prevention , and Treatment of Malaria Including Perspectives in Ethiopia. *The Scientific World Journal*, *2020*.

Ogutu, B., Oloo, F., Swai, H., Melariri, P., Mahanga, G. M., & Waweru, J. (2014). Preparation, characterization, and optimization of primaquine-loaded solid lipid nanoparticles. *International Journal of Nanomeidicine*, *9*, 3865–3874.

Opadokun, T., & Rohrbach, P. (2021). Extracellular vesicles in malaria: an agglomeration of two decades of research. *Malaria Journal*, *20*(1), 1–16. https://doi.org/10.1186/s12936-021-03969-8

Pandya, A., Pulakkat, S., & Patravale, V. (2022). Exosomes for Drug Delivery Applications in Cancer and Cardiac Indications. *Targeted Drug Delivery*, 193–220.

Parashar, D., Aditya, N. P., & Murthy, R. S. R. (2016). Development of artemether and lumefantrine co-loaded nanostructured lipid carriers: Physicochemical characterization and in vivo antimalarial activity. *Drug Delivery*, *23*(1), 123–129. https://doi.org/10.3109/10717544.2014.905883

Pasternak, N. D., & Dzikowski, R. (2009). PfEMP1 : An antigen that plays a key role in the pathogenicity and immune evasion of the malaria parasite Plasmodium falciparum. *The International Journal of Biochemistry*, *41*, 1463–1466. https://doi.org/10.1016/j.biocel.2008.12.012

Patil, J., Rajput, R., Nemade, R., & Naik, J. (2020). Preparation and characterization of artemether loaded solid lipid nanoparticles: a 32 factorial design approach. *Materials Technology*, *35*(11–12), 719–726. https://doi.org/10.1080/10667857.2018.1475142

Prabhu, P., Suryavanshi, S., Pathak, S., Patra, A., Sharma, S., & Patravale, V. (2016). Nanostructured lipid carriers of artemether–lumefantrine combination for intravenous therapy of cerebral malaria. *International Journal of Pharmaceutics*. https://doi.org/10.1016/j.ijpharm.2016.09.008

Prabhu, P., Suryavanshi, S., Pathak, S., Sharma, S., & Patravale, V. (2016a). Artemether–lumefantrine nanostructured lipid carriers for oral malaria therapy: Enhanced efficacy at reduced dose and dosing frequency. *International Journal of Pharmaceutics*. https://doi.org/10.1016/j.ijpharm.2016.07.021

Prabhu, P., Suryavanshi, S., Pathak, S., Sharma, S., & Patravale, V. (2016b). Artemether–lumefantrine nanostructured lipid carriers for oral malaria therapy: Enhanced efficacy at reduced dose and dosing frequency. *International Journal of Pharmaceutics*, *511*(1), 473–487. https://doi.org/10.1016/j.ijpharm.2016.07.021

Prudêncio, M., Rodriguez, A., & Mota, M. M. (2006a). The silent path to thousands of

merozoites: The Plasmodium liver stage. In *Nature Reviews Microbiology*. https://doi.org/10.1038/nrmicro1529

Prudêncio, M., Rodriguez, A., & Mota, M. M. (2006b). The silent path to thousands of merozoites: The Plasmodium liver stage. In *Nature Reviews Microbiology*. https://doi.org/10.1038/nrmicro1529

Puttappa, N., Kumar, R. S., Kuppusamy, G., & Radhakrishnan, A. (2019). Acta Tropica Nano-facilitated drug delivery strategies in the treatment of plasmodium infection. *Acta Tropica*, *195*, 103–114. https://doi.org/10.1016/j.actatropica.2019.04.020

Rai, M., Ingle, A. P., Paralikar, P., Gupta, I., Medici, S., & Santos, C. A. (2017). Recent advances in use of silver nanoparticles as antimalarial agents. In *International Journal of Pharmaceutics*. https://doi.org/10.1016/j.ijpharm.2017.04.042

Rathod, P. K., Ghori, N., & Haldar, K. (1997). Membrane Network for Nutrient Import in Red Cells Infected with the Malaria Parasite. *Science*, *276*, 1122–1125.

Rodrigues, T., Prudêncio, M., Moreira, R., Mota, M. M., & Lopes, F. (2012). Targeting the Liver Stage of Malaria Parasites: A Yet Unmet Goal. *Journal of Medicinal Chemistry*, *55*(3), 995–1012. https://doi.org/10.1021/jm201095h

Rodriguez, L. E., Curtidor, H., Urquiza, M., Cifuentes, G., Reyes, C., & Patarroyo, M. E. (2008). Intimate Molecular Interactions of P . falciparum Merozoite Proteins Involved in Invasion of Red Blood Cells and Their Implications for Vaccine Design. *Chem Rev*, *108*, 3656–3705.

Rogerson, S. J., & Brown, G. V. (1997). Chondroitin Sulphate A as an Adherence Receptor for Plasmodium faiciparum . infected Erythrocytes. *Parasitology Today*, *13*(2), 0–5.

Rosen, B. M., Wilson, C. J., Wilson, D. A., Peterca, M., Imam, M. R., & Percec, V. (2009). Dendron-mediated self-assembly, disassembly, and self-organization of complex systems. *Chem Soc Rev*, *109*, 6275–6540. https://doi.org/10.1021/cr900157q

Rotmann, A., Sanchez, C., Guiguemde, A., Rohrbach, P., Dave, A., Bakouh, N., Planelles, G., & Lanzer, M. (2010). PfCHA is a mitochondrial divalent cation / H + antiporter in Plasmodium falciparum. *Molecular Microbiology*, *76*(May), 1591–1606. https://doi.org/10.1111/j.1365-2958.2010.07187.x

Rowe, R. C., Sheskey, P. J., & Quinn, M. E. (2009). Handbook of Pharmaceutical Excipients 6th Ed.(2009) - (Malestrom). In *Handbook of Pharmaceutical Excipients*.

Sage, J., & Carruthers, A. (2014). Human erythrocytes transport dehydroascorbic acid and sugars using the same transporter complex. *American Journal of Physiology Cell Physiology*, *306*(10), C910–C917.

San Anselmo, M., Lantero, E., Avalos-Padilla, Y., Bouzón-Arnáiz, I., Ramírez, M., Postigo, A., Serrano, J. L., Sierra, T., Hernández-Ainsa, S., & Fernàndez-Busquets, X. (2022). Heparin-Coated Dendronized Hyperbranched Polymers for Antimalarial Targeted Delivery. *ACS Applied Polymer Materials*. https://doi.org/10.1021/acsapm.2c01553

Satchwell, T. J. (2016a). Erythrocyte invasion receptors for Plasmodium falciparum: New and old. *Transfusion Medicine*. https://doi.org/10.1111/tme.12280

Satchwell, T. J. (2016b). Erythrocyte invasion receptors for Plasmodium falciparum: New and old. *Transfusion Medicine*. https://doi.org/10.1111/tme.12280

Shafi, H., Reddy, D. V. S., Khan, T., Ranjan, R., Srivastava, A., Vaishya, S., Sharma, T., Siddiqui, M. I., Habib, S., & Misra, A. (2017). Dehydroascorbate-derivatized chitosan particles for targeting antimalarial agents to infected erythrocytes. *International Journal of Pharmaceutics*. https://doi.org/10.1016/j.ijpharm.2017.03.088

Sharma, L., & Shukla, G. (2017). Placental Malaria: A new insight into the pathophysiology. *Frontiers in Medicine*, *4*(JUL), 1–6. https://doi.org/10.3389/fmed.2017.00117

Sidhaye, A. A., Bhuran, K. C., Zambare, S., Abubaker, M., Nirmalan, N., & Singh, K. K.

(2016). Bio-inspired artemether-loaded human serum albumin nanoparticles for effective control of malaria-infected erythrocytes. *Nanomedicine*. https://doi.org/10.2217/nnm-2016-0235

Singh, B., & Daneshvar, C. (2013). Human Infections and Detection of Plasmodium knowlesi. *Clinical Microbiology Reviews*, *26*(2), 165–184. https://doi.org/10.1128/CMR.00079-12

Slavic, K., Krishna, S., Derbyshire, E. T., & Staines, H. M. (2011). Plasmodial sugar transporters as anti-malarial drug targets and comparisons with other protozoa. *Malaria Journal*, *10*, 1–10. https://doi.org/10.1186/1475-2875-10-165

Smith D, J. (2014). The role of PfEMP1 adhesion domain classification in Plasmodium falciparum pathogenesis research. *Molecular Biochem Parasitol*, *195*(2), 82–87. https://doi.org/10.1016/j.molbiopara.2014.07.006.The

Somner, E. A., Black, J., & Pasvol, G. (2000). Multiple human serum components act as bridging molecules in rosette formation by Plasmodium falciparum-infected erythrocytes. *Blood*. https://doi.org/10.1182/blood.v95.2.674

Steel, R. W. J., Pei, Y., Camargo, N., Kaushansky, A., Dankwa, D. A., Martinson, T., Nguyen, T., Betz, W., Cardamone, H., Vigdorovich, V., Dambrauskas, N., Carbonetti, S., Vaughan, A. M., Sather, D. N., & Kappe, S. H. I. (2018). Plasmodium yoelii S4/CelTOS is important for sporozoite gliding motility and cell traversal. *Cellular Microbiology*. https://doi.org/10.1111/cmi.12817

Tagami, T., Yanai, H., Terada, Y., & Ozeki, T. (2015). Evaluation of Phosphatidylserine-Specific Peptide-Conjugated Liposomes Using a Model System of Malaria-Infected Erythrocytes. *Biol. Pharm. Biull.*, *38*(10), 1649–1651.

Tahir, A. E. L., Malhotra, P., & Chauhan, V. S. (2003). Uptake of proteins and degradation of human serum albumin by Plasmodium falciparum - Infected human erythrocytes. *Malaria Journal*. https://doi.org/10.1186/1475-2875-2-1

Tamez, P. A., Bhattacharjee, S., Ooij, C. Van, Hiller, N. L., Llina, M., Balu, B., Adams, J. H., & Haldar, K. (2008). An Erythrocyte Vesicle Protein Exported by the Malaria Parasite Promotes Tubovesicular Lipid Import from the Host Cell Surface. *PLoS Pathogens*, *4*(8). https://doi.org/10.1371/journal.ppat.1000118

Tian, Y., Zheng, Z., Wang, X., Liu, S., Gu, L., Mu, J., Zheng, X., Li, Y., & Shen, S. (2022). Establishment and evaluation of glucose-modified nanocomposite liposomes for the treatment of cerebral malaria. *Journal of Nanobiotechnology*, *20*(1), 1–22. https://doi.org/10.1186/s12951-022-01493-8

Tougan, T., Edula, J. R., Morita, M., Takashima, E., Honma, H., Tsuboi, T., & Horii, T. (2020). The malaria parasite Plasmodium falciparum in red blood cells selectively takes up serum proteins that affect host pathogenicity. *Malaria Journal*. https://doi.org/10.1186/s12936-020-03229-1

Urbán, P., Estelrich, J., Adeva, A., Cortés, A., & Fernàndez-busquets, X. (2011). Study of the efficacy of antimalarial drugs delivered inside targeted immunoliposomal nanovectors. *Nanoscale Research Letters*, *6*(620), 1–9.

Urbán, P., Estelrich, J., Cortés, A., & Fernàndez-busquets, X. (2011). A nanovector with complete discrimination for targeted delivery to Plasmodium falciparum -infected versus non-infected red blood cells in vitro. *Journal of Controlled Release*, *151*(2), 202–211. https://doi.org/10.1016/j.jconrel.2011.01.001

Urbán, P., Ranucci, E., & Fernàndez-, X. (2015). Polyamidoamine nanoparticles as nanocarriers for the drug delivery to malaria parasite stages in the mosquito vector. *Nanomedicine(Lond.)*, *10*(22), 3401–3414.

Urbán, P., Valle-delgado, J. J., Mauro, N., Marques, J., Manfredi, A., Rottmann, M., Ranucci, E., Ferruti, P., & Fernàndez-busquets, X. (2014). Use of poly (amidoamine) drug

conjugates for the delivery of antimalarials to Plasmodium. *Journal of Controlled Release*, *177*, 84–95. https://doi.org/10.1016/j.jconrel.2013.12.032

Vader, P., Mol, E. A., Pasterkamp, G., & Schiffelers, R. M. (2016). Extracellular vesicles for drug delivery. *Advanced Drug Delivery Reviews*, *106*, 148–156. https://doi.org/10.1016/j.addr.2016.02.006

Viebig, N. K., Wulbrand, U., Förster, R., Andrews, K. T., Lanzer, M., & Knolle, P. A. (2005). Direct activation of human endothelial cells by Plasmodium falciparum-infected erythrocytes. *Infection and Immunity*, *73*(6), 3271–3277. https://doi.org/10.1128/IAI.73.6.3271-3277.2005

Vogt, A. M., Barragan, A., Chen, Q., Kironde, F., Spillmann, D., & Wahlgren, M. (2003). Heparan sulfate on endothelial cells mediates the binding of Plasmodium falciparum – infected erythrocytes via the DBL1 ⎵ domain of PfEMP1. *Blood*, *101*(6), 2405–2411. https://doi.org/10.1182/blood-2002-07-2016.Supported

Walvekar, P., Gannimani, R., & Govender, T. (2018). COmbination drug therapy via nanocarriers against infectious diseases. *European Journal of Pharmaceutical Sciences*, *127*, 121–141. https://doi.org/10.1016/j.ejps.2018.10.017

Wang, B., Sun, Y., Davis, T., Chun Ke, P., Wu, Y., & Ding, F. (2018). Understanding Effects of PAMAM Dendrimer Size and Surface Chemistry on Serum Protein Binding with Discrete Molecular Dynamics Simulations. *ACS Sustain Chem Eng*, *6*(9). https://doi.org/10.1053/j.gastro.2016.08.014.CagY

Wang, F., Zhang, G., Zang, C., Pan, H., Ma, L., Li, C., Hou, H., Su, P., Gao, Y., Sun, J., & Ye, Z. (2020). Preparation and In Vitro / Vivo Evaluation of Nano-Liposomal Form of Febrifugine Hydrochloride. *Journal of Nanoscience and Nanotechnology*, *20*, 2558–2566. https://doi.org/10.1166/jnn.2020.17186

Wassmer, S. C., Cianciolo, G. J., Combes, V., & Grau, G. E. (2005). Inhibition of endothelial activation: A new way to treat cerebral malaria? *PLoS Medicine*, *2*(9), 0885–0890. https://doi.org/10.1371/journal.pmed.0020245

Wells, T. N. C., Burrows, J. N., & Baird, J. K. (2010). Targeting the hypnozoite reservoir of Plasmodium vivax: the hidden obstacle to malaria elimination. *Trends in Parasitology*, *26*(3), 145–151. https://doi.org/10.1016/j.pt.2009.12.005

WHO. (2018). *High burden to high impact A targeted malaria response*.

World Malaria Report 2020. (n.d.).

Wright, K. E., Hjerrild, K. A., Bartlett, J., Douglas, A. D., Jin, J., Brown, R. E., Illingworth, J. J., Ashfield, R., Clemmensen, S. B., De Jongh, W. A., Draper, S. J., & Higgins, M. K. (2014). Structure of malaria invasion protein RH5 with erythrocyte basigin and blocking antibodies. *Nature*. https://doi.org/10.1038/nature13715

Yaméogo, J. B. G., Gze, A., Choisnard, L., Putaux, J. L., Gansané, A., Sirima, S. B., Semdé, R., & Wouessidjewe, D. (2012). Self-assembled biotransesterified cyclodextrins as Artemisinin nanocarriers - I: Formulation, lyoavailability and in vitro antimalarial activity assessment. *European Journal of Pharmaceutics and Biopharmaceutics*. https://doi.org/10.1016/j.ejpb.2011.12.007

Yanan, Z., Rauf, K. A., Manfei, F., Jianbo, J., Larisa, B., & Guangxi, Z. (2019). Advances in Curcumin Loaded Nanopreparations: Improving Bioavailability and Overcoming Inherent Drawbacks. *Journal of Drug Targeting*, *27*(9). https://doi.org/10.1080/1061186X.2019.1572158

Yang, A. S. P., & Boddey, J. A. (2017a). Molecular mechanisms of host cell traversal by malaria sporozoites. In *International Journal for Parasitology*. https://doi.org/10.1016/j.ijpara.2016.09.002

Yang, A. S. P., & Boddey, J. A. (2017b). Molecular mechanisms of host cell traversal by

malaria sporozoites. In *International Journal for Parasitology*. https://doi.org/10.1016/j.ijpara.2016.09.002

Yang, A. S. P., O'Neill, M. T., Jennison, C., Lopaticki, S., Allison, C. C., Armistead, J. S., Erickson, S. M., Rogers, K. L., Ellisdon, A. M., Whisstock, J. C., Tweedell, R. E., Dinglasan, R. R., Douglas, D. N., Kneteman, N. M., & Boddey, J. A. (2017). Cell Traversal Activity Is Important for Plasmodium falciparum Liver Infection in Humanized Mice. *Cell Reports*. https://doi.org/10.1016/j.celrep.2017.03.017

Zakama, A. K., Ozarslan, N., & Gaw, S. L. (2020a). Placental Malaria. *Current Tropical Medicine Reports*, *7*(4), 162–171. https://doi.org/10.1007/s40475-020-00213-2

Zakama, A. K., Ozarslan, N., & Gaw, S. L. (2020b). Placental Malaria. *Current Tropical Medicine Reports*, *7*(4), 162–171. https://doi.org/10.1007/s40475-020-00213-2

Zhong, H., He Zhi-Guo, Z. G., Li, Z., Li, G. Y., Shen, S. R., & Li, X. L. (2008). Studies on polyamidoamine dendrimers as efficient gene delivery vector. *Journal of Biomaterials Applications*, *22*(6), 527–544. https://doi.org/10.1177/0885328207080005

Zuzarte-Luis, V., & Mota, M. M. (2020). The Hepatocyte as a Household for Plasmodium Parasites . *The Liver*, 1075–1080. https://doi.org/10.1002/9781119436812.ch86

Zwain, T., Zwayen, S., Singh, K. K., Taneja, N., Shidhaye, A., & Palshetkar, A. (2022). Albumin nanoparticles—A versatile and a safe platform for drug delivery applications. In *Nanoparticle Therapeutics: Production Technologies, Types of Nanoparticles, and Regulatory Aspects*. Elsevier Inc. https://doi.org/10.1016/B978-0-12-820757-4.00008-9

Chapter 2.1: Development and validation of RP-HPLC based analytical method for quantification of artemether

2.1.1 Introduction

Artemether (ART), 10-methoxy-3,6,9-trimethyldecahydro-12H-3,12-epoxy[1,2]dioxepino[4,3-i]isochromene is a semi-synthetic derivative of Artemisinin which is obtained from the plant Artemisia annua (Gilmore et al., 2014). Chemically, ART is a sesquiterpene lactone having one endoperoxide functionality. It is white in colour and crystalline in nature, insoluble in water and soluble in ethanol, dimethyl sulfoxide, and dimethylformamide (*Product Information*, n.d.). ART has a log P value of 3.48 (Amin et al., 2013) and exhibits high plasma protein binding (95 – 98 %) (Colussi et al., 1999). The compound has a melting point range of 86 – 90 ºC (*Artemether*, n.d.).

Analysis of ART using reverse-phase high-performance liquid chromatography (RP-HPLC) with different detectors including UV – photodiode array (UV-PDA) (I. D. C. César & Pianetti, 2009), electron capture detector (Mount et al., 1995), polarographic detector (Huang et al., 1987) have been extensively reported for the quantification of ART in bulk drugs (Ubale & Choudhari, 2015), formulations (I. da C. César et al., 2008) and biological fluids (Huang et al., 1987). Recently, Resende et. al.(Resende et al., 2019), reviewed different analytical techniques for quantification of ART alone or in combination with lumefantrine in fixed-dose combination (Resende et al., 2019). The structure of ART lacks the chromophoric group, leading to poor sensitivity when quantified using an HPLC-UV detector (Fig. 2.1.1.). However, it has been reported that ART can be transformed to α, β-unsaturated decalones by acid treatment which exhibits enhanced absorption in the UV-visible region as compared to ART (Christian et al., 2017). This transformation has enabled the quantification of ART using a UV-visible spectrophotometer. Many literature reports demonstrated that the sensitivity of ART towards UV-visible detectors was increased after treatment with acids (Christian et al., 2017), bases (Shishan & Mel-Yi, 1986), or coupling with UV-sensitive entities (Adegoke et al., 2012). However, multistep sample preparation technique still exerted significant challenge in the quantification of ART in biological fluids using the above strategies. To the best of our knowledge, no method has been reported for analysis of ART from nanoformulation by acid treatment of ART utilizing HPLC-UV.

Hence, the objective of the present study is to develop and validate a simple and sensitive RP-HPLC method using a UV-visible detector for the quantification of ART from polymeric

nanoparticles. The pre-column acid treatment approach was adapted to increase the sensitivity of ART during quantification by HPLC using UV-detector.

2.1.2 Materials

Artemether (>98.0%) was purchased from Tokyo Chemical Industry Co. Ltd. (Tokyo, Japan). HPLC grade acetonitrile and methanol were purchased from Merck Limited (Mumbai, India). All other chemicals, solvents and reagents utilized, were either HPLC or analytical grade. HPLC grade water was obtained from Milli-Q system (Millipore GmbH, Germany) used throughout the analysis. The solvents and buffers prepared were suitably filtered through 0.22 MilliporeTM membrane filter (Merck, Darmstadt, Germany) and suitably degassed using an ultrasonic bath for 30 min.

2.1.3 Methods

2.1.3.1 Instrument and software

The HPLC method for ART was developed with the Shimadzu HPLC system (Kyoto, Japan) with a binary pump (LC-20AD), UV-visible detector (SPD-20A) and autosampler (SIL-20AC HT). The column used for analysis was Waters Spherisorb® 5µm ODS(C18) column with the dimensions of 4.6 x 250mm. The instrument was operated by the software LC solution version 5.97.

Gradient RP-HPLC method with a mobile phase composed of A – ACN and B – Phosphate buffer solution (PBS) (10mM; pH 6.0) consisting of T (min)/% B (v/v) of 0/50, 2/40, 3/30, 14/50, 20/50 as gradient at 1 ml/min was utilized for quantification of ART. The analysis was carried out at λ_{max} of 253nm with 20min and 20µL being run time and injection volume respectively.

2.1.3.2 Pre-column acid treatment of ART

Accurately weighed 25mg of ART was dissolved in 25mL of methanol to prepare 1mg/ml of the stock solution. Pre-column acid treatment of ART was carried out as described previously by Christian *et al.* with some modification.(Christian et al., 2017) Briefly, 5ml of the solution of ART (1mg/ml) was taken in a test tube and 0.5ml of concentrated HCl (35% v/v) was added into it (solution 1). Solution 1 was then incubated at 40ºC for 4h. After the incubation period, the solution was immediately transferred into an ice bath to cease the reaction. Thereafter, the volume of solution 1 was made up to 50ml with methanol to get a concentration of 100µg/ml (solution 2). Aliquot of 3ml was withdrawn from solution 2 and diluted with methanol up to 10mL to get a solution of 30µg/ml concentration. This solution of 30µg/ml concentration was serially diluted with methanol to get solutions of 20µg/ml and 15µg/ml respectively. These

solutions were analysed at λ_{max} of 253nm using Shimadzu-3600 UV-VIS spectrophotometer (Kyoto, Japan). The process of pre-column acid treatment of ART was optimized by varying different reaction conditions as presented in Table 2.1.1.

Table 2.1.1. Optimization of pre-column acid treatment reaction conditions for ART

Parameter	Reaction Conditions
Temperature (ºC)	25, 40, 60
Acid concentration (M)	5, 10, ≈11.65
Acid volume (ml)	0.25, 0.5, 1.3
Time (h)	2, 4, 6

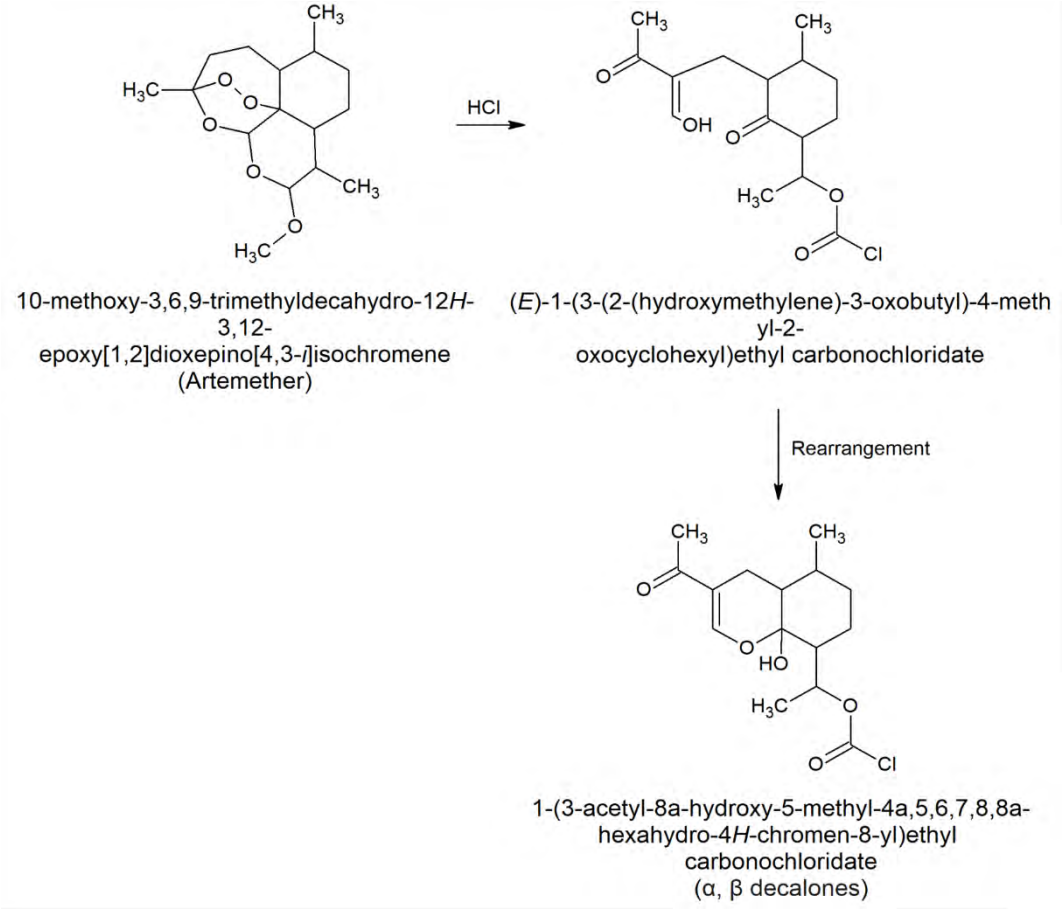

Fig. 2.1.1. Reaction scheme of acid treated ART

2.1.3.3 Preparation of standard solution

Accurately weighed 10mg of ART was dissolved in 10mL of methanol to prepare 1mg/ml of the stock solution. 5ml of the stock solution was treated with acid as described in the section pre-column acid treatment of ART. After acid treatment and dilution, an aliquot of 1ml was withdrawn and diluted with methanol up to 10ml in a volumetric flask to prepare a solution of 10µg/ml (solution 3). Solution 3 was then serially diluted to get various solutions of

concentrations 8, 6, 4, 2, 1, 0.75, and 0.5µg/ml respectively.

2.1.3.4 Preparation of sample solution

Aliquot of 5ml supernatant obtained after centrifugation of nanoparticles, was acid-treated as described in the pre-column acid treatment of ART. After acid treatment, the solution was diluted up to 50ml and was analysed by HPLC using the chromatographic conditions as stated in instrumentation and chromatographic conditions.

2.1.3.5 Validation

The developed method was validated as per ICH Q2R(1) guidelines for specificity, linearity and range, limit of detection (LOD) and limit of quantitation (LOQ), accuracy, precision, robustness, stability, and system suitability (*Validation of Analytical Procedures: Text and Methdology Q2(R1)*, 2005). To confirm the specificity, chromatogram obtained from the supernatant of the blank nanoformulation was compared to the standard ART reaction product for the presence of any interfering peaks.

Calibration curves were prepared by injecting different concentrations of ART including 0.5, 0.75, 1, 2, 4, 6, 8, and 10µg/ml in six replicates. The data were tested for homoscedasticity using both the Ordinary Least Squares (OLS) and Weighted Least Squares (WLS) method. The F-values ($F_{obsearved}$ and F_{table}) were calculated and the regression analysis was performed on weights $\sqrt{x}$, $1/\sqrt{x}$, $1/x$, x^2, $1/x^2$, $\sqrt{y}$, $1/\sqrt{y}$, $1/y$, y^2, $1/y^2$. % Relative error (% RE) and total % Relative error (Σ% RE) were calculated for each model. The model with least Σ% RE was selected to determine linearity.(Surve & Jindal, 2019) The range of developed analytical method was determined from the peak area versus concentration curve and response factor versus concentration curve. %RSD of response obtained from each concentration was calculated to establish concentration range. LOD and LOQ were calculated by using Eq. (2.1) and (2.2) respectively.

$$LOD = \frac{3.3\ x\ \sigma}{S} \qquad (2.1)$$

$$LOQ = \frac{10\ x\ \sigma}{S} \qquad (2.2)$$

Where σ is the standard deviation of response and S is the slope of the calibration curve.

Accuracy was determined by spiking a known concentration (4µg/ml) of ART into three working standards (1, 4, and 8µg/ml) each in triplicate. % Recovery was then calculated while considering the %RSD to confirm the accuracy of the method. The intra-day precision was determined by analyzing the quality control samples of three different concentrations including 1µg/ml (LQC), 4µg/ml (MQC), and 8µg/ml (HQC) each in triplicate within a day. Inter-day

precision was determined by analyzing the above quality control samples in triplicate for three consecutive days. %RSD of peak area was calculated to establish inter-day and intra-day precision. To confirm the robustness of the method, quality control samples of ART (1, 4, and 8µg/ml) were analyzed after deliberately changing the different chromatographic parameters including pH of PBS and column temperature. The pH of PBS and column temperature were varied from 5.8 to 6.2 and from 28ºC to 32ºC respectively. % Recovery obtained from each concentration was determined.

Stability of ART (1mg/mL) after pre-column acid treatment was assessed till 24h, the above solution was kept at room temperature in a vial and analysed at pre-determined time points (0, 6, 18, 24h). The concentration of the solution was obtained from the peak area and %recovery was calculated. To assess the system suitability of the method, five replicate injections of ART (5µg/ml) obtained after acid treatment was injected and %RSD of retention time, tailing factor, height equivalent to theoretical plates (HETP), resolution and number of theoretical plates (N) were calculated.

2.1.4 Results

2.1.4.1 Optimization of reaction conditions for pre-column acid treatment of ART

ART does not exhibit significant absorption in the UV-visible region due to the absence of any chromatographic group in chemical structure. It also lacks chemical groups which can react with other reagents to form coloured compounds (Tayade & Nagarsenker, 2007). Hence, ART was treated with HCl to get α, β unsaturated decalones (Fig. 2.1.1.) for which the probable mechanism involves protonation of ART in methanol to generate hydroperoxyl acetal. This hydroperoxyl acetal forms cyclic peroxides by aldolization due to its strong nucleophilic properties. The cyclic peroxides further rearrange to α, β-unsaturated decalones which exhibits improved UV absorbance. The reaction also involves the formation of tricyclic dihydropyrans as secondary byproducts (Jefford, 1996).

Therefore, pre-column acid treatment was carried out, to enable the quantification of ART by HPLC using a UV detector. Until now, acid treatment of ART was carried at 53°C for 15min (Jefford, 1996; Thomas & Ward, 1992). However, it was observed that various reaction parameters including reaction temperature, volume, and strength of hydrochloric acid and reaction time played a significant role in the formation of α, β-unsaturated decalones. Effect of different reaction conditions on UV absorbance of solutions of different concentrations of 15, 20, and 30µg/ml reaction products are shown in Fig. 2.1.2. The absorbance of acid-treated ART was found to be increased when the temperature was increased from room temperature to 40ºC or

60ºC (Fig. 2.1.2A.). However, considering the appreciable absorbance at 40ºC and further utilization of the method for quantification of the drug in biological samples, the reaction was carried out at 40ºC to optimize other parameters. Furthermore, the absorbance of acid-treated ART was also found to be increased with an increase in acid strength (Fig. 2.1.2B.). The absorbance of acid-treated ART in the case of concentrated HCl was found to be significantly higher when compared to the absorbance of acid-treated ART obtained after treatment with 10M and 5M HCl. The volume of acid used during the reaction also exerted a significant impact on the absorbance of acid-treated ART. Higher absorbance was observed when 1.3ml of HCl was used during the reaction as compared to 0.5 to 0.25mL of HCl (Fig. 2.1.2C.). To utilize the minimum amount of acid during separation and quantification by HPLC, 0.5mL of HCl was found to be suitable to obtain acid-treated ART. The absorbance of acid-treated ART was found to be increased by 1.78 ± 0.011 folds when the reaction time was increased from 2h to 4h. While, only a slight increase of 1.15 ± 0.022 folds in the absorption of unsaturated α, β-decalones was observed when the reaction time was increased to 6h from 4h (Fig. 2.1.2D.).

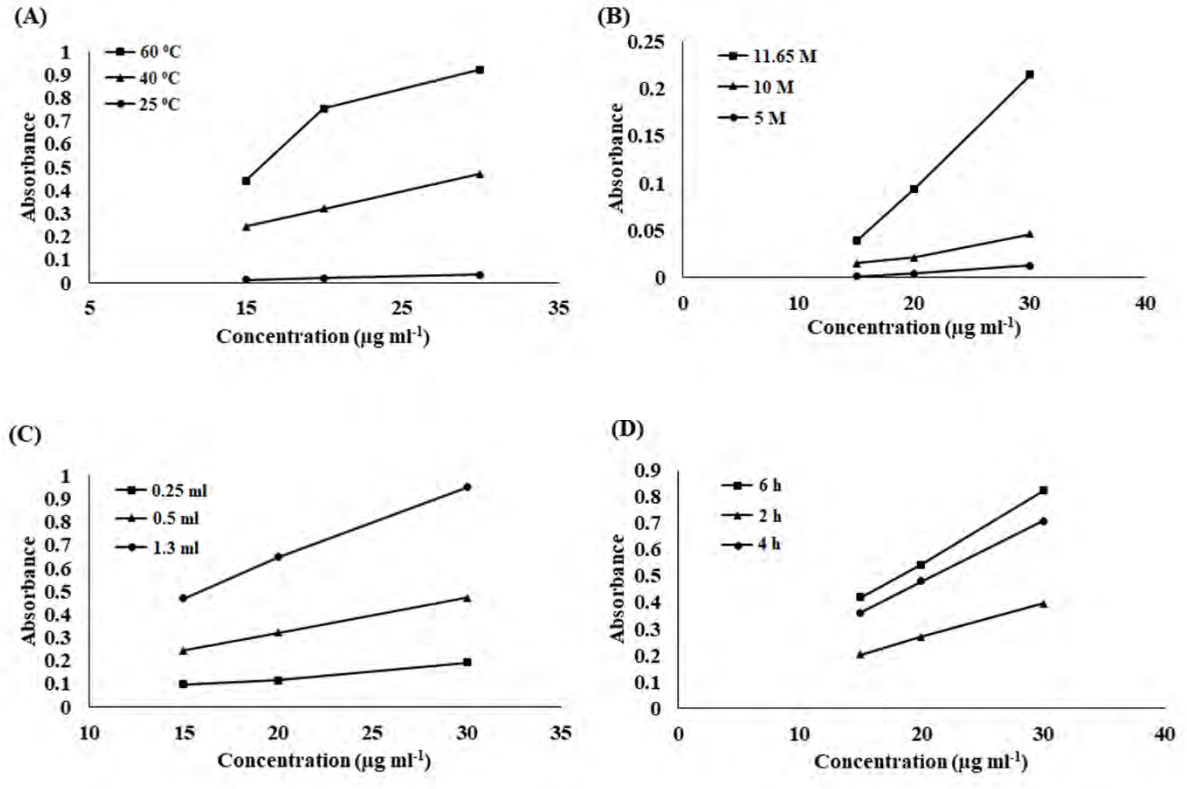

Fig. 2.1.2. Effect of different reaction conditions including (A) temperature (B) acid molarity (C) acid volume (D) reaction time on acid treated ART (n=3).

2.1.4.2 Method development

A solution of 100 µg/ml of the reaction product was obtained after acid treatment of ART as

described in the section of the pre-column acid treatment of ART. It was diluted with methanol to prepare a solution of a concentration of 1 µg/ml. Initially, the separation of acid-treated ART was attempted under isocratic conditions. Different mobile phases were used to optimize the isocratic separation of acid-treated ART. However, in all the conditions, poor peak shape and/or resolution was observed as presented in Table 2.1.2. It was difficult to separate those multiple peaks resolving at the same time leading to interference with the reaction product peak under isocratic conditions. Therefore, gradient elution of acid-treated ART was attempted to resolve the peaks eluting at the same time by subjecting the analyte solution in the column with different mobile phase ratios.

Table 2.1.2. Different mobile phase composition used for separation of acid treated ART under isocratic conditions

Mobile Phase	Comment
A – ACN and B – Water in the ratio of %A: %B = 85: 15	Poor resolution between peaks
A – Methanol and B – Water in the ratio of %A: %B = 70: 30	Poor resolution
A – Methanol and B – Acetic acid in the ratio of %A: %B = 60: 40	Shoulder peak and broadening
A – ACN and B – PBS (pH 3.5, 10 mM) in the ratio of %A: %B = 83: 17	Peak broadening
A – ACN and B – PBS (pH 6.0, 10 mM) in the ratio of %A: %B = 55: 45	Peak splitting at higher concentrations

Peak resolution was found to be affected by a change in gradient steepness and range. As the initial mobile phase composition was changed from 20% B to 50% B and run time from 6min or 10min to 14min. Significant improvement in peak and resolution (k = 0.084) was observed. The peaks obtained at 9.0min, 10.7min, and 12.2min were attributed to reaction byproducts while the peak at 9.7min was of α, β- unsaturated decalones (Idowu et al., 1989). A chromatogram of acid-treated ART separated by gradient elution is presented in Fig. 2.1.3.

2.1.4.3 Method validation

The method validity was analysed by a series of analytical tests as mentioned above. The tests for specificity involved comparison of the supernatant of the blank formulation with that of the ART standard. No interference was observed in the case of blank nanoparticles at the retention time of acid-treated ART indicating the specificity of the method for the quantification of ART from polymeric nanoparticles (Fig. 2.1.4). Moreover, the resolution of the by-product and acid-treated ART was found to be greater than 2.

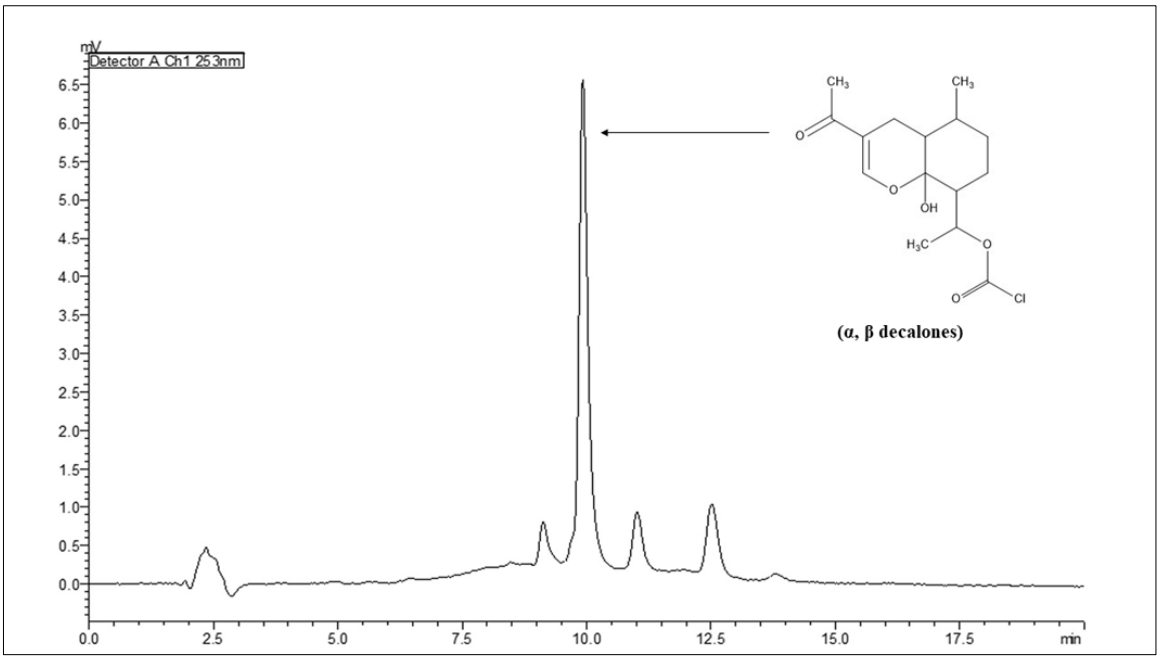

Fig. 2.1.3. Representative chromatogram of acid treated ART (5 mg/ml) by gradient elution.

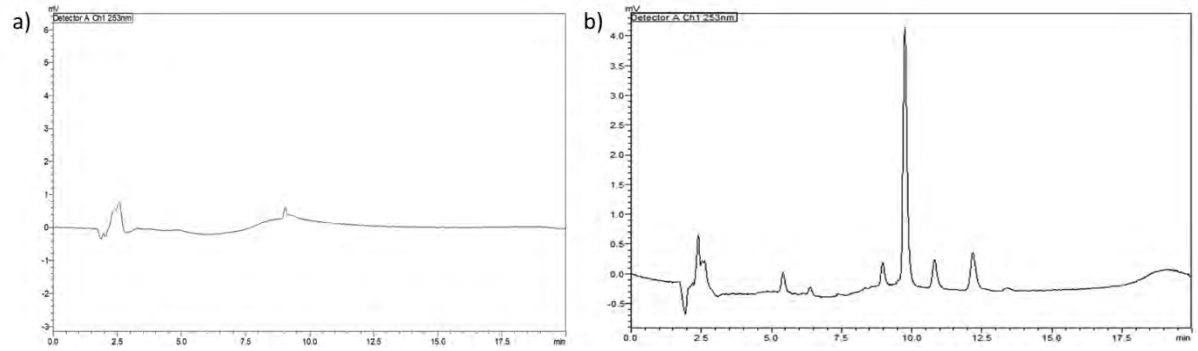

Fig. 2.1.4. Representative chromatogram of a) blank nanoparticles b) ART loaded nanoparticles

All the six calibration curves were found to be linear in the concentration range of 0.5 to 10µg/mL with R^2 values of 0.9996 (Fig. 2.1.5A.). Linearity was further confirmed from the slope, %RSD, and a plot of response factor versus standard concentrations (Fig. 2.1.5B.). A negative slope of a small value and low %RSD (1.19 – 1.95%) further confirmed the linearity of the method. However, the OLS regression analysis is only suitable when data is homoscedastic. Therefore, obtained results were tested for homoscedasticity using F-test. The data can be considered statistically homoscedastic if $F_{observed} < F_{table}$. Since $F_{observed} > F_{table}$ (Table 2.1.3) therefore the obtained responses were heteroscedastic at lower concentrations. WLS regression equation, regression coefficient, and Σ% RE for each weighed factor were obtained (Table 2.1.4) and represented graphically in Fig. 2.1.6.

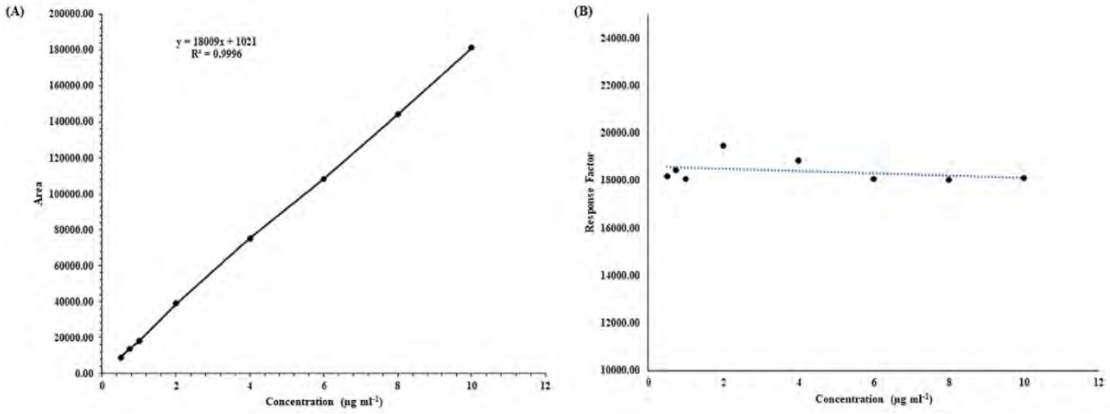

Fig. 2.1.5. A.) Calibration curve of ART B.) Response factor versus standard concentration plot of ART

Table 2.1.3. Test for homogeneity of variance, F-test

Concentration (µg/ml)	Responses	Variance (S^2)
0.5	9209 9032 9205 9075 8827 9137	S_1^2: 20369.77
10	181347 184804 184722 180121 179263 176792	S_2^2: 9951556.57
$F_{observed}$ (S_2^2/S_1^2) - 488.55 F_{table} (0.99,5,5) - 10.97		

Table 2.1.4. Regression equation, correlation coefficient and sum of the relative errors (Σ%RE) for each weighted and unweighted factor

W_i	WLS/LS regression equation	Correlation coefficient (R^2)	Σ%RE
$\sqrt{x}$	y = 17933.116 5 x + 1509.5497	0.9998	39.4023
$1/\sqrt{x}$	y = 18093.206 4 x + 605.1912	0.9997	22.7108
1/x	y = 18183.466 9 x + 306.4489	0.9996	18.1644
x^2	y = 17899.472 2 x + 1 749.3452	0.9998	44.0363
$1/x^2$	y = 18406.186 9 x - 44.5227	0.9993	16.3874
$\sqrt{y}$	y = 17930.441 8 x + 1537.1258	0.9998	39.9491
$1/\sqrt{y}$	y = 18092.724 1 x + 591.6367	0.9997	22.4009
1/y	y = 18182.172 2 x + 292.8082	0.9996	17.8343
y^2	y = 17884.711 7 x + 1 887.0903	0.9998	46.7510
$1/y^2$	y = 18409.385 8 x - 55.935	0.9993	16.3385
Unweighted	y = 18008.836 7 x + 1021.0227	0.9998	30.0449

Table 2.1.5. Calibration curve parameters

Parameter	Result

Range (µg/ml)	0.5 - 10
Regression equation	y = 18009x + 1021
Correlation coefficient (R^2)	0.9996
Limit of Detection (µg/ml)	0.09
Limit of Quantification (µg/ml)	0.27

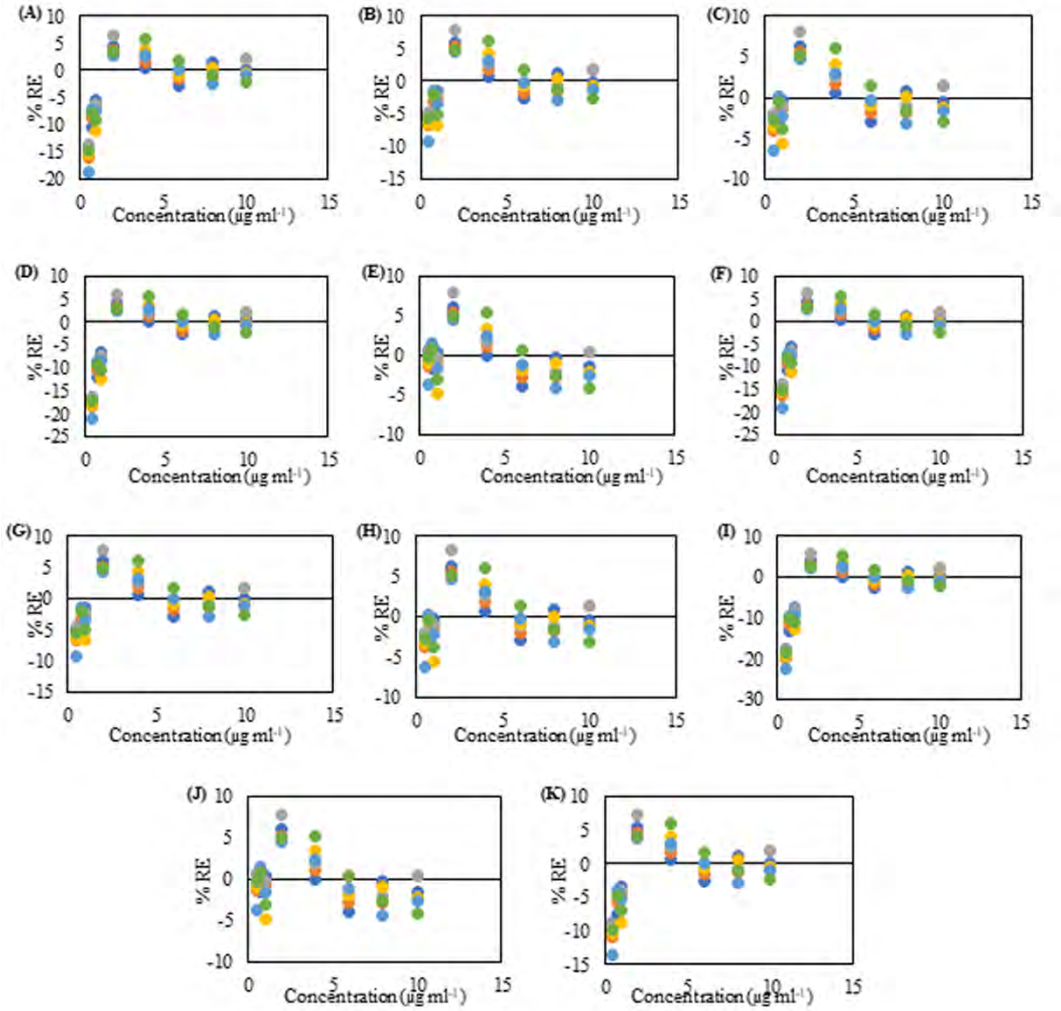

Fig. 2.1.6. % Relative error distribution based on concentration for unweighted and weighted factors. model A) √x, model B) 1/√x, model C) 1/x, model D) x2, model E) 1/ x2, model F) √y, model G) 1/√y, model H) 1/y, model I) y2, model J) 1/y2 and model K) Unweighted.

Among the models screened, $1/y^2$ was chosen as it resulted in least Σ % RE (16.34%), highest correlation coefficient amongst other weighted models (0.999) and uniform distribution of the response towards x axis with respect to the other models (Fig. 2.1.6.). Upon validation of the developed RP-HPLC method for weighted and unweighted models, higher accuracy for weighted model (% ias = 0.34 ± 1.79) was obtained compared with unweighted model (% bias = 1.76 ± 1.70). Similarly, %RSD was found to be least in case of weighted model for intraday precision (1.43 ± 0.11%) and interday precision (1.60 ± 0.36 %) compared with unweighted

model for intraday precision (1.46 ± 0.09 %) and interday precision (1.64 ± 0.36 %) depicting significance of weighted model for heteroscedastic values.(Almeida et al., 2002)

LOD and LOQ of the method are presented in Table 2.1.5. The values of LOD and LOQ demonstrated the sensitivity of the method suitable for the quantification of acid-treated ART from the polymeric nanoparticles.

Accuracy determined by calculating %recovery at three concentration levels (1, 4, and 8µg mL-1) of the calibration curve was found to be over the linear range of acid-treated ART. %Recovery at all the three concentrations found to be between 100.14% - 103.50% which was well within the acceptance criteria of 80 – 120% while the %RSD was found to be not more than 2.04% (Table 2.1.6). Both inter-day and intra-day precision of the method was assessed at three concentration levels over calibration ranges and presented in Table 2.1.6. %RSD for inter-day and intra-day precision were found to be between 1.22 - 1.93% and 1.35 - 1.56% respectively. The method was found to accurate and precise for quantification of ART from polymeric nanoparticles.

Table 2.1.6. Accuracy and Precision results

Accuracy (n=3)			
Target (%)	**%Recovery**	**S.D.**	**%RSD**
80	101.59	0.41	0.40
100	103.50	2.11	2.04
120	100.14	1.23	1.22
Inter-day Precision (n=3)			
Concentration (µg ml^{-1})	**Measured Concentration (µg ml^{-1})**	**S.D.**	**%RSD**
1	1.05	0.02	1.65
4	4.13	0.05	1.22
8	7.91	0.15	1.93
Intraday Precision (n=3)			
Concentration (µg ml^{-1})	**Measured Concentration (µg ml^{-1})**	**S.D.**	**%RSD**
1	1.04	0.01	1.35
4	4.11	0.06	1.39
8	7.90	0.12	1.56

In robustness studies, no significant difference in % recovery of acid-treated ART observed at three quality controls (1 µg/ml, 4 µg/mL, and 8 µg/mL) after deliberate changes in chromatographic conditions. %Recovery was found to be between 87.94 ± 3.30% to 100.78 ± 0.24% (Table 2.1.7).

Table 2.1.7. Robustness results

Condition	**%Recovery**

	1µg/ml	4µg/ml	8µg/ml
Column Temperature (32 ºC)	96.58 ± 2.61	96.27 ± 8.52	100.78 ± 0.24
Column Temperature (28 ºC)	91.83 ± 1.59	97.21 ± 4.16	95.47 ± 1.49
Phosphate Buffer (10mM; pH 6.2)	90.10 ± 1.10	92.62 ± 3.09	92.35 ± 0.45
Phosphate Buffer (10mM; pH 5.8)	87.94 ± 3.30	91.79 ± 3.56	92.24 ± 4.72

Each value represents Mean ± SD; n = 3

The methanolic solution containing acid-treated ART showed 95.19 ± 2.19, 97.91 ± 1.44, 102.95 ± 4.9 and 101.58 ± 2.97% (n = 3) recovery after 0, 6, 18 and 24h respectively which indicated that acid-treated ART was stable for at least 24h in the solution state.

Different system suitability parameters including tailing factor, HETP, resolution, and number of theoretical plates obtained from 5 replicates of standard acid-treated ART solution are presented in Table 2.1.8. All the parameters were found to be within the limits as specified by Food and Drugs Administration (*No Title*, n.d.)

Table 2.1.8. System suitability parameters

Parameter	Value ± SD
Retention Time (min)	9.91 ± 0.00
Tailing factor	1.23 ± 0.02
HETP	9.81 ± 0.05
Resolution	2.54 ± 0.02
Number of Theoretical Plates	15298 ± 80.55

Each value represents Mean ± SD; n = 3

2.1.5 Conclusion

Pre-column acid treatment of ART showed a significant increase in the sensitivity of ART during quantification by HPLC using UV-detector due to the formation of α, β-unsaturated decalones. The method was validated as per ICH guideline Q2(R1) for estimation of ART and could be successfully utilized for determination of % EE, and in vitro drug release from ART-loaded polymeric nanoparticles.

References

Adegoke, O. A., Xiang, L. L., Idowu, O. S., & Chen, D. Y. (2012). Highly sensitive liquid chromatographic analysis of artemisinin and its derivatives after pre-column derivatization with 4-carboxyl-2,6-dinitrobenzene diazonium ion. *Acta Chromatographica*, *24*(3), 445–462. https://doi.org/10.1556/AChrom.24.2012.3.8

Almeida, A. M., Castel-Branco, M. M., & Falcão, A. C. (2002). Linear regression for calibration lines revisited: Weighting schemes for bioanalytical methods. *Journal of Chromatography B: Analytical Technologies in the Biomedical and Life Sciences*. https://doi.org/10.1016/S1570-0232(02)00244-1

Amin, N. C., Fabre, H., Blanchin, M. D., Montels, J., & Aké, M. (2013). Determination of artemether and lumefantrine in anti-malarial fixed-dose combination tablets by microemulsion electrokinetic chromatography with short-end injection procedure. *Malaria Journal*, *12*(1), 1–8. https://doi.org/10.1186/1475-2875-12-202

Artemether. (n.d.). Retrieved May 31, 2020, from https://www.drugbank.ca/drugs/DB06697

César, I. D. C., & Pianetti, G. A. (2009). Quantitation of artemether in pharmaceutical raw material and injections by high performance liquid chromatography. *Brazilian Journal of Pharmaceutical Sciences*, *45*(4), 737–742. https://doi.org/10.1590/S1984-82502009000400018

César, I. da C., Andrade Nogueira, F. H., & Antônio Pianetti, G. (2008). Simultaneous determination of artemether and lumefantrine in fixed dose combination tablets by HPLC with UV detection. *Journal of Pharmaceutical and Biomedical Analysis*, *48*(3), 951–954. https://doi.org/10.1016/j.jpba.2008.05.022

Christian, J., Shah, P., Patel, M., Patel, K., & Gandhi, T. (2017). Optimizing derivatization conditions using an experimental design and simultaneous estimation of artemether and lumefantrine by ratio first order derivative spectrophotometric method. *Journal of Taibah University for Science*, *11*, 729–740. https://doi.org/10.1016/j.jtusci.2016.08.003

Colussi, D., Parisot, C., Legay, F., & Lefèvre, G. (1999). Binding of artemether and lumefantrine to plasma proteins and erythrocytes. *European Journal of Pharmaceutical Sciences*, *9*(1), 9–16. https://doi.org/10.1016/S0928-0987(99)00037-8

Gilmore, K., Kopetzki, D., Lee, J. W., Horváth, Z., McQuade, D. T., Seidel-Morgenstern, A., & Seeberger, P. H. (2014). Continuous synthesis of artemisinin-derived medicines. *Chemical Communications*, *50*(84), 12652–12655. https://doi.org/10.1039/c4cc05098c

Huang, Y., Xie, G., Zhou, Z., Sun, X., & Wang, Y. (1987). Determination of artemether in plasma and whole blood using HPLC with flow-through polarographic detection. *Biomedical Chromatography*, *2*(2), 53–56. https://doi.org/10.1002/bmc.1130020203

Idowu, O. R., Edwards, G., Ward, S. A., Orme, M. L. E., & Breckenridge, A. M. (1989). Determination of arteether in blood plasma by high-performance liquid chromatography with ultraviolet detection after hydrolysis with acid. *Journal of Chromatography B: Biomedical Sciences and Applications*, *493*(C), 125–136. https://doi.org/10.1016/S0378-4347(00)82715-2

Jefford, C. W. (1996). Six-membered Rings with no Bridgehead Heteroatom and Fused Carbocyclic Derivatives. In *Comprehensive Heterocyclic Chemistry II*.

Mount, D. L., Todd, G. D., & Navaratnam, V. (1995). Packed-column supercritical fluid chromatography of artemisinin (qinghaosu) with electron-capture detection. *Journal of Chromatography B: Biomedical Sciences and Applications*, *666*(1), 183–187. https://doi.org/10.1016/0378-4347(94)00560-R

No Title. (n.d.). Retrieved May 31, 2020, from https://www.fda.gov/media/75643/download

Product Information. (n.d.). Retrieved May 31, 2020, from https://www.caymanchem.com/pdfs/11815.pdf

Resende, L. A., da Silva, P. H. R., & Fernandes, C. (2019). Quantitative determination of the antimalarials artemether and lumefantrine in biological samples: A review. *Journal of Pharmaceutical and Biomedical Analysis*, *165*, 304–314. https://doi.org/10.1016/j.jpba.2018.12.021

Shishan, Z., & Mel-Yi, Z. (1986). Application of Precolumn Reaction to High-Performance Liquid Chromatography of Qinghaosu in Animal Plasma. *Analytical Chemistry*, *58*(2), 289–292. https://doi.org/10.1021/ac00293a006

Surve, D. H., & Jindal, A. B. (2019). Journal of Pharmaceutical and Biomedical Analysis Development and validation of reverse-phase high-performance liquid chromatographic (RP-HPLC) method for quantification of Efavirenz in Efavirenz-Enfuvirtide co-loaded polymer-lipid hybrid nanoparticles. *Journal of Pharmaceutical and Biomedical Analysis*, *175*, 112765. https://doi.org/10.1016/j.jpba.2019.07.013

Tayade, N. G., & Nagarsenker, M. S. (2007). Validated HPTLC method of analysis for artemether and its formulations. *Journal of Pharmaceutical and Biomedical Analysis*, *43*(3), 839–844. https://doi.org/10.1016/j.jpba.2006.08.029

Thomas, C. G., & Ward, S. A. (1992). Selective determination , in plasma , of artemether and its major metabolite , dihydroartemisinin , by high- performance liquid chromatography with ultraviolet detection. *Journal of Chromatography*, *583*, 131–136.

Ubale, M., & Choudhari, V. (2015). Stability-Indicating Hplc Determination of Artemether in Bulk Drug and Pharmaceutical Form. *World Journal of Pharmaceutical Research*, *5*(1), 609–625. https://doi.org/10.13140/RG.2.1.4508.7760

Validation of Analytical Procedures: Text and Methdology Q2(R1) (Vol. 1994, Issue October 1994). (2005).

Chapter 2.2: Development and validation of LC-MS-MS based bioanalytical method for quantification of artemether

2.2.1 Introduction

Artemether (ART), 10-methoxy-3,6,9-trimethyldecahydro-12H-3,12-epoxy[1,2]dioxepino[4,3-i]isochromene is a semi-synthetic derivative of Artemisinin which is obtained from the plant Artemisia annua (Gilmore et al., 2014). Chemically, ART is a sesquiterpene lactone having one endoperoxide functionality. It is white in colour and crystalline in nature, insoluble in water and soluble in ethanol, dimethyl sulfoxide, and dimethylformamide (*Product Information*, n.d.). ART has a log P value of 3.48 (Amin et al., 2013) and exhibits high plasma protein binding (95 – 98 %) (Colussi et al., 1999). The compound has a melting point range of 86 – 90 ºC (*Artemether*, n.d.).

Analysis of ART using reverse-phase high-performance liquid chromatography (RP-HPLC) with different detectors including UV – photodiode array (UV-PDA) (I. D. C. César & Pianetti, 2009), electron capture detector (Mount et al., 1995), polarographic detector (Huang et al., 1987) have been extensively reported for the quantification of ART in bulk drugs (Ubale & Choudhari, 2015), formulations (I. da C. César et al., 2008) and biological fluids (Huang et al., 1987). Recently, Resende et. al.(Resende et al., 2019), reviewed different analytical techniques for quantification of ART alone or in combination with lumefantrine in fixed-dose combination (Resende et al., 2019). The structure of ART lacks the chromophoric group, leading to poor sensitivity when quantified using an HPLC-UV detector (Chaturvedi et al., 2010; Christian et al., 2017; Stringham et al., 2009). Hence, it has been difficult to quantify ART in formulations as well as in *in vitro* release media. A pre-column acid treatment of ART with HCl leading to formation of α, β decalones has been reported thus increasing the sensitivity of ART by UV spectroscopy. However, the method is not suitable for the quantification of ART in biological matrices. ART has a therapeutic plasma drug concentration of around 5 to 150ng/ml (Tarning et al., 2013). It is difficult to develop an analytical method using UV-vis spectroscopy capable of quantifying ART in the plasma at its therapeutic concentrations (Bhide et al., 2020).

Therefore, here we developed a sensitive LC-MS-MS based bioanalytical method for the quantification of ART in rat plasma. The chapter covers the steps used for the development, optimization and the validation of the LC-MS-MS based bioanalytical method for the quantification of ART.

2.2.2 Materials

Artemether (>98.0%) was purchased from Tokyo Chemical Industry Co. Ltd. (Tokyo, Japan). Curcumin was purchased from HiMedia Laboratories Pvt. Ltd. (Mumbai, India). LC-MS grade and HPLC grade formic acid, acetonitrile and methanol were purchased from Merck Limited (Mumbai, India). All other chemicals, solvents and reagents utilized, were either HPLC or analytical grade. HPLC grade water was obtained from Milli-Q system (Millipore GmbH, Germany) used throughout the analysis. The solvents and buffers prepared were suitably filtered through 0.22 MilliporeTM membrane filter (Merck, Darmstadt, Germany) and suitably degassed using an ultrasonic bath for 30 min.

2.2.3 Methods

2.3.3.1 Instrumentation, software and chromatographic conditions

The bioanalytical method for the quantification of ART was developed with liquid chromatography coupled with tandem mass spectrometry (LC−MS/MS) (Waters Acquity UPLC H Class system with a Waters Xevo Triple Quadrupole mass spectrometer). Mass Lynx software version 4.1 was used to control the machine and analyse the data. The column utilized during the analysis was Acquity UPLC BEH C18 (50 mm × 2.1 mm, 1.7 μm) column.

Isocratic method with a mobile phase system consisted of reservoir A (methanol) and reservoir B (0.1% v/v formic acid) with a ratio of 80:20 (%A: %B) with a flow rate of 0.4ml/min. The injection volume was set to 10μL with a column temperature of 35°C with a total run time of 5min. With the use of an ESI source, a mass spectrometer was able to identify the drug and the internal standard. For the measurement of ART, the ART ammonium adduct $[M^+ + NH4]^+$, m/z 16.02 → 267.14 and m/z 368.84 → 177 for curcumin (CUR), were the molecular transition ions that were analyzed.

2.3.3.2 Preparation of standard solutions

10 mg of ART and CUR each were precisely weighed and then added to volumetric flasks to prepare stock solutions. The volume was increased to 10 ml by adding methanol, and the resultant solutions were stored at 2-8ºC until further use. Calibration curve samples were prepared at concentrations of 1.56, 3.12, 6.25, 12.5, 25, 50 and 100ng/mL using working solutions of 1μg/mL. To get final concentrations of 6.5, 12.5, and 50 ng/mL, quality control (QC) samples were also made via serial dilutions from stock solution at concentrations of 1000ng/mL. Methanol and water were diluted one at a time to provide all working solutions needed for preparing ART samples and producing the calibration curve.

2.3.3.3 Extraction procedure

Two techniques— protein precipitation and liquid-liquid extraction (LLE)—were assessed for the extraction of ART from plasma. Tert-butyl methyl ether (TBME), diethyl ether, TBME: IPA (80:20), chloroform, hexane, ethyl acetate and dichloromethane—were tried for LLE. Furthermore, several water-miscible organic solvents (acetonitrile and methanol) were used in different ratios to extract ART from plasma in order to assess plasma protein precipitation.

LLE was chosen for additional sample processing because it was found to be the most efficient technique for the extraction of drug. By comparing the chromatographic peak areas of non-biological standard samples with the biological plasma samples with spiked drug at the same concentration level, the extraction efficiency was assessed.

2.3.3.4 Preparation of plasma samples

90µL of pooled rat plasma (n=6) was spiked with 5µL of ART (0.031, 0.062, 0.125, 0.25, 0.5, 1 and 2µg/ml) and 5µL of CUR (1µg/ml) (IS). The sample were vortexed for 30sec. Then, 1ml of TBME was added to the samples and the samples were vortexed for 15min followed by centrifugation (10,000rpm; 15min). Post centrifugation, the TBME was separated and placed in a vacuum oven at 37ºC until all TBME was completely evaporated. The residue was then reconstituted in 100µL of 8:2 mixture of methanol and water followed by vortex mixing and centrifugation (10,000rpm; 15min). A 0.22µm nylon syringe filter was used to filter the supernatant, and 10µL of the resultant solution was then injected into the LC-MS-MS system for chromatographic analysis.

2.3.3.5 Bioanalytical Method validation

The developed LC-MS-MS method was validated for range, limit of detection (LOD), limit of quantitation (LOQ) and precision.

The linearity and range of the devised analytical technique were assessed by injecting six times a set of calibration standards with concentrations ranging from 1.56 to 100ng/mL. Six calibration curves were prepared by plotting the drug: IS peak area ratios on the Y-axis and the nominal plasma concentrations on the X-axis. Using the correlation coefficient and ordinary least square regression equation that were previously acquired via the analytical method's optimisation, the linearity of the approach was evaluated.

Three replicates at three distinct QC levels (LQC, MQC, HQC) were analysed in order to assess the intra-day and inter-day precision of the developed bioanalytical method. Samples were tested on the same day to assess the precision for intra-day, whereas, samples were analysed on three separate days to establish precision and accuracy for inter-day. The acceptance

standards for precision were within ±15% (reported as percentage deviation, or % CV).

The developed method's limits of detection (LOD) and quantification (LOQ) were ascertained through the measurement of the signal-to-noise ratio (S/N) acquired in the chromatogram containing the standard and blank quantities of ART. The concentrations designated as LOD and LOQ, respectively, were those at which the S/N ratio was larger than 3 and 10.

2.2.4 Results

Using polynomial regression, the calibration plots demonstrated an excellent linear relationship throughout the concentration range of 1.56–100ng/ml, with a high correlation coefficient (R^2) of 0.994 and the equation y = 1.4617x + 4.3566. Fig. 2.2.1. represents the linear regression calibration curve of ART. It was found that the total %recovery for the three different concentration levels fell between 80 and 120% of the acceptable range.

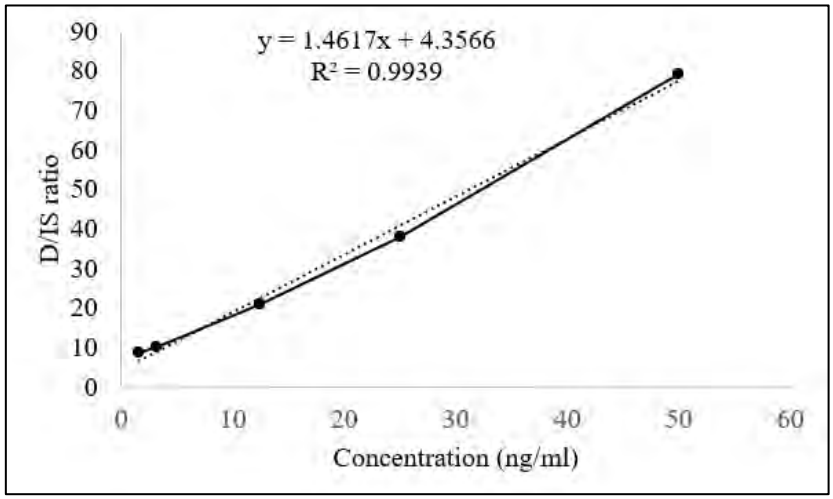

Fig. 2.2.1. Linear regression calibration curve of ART

2.3.4.1 Optimization of chromatographic conditions

To find the ideal mobile phase composition, column choice, flow rate, and injection volume for the measurement of ART in rat plasma, a range of chromatographic settings were evaluated. The chromatographic settings were optimized with the use of information obtained throughout the development of the analytical method. By increasing the flow rate from 0.3 to 0.4ml/min, a significant shift in the analyte retention time was noted. Using an Acquity UPLC BEH C18 (50mm × 2.1mm, 1.7µm) column, with a mobile phase made up of 80:20 ammonium acetate buffer with 0.1% v/v formic acid, 0.4 mL/min flow rate, and 10 µL injection volume was the final optimised separation technique for the quantification of ART. The retention times for ART and the IS were 1.05 and 0.45min, respectively, with a total run duration of 2min. A typical chromatogram of a bioanalytical sample comprising ART and CUR (I.S.) is displayed in Fig. 2.2.2.

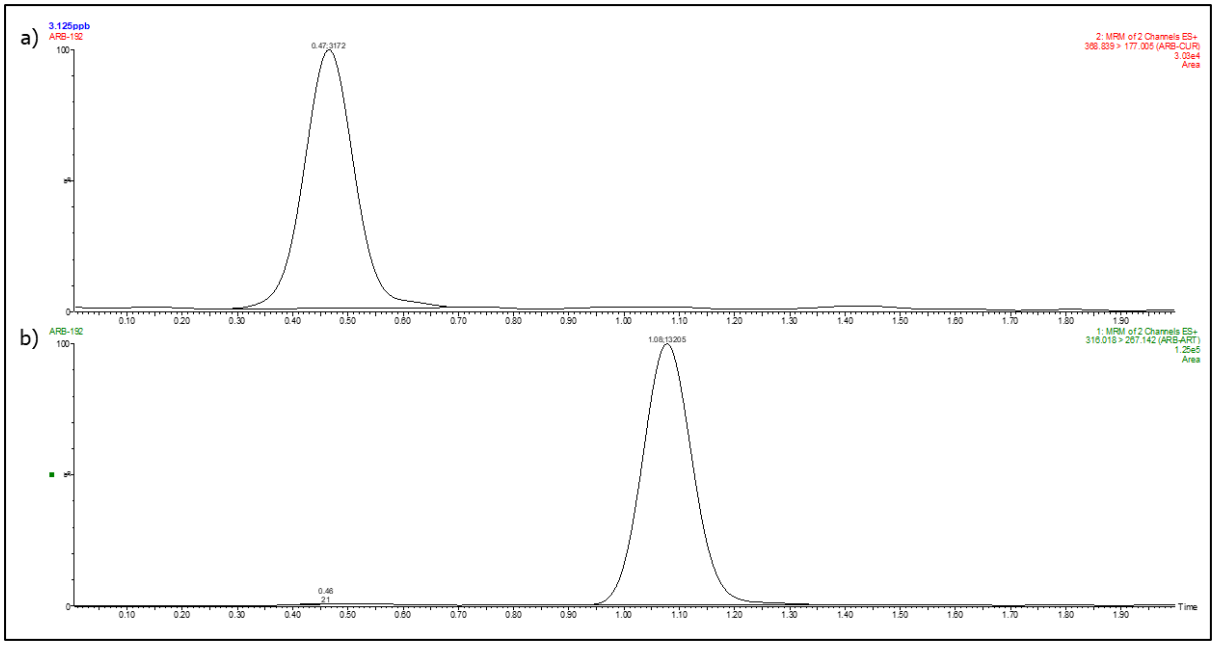

Fig. 2.2.2. Chromatograms of bioanalytical samples of a) curcumin and b) artemether from the developed bioanalytical method of LC-MS-MS

2.3.4.2 Optimization of sample preparation method

The process of cleaning up the plasma sample is essential to the development of bioanalytical methods since it influences the method's sensitivity and selectivity. The recovery of a known concentration of the analyte following sample extraction methods is referred to as the analytical process's extraction efficiency. An increased extraction efficiency results in a more precise procedure. Amongst the different techniques used for the extraction of the drug, liquid-liquid extraction method produced the most recovery. Table 2.2.1. lists the different solvents and how they extracted ART from plasma as efficiently as possible.

Table. 2.2.1. Extraction efficiency of different solvents

Solvent	Qty added (µL)	Vortex time (min)	Centrifugation [speed (rpm), time (min)]	% Recovery
Acetonitrile	1000	15	10000, 10	7.6%
Methanol	1000	15	10000, 10	1.98%
Diethyl ether	1000	15	10000, 10	1.72%
TBME	1000	15	10000, 10	1.46%
TBME: IPA (80:20)	1000	15	10000, 10	10%
Chloroform	1000	15	10000, 10	67.15%
Hexane	1000	15	10000, 10	2.28%
Ethyl acetate	1000	15	10000, 10	9.07%
Dichloromethane	1000	15	10000, 10	81%
Dichloromethane + Diethyl ether (50:50)	1000	15	10000, 10	27.27%

2.3.4.3 Bioanalytical method validation

The peak area ratios of ART to IS at different concentrations of ART in plasma were plotted to generate a calibration curve that exhibited linearity in the concentration range of 1.56-100ng/mL with a high regression coefficient of 0.994, indicating good reproducibility. Fig 2.2.2. shows the chromatograms of ART and the IS respectively whereas, Table 2.2.2. displays the regression data.

Table 2.2.2. Linear regression data for the calibration curve of ART in rat plasma (n = 6).

Parameters	Values
Range (ng/mL)	1.56-100
Correlation coefficient (r^2)	0.9939
Slope	1.4617
Intercept	4.3566

The plasma ART detection and quantification limit were found to be 0.30 ± 0.05 and 0.99 ± 0.17.

Table 2.2.3 enlists the QC values of LQC, MQC, and HQC, including LLOQ, for the inter-day precision. All the values for these QC samples were found to be within the acceptable range thus rendering the method suitable for the quantification of PQ-PAL in the biological matrices (% bias and RSD <±15% at LQC, MQC, and HQC).

Table 2.2.3. Precision (% CV) of the PQ-PAL in rat plasma samples at QC concentrations of the calibration ranges

Level	Nominal conc. (ng/mL)	Inter-day	
		Measured concentration	Precision (%CV)
LQC	6.25	7.67	16.20
MQC	12.5	10.96	11.28
HQC	50	49.78	12.38

2.2.5 Conclusion

A sensitive LC-MS-MS based bioanalytical was developed which could quantify ART in rat plasma upto 1ng/ml. The method was validated for precision as per ICH guideline Q2(R1) for estimation of ART and could be successfully utilized in the pharmacokinetic studies for the quantification of ART in the rat plasma.

References

Amin, N. C., Fabre, H., Blanchin, M. D., Montels, J., & Aké, M. (2013). Determination of artemether and lumefantrine in anti-malarial fixed-dose combination tablets by microemulsion electrokinetic chromatography with short-end injection procedure. *Malaria Journal*, *12*(1), 1–8. https://doi.org/10.1186/1475-2875-12-202

Artemether. (n.d.). Retrieved May 31, 2020, from https://www.drugbank.ca/drugs/DB06697

Bhide, A. R., Surve, D. H., Guha, S., & Jindal, A. B. (2020). A sensitive RP-HPLC method for estimation of artemether from polymeric nanoparticles after pre-column acid treatment using UV-visible detector. *Journal of Liquid Chromatography and Related Technologies*. https://doi.org/10.1080/10826076.2020.1777564

César, I. D. C., & Pianetti, G. A. (2009). Quantitation of artemether in pharmaceutical raw material and injections by high performance liquid chromatography. *Brazilian Journal of Pharmaceutical Sciences*, *45*(4), 737–742. https://doi.org/10.1590/S1984-82502009000400018

César, I. da C., Andrade Nogueira, F. H., & Antônio Pianetti, G. (2008). Simultaneous determination of artemether and lumefantrine in fixed dose combination tablets by HPLC with UV detection. *Journal of Pharmaceutical and Biomedical Analysis*, *48*(3), 951–954. https://doi.org/10.1016/j.jpba.2008.05.022

Chaturvedi, D., Goswami, A., Pratim Saikia, P., Barua, N. C., & Rao, P. G. (2010). Artemisinin and its derivatives: a novel class of anti-malarial and anti-cancer agents. *Chem. Soc. Rev.*, *39*(2), 435–454. https://doi.org/10.1039/B816679J

Christian, J., Shah, P., Patel, M., Patel, K., & Gandhi, T. (2017). Optimizing derivatization conditions using an experimental design and simultaneous estimation of artemether and lumefantrine by ratio first order derivative spectrophotometric method. *Journal of Taibah University for Science*, *11*(5), 729–740. https://doi.org/10.1016/j.jtusci.2016.08.003

Colussi, D., Parisot, C., Legay, F., & Lefèvre, G. (1999). Binding of artemether and lumefantrine to plasma proteins and erythrocytes. *European Journal of Pharmaceutical Sciences*, *9*(1), 9–16. https://doi.org/10.1016/S0928-0987(99)00037-8

Gilmore, K., Kopetzki, D., Lee, J. W., Horváth, Z., McQuade, D. T., Seidel-Morgenstern, A., & Seeberger, P. H. (2014). Continuous synthesis of artemisinin-derived medicines. *Chemical Communications*, *50*(84), 12652–12655. https://doi.org/10.1039/c4cc05098c

Huang, Y., Xie, G., Zhou, Z., Sun, X., & Wang, Y. (1987). Determination of artemether in plasma and whole blood using HPLC with flow-through polarographic detection. *Biomedical Chromatography*, *2*(2), 53–56. https://doi.org/10.1002/bmc.1130020203

Mount, D. L., Todd, G. D., & Navaratnam, V. (1995). Packed-column supercritical fluid chromatography of artemisinin (qinghaosu) with electron-capture detection. *Journal of Chromatography B: Biomedical Sciences and Applications*, *666*(1), 183–187. https://doi.org/10.1016/0378-4347(94)00560-R

Product Information. (n.d.). Retrieved May 31, 2020, from https://www.caymanchem.com/pdfs/11815.pdf

Resende, L. A., da Silva, P. H. R., & Fernandes, C. (2019). Quantitative determination of the antimalarials artemether and lumefantrine in biological samples: A review. *Journal of Pharmaceutical and Biomedical Analysis*, *165*, 304–314. https://doi.org/10.1016/j.jpba.2018.12.021

Stringham, R. W., Lynam, K. G., Mrozinski, P., Kilby, G., Pelczer, I., & Kraml, C. (2009). High performance liquid chromatographic evaluation of artemisinin, raw material in the synthesis of artesunate and artemether. *Journal of Chromatography A*, *1216*(51), 8918–8925. https://doi.org/10.1016/j.chroma.2009.10.056

Tarning, J., Kloprogge, F., Dhorda, M., Jullien, V., Nosten, F., White, N. J., Guerin, P. J., & Piola, P. (2013). Pharmacokinetic Properties of Artemether, Dihydroartemisinin, Lumefantrine, and Quinine in Pregnant Women with Uncomplicated Plasmodium falciparum Malaria in Uganda. *Antimicrobial Agents and Chemotherapy*, *57*(10), 5096–5103. https://doi.org/10.1128/AAC.00683-13

Ubale, M., & Choudhari, V. (2015). Stability-Indicating Hplc Determination of Artemether in Bulk Drug and Pharmaceutical Form. *World Journal of Pharmaceutical Research*, *5*(1), 609–625. https://doi.org/10.13140/RG.2.1.4508.7760

Chapter 2.3: Development and validation of RP-HPLC based analytical method for quantification of primaquine prodrug

2.3.1 Introduction

Primaquine diphosphate (PQ), 4-N-(6-methoxyquinolin-8-yl)pentane-1,4-diamine;phosphoric acid is an 8-aminoquinoline derivative used for the prophylaxis and treatment of *P. vivax* caused malaria (Baird & Rieckmann, 2003; Waters & Edstein, 2011). Primaquine itself is a viscous liquid, hence is available in the diphosphate salt form which is orange crystalline powder and soluble in water (Al-Badr, 2005; Chung et al., 1997). It has a log P of 2.1 (Davanço et al., 2014).

However, the drug poses few complications while use. For instance, PQ is a hydrophilic drug (solubility – 66mg/ml) (*PRIMAQUINE PHOSPHATE*, n.d.) and hence it poses challenge in loading ion the nanocarriers (Singh & Vingkar, 2008). Furthermore, PQ has a short half-life (4-5h) (Jittamala et al., 2015; Li et al., 2014) and hence, the PQ formulation needs to be administered daily (Galappaththy et al., 2013; Milligan et al., 2020). In order to resolve this, hydrophilic PQ was conjugated to palmitic acid in order to synthesize a lipophilic prodrug (PQ-PAL) (Sloat et al., 2011). The prodrug due to its lipophilic nature, was suitable for loading on nanoformulations (Barichello et al., 1999). Hence, now a sensitive analytical method was required for the analysis of PQ-PAL in the solvents. PQ-PA needed to evaluated for its solubility in various solvents and release medias. Furthermore, the nanoformulations loaded with PQ-PAL were to be prepared and evaluated for %EE, %DL and drug content. Although, UV spectrophotometer was useful for the determination of solubility and λ_{max} of PQ-PAL (266nm), it was not specific for the analysis of PQ-PAL in the formulations and the *in vitro* release media due to the interference of the inactive components present in it.

Therefore, a sensitive analytical method was required for the detection and quantification of PQ-PAL in the nanoformulations as well as the *in vitro* release media.

Hence the objective of the present study was development, optimization and validation of the RP-HPLC method for the detection and quantification of PQ-PAL in the nanoformulations and release medias.

2.3.2 Materials

Primaquine diphosphate was a gift sample from IPCA Laboratories, Maharashtra India. Primaquine prodrug was synthesized in the laboratory. LC-MS grade and HPLC grade formic

acid, acetonitrile and methanol were purchased from Merck Limited (Mumbai, India). All other chemicals, solvents and reagents utilized, were either HPLC or analytical grade. HPLC grade water was obtained from Milli-Q system (Millipore GmbH, Germany) used throughout the analysis. The solvents and buffers prepared were suitably filtered through 0.22 MilliporeTM membrane filter (Merck, Darmstadt, Germany) and suitably degassed using an ultrasonic bath for 30 min.

2.3.3 Methods

2.3.3.1 Instrumentation, software and chromatographic conditions

The analytical method for the quantification of PQ-PAL was developed with Shimadzu HPLC system (Kyoto, Japan) equipped with a binary pump (LC-20AD), autosampler (SIL-20AC HT) and UV-visible detector (SPD-20A). The hardware control and data processing were done using LC solution software version 5.97. The column utilized during the analysis was Thermo Scientific HyPURITY ADVANCE 5µm ODS(C18) column with the dimensions of 50 × 4.6mm.

Isocratic RP-HPLC method with a mobile phase system consisted of reservoir A (acetonitrile) and reservoir B [Phosphate buffer solution (PBS), 10mM; pH 3.5] with a ratio of 60:40 (%A: %B) with a flow rate of 1ml/min. The injection volume was set to 20µL with a column temperature of 30°C with a total run time of 7min at a wavelength of 266nm.

2.3.3.2 Preparation of standard solutions

Standard solution of PQ-PAL was prepared by dissolving accurately weighed 25mg of PQ-PAL in 25ml of methanol in a volumetric flask. A working standard solution of 100µg/ml was prepared by diluting 1mL of the stock solution to 10mL in a volumetric flask (10mL) using methanol. For the preparation of secondary working standard solutions of PQ-PAL, the working standard solution (100µg/mL) was suitably diluted with 6:4 acetonitrile: Milli-Q water. Further, 100µL of standard stock solution was diluted up to 1mL to obtain a final concentration of 10µg/mL, which was further serially diluted to yield 5, 2.5, 1.25, 0.625, 0.312, 0.156µg/mL concentration standards.

2.3.3.3 Analytical Method validation of PQ-PAL

In accordance to the International Conference on Harmonization (ICH) guideline Q2 (R1)(ICH, 2005), the method was validated for specificity, linearity, range, limit of detection (LOD), limit of quantitation (LOQ), precision, accuracy and robustness.

In order to assess the specificity of the developed analytical method, a PQ-PAL standard solution (0.5µg/mL) was spiked in the placebo formulation, which contained all the

formulation components namely PLGA, albumin, PVA and ethanol. Furthermore, release media was also spiked with the PQ-PAL standard (0.5µg/mL) and the resulting chromatograms were observed for the presence of other peaks.

The linearity and range of the devised analytical technique were assessed by injecting six times a set of calibration standards with concentrations ranging from 0.156 to 10 µg/mL. A calibration curve was then created by plotting each standard's peak area against the respective concentration. Using the correlation coefficient and ordinary least square regression equation that were previously acquired via the analytical method's optimization, the linearity of the approach was evaluated.

Samples were analyzed in triplicate after known amounts of PQ-PAL were injected into three calibration standards (0.312, 1.25, and 5µg/mL) in order to assess the accuracy of the established RP-HPLC technique. Comparing the measured concentrations to the anticipated concentrations of the spiked samples allowed for the computation of the recovery of PQ-PAL. The percent recovery and percent relative standard deviation (%RSD) for each calibration standard were computed in order to evaluate the method's accuracy. This approach provides a reliable and comprehensive assessment of the accuracy of the developed method and ensures the reliability of subsequent analysis.

To analyze the precision of the developed method, the peak areas of three calibration standards were examined in triplicate, three times a day. Whereas, the for the inter-day precision the peak areas of three calibration standards were analyzed in triplicate for three consecutive days. The method's accuracy was evaluated by computing the relative standard deviation (%RSD) for every set of measurements made in triplicate.

The developed method's limits of detection (LOD) and quantification (LOQ) were ascertained through the measurement of the signal-to-noise ratio (S/N) acquired in the chromatogram containing the standard and blank quantities of PQ-PAL. The concentrations designated as LOD and LOQ, respectively, were those at which the S/N ratio was larger than 3.3 and 10.

For determination of the robustness of the method, deliberate modifications were made to the chromatographic settings, such column temperature (28 and 32°C). By calculating the percentage recovery of the three calibration standards, the impact of these modifications on the method's accuracy was assessed

2.3.4 Results

2.3.4.1 Analytical method development

Considering the lipophilic nature and solubility of the drug, it was assumed that a mobile phase

with higher proportion of ACN in the mobile phase would result in poor retention. However, the compound's high hydrophobicity resulted in extensive interaction of the compound with the C18 column [5µm ODS(C18); 250 × 4.6mm] leading to longer retention times. A method with longer retention times would have involved a longer run time and excessive use of solvents with no commensurate advantages. Hence, in order to decrease the retention time, a column with similar characteristics but with a shorter length was chosen. A column with the dimensions of 50 × 4.6mm with 5µm ODS(C18) was selected for further analysis. Initial trial runs were conducted at a ratio of 50:50 (%A: %B), while the mobile phase ratio was changed in further trials to understand its effect on the retention time and peak shape. A mobile phase ratio of 60:40 (%A: %B) consisting of reservoir A (acetonitrile) and reservoir B (PBS, 10mM; pH 3.5) with a flow rate of 1ml/min were optimized. The column temperature was set to 30°C. Table 2.4.1. represents various chromatographic parameters of the peak obtained during the optimization of mobile phase ratio.

Table 2.3.1. Mobile phase optimization

Chromatographic conditions	**Acceptance criteria**	**Results**			
A: Acetonitrile, B: PBS, 10mM; pH 3.5	-	50:50	60:40	65:35	80:20
Retention time of PQ-PAL		18.14	5.27	3.38	1.47
Tailing factor	0.8-1.5	0.94	1.02	1.07	1.25
Number of theoretical plates	>2000	1590	2087	1573	461

2.3.4.2 Analytical method validation

Using polynomial regression, the calibration plots demonstrated an excellent linear relationship throughout the concentration range of 0.156–10µg/ml, with a high correlation coefficient (R^2) of 1 and the equation y = 58447x + 606.47. Fig. 2.3.1a. shows the calibration curve Linear regression calibration curve of PQ-PAL in RP-HPLC. A representative chromatogram of PQ-PAL (1.25µg/mL) ACN: PBS, 10mM; pH 3.5 (60:40) is shown in Fig. 2.3.1b.

It was found that the total %recovery for the three different concentration levels fell between 80 and 120% of the acceptable range. The devised method's %RSD was less than 2%, indicating that the inter-day and intra-day precision.

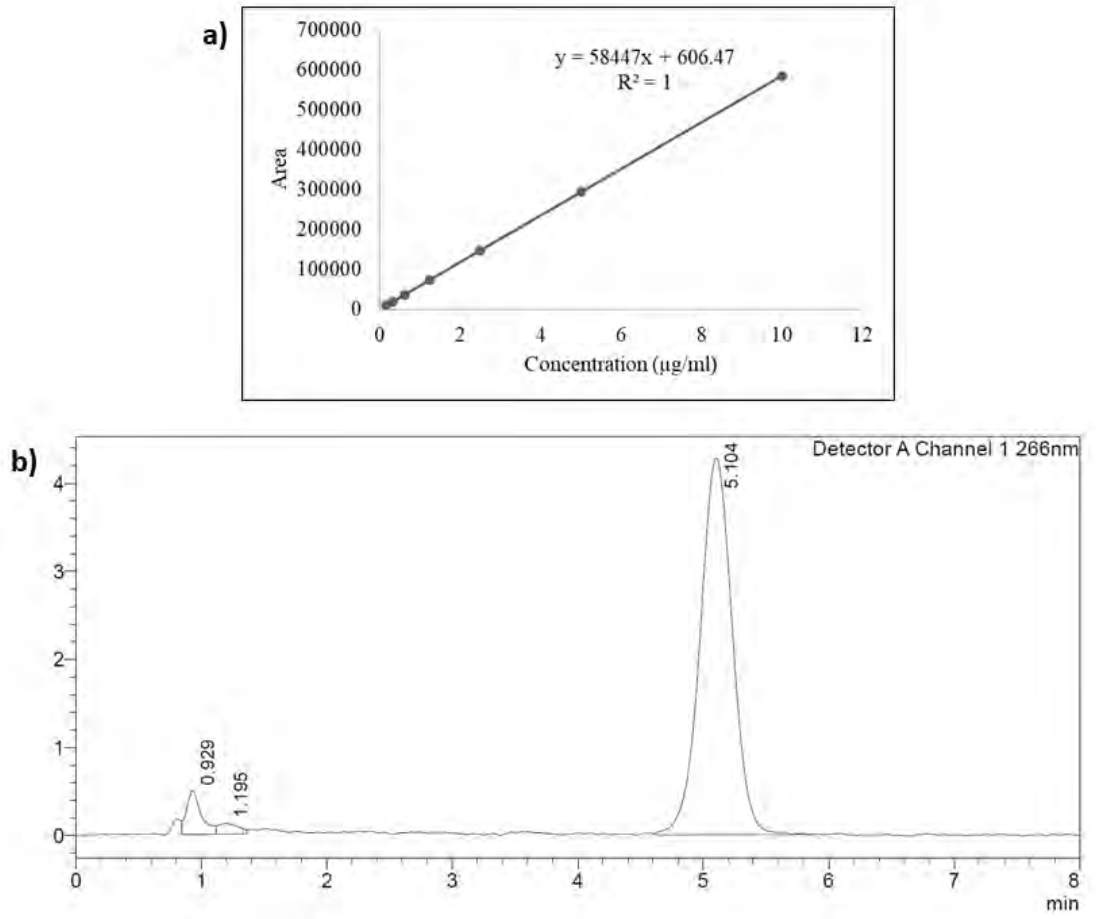

Fig. 2.3.1. a) Linear regression calibration curve of PQ-PAL in RP-HPLC, and b) Representative chromatogram of PQ-PAL (1.25µg/mL) ACN: PBS, 10mM; pH 3.5 (60:40)

The absence of interference from the excipients used in the formulation proved the selectivity of the devised RP-HPLC technique for quantifying PQ-PAL (Fig. 2.3.2).

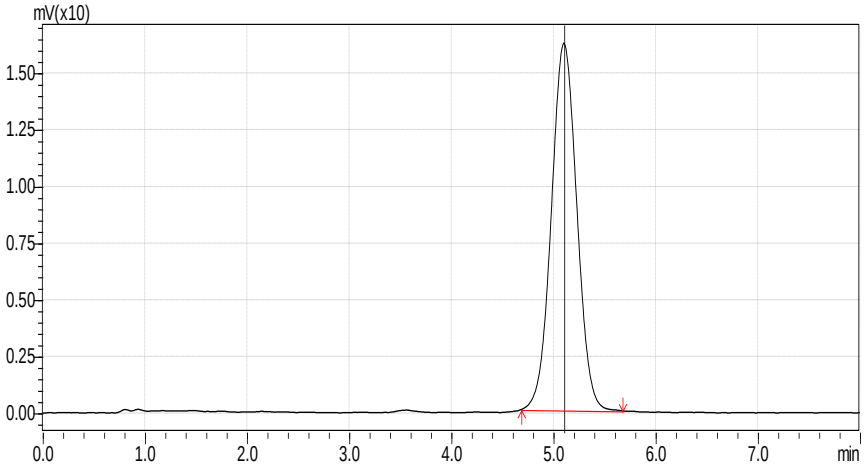

Fig. 2.3.2. Representative chromatogram of PQ-PAL formulation sample

Furthermore, the method's robustness was confirmed when minor adjustments were made in the column temperature and buffer pH. The percentage recovery of PQ-PAL remained within

the permissible range of 80–120%. It was discovered that the limits of detection and quantitation were, respectively, 30.23µg/ml and 100.77ng/ml. Table 2.3.2. displays the findings from the PQ-PAL method accuracy and precision. Additionally, it was found out that the method was selective since no interference from the formulation's excipients. The results of the method robustness are given in table 2.3.3.

Table 2.3.2. Accuracy and precision

Accuracy (n=3)			
Concentration (µg/ml)	% Recovery	Standard Deviation	%RSD
LQC (0.312µg/ml)	96.61	0.91	0.94
MQC (1.25µg/ml)	96.93	0.68	0.70
HQC (5µg/ml)	96.32	1.22	1.26
Inter-day precision (n=3)			
Concentration (µg/ml)	Measured concentration (µg/ mL)	Standard Deviation	%RSD
LQC (0.312µg/ml)	0.30	0.00	1.25
MQC (1.25µg/ml)	1.28	0.03	2.04
HQC (5µg/ml)	5.11	0.08	1.65
Intraday precision (n=3)			
Concentration (µg/ml)	Measured concentration (µg/ mL)	Standard Deviation	%RSD
LQC (0.312µg/ml)	0.31	0.00	1.35
MQC (1.25µg/ml)	1.30	0.02	1.68
HQC (5µg/ml)	5.17	0.10	1.98

Table 2.3.3. Robustness

	% Recovery ± SD		
Condition	LQC (0.312µg/ml)	MQC (1.25µg/ml)	HQC (5µg/ml)
Column temperature (32ºC)	97.80 ± 1.14	103.58 ± 1.86	103.74 ± 0.80
Phosphate buffer (10 mM; pH 3.8)	99.35 ± 1.59	104.36 ± 2.33	104.57 ± 3.08

2.3.5 Conclusion

A sensitive HPLC based analytical was developed which could detect PQ-PAL. The method was validated for accuracy, precision and robustness as per ICH guideline Q2(R1) for the estimation of PQ-PAL and could be used for the quantification of PQ-PAL from the formulations and other analytical matrices for the determination of %EE, %DL and drug content.

References

Al-Badr, A. A. (2005). *Primaquine Diphosphate: Comprehensive Profile* (pp. 153–208). https://doi.org/10.1016/S0099-5428(05)32007-7

Baird, J. K., & Rieckmann, K. H. (2003). Can primaquine therapy for vivax malaria be improved? *Trends in Parasitology*, *19*(3), 115–120. https://doi.org/10.1016/S1471-4922(03)00005-9

Barichello, J. M., Morishita, M., Takayama, K., & Nagai, T. (1999). Encapsulation of Hydrophilic and Lipophilic Drugs in PLGA Nanoparticles by the Nanoprecipitation Method. *Drug Development and Industrial Pharmacy*, *25*(4), 471–476. https://doi.org/10.1081/DDC-100102197

Chung, M. C., Gonçalves, M. F., Colli, W., Ferreira, E. I., & Miranda, M. T. M. (1997). Synthesis and in Vitro Evaluation of Potential Antichagasic Dipeptide Prodrugs of Primaquine. *Journal of Pharmaceutical Sciences*, *86*(10), 1127–1131. https://doi.org/10.1021/js970006v

Davanço, M. G., Aguiar, A. C. C., dos Santos, L. A., Padilha, E. C., Campos, M. L., de Andrade, C. R., da Fonseca, L. M., dos Santos, J. L., Chin, C. M., Krettli, A. U., & Peccinini, R. G. (2014). Evaluation of Antimalarial Activity and Toxicity of a New Primaquine Prodrug. *PLoS ONE*, *9*(8), e105217. https://doi.org/10.1371/journal.pone.0105217

Galappaththy, G. N., Tharyan, P., & Kirubakaran, R. (2013). Primaquine for preventing relapse in people with *Plasmodium vivax* malaria treated with chloroquine. *Cochrane Database of Systematic Reviews*. https://doi.org/10.1002/14651858.CD004389.pub3

Jittamala, P., Pukrittayakamee, S., Ashley, E. A., Nosten, F., Hanboonkunupakarn, B., Lee, S. J., Thana, P., Chairat, K., Blessborn, D., Panapipat, S., White, N. J., Day, N. P. J., & Tarningb, J. (2015). Pharmacokinetic interactions between primaquine and pyronaridine-artesunate in healthy adult Thai subjects. *Antimicrobial Agents and Chemotherapy*, *59*(1), 505–513. https://doi.org/10.1128/AAC.03829-14

Li, Q., O'Neil, M., Xie, L., Caridha, D., Zeng, Q., Zhang, J., Pybus, B., Hickman, M., & Melendez, V. (2014). Assessment of the prophylactic activity and pharmacokinetic profile of oral tafenoquine compared to primaquine for inhibition of liver stage malaria infections. *Malaria Journal*, *13*(1), 141. https://doi.org/10.1186/1475-2875-13-141

Milligan, R., Daher, A., Villanueva, G., Bergman, H., & Graves, P. M. (2020). Primaquine alternative dosing schedules for preventing malaria relapse in people with *Plasmodium vivax*. *Cochrane Database of Systematic Reviews*. https://doi.org/10.1002/14651858.CD012656.pub3

PRIMAQUINE PHOSPHATE. (n.d.). Https://Lktlabs.Com/Product/Primaquine-Phosphate/#:~:Text=Soluble%20in%20water%20(66%20mg%2FmL).

Singh, K. K., & Vingkar, S. K. (2008). Formulation, antimalarial activity and biodistribution of oral lipid nanoemulsion of primaquine. *International Journal of Pharmaceutics*, *347*(1–2), 136–143. https://doi.org/10.1016/j.ijpharm.2007.06.035

Sloat, B. R., Sandoval, M. A., Li, D., Chung, W.-G., Lansakara-P, D. S. P., Proteau, P. J., Kiguchi, K., DiGiovanni, J., & Cui, Z. (2011). In vitro and in vivo anti-tumor activities of a gemcitabine derivative carried by nanoparticles. *International Journal of Pharmaceutics*, *409*(1–2), 278–288. https://doi.org/10.1016/j.ijpharm.2011.02.037

Waters, N. C., & Edstein, M. D. (2011). 8-Aminoquinolines: Primaquine and Tafenoquine. In *Treatment and Prevention of Malaria* (pp. 69–94). Springer Basel. https://doi.org/10.1007/978-3-0346-0480-2_4

Chapter 2.4: Development and validation of LC-MS-MS based bioanalytical method for quantification of primaquine prodrug

2.4.1 Introduction

Primaquine diphosphate (PQ), 4-N-(6-methoxyquinolin-8-yl)pentane-1,4-diamine;phosphoric acid is an 8-aminoquinoline derivative used for the prophylaxis and treatment of P. *vivax* caused malaria (Baird & Rieckmann, 2003; Waters & Edstein, 2011). Primaquine itself is a viscous liquid, hence is available in the diphosphate salt form which is orange crystalline powder and soluble in water (Al-Badr, 2005; Chung et al., 1997). It has a log P of 2.1 (Davanço et al., 2014).

However, the drug poses few complications while use. For instance, PQ is a hydrophilic drug (solubility – 66mg/ml) (*PRIMAQUINE PHOSPHATE*, n.d.) and hence it poses challenge in loading ion the nanocarriers (Singh & Vingkar, 2008). Furthermore, PQ has a short half-life (4-5h) (Jittamala et al., 2015; Li et al., 2014) and hence, the PQ formulation needs to be administered daily (Galappaththy et al., 2013; Milligan et al., 2020). In order to resolve this, hydrophilic PQ was conjugated to palmitic acid in order to synthesize a lipophilic prodrug (PQ-PAL) (Sloat et al., 2011). The prodrug due to its lipophilic nature, was suitable for loading on nanoformulations (Barichello et al., 1999). Initially, for the analysis of PQ-PAL a sensitive RP-HPLC was developed and validated. The LOQ value for PQ-PAL was found to be around 100ng/ml. This limit for the quantification of PQ-PAL was suitable for the quantification of PQ-PAL in the nanoformulation and *in vitro* studies where higher quantity of drug is used during the study. However, such is not the case in *in vivo* pharmacokinetic studies (Moein et al., 2017). Additionally, the ability of PQ-PAL to remain in the system was evaluated using long-acting formulations. In such case, following the administration of the formulations, the latter time points frequently exhibited lower plasma drug concentrations, falling below the detection limit of the developed RP-HPLC method. Hence, a bioanalytical method sensitive enough for the quantification of PQ-PAL in the biological matrices was required. Therefore, we developed a sensitive LC-MS-MS method for the quantification of PQ-PAL in the biological matrices.

This chapter discusses about the steps which were involved in the development, optimization, and validation of the LC-MS-MS method for the detection and quantification of PQ-PAL in the rat plasma.

2.4.2 Materials

Primaquine prodrug was synthesized in the laboratory. Lumefantrine was purchased from Yarrow Chem Products (Mumbai, Maharashtra). LC-MS grade and HPLC grade formic acid, acetonitrile and methanol were purchased from Merck Limited (Mumbai, India). All other chemicals, solvents and reagents utilized, were either HPLC or analytical grade. HPLC grade water was obtained from Milli-Q system (Millipore GmbH, Germany) used throughout the analysis. The solvents and buffers prepared were suitably filtered through 0.22 MilliporeTM membrane filter (Merck, Darmstadt, Germany) and suitably degassed using an ultrasonic bath for 30 min.

2.4.3 Methods

2.4.3.1 Instrumentation, software and chromatographic conditions

The bioanalytical method for the quantification of PQ-PAL was developed with liquid chromatography coupled with tandem mass spectrometry (LC−MS/MS) (Waters Acquity UPLC H Class system with a Waters Xevo Triple Quadrupole mass spectrometer). Mass Lynx software version 4.1 was used to control the machine and analyse the data. The column utilized during the analysis was Acquity UPLC BEH C18 (50 mm × 2.1 mm, 1.7 μm) column.

Isocratic method with a mobile phase system consisted of reservoir A (acetonitrile) and reservoir B (0.1% v/v formic acid) with a ratio of 90:10 (%A: %B) with a flow rate of 0.2ml/min. The injection volume was set to 10μL with a column temperature of 35°C with a total run time of 5min. With the use of an ESI source, a mass spectrometer was able to identify the drug and the internal standard. The molecular transition ions analyzed for the measurement of PQ-PAL and LUM were m/z 498.11 → 324.24 and m/z 527.86 → 510.07 respectively.

2.4.3.2 Extraction procedure

Two techniques— protein precipitation and liquid-liquid extraction (LLE)—were assessed for the extraction of PQ-PAL from plasma. Diethyl ether and dichloromethane—were tried for LLE. Furthermore, several water-soluble organic solvents (acetonitrile, methanol and acetone) were used in diverse ratios to extract PQ-PAL from plasma in order to assess plasma protein precipitation.

Protein precipitation was chosen for additional sample processing because it was found to be the most efficient technique for the extraction of drug. By comparing the chromatographic peak areas of non-biological standard samples with the biological plasma samples with spiked drug at the same concentration level, the extraction efficiency was assessed.

2.4.3.3 Preparation of plasma samples

90µL of pooled rat plasma was spiked with 5µL of PQ-PAL (0.016, 0.031, 0.062, 0.125, 0.25, 0.5, 1 and 2µg/ml) and 5µL of LUM (0.5µg/ml) (IS). The sample were vortexed for 30sec. Then 1ml of ACN was added to the samples and the samples were vortexed for 15min followed by centrifugation (10,000rpm; 15min). Post centrifugation the supernatant was separated and placed in a vacuum oven at 37ºC until all ACN was completely evaporated. The residue was then reconstituted in 100µL of 8:2 mixture of acetonitrile and water followed by vortexing and centrifugation (10,000rpm; 15min). A 0.22µm nylon syringe filter was used to filter the supernatant, and 10µL of the resultant solution was then injected into the LC-MS-MS system for chromatographic analysis.

2.4.3.4 Bioanalytical Method validation of PQ-PAL

In accordance to the International Conference on Harmonization (ICH) guideline Q2 (R1)(ICH, 2005), the method was validated for range, limit of detection (LOD), limit of quantitation (LOQ), precision and accuracy.

The linearity and range of the devised analytical technique were assessed by injecting six times a set of calibration standards with concentrations ranging from 0.078to 100ng/mL. Six calibration curves were prepared by plotting the drug: IS peak area ratios on the Y-axis and the nominal plasma concentrations on the X-axis. Using the correlation coefficient and ordinary least square regression equation that were previously acquired via the analytical method's optimisation, the linearity of the approach was evaluated.

Three replicates at three distinct QC levels (LQC, MQC, HQC, and LLOQ) were analysed in order to assess the intra-day and inter-day precision and accuracy of the developed bioanalytical method. Samples were tested on the same day to assess the precision and accuracy for intra-day, whereas, samples were analysed on three separate days to establish precision and accuracy for inter-day. With the exception of LLOQ, where its value should not exceed ±20% for both accuracy and precision, the acceptance standards for accuracy are within ±15% (represented as percentage of variation from nominal concentration, or % bias) and for precision within ±15% (reported as percentage deviation, or % CV).

The developed method's limits of detection (LOD) and quantification (LOQ) were ascertained through the measurement of the signal-to-noise ratio (S/N) acquired in the chromatogram containing the standard and blank quantities of PQ-PAL. The concentrations designated as LOD and LOQ, respectively, were those at which the S/N ratio was larger than 3.3 and 10

2.4.4 Results

2.4.4.1 Bioanalytical method development

Using polynomial regression, the calibration plots demonstrated an excellent linear relationship throughout the concentration range of 0.78–100ng/ml, with a high correlation coefficient (R^2) of 0.9974 and the equation y = 0.2068x - 0.0049. Fig. 2.4.1. represents the linear regression calibration curve of PQ-PAL. It was found that the total %recovery for the three different concentration levels fell between 80 and 120% of the acceptable range.

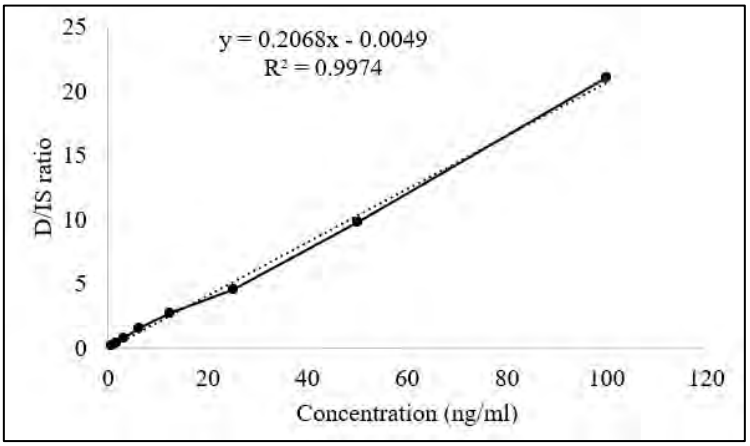

Fig. 2.4.1. Linear regression calibration curve of PQ-PAL

2.4.4.2 Optimization of chromatographic conditions

To find the ideal mobile phase composition, column choice, flow rate, and injection volume for the measurement of PQ-PAL in rat plasma, a range of chromatographic settings were evaluated. The chromatographic settings were optimized with the use of information obtained throughout the development of the analytical method. Using an Acquity UPLC BEH C18 (50 mm × 2.1 mm, 1.7 µm) column, with a mobile phase made up of 90:10 ACN: ammonium acetate buffer with 0.1% v/v formic acid, 0.2 mL/min flow rate, and 10 µL injection volume was the final optimised separation technique for the quantification of PQ-PAL. The retention times for PQ-PAL and the IS were 3.98 and 3.41min, respectively, with a total run duration of 5min. A typical chromatogram of a sample comprising PQ-PAL (50ng/ml) and IS (50ng/ml) is displayed in Fig. 2.4.2.

2.4.4.3 Optimization of sample preparation method

The process of cleaning up the plasma sample is essential to the development of bioanalytical methods since it influences the method's sensitivity and selectivity. The recovery of a known concentration of the analyte following sample extraction methods is referred to as the analytical process's extraction efficiency. An increased extraction efficiency results in a more precise

procedure. Amongst the different techniques used for the extraction of the drug, protein precipitation method produced the most recovery. Table 2.4.1. lists the different solvents and their extraction capacity of PQ-PAL from plasma.

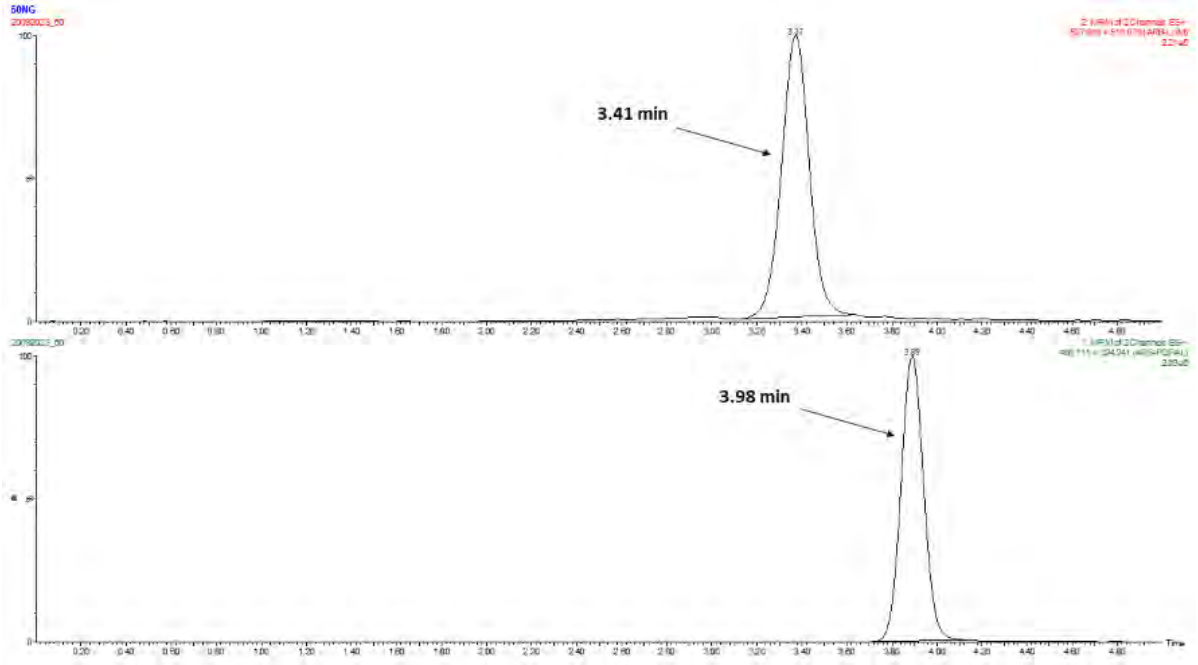

Fig. 2.4.2. Chromatogram of PQ-PAL (50ng/ml) and IS (50ng/ml) from the developed bioanalytical method of LC-MS-MS

Table 2.4.1. Extraction efficiency of PQ-PAL of different organic solvents

Solvent	Qty added (µL)	Vortex time (min)	Centrifugation [speed (rpm), time (min)]	% Recovery
Acetonitrile	1000	15	10000, 10	79%
Methanol	1000	15	10000, 10	84%
Dichloromethane	1000	15	10000, 10	34%
Diethyl ether	1000	15	10000, 10	9%
Ethyl acetate	1000	15	10000, 10	10%

2.4.4.4 Bioanalytical method validation

The peak area ratios of PQ-PAL to IS at different concentrations of QS in plasma were plotted to generate a calibration curve that exhibited linearity in the concentration range of 0.78-100 ng/mL with a high regression coefficient of 0.997, indicating good reproducibility. Table 2.4.2. displays the regression data for the calibration curve of PQ-PAL.

Table 2.4.2. Linear regression data for the calibration curve of PQ-PAL in rat plasma (n=6).

Parameters	Values
Range (ng/mL)	0.78-100
Correlation coefficient (r^2)	0.9974
Slope	0.2068
Intercept	(-0.0049)
LLOQ (ng/mL)	0.585

The plasma PQ-PAL detection and quantification limit were found to be 0.044 and 0.164ng/ml. Table 2.4.3. enlists the QC values of LQC, MQC, and HQC, including LLOQ, for the inter- and intra-day precision and accuracy. All the values for these QC samples were found to be within the acceptable range thus rendering the method suitable for the quantification of PQ-PAL in the biological matrices (% bias and RSD <±15% at LQC, MQC, and HQC while, <±20% for LLOQ).

Table 2.4.3. Precision (% CV) and accuracy (% bias) of the PQ-PAL in rat plasma samples at QC concentrations of the calibration ranges

Level	Nominal conc. (ng/mL)	Inter-day		
		Measured concentration	Precision (%CV)	Accuracy (% Bias)
LLOQ	0.585	0.56	17.14	-3.82
LQC	2	2.07	10.28	3.31
MQC	30	29.75	7.60	-0.83
HQC	60	59.02	7.29	-1.64
Level	**Nominal conc. (ng/mL)**	**Intra-day**		
		Measured concentration	**Precision (%CV)**	**Accuracy (% Bias)**
LLOQ	0.585	0.54	15.92	-7.82
LQC	2	1.97	10.43	-1.45
MQC	30	30.14	6.63	0.48
HQC	60	63.19	8.10	5.32

2.4.5 Conclusion

A sensitive LC-MS-MS based bioanalytical was developed which could quantify PQ-PAL in rat plasma upto 0.164ng/ml. The method was validated for precision as per ICH guideline Q2(R1) for estimation of PQ-PAL and could be successfully utilized in the pharmacokinetic studies for the quantification of PQ-PAL in the rat plasma.

References

Al-Badr, A. A. (2005). *Primaquine Diphosphate: Comprehensive Profile* (pp. 153–208). https://doi.org/10.1016/S0099-5428(05)32007-7

Baird, J. K., & Rieckmann, K. H. (2003). Can primaquine therapy for vivax malaria be improved? *Trends in Parasitology*, *19*(3), 115–120. https://doi.org/10.1016/S1471-4922(03)00005-9

Barichello, J. M., Morishita, M., Takayama, K., & Nagai, T. (1999). Encapsulation of Hydrophilic and Lipophilic Drugs in PLGA Nanoparticles by the Nanoprecipitation Method. *Drug Development and Industrial Pharmacy*, *25*(4), 471–476. https://doi.org/10.1081/DDC-100102197

Chung, M. C., Gonçalves, M. F., Colli, W., Ferreira, E. I., & Miranda, M. T. M. (1997). Synthesis and in Vitro Evaluation of Potential Antichagasic Dipeptide Prodrugs of Primaquine. *Journal of Pharmaceutical Sciences*, *86*(10), 1127–1131. https://doi.org/10.1021/js970006v

Davanço, M. G., Aguiar, A. C. C., dos Santos, L. A., Padilha, E. C., Campos, M. L., de Andrade, C. R., da Fonseca, L. M., dos Santos, J. L., Chin, C. M., Krettli, A. U., & Peccinini, R. G. (2014). Evaluation of Antimalarial Activity and Toxicity of a New Primaquine Prodrug. *PLoS ONE*, *9*(8), e105217. https://doi.org/10.1371/journal.pone.0105217

Galappaththy, G. N., Tharyan, P., & Kirubakaran, R. (2013). Primaquine for preventing relapse in people with *Plasmodium vivax* malaria treated with chloroquine. *Cochrane Database of Systematic Reviews*. https://doi.org/10.1002/14651858.CD004389.pub3

Jittamala, P., Pukrittayakamee, S., Ashley, E. A., Nosten, F., Hanboonkunupakarn, B., Lee, S. J., Thana, P., Chairat, K., Blessborn, D., Panapipat, S., White, N. J., Day, N. P. J., & Tarningb, J. (2015). Pharmacokinetic interactions between primaquine and pyronaridine-artesunate in healthy adult Thai subjects. *Antimicrobial Agents and Chemotherapy*, *59*(1), 505–513. https://doi.org/10.1128/AAC.03829-14

Li, Q., O'Neil, M., Xie, L., Caridha, D., Zeng, Q., Zhang, J., Pybus, B., Hickman, M., & Melendez, V. (2014). Assessment of the prophylactic activity and pharmacokinetic profile of oral tafenoquine compared to primaquine for inhibition of liver stage malaria infections. *Malaria Journal*, *13*(1), 141. https://doi.org/10.1186/1475-2875-13-141

Milligan, R., Daher, A., Villanueva, G., Bergman, H., & Graves, P. M. (2020). Primaquine alternative dosing schedules for preventing malaria relapse in people with *Plasmodium vivax*. *Cochrane Database of Systematic Reviews*. https://doi.org/10.1002/14651858.CD012656.pub3

Moein, M. M., El Beqqali, A., & Abdel-Rehim, M. (2017). Bioanalytical method development and validation: Critical concepts and strategies. *Journal of Chromatography B*, *1043*, 3–11. https://doi.org/10.1016/j.jchromb.2016.09.028

PRIMAQUINE PHOSPHATE. (n.d.). Https://Lktlabs.Com/Product/Primaquine-Phosphate/#:~:Text=Soluble%20in%20water%20(66%20mg%2FmL).

Singh, K. K., & Vingkar, S. K. (2008). Formulation, antimalarial activity and biodistribution of oral lipid nanoemulsion of primaquine. *International Journal of Pharmaceutics*, *347*(1–2), 136–143. https://doi.org/10.1016/j.ijpharm.2007.06.035

Sloat, B. R., Sandoval, M. A., Li, D., Chung, W.-G., Lansakara-P, D. S. P., Proteau, P. J., Kiguchi, K., DiGiovanni, J., & Cui, Z. (2011). In vitro and in vivo anti-tumor activities of a gemcitabine derivative carried by nanoparticles. *International Journal of Pharmaceutics*, *409*(1–2), 278–288. https://doi.org/10.1016/j.ijpharm.2011.02.037

Waters, N. C., & Edstein, M. D. (2011). 8-Aminoquinolines: Primaquine and

Tafenoquine. In Treatment and Prevention of Malaria (pp. 69–94). Springer Basel. https://doi.org/10.1007/978-3-0346-0480-2_4

Chapter 3: Development and evaluation of artemether loaded polymeric nanorods for enhanced antimalarial effect

3.1 Introduction

Recently, particle shape has been recognized as an important parameter to design the nanocarriers for site-specific drug delivery. The *in vivo* journey of nonspherical nanocarriers largely depends upon the shape and the dimensions of the particle (Jindal, 2017). Nanocarriers, based on the particle shape, have shown a significant difference in several biological processes including phagocytosis (Champion & Mitragotri, 2009), cellular uptake mechanism and kinetics (Jurney et al., 2017), particle-cell interaction (Dasgupta et al., 2014), intracellular distribution of the particles (Yoo et al., 2010), margination of the particles in the blood vessels (Jurney et al., 2017) and tissue distribution of particles (Zhu et al., 2019). Moreover, the impact of particle shape on the cytotoxicity and *in vivo* antitumor efficacy of anticancer agents have been extensively investigated (L. Wang et al., 2019). It has also been reported that the nonspherical nanocarriers (needle-shaped) showed improved cytoplasmic delivery of siRNA as compared to its spherical counterpart (Kolhar et al., 2011).

The significant impact of the nanocarrier geometry on the *in vivo* performance of the nanoparticles directed the researchers towards the exploitation of methods for the fabrication of nonspherical nanoparticles. Several techniques including PRINT® (Rolland et al., 2005), microfluidics (Dendukuri et al., 2005), modified nanoprecipitation (Jindal & Devarajan, 2015), solvent evaporation (Zhang et al., 2021), sol-gel technique (Shukla & Seal, 2004), co-precipitation (Aphesteguy et al., 2015), template assembly (Mathaes et al., 2015), self-assembly (Mhatre & Sodha, 2019) and solvent moulding methods (Caldorera-Moore et al., 2010) have been reported for the design of nonspherical nanoparticles of varied geometries.

Ho et. al. reported the fabrication of ellipsoidal shaped polystyrene-based micro- and nanoparticles of different aspect ratio (AR) using the film stretching method (Ho et al., 1993). Later, Champion et. al. also used the same method to prepare polystyrene-based nonspherical micro- and nanoparticles of more than 20 different shapes and sizes ranging from 60 nm to 30 μm (Champion et al., 2007). In another study, Palazzo et. al. reported the fabrication of elongated chitosan coated poly(alkylcyanoacrylate) nanoparticles by mechanical stretching of water-soluble film (Palazzo et al., 2017). Although, the film stretching method has been investigated for the fabrication of polystyrene-based nonspherical nanoparticles, yet there are

very few reports present on the fabrication of biodegradable polymer-based nonspherical nanoparticles. Cao et. al. reported fabrication of functionalized biodegradable poly(lactic-co-glycolic acid) (PLGA) nanorods of the dimensions 380 x 100 (nm) with AR of 4 using the film stretching method (Cao et al., 2019). In another study, Castoldi et al. prepared drug-loaded functionalized PLGA nanorods with an AR of 2.6. They observed significantly enhanced intracellular inhibition of bacteria by nanorods as compared to nanospheres (Castoldi et al., 2019). To enable successful translation of the nanocarriers from lab to clinic, fabrication of nonspherical nanoparticles using biodegradable polymers is extremely important. To the best of our knowledge, biodegradable polymer based nonspherical nanoparticles encapsulating antimalarial drugs have not been attempted yet.

Therefore, the objective of the present study was the preparation and evaluation of artemether-loaded PLGA based nanorods by mechanical stretching of nanospheres. In the present study, artemether-loaded PLGA nanospheres were prepared by the standard nanoprecipitation method and loaded into the polyvinyl alcohol (PVA) film. The nanosphere loaded film was then stretched using an *in-house* fabricated film stretching apparatus to form nanorods by mechanical stretching of nanospheres. The influence of process parameters and material related properties on the AR of nanorods was investigated. The nanorods were further evaluated for *in vitro* release, cytotoxicity, and hemolysis.

3.2 Materials and methods

3.2.1 Materials

Artemether (>98.0%) was purchased from Tokyo Chemical Industry Co. Ltd. (Tokyo, Japan). Poly(lactic-co-glycolic) acid (PLGA) (50:50, MW 30,000- 60,000) and (75:25, MW 4000-15,000), polyvinyl alcohol (PVA, MW 9000- 10,000) were purchased from Sigma-Aldrich Chemicals Company (Missouri, United States). Glycerol was purchased from S D Fine-Chem Ltd (Mumbai, India). Silicon oil was purchased from Rankem™ (Bangalore, India). Trehalose was purchased from Spectrochem (Mumbai, India). Emplura® grade acetone was procured from Merck Life Science Pvt. Ltd. (Mumbai, India). Water was obtained from Milli-Q system (Millipore GmbH, Germany). All other chemicals, solvents, and reagents utilized were either HPLC or analytical grade.

3.2.2 Methods

3.2.2.1 Preparation of artemether loaded PLGA nanospheres

Artemether loaded PLGA nanospheres were prepared by the standard nanoprecipitation method. Briefly, PLGA (50:50, MW 30,000- 60,000) or (75:25, MW 4000- 15,000) (75mg)

and artemether (5mg or 10mg) were dissolved in acetone (5-15ml) to prepare the organic phase. The aqueous phase was prepared by dissolving the PVA (molecular weight 9000- 10,000) (0.25-1% w/v) in Milli-Q water at 65ºC. The organic phase was added drop-wise to the aqueous phase under constant stirring (400rpm). Thereafter, the organic phase was evaporated using a rotary vacuum evaporator (Buchi Rotavapor, Switzerland) at 40ºC under reduced pressure. After the evaporation of the organic phase, the aqueous dispersion was centrifuged at 20,000rpm for 40min to separate the artemether loaded PLGA nanospheres. The obtained pellet was redispersed in 1 ml of Milli-Q water by sonication. Nanospheres were characterized for particle size, polydispersity index (PDI), % entrapment efficiency, scanning electron microscopy and % drug loading. The artemether loaded PLGA nanospheres were freeze-dried using trehalose (10% w/v) as a cryoprotectant and stored at 4 ºC until further use.

3.2.2.2 Preparation of artemether loaded PLGA nanorods

Artemether loaded PLGA nanorods were prepared as reported previously by Champion et. al. with modification (Champion et al., 2007). Briefly, a film-forming solution was prepared by dissolving PVA (5% w/v) and glycerol (2.5% w/v) in Milli-Q water. Thereafter, 1 ml of aqueous dispersion of artemether loaded PLGA nanospheres (equivalent to 10 mg of artemether) prepared from (50:50, MW 30,000- 60,000) or (75:25, MW 4000- 15,000) was added to the above film-forming solution (10ml) under stirring which was then added to a 6 x 6 (cm) glass mould and dried at room temperature for 24h to form the artemether loaded PLGA nanospheres embedded polymeric film. The film was stretched by using an *in-house* fabricated film stretching apparatus (fig. 3.1.) in one dimension at the rate of 10mm/min in acetone or silicon oil (65ºC). In the case of acetone, the film was immersed in acetone for 15min, removed, and stretched in the air. While in case of heat stretching, the film was immersed in hot oil, for 15 min and stretched while still in the oil. The extent of stretching was varied from 2- to 4-fold of the initial length of the film. After stretching, the film was removed from the apparatus and dissolved in Mill-Q-water. The particles were washed with water to remove the PVA absorbed onto the particle surface and separated by centrifugation. The particles were freeze-dried and stored at 4ºC until further use (Bhide & Jindal, 2021).

3.2.2.3 Characterization of nanospheres and nanorods

A) Particle size and PDI

The aqueous nanodispersion of artemether loaded nanospheres was centrifuged at 20,000 rpm for 40 min (Sorvall 150+ Micro Ultracentrifuge, United States). The supernatant was removed, and the pellet was re-dispersed in Milli-Q water to get a dispersion of 83.7 mg/ml

concentration. The particle size and PDI was determined using Malvern Nano ZS (Malvern Instruments Ltd. UK) after appropriate dilution of the re-dispersed sample.

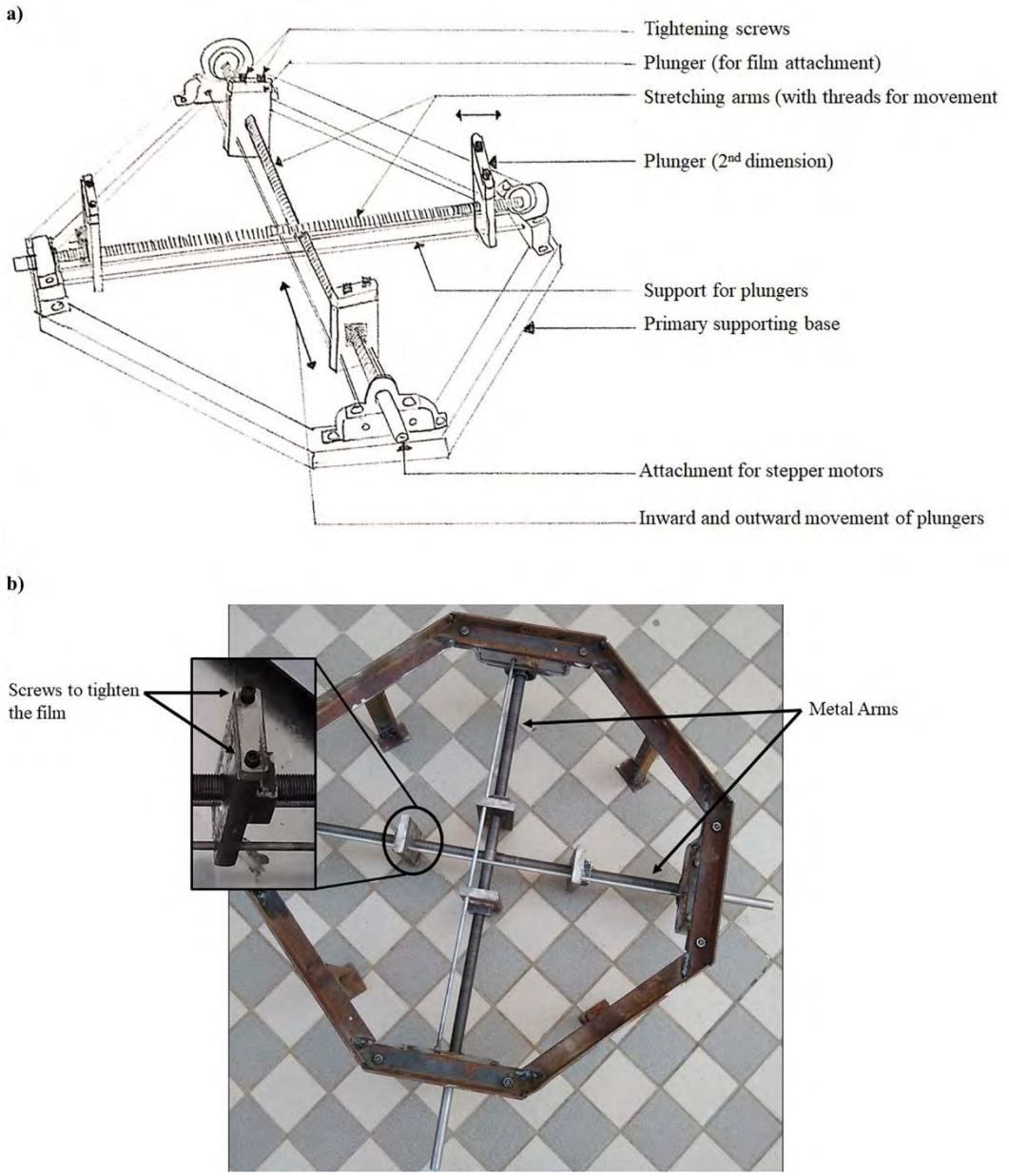

Fig. 3.1. *In house* fabricated film stretching apparatus a) Schematic representation of the apparatus b) Image acquired by digital camera.

B) % Entrapment efficiency (EE)

The supernatant obtained after centrifugation of the nanoformulation was analysed by the RP-HPLC method reported previously by our group (Bhide et al., 2020). %EE was calculated using equation (1)

$$\%\ EE\ = \frac{Total\ quantity\ of\ drug\ used - Drug\ content\ in\ the\ supernatant}{Total\ quantity\ of\ drug\ used} x\ 100 \quad \ldots\ldots\ldots\ldots\ldots(1)$$

C) % Drug loading

The drug loading is calculated by determining the entrapped drug in the formulation. It can be expressed as the mass ratio of artemether to the artemether loaded nanospheres (Liu et al., 2020). The % drug loading can be calculated using equation (2)

$$\% DL = \frac{Total\ quantity\ of\ drug\ entrapped}{(Total\ quantity\ of\ drug\ used + Total\ quantity\ of\ polymer\ used)} x\ 100 \ldots\ldots\ldots\ldots (2)$$

D) Drug content

The accurately weighed (10 mg) of the lyophilized nanorods was dispersed in 1 mL of methanol and vortexed and sonicated for 5 min. The dispersion was centrifuged and supernatant was then acid treated and analysed using the RP-HPLC method previously reported by our group (Bhide et al., 2020).

E) Field emission scanning electron microscopy

Aliquot of aqueous dispersion of nanospheres or nanorods was placed onto the coverslip and dried at room temperature. The coverslip was then placed on the metal stub and gold coated for 45 sec by sputter coater (Quorum Technologies Q150TES, East Sussex, England). The coated nanoparticles were then analysed by FEI scanning electron microscope (Hillsboro, Washington) at 20kV high vacuum, with 9.0 as the spot size and the scale set to 300 to 1000 nm.

F) Calculation of shape descriptors of nanorods

Feret diameter, minor Feret diameter, AR, major axis, and minor axis were used as shape descriptors to characterize the nanorods. The shape descriptors were determined from the SEM images of the nanorods using Fiji ImageJ software (Version 1.52p).

G) Feret diameter and minor Feret diameter

Feret diameter is the distance between two parallel tangents drawn perpendicular to the two ends of the particle having maximal distance from each other. While, in case of minor Feret diameter, the distance calculated is between two endpoints having minimal distance from each other (Baybay et al., 2020; Yu & Hancock, 2008). It is primarily calculated for asymmetrical particles. Feret diameter and minor Feret diameter of a nanorod are depicted schematically in fig. 3.2.

H) Major axis, minor axis and aspect ratio

Major axis is the distance of the segment connecting the farthest points of the particle comprising its maximum length. While minor axis is the distance of the segment connecting the closest points of the particle. Aspect ratio is the ratio of the major axis to the minor axis of

the particle. Major axis and minor axis of a nanorod are depicted schematically in fig. 3.2.

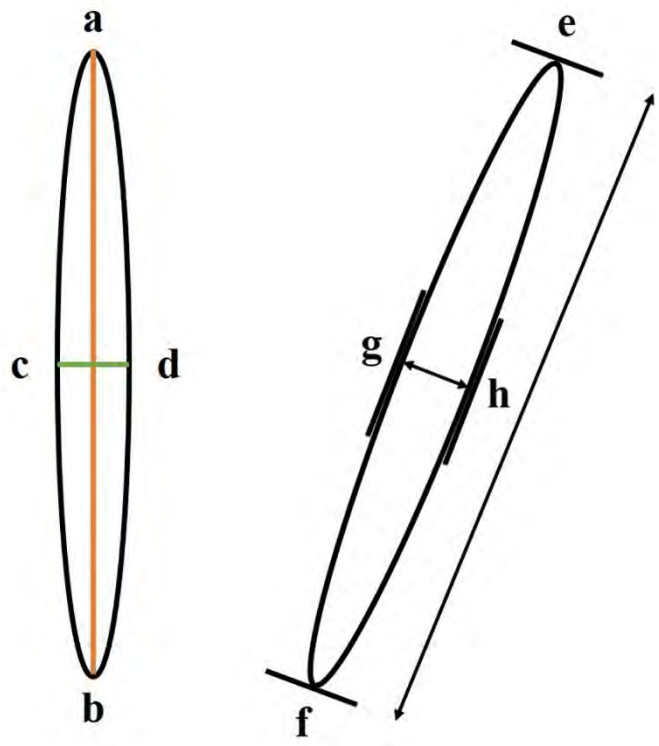

Fig. 3.2. Schematic representation of the shape descriptors used for the characterization of a rod-shaped particle. Segment a-b and c-d represent the major axis and minor axis of the nanorod, respectively. Distance between point e to f and point g to h represent the Feret diameter and minor Feret diameter.

I) Size distribution of nanorods

The percentage frequency of distribution of major and minor axis of nanorods was determined and data was represented in the form of size-frequency distribution curve by plotting percentage frequencies of various particles against particle size. The D_{10}, D_{50} and D_{90} values were calculated from size-frequency distribution curve.

3.2.2.4 Release study

In vitro release of artemether from nanospheres and nanorods was determined using the dialysis bag method as described previously with modifications (Raina et al., 2017). Nanospheres or nanorods (equivalent to 5 mg of artemether) were dispersed in 2 ml of Milli-Q water and was filled in a dialysis bag (SnakeSkin^{TM}, 3.5K MWCO, Thermo Scientific, USA). The dialysis bag was immersed in 50 mL of 10 mM phosphate buffer pH 7.4 with sodium lauryl sulphate (SLS) (1% w/v) for 72 h under stirring (100 rpm) at 37º C. SLS was used to maintain the sink conditions during the release studies as reported previously by the researchers.(Belew et al., 2020; Pawar et al., 2016; Shende et al., 2017). 2 mL of sample was withdrawn at predetermined time points (0.25, 0.5, 1, 2, 4, 6, 12, 24, 48, and 72 h) and was replaced with an equal amount

of fresh media. The samples were analysed by HPLC after pre-column acid treatment as reported previously by our group (Bhide et al., 2020). The study was carried out in triplicate.

3.2.2.5 Cytotoxicity study

THP-1 suspension cell line was cultured in RPMI 1640 media with 10% (foetal bovine serum) FBS and gentamycin (0.005%) in a T-75 culture flask till an optimal cell count was obtained. THP-1 cells were seeded in a 96-well plate with phorbol 12-myristate 13-acetate (PMA) to differentiate it at a count of 10,000 cells per well. The cells were incubated with artemether, nanospheres (artemether equivalent to 0.001, 0.01, 0.1, 1, 10, 100, and 200 µg/mL), nanorods (artemether equivalent to 0.001, 0.01, 0.1, 1, 10, 100, and 200 µg/mL), blank nanospheres and blank nanorods for 24 h. Then, 100 µL of 3-(4,5-dimethylthiazol-2-yl)-2,5-diphenyl tetrazolium bromide (MTT) solution (0.5 µg/mL) was added to each well and incubated for 4 h. After 4 h, the MTT solution was replaced by DMSO and the absorbance was recorded at 540nm using an Epoch ELISA plate reader (BioTek, Winooski, United States). % cell viability was calculated by using the equation (3)

$$\%\ cell\ viability = \frac{(absorbance\ of\ sample - absorbance\ of\ blank)}{(absorbance\ of\ control - absorbance\ of\ blank)}\ x\ 100 \quad \ldots\ldots\ldots\ldots\ (3)$$

3.2.2.6 Hemolysis study

In vitro hemolysis study was carried out as reported previously by our group (Jindal et al., 2020). Blood was collected from Wistar rats in microcentrifuge tubes containing Ethylenediamine tetraacetic acid (EDTA) (10% w/v). Red blood cells (RBCs) were collected after centrifugation of blood at 1000 rpm for 5 min and washed thrice with normal saline (0.9 % w/v sodium chloride). 5µL of the packed erythrocytes were treated with 95 µL of the nanospheres (artemether equivalent to 0.001, 0.01, 0.1, 1, 10, 100, and 200 µg/mL) or nanorods (artemether equivalent to 0.001, 0.01, 0.1, 1, 10, 100, and 200 µg/mL). Thereafter, the samples were centrifuged at 1000 rpm for 5 min and the supernatant was analysed at 540 nm using an Epoch ELISA plate reader (BioTek, Winooski, United States). Normal saline and Milli-Q water were used as a negative control and positive control respectively during the study. % haemolysis was calculated using the equation (4)

$$\%\ hemolysis = \frac{absorbance\ of\ the\ sample}{absorbance\ of\ the\ positive\ control}\ x\ 100 \quad \ldots\ldots\ldots\ldots\ (4)$$

3.2.2.7 Interaction of artemether-loaded poly(lactic-co-glycolic) acid nanorods with rat erythrocytes

Interaction of polymeric nanorods with erythrocytes isolated from rat blood were studied using scanning electron microscopy and confocal imaging techniques.

A. Isolation of erythrocytes from the rat blood

Fresh blood (200µL) was collected from the retro-orbital plexus and erythrocytes were isolated from the blood by centrifugation at 1000 rpm for 5 min. Thereafter, isolated erythrocytes were washed thrice with normal saline and 5 µL of it was redispersed in 1 mL normal saline.

B. Scanning electron microscopy

10µL of freshly prepared artemether nanospheres or artemether nanorods were diluted 640 times by normal saline. Thereafter, to the 500µL of the above diluted nanodispersion, 500µL of resuspended erythrocytes and 500µL of 1 % v/v glutaraldehyde solution were added, vortexed and incubated for 10min at room temperature. After incubation, aliquot of above solution was spread on a cover slip and dried at 37ºC. Then, the sample was chromium coated for 45sec by placing it on a metal stub in a sputter coater (Quorum Technologies Q150TES, East Sussex, England). The images were acquired using a FEI scanning electron microscope (Hillsboro, Washington).

3.2.2.8 Confocal microscopy

Coumarin-6 (C-6) loaded nanospheres and nanorods were used as a surrogate to study the interaction of nanoformulation with erythrocytes using confocal microscopy. 10µL of freshly prepared C-6 nanospheres or C-6 nanorods dispersion were diluted 640 times in normal saline followed by incubation with the erythrocytes. After incubation with erythrocytes, the samples were fixed in 1 % w/v glutaraldehyde solution and spread on glass slide and dried at 4ºC followed by analysis laser scanning confocal microscope (ZEISS LSM 880, Axio Observer). The images were processed and analyzed with ZEN 2.3 software.

3.2.2.9 Pharmacokinetic study

Pharmacokinetics of artemether nanospheres and artemether nanorods were studied in Sprague Dawley rats (250 ± 50 g) after intravenous administration. The animal study protocol was approved by the Institutional Animal Ethics Committee of Birla Institute of Technology and Science, Pilani campus, Pilani (Protocol no.: IAEC/RES/26/04/Rev-1/29/15). The animals were fed with regular food and water *ad libitum* and were subjected to 12 h light-dark cycle before the study. During the study, the animals were divided into two groups (n = 4). Artemether-loaded nanospheres and artemether-loaded nanorods (dose: 1.2 mg/kg) were administered to rats in group I and group II, respectively by intravenous route. Thereafter, 300 µL of blood was withdrawn through the retro-orbital plexus of the rat at 0, 0.08, 0.25, 0.5, 1, 2, 4, 6, 12 and 24 h in a microcentrifuge tube containing 20 µL of 10 % w/v EDTA. The blood

was centrifuged at 10,000 rpm for 10 min, the plasma was separated and stored at -23 ºC until further analysis. 95µL of plasma was spiked with 5µL of internal standard (1 µg/mL curcumin). artemether and curcumin were separated from plasma by liquid-liquid extraction using dichloromethane (1mL) as extracting solvent. The samples were vortexed and dichloromethane was evaporated at room temperature. Then, the samples were reconstituted using 100µL of mobile phase. artemether was analysed using the developed LC-MS-MS bioanalytical method.

3.2.2.10 Biodistribution study

DiR nanospheres and DiR nanorods were used as a surrogate to study *in vivo* biodistribution in BALB/c mice after intravenous administration using PerkinElmer IVIS Lumina Series III (Waltham, United States). The procedures and protocols for the study were approved by the Institutional Animal Ethics Committee at National Institute for Research in Reproductive Health, ICMR, Parel, Mumbai (Protocol no.: IAEC/14/19). DiR loaded nanospheres or nanorods was administered intravenously through the tail vein of mice. Whole-body imaging of mice was carried out at different time points including 0.5, 1, 2, 4, 8 and 24 h post intravenous administration of nanospheres and nanorods. After 24 h, the animals were sacrificed and the vital organs including brain, heart, kidneys, liver, lungs, female reproductive organs (F.R.O.) and spleen were isolated. The fluorescence intensity due to the presence of DIR in different organs was determined and the % injected dose in each organ was calculated.

3.2.2.11 *In vitro* schizont maturation inhibition assay against Plasmodium berghei (ANKA)

The *in vitro* anti-plasmodial activity of artemether, artemether-loaded nanospheres and artemether-loaded nanorods was determined by the schizont maturation inhibition assay as reported previously with modification (*World Health Organization (WHO). Geneva. (2001) CTD/MAL/ 97, 20.*, n.d.).

The stock solution of artemether was prepared in DMSO and the formulations were prepared in PBS. These stock solutions were further diluted in incomplete medium for *in vitro* studies. Short-term *in vitro* culture of *P. berghei* ANKA blood stages was maintained using the method as reported by Trager and Jensen with modification (1976) (*Trager, W., & Jensen, J. B. (1976). Human Malaria Parasites in Continuous Culture. Science (New York, N.Y.), 193(4254), 673–675.*, n.d.).

RPMI-1640 (GIBCO) supplemented with sodium bicarbonate, antibiotics [gentamicin (50 µg/ml), penicillin (100 µg/ml) and streptomycin (100 µg/ml)] and foetal bovine serum (20 %) was used for the study. The parasite was treated with artemether, artemether-loaded

nanospheres and artemether-loaded nanorods (artemether equivalent to 2, 4 and 8 µg/ml), blank nanospheres and blank nanorods in a 24 well plate and incubated at 37 ºC for 24 h. The % inhibition of schizont maturation was calculated using the equation (1)

$$\%\ inhibition = 100 - \frac{Number\ of\ schizonts\ in\ drug\ treated\ well}{Number\ of\ schizonts\ in\ control\ well}\ X\ 100 \quad \text{.....(1)}$$

3.2.2.12 Antimalarial efficacy of nanoformulations in *P. berghei* infected mice

The procedures and protocols for the study were approved by the Institutional Animal Ethics Committee (Protocol no.: PU/45/99/CPCSEA/IAEC/2021/580) at Panjab University, Chandigarh. Female BALB/c mice (6 – 8 weeks) were used for the experiment. Animals were housed at room temperature (24 ºC ± 1 ºC) and were given food and water *ad libitum*. Erythrocyte stage of the parasite was maintained in donor (BALB/c) mice with high parasitaemia (5 - 20 %). The mice were divided into 7 groups (n = 6). The animals were induced parasitaemia by injecting 1.0 x 10^7 *Plasmodium*-infected erythrocytes *i.p.* (5 - 20 % parasitemia). The animals were divided into groups on the basis of treatment formulation, as follows. Group I (negative control), Group II (vehicle control; 0.9 % normal saline), Group III (artemether free drug), Group IV (blank nanospheres), Group V (artemether-loaded nanospheres), Group VI (Blank nanorods) and Group VII (artemether-loaded nanorods). The stock solutions of all the drugs were diluted in 0.9 % normal saline for dosing. After 24 h of parasitaemia induction, blank and artemether-loaded nano formulations were administered intravenously at the dose of 4.8 mg/kg while in the case of Group III, the free drug artemether (4.8 mg/kg) was administered orally as suspension. The treatment was continued for 4 consecutive days. 20 µL of blood was collected from the tail vein on predetermined time points (day 0, day 5, day 7, day 10, day 14 and day 21) and thin smears were prepared from it. The smears were air-dried, fixed with methanol and finally stained with Giemsa stain. The average parasitemia of each group of mice was used to calculate the percentage reduction of parasitemia (% chemosuppression) using the following equation (2)

$$(A - B/A) \times 100 \quad \text{.....(2)}$$

where A is the mean parasitemia in the negative control group and B is the parasitemia of each treated group. The mean survival time [MST] was used to assess the efficacy of the nanoformulations. Mortality was checked regularly and the number of days from the time of inoculation of the parasite up to death was recorded for each mouse within the treatment and control groups all through the follow-up period of 28 days. Results of parasitaemia and changes in survival time were analyzed using GraphPad Prism software version 9.3.1. for each

treatment group. Two-way ANOVA and Tukey post hoc tests were used to analyze differences between groups and subgroups, within groups, respectively. Differences were considered as statistically significant in case the value is $p < 0.05$ (*Knight, D. J., & Peters. W. (1980). The Antimalarial Activity of N-Benzyloxydihydrotriazines. I. The Activity of Clociguanil (BRL 50216) against Rodent Malaria, and Studies on Its Mode of Action. Annals of Tropical Medicine and Parasitology, 74(4):393–404*, n.d.).

Statistical Analysis

The data was analyzed using a student t-test or ANOVA with $p < 0.05$ as a minimal level of significance. All the results expressed in mean ± standard deviation.

3.3 Results

3.3.1 Preparation of nanospheres

Artemether loaded PLGA nanospheres were prepared by the nanoprecipitation method. Particle size, PDI, zeta potential, and % EE of nanospheres obtained after varying different parameters are presented in table 3.1. Particle size, PDI, zeta potential, and % EE were found to be affected by the ratio of organic to aqueous phase, surfactant concentration, and amount of drug used during the preparation of nanospheres. There was an increase in particle size observed when the ratio of aqueous to organic phase was increased from 1:2 to 1:3. Similarly, when the drug amount was increased from 5mg to 10mg, particle size was increased from 196nm to 214nm. Furthermore, the effect of surfactant concentration on particle size was found to be dependent upon the amount of drug used in the study. Surprisingly, at lower drug concentration (5mg), an increase in particle size was observed with an increase in surfactant concentration, while, in the case of 10mg drug, particle size was decreased from 245nm to 196nm when surfactant concentration was increased. Moreover, an increase in organic phase to aqueous phase ratio resulted in narrow particle size distribution with a PDI of 0.06 ± 0.01. The type of the polymer (50:50, MW 30,000- 60,000) and (75:25, MW 4000- 15,000) did not seem to play a role on the size or surface charge of the nanoparticles. In all the cases, the zeta potential was found between -1mV and -8mV and the % EE was found to be more than 70%.

3.3.2 Preparation of nanorods

PLGA nanospheres of diameter 129.33 ± 3.64nm were used to obtain nanorods by mechanical stretching after embedded into the PVA film. The film was kept in acetone for 15min, removed, and stretched in air to obtain nanorods. The effect of various parameters including film thickness (100µm vs 150µm), the ratio of lactide to glycolide (50:50 vs 75:25), extent of

stretching (2x vs 4x), and liquefaction method (acetone vs heat) on the dimensions of the nanorods including major axis, minor axis, AR, Feret diameter and minor Feret diameter are presented in table 3.2.

Size-frequency distribution curve of major and minor axis of nanorods obtained from stretching of nanospheres after solvent treatment are presented in figure 3.3 (a-d) and figure 3.3 (e-h) respectively. SEM images of nanospheres and nanorods obtained from mechanical stretching of nanospheres after solvent treatment are presented in figure 3.3 (i-m). AR of nanorods was found to be 3.82 ± 0.82 when nanospheres were stretched in a thin film (100 µm) 4x of its initial length. While in the case of thick film (150µm), nanorods with AR 5.13 ± 0.85 were produced. The particles were observed to be uniformly elongated in both the cases ($D_{90\ major}$ = 340nm and $D_{90\ minor}$ = 75nm for 100 µm film and $D_{90\ major}$ = 395nm and $D_{90\ minor}$ = 80nm for 150µm film). Moreover, it has been observed that as the film thickness was increased, the major axes were found to be increased (1.26-fold) while the minor axis was decreased (1.05-fold). Thick film produced nanorods with an aspect ratio higher than the nanorods obtained from the thin film. In general, a solid body deforms when it is subjected an opposing force (Terzopoulos & Fleischer, 1988). In this method, it was expected that deformation of the particles could be the function of stress experienced by the nanospheres during stretching of the polymeric film. Under stress conditions, the change in geometry of the particles was opposed by the cohesive forces present in the PLGA. When the stress on the particles overcome the cohesive forces, nanospheres transform into nanorods. Treatment of PLGA nanospheres embedded PVA film with solvent or heat could have resulted in a decrease in the cohesive forces of the PLGA, which could have ultimately resulted in the elongation of nanospheres. To produce the same amount of strain, thick film required higher stress than the thin film which could have led to the generation of nanorods with high AR from the thick film. However, Champion et. al. reported that AR of the rod-shaped polystyrene particles was decreased with an increase in the film thickness (Champion et al., 2007). The difference in the findings could be due to the difference in the cohesive forces and applied stress during stretching. There was an almost 2-fold increase in the AR and major axis observed with a 2-fold increase in extent of stretching. However, the minor axis of nanorods was not changed with an increase in stretching extent. During the deformation, the stress experienced by the nanospheres was directly proportional to the strain produced in the PVA film by stretching. The increase in the major axis with the preserving action of the minor axis could be due to the higher stress on the nanospheres in one direction during 4x stretching.

Table 3.1. Particle size, PDI, %EE, %DL and zeta potential of the artemether loaded nanospheres

Composition					Particle size (nm)	PDI	Zeta potential (mV)	%EE	% DL
Artemether (mg)	PLGA (mg)	PVA (mg)	Acetone (mL)	Aqueous phase (mL)					
5	75	75	5	15	190.2 ± 18.0	0.06 ± 0.01	-8.0 ± 0.58	78.5 ± 1.8	4.9 ± 0.1
5	75	150	5	15	214.3 ± 6.2	0.238	-1.8 ± 0.22	80.0 ± 0.1	5.0 ± 0.0
10	75	300	10	30	196.8 ± 1.1	0.214	-2.2 ± 0.16	78.3 ± 0.0	9.2 ± 0.0
10	75	150	10	30	245.5 ± 44.5	0.183	-3.2 ± 0.24	80.6 ± 0.4	9.5 ± 0.0
10	75	150	15	30	129.3 ± 3.6	0.06 ± 0.01	-7.4 ± 0.69	86.9 ± 0.2	10.2 ± 0.0

Each value presented as mean ± SD, n=3

Table 3.2. Physicochemical parameters of nanorods obtained by varying the process conditions

Process conditions					Major axis (nm)	Minor axis (nm)	AR	Feret's diameter (nm)	Minor Feret's diameter (nm)	Drug content (µg/mg)
Film thickness (µm)	PLGA type (lactide: glycolide)	Extent of stretching	Liquefaction method	Incubation period (min)						
100	75:25	4x	Acetone	15	234.1 ± 61.7	61.3 ± 8.7	3.8 ± 0.8	237.2 ± 61.9	77.8 ± 13.3	1.8
150	75:25	4x	Acetone	15	295.1 ± 64.9	58.1 ± 12.0	5.1 ± 0.8	265.4 ± 66.3	59.6 ± 15.2	1.4
100	50:50	4x	Acetone	15	211.3 ± 44.1	61.1 ± 11.6	3.5 ± 0.7	198.1 ± 37.5	67.7 ± 10.4	2.6
100	75:25	2x	Acetone	15	128.1 ± 23.1	61.5 ± 10.3	2.1 ± 0.3	127.5 ± 22.9	61.3 ± 10.4	1.6
100	75:25	4x	Heat*	5	241.7 ± 76.3	140.1 ± 31.3	1.7 ± 0.3	294.0 ± 85.8	157.6 ± 32.8	0.9
100	75:25	2x	Heat*	15	329.6 ± 79.3	92.2 ± 14.9	3.6 ± 0.7	343.0 ± 79.7	98.9 ± 17.8	0.8
100	75:25	4x	Heat*	15	510.7 ± 114.6	102.0 ± 23.7	5.1 ± 0.9	559.5 ± 102.8	119.3 ± 28.8	3.2

*In case of heat treatment, 65^{o}C temperature was used;

To study the impact of the extent of stretching on the nanorods, the film (100µm) was stretched to 2x and 4x to its initial length. It was observed that the film which was stretched to 2x produced nanorods with an AR = 2.11 ± 0.35, while nanorods with AR = 3.82 ± 0.82 were obtained from the film which was stretched 4x of its initial length ($D_{90\ major}$ = 170nm and $D_{90\ minor}$ = 75nm for 2x stretched film). Moreover, an almost 1.82-fold increase in the major axis of nanorods was obtained when film was stretched 4x as compared to the stretching extent of 2x. However, there was no effect of stretching extent on the minor axis of nanorods observed. Impact of lactide: glycolide ratio in the PLGA on the dimension of nanorods was also studied. Nanospheres prepared using PLGA (lactide: glycolide 50:50 or lactide: glycolide 75:25) were embedded in the film and stretched 4x to the initial length of the film. In both the cases, the AR of nanoparticles was found to be 3.52 ± 0.71 and 3.82 ± 0.82 respectively. ($D_{90\ major}$ = 300nm and $D_{90\ minor}$ = 80nm for PLGA 50:50). Here, the AR of nanorods was not affected by an increase in the hydrophobicity of the polymer. However, there was an increase in the major and minor axis of the nanorods observed. It was reported that PVA formed an interconnected network with the PLGA polymer and hence adhered onto the surface of the nanoparticles (Sahoo et al., 2002). Therefore, it was expected that the PVA interacted with the polymer and led to the formation of nanorods. The viscosity of PLGA 50:50 was reported as 0.55 to 0.75 dL/g while that of PLGA 75:25 was 0.14 to 0.22 dL/g respectively. Since viscosity is considered as the resistance in the deformation of the particles, the higher the viscosity, the lower the deformation, and hence the lower the AR of the nanorods. The lower viscosity of the polymer could have contributed to the higher elongation of the nanorods during stretching (Makadia & Siegel, 2011).

Size-frequency distribution curve of major and minor axis of nanorods obtained from stretching of nanospheres after heat treatment are presented in figure 3.4 (a-c) and figure 3.4 (d-f) respectively SEM images of nanospheres and nanorods obtained from mechanical stretching of nanospheres after heat treatment are presented in figure 3.4 (g-j). Replacing acetone with heat to liquefy the particles also resulted in the formation of nanorods.

Moreover, the incubation time of the film in the oil exerted a significant impact on the shape and dimensions of the particles. Oval-shaped particles with AR = 1.72 ± 0.33 were obtained when the film was incubated for 5min and stretched 4x of its initial length in the oil. While in the case of incubation time of 15min, nanorods of AR = 5.07 ± 0.92 were produced ($D_{90\ major}$ = 355nm and $D_{90\ minor}$ = 195nm for film incubated for 5min and $D_{90\ major}$ = 700nm and $D_{90\ minor}$ = 130nm for film incubated for 15 min). As the incubation time was increased from 5 min to 15

min, particle shape was converted from oval to rods which could be due to the decrease in viscosity of the polymer at a longer incubation time. Also, after 5 min of incubation period, the viscosity of the nanoparticles might not be uniform thus leading to an oval shape. Similar observations were reported by the other researchers (Champion et al., 2007; Yoo & Mitragotri, 2010).

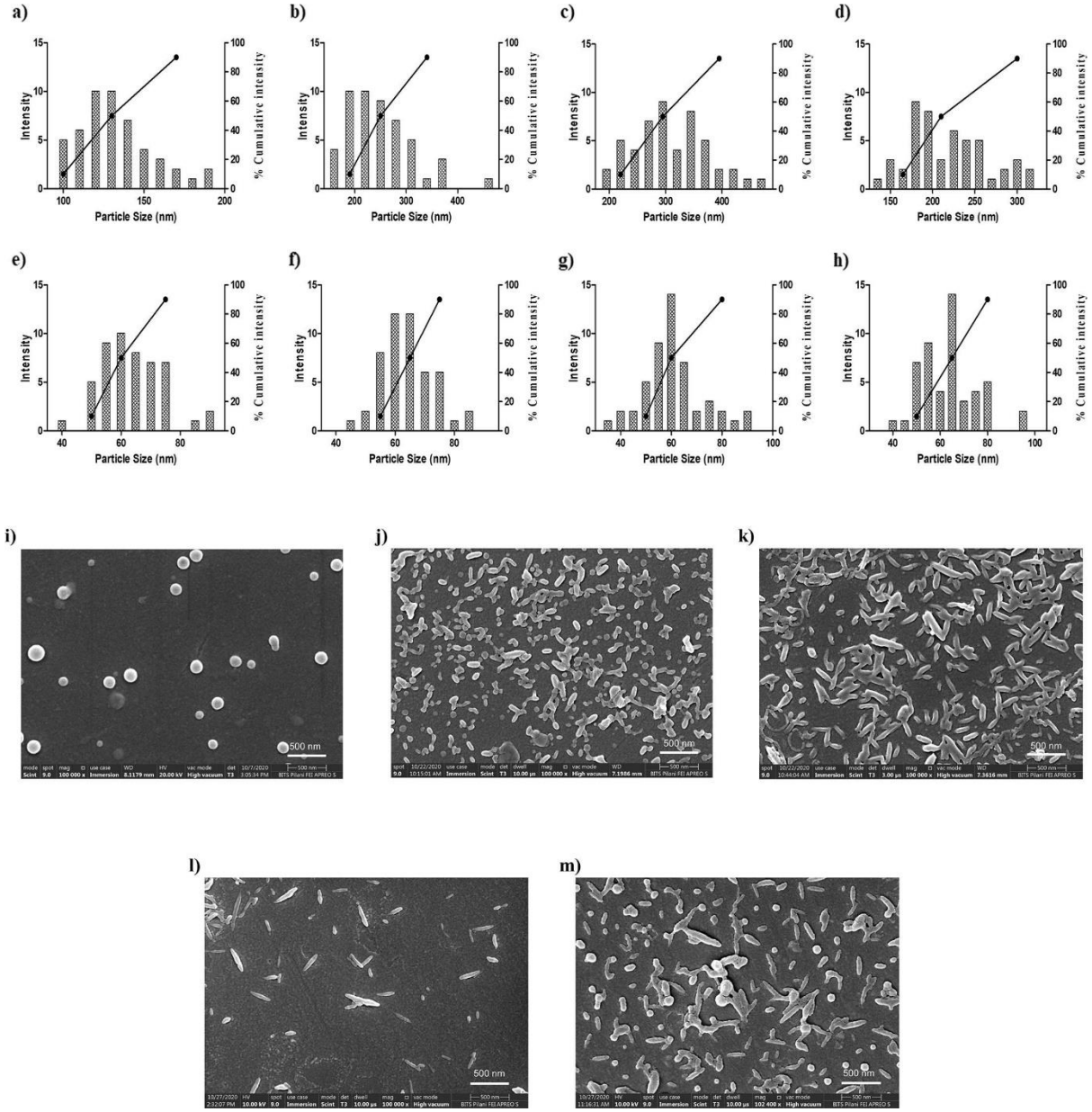

Fig. 3.3. Characterization of size and shape of the nanorods obtained from mechanical stretching of nanospheres after solvent treatment. Size-frequency distribution curves of major axis (a-d), minor axis (e-h) and SEM images (j-m) of nanorods, (i) of nanospheres; a) major axis, e) minor axis and j) SEM image of nanorods (film thickness = 100 µm, L/G ratio = 75: 25, stretching extent = 2x), b) major axis, f) minor axis and k) SEM image of nanorods (film thickness = 100 µm, L/G ratio = 75: 25, stretching extent = 4x), c) major axis, g) minor axis and l) SEM image of nanorods (film thickness = 150 µm, L/G ratio = 75: 25, stretching extent = 4x), d) major axis, h) minor axis and m) SEM image of nanorods (film thickness = 100 µm, L/G ratio = 50: 50, stretching extent = 4x).

Furthermore, AR of nanorods was found to be 3.60 ± 0.75 and 5.07 ± 0.92 when the film was stretched 2x and 4x of its initial length, respectively ($D_{90\ major}$ = 430nm and $D_{90\ minor}$ = 116nm for 2x stretched film). The method of liquefaction of the nanosphere during stretching exerted a significant impact on the AR of nanorods. When acetone is replaced by heat as a method of liquefaction, an almost 1.44-fold increase in the AR of nanorods was observed. The method of liquefaction during stretching produced a significant impact on the dimension of nanorods while the shape of the nanoparticle was not affected. Nanospheres to be stretched can be liquefied at two instances, either before the stretching or after the stretching as reported by Champion et. al. (Champion et al., 2007). Here, the nanospheres are liquefied before the stretching. In case of heat treatment, a significant increase in the major axis, minor axis, and AR of nanorods were observed. This could be due to the difference in the extent of reduction in cohesive forces of nanospheres by solvent and heat during stretching. Heating the film at 65 ºC which is larger than the Tg of PLGA resulted in the conversion of the glassy state to the rubbery state of the polymer. The presence of polymer in the rubbery state at 65 ºC could have contributed significantly to the elongation of particles. In all the cases, the Feret diameter and minor Feret diameter of nanorods were found to be similar to the major axis and minor axis respectively, indicating that the particles obtained from the film stretching method were symmetric in shape.

The drug content was less in the nanorods than nanospheres due to its solubility in acetone and silicon oil. Hence, utilization of a solvent which exhibits affinity for the polymer instead of the drug can lead to minimization of drug loss.

3.3.3 Release study

Fig. 3.5a. represents the *in vitro* release profile of artemether loaded nanospheres and nanorods. A sustained release of artemether was observed from both nanospheres and nanorods. Till 24h, the release of artemether from nanorods was found to be significantly slow ($p < 0.05$) as compared to nanospheres. However, almost 85% drug was found to be released from both nanosphere and nanorods at the end of 72h.

3.3.4 Cytotoxicity study

In vitro cytotoxicity of both artemether loaded nanosphere and nanorods were studied at different concentrations of artemether using THP-1 monocyte cell line. There was no difference observed in % cell viability of THP-1 cell lines treated with artemether, nanospheres, and nanorods at all the concentrations of the drug (Fig. 3.5b.). Furthermore, almost 90% cell viability was found when THP-1 cells were treated with artemether, nanospheres, and nanorods

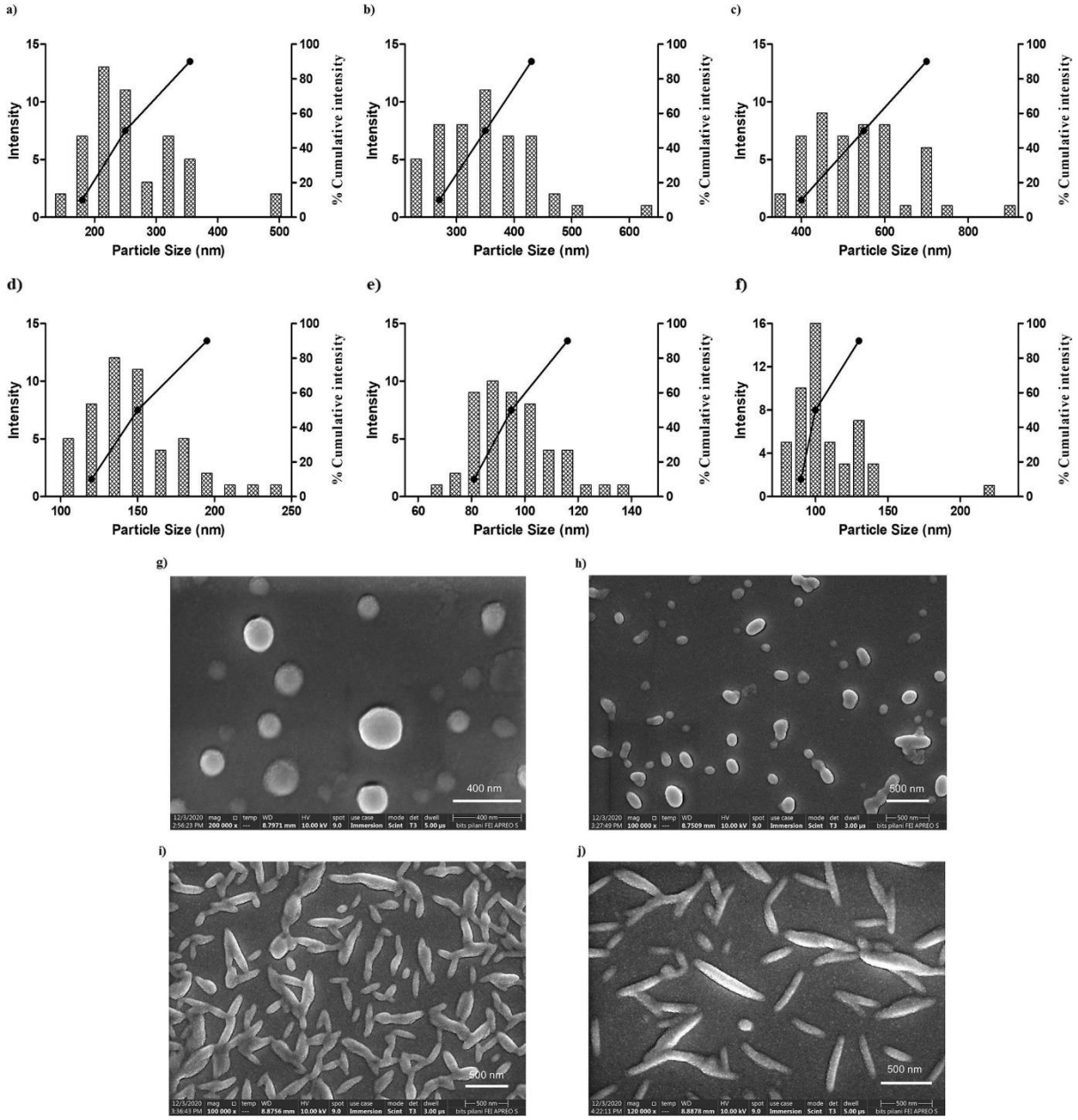

Fig. 3.4. Characterisation of size and shape of the nanorods obtained from mechanical stretching of nanospheres after heat treatment. Size-frequency distribution curves of major axis (a-c), minor axis (d-f) and SEM images (h-j) of nanorods, (g) of nanospheres; a) major axis, d) minor axis and h) SEM image of nanorods (film thickness = 100 µm, L/G ratio = 75: 25, stretching extent = 4x, incubation time = 5 min), b) major axis, e) minor axis and i) SEM image of nanorods (film thickness = 100 µm, L/G ratio = 75: 25, stretching extent = 2x, incubation time = 15 min), c) major axis, f) minor axis and j) SEM image of nanorods (film thickness = 100 µm, L/G ratio = 75: 25, stretching extent = 4x, incubation time = 15 min).

equivalent to 0.001 to 100 µg/mL of artemether. However, at higher artemether concentration (200 µg/mL), a significant decrease in % cell viability was observed when cells were treated with artemether, nanospheres, and nanorods. Furthermore, at a concentration equivalent to 200 µg/mL of artemether, nanorods showed significantly less % cell viability as compared to nanospheres and free drug.

3.3.5 Hemolysis study

In vitro hemolytic potential of nanospheres and nanorods were studied using erythrocytes obtained from rat blood. At all the concentrations of artemether, nanorods showed less hemolysis of red blood cells (RBCs) than the nanospheres (Fig. 3.5c.). However, both nanospheres and nanorods showed less than 10% hemolysis at all concentrations.

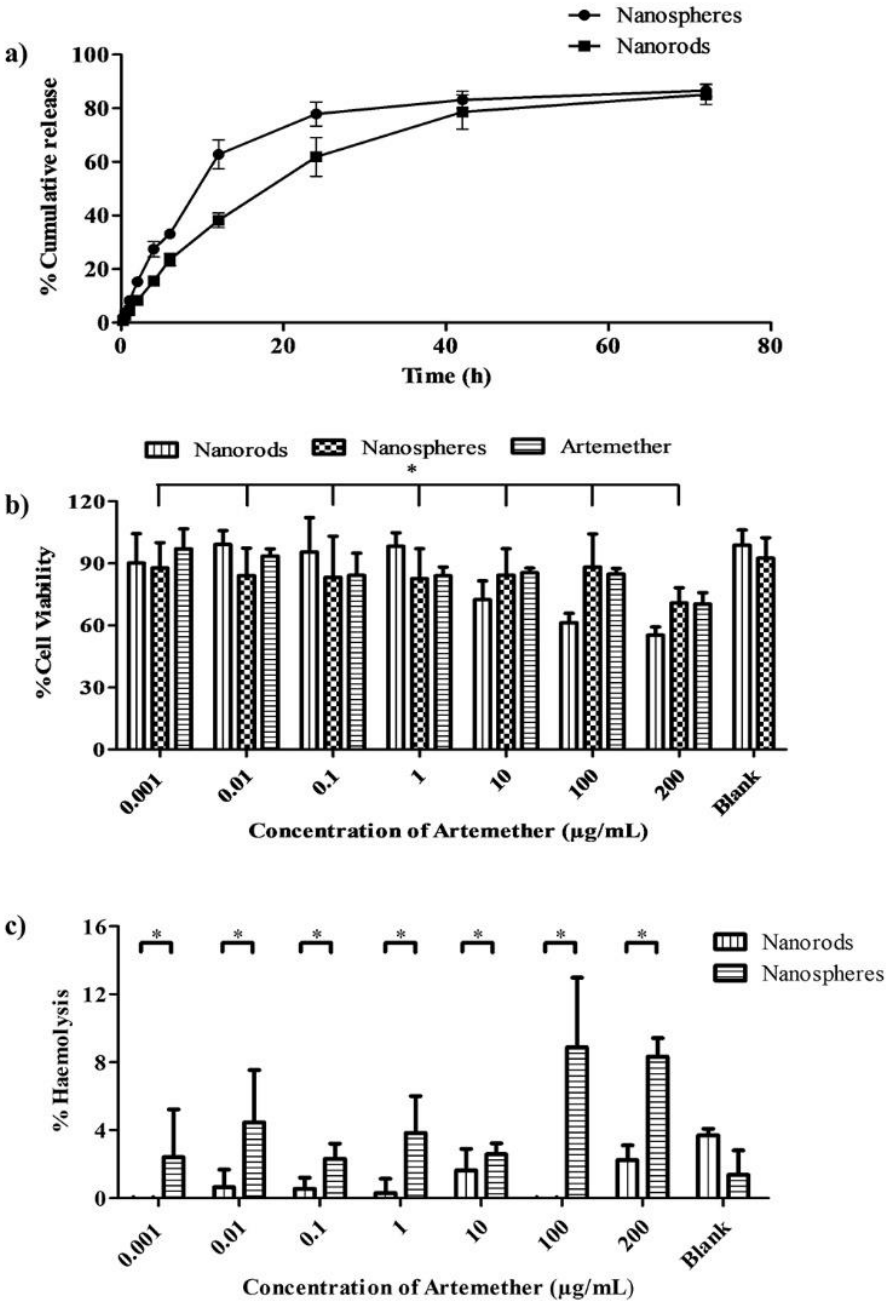

Fig. 3.5. *In vitro* evaluation of nanospheres and nanorods a) *In vitro* release profile of nanosphere and nanorods in 50 ml of 10 mM phosphate buffer pH 7.4 with sodium lauryl sulphate (SLS) (1% w/v) for 72 h under stirring (100 rpm) at 37 C b) % cell viability of artemether loaded nanospheres, artemether loaded nanorods and artemether free drug at different artemether concentrations in THP-1 monocyte cell lines, c) % hemolysis of RBCs obtained from rat blood after treatment with artemether loaded nanospheres, artemether loaded nanorods at different artemether concentrations, Each data represents the mean ± SD; n = 3; * represents $p < 0.05$.

3.3.6 Interaction of nanoparticles with rat erythrocytes

Fig. 3.6. shows interaction of nanoparticles with rat erythrocytes. Supporting information files SI1 and SI2 shows videos of confocal micrographs demonstrating interaction of nanospheres and nanorods with rat erythrocytes taken from different z-positions respectively. In case of malaria, the parasite resides and survives within the erythrocytes. Hence, it is desirable to deliver the antimalarial drug within erythrocytes for complete eradication of the parasite. Recently, we reported that nanorods showed low hemolysis of rat erythrocytes as compared to nanospheres. However, both nanospheres and nanorods showed < 10 % hemolysis of rat erythrocytes [21]. In the present study, we attempted to understand the interaction of nanospheres and nanorods with erythrocytes isolated from rat blood. The interaction of nanoparticles with erythrocytes is not well understood. However, it is extremely important in case of intravenous delivery of antimalarial formulations. SEM images revealed that both nanospheres and nanorods were adsorbed onto the surface of erythrocytes. However, due to the higher surface area of nanorods than nanospheres, the retention of nanorods on the cell surface could be more than the nanospheres in blood flow. Moreover, the particle cell interaction depends upon the energy released upon interaction and the energy required for bending the cell membrane. Energy released upon interaction depends upon surface area while the energy required for bending depends upon the size of the particles. It has been reported that the higher the surface area, the higher the free energy released upon the interaction (Brenner et al., 2018). On the other hand, the lower the size, higher the bending energy required for wrapping the particles. We, therefore, assumed that both nanospheres and nanorods, although interacted with erythrocytes, nanorods could retain and be wrapped by the erythrocytes more efficiently than nanospheres, probably due to high surface area of nanorods (Brenner et al., 2018). It could lead to maintenance of higher concentration within the erythrocytes than the nanospheres. Nevertheless, interaction of the nanoparticles with erythrocytes needs to be studied after intravenous administration of the formulation to establish an *in vivo* proof of concept.

3.3.7 Pharmacokinetic study

Pharmacokinetic profiles of artemether-loaded nanospheres and artemether-loaded nanorods are presented in fig. 3.7. It was observed that in case of artemether-loaded nanorods, plasma drug concentration was higher when compared with nanospheres. Interestingly, during the initial 15 mins, a rapid decrease in plasma drug concentration was observed in case of

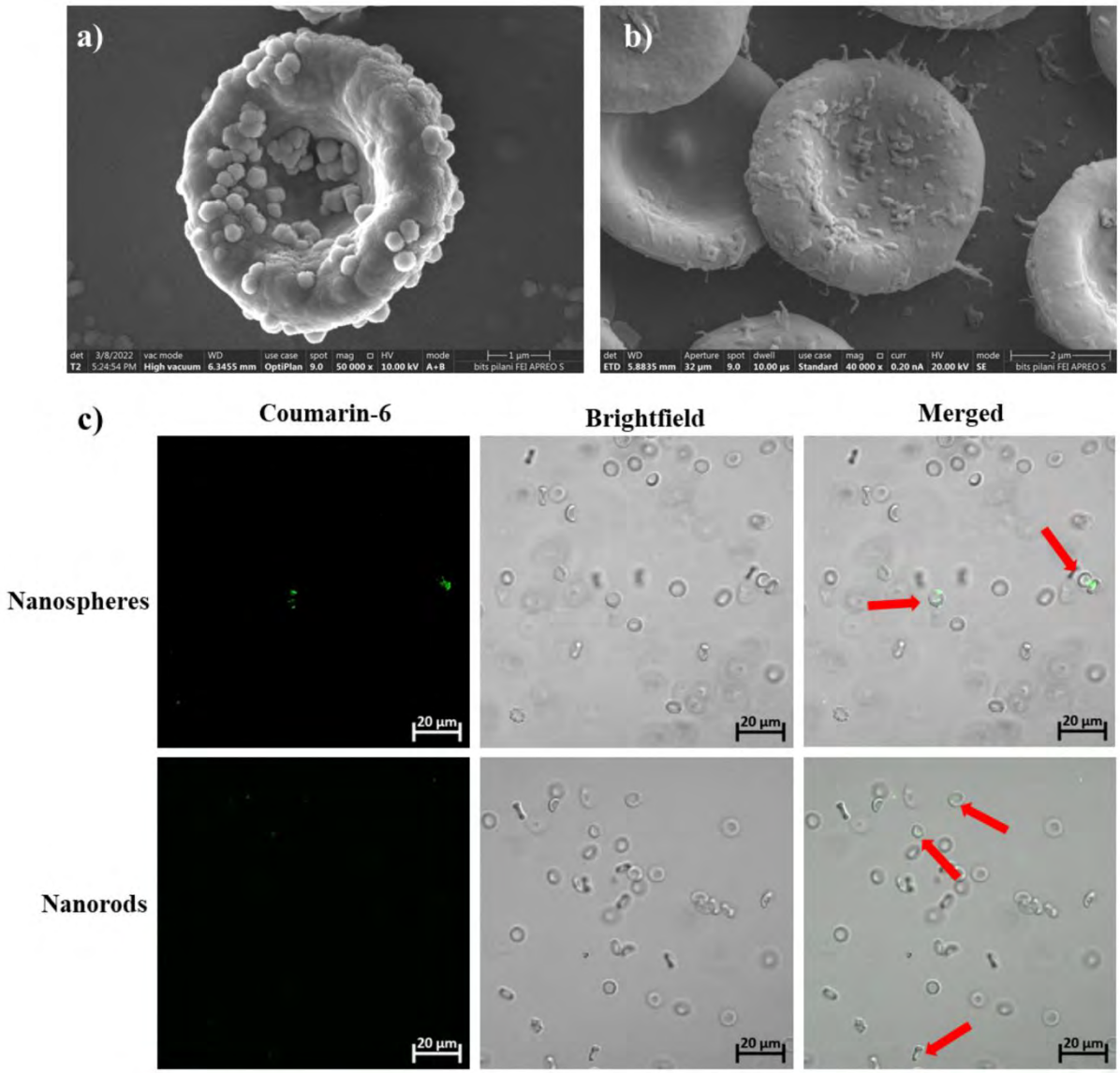

Fig. 3.6. Erythrocyte nanoparticle interaction study. SEM image of a) nanospheres adsorbed on erythrocyte & b) nanorods adsorbed on erythrocytes; Confocal image of c) nanospheres and nanorods, adsorbed on erythrocyte

nanospheres when compared with nanorods. The pharmacokinetic parameters of artemether nanospheres and artemether nanorods are presented in table 3.3. In case of nanospheres, C_{max} was found to be 1.64 - fold higher than nanorods. A lower C_{max} in case of artemether nanorods could result in a decrease in concentration-dependent side effects of artemether. Moreover, $t_{1/2}$ was found to be 3.09 - fold higher in case of nanorods than nanospheres. The difference in the pharmacokinetic parameters of nanorods and nanospheres after intravenous administration can be explained based upon the particle shape. Higher surface area and contact angle of nanorods than nanospheres could have led to an enhanced interaction of nanoparticles with endothelial cells and erythrocytes present in the circulatory system. The enhanced interaction of the

nanorods with blood components could have contributed to the higher $t_{1/2}$ of the drug in case of nanorods. Moreover, nanorods have an ability to marginate towards the blood vessel walls which would result in the retention of particles in the circulatory system for longer duration and creation of a depot in the blood vessel for the sustained release of drug (da Silva-Candal et al., 2019). The malaria parasite resides and survives within the erythrocyte which emerges out from the erythrocyte into the blood after 48 h. Hence, it is desirable to maintain the plasma concentration of antimalarial drugs for an extended duration for the complete elimination of parasites from blood. Furthermore, in case of nanorods, AUC was also found to be 1.8 - fold higher than nanospheres which indicated higher exposure of the parasite to the drug after treatment with artemether nanorods when compared with the artemether nanospheres. The longer circulation time of nanorods in combination with sustained drug release could be the possible reason of higher AUC in case of nanorods as compared to nanospheres. In case of nanorods, their low clearance (2 - fold) and high volume of distribution when compared with nanospheres indicated the presence of drug for an extended period in plasma. Comparative pharmacokinetics of nanorods and nanospheres in Sprague Dawley rats revealed that nanorods could maintain the plasma concentration of the drug for an extended duration which could lead to reduced dosing frequency.

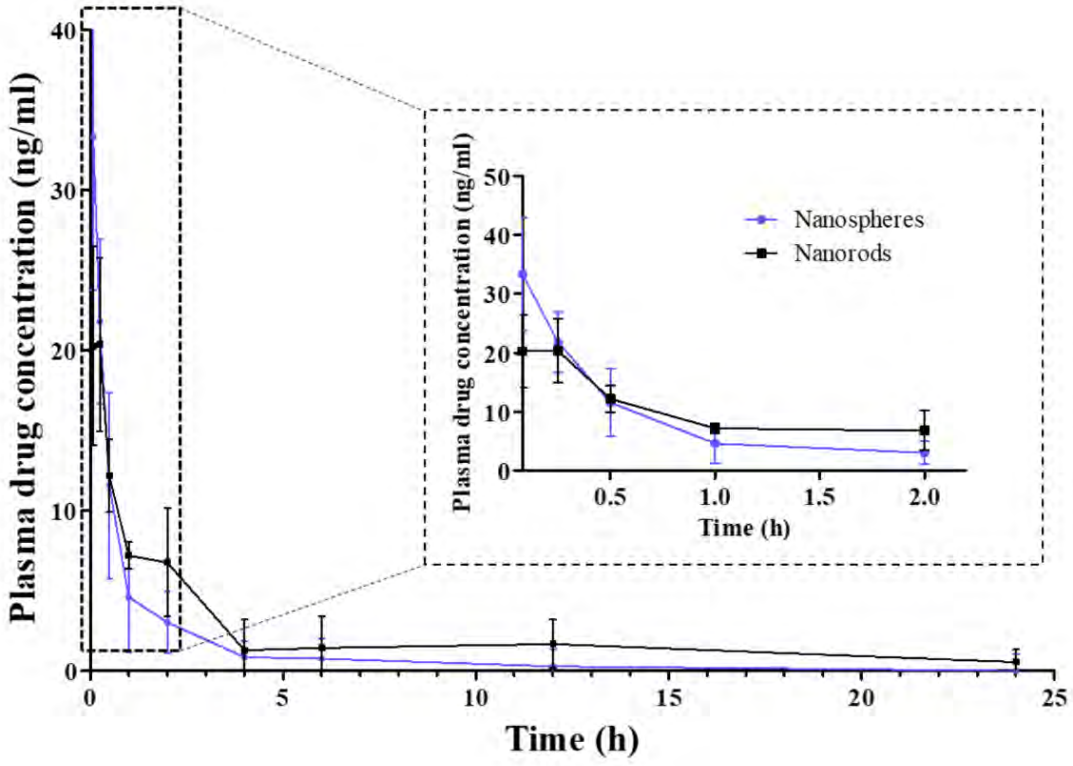

Fig. 3.7. Pharmacokinetic profile of nanospheres (blue) and nanorods (black) after intravenous administration of artemether-loaded nanospheres and artemether-loaded nanorods

Table 3.3: Pharmacokinetic parameters of artemether-loaded nanospheres and artemether-loaded nanorods after intravenous administration to rats

Pharmacokinetic parameter	Nanospheres	Nanorods
C_{max} (ng/ml)	29.33 ± 19.98	26.44 ± 10.89
t_{max} (h)	0.10±0.11	0.12±0.09
$t_{1/2}$ (h)	0.43 ± 0.08	1.17 ± 0.85
AUC (ng*h/L)	12.54 ± 4.71	62.18 ± 47.03
Volume of distribution (ml/kg)	17079.45 ± 8398.52	8305.41 ± 2477.34
Clearance (ml/h/kg)	26796.44 ± 8697.65	7783.66 ± 6369.11
Mean Residence Time (h)	0.67 ± 0.19	5.20 ± 4.95

Each value represents mean ± SD; (n = 4)

3.3.8 Biodistribution study

A comparative biodistribution profile of DIR loaded nanospheres and nanorods after intravenous administration is presented in fig. 3.8. Both nanospheres and nanorods showed significantly higher fluorescent intensity in liver and spleen as compared to other organs. At 30 min, the liver concentration of nanorods was found to be significantly less as compared to nanospheres. This observation indicated that the nanorods were present in the bloodstream for the longer duration and were not phagocytosed when compared to the nanospheres. It could provide a better opportunity for nanorods to interact with erythrocytes. Moreover, an increase in the fluorescence intensity at 24h indicates the sustained release of the dye from the nanoparticles.

3.3.9 *In vitro* schizont maturation inhibition assay against Plasmodium berghei (ANKA)

Artemether, blank nanospheres, blank nanorods, artemether-loaded nanospheres and artemether-loaded nanorods were evaluated for inhibition of *Plasmodium berghei* schizont maturation. All the drug loaded nanoformulations showed concentration-dependent inhibition of *P. berghei* schizont maturation. In the case of artemether, almost 70 % parasite inhibition was observed at all three concentrations. While in the case of artemether-loaded nanospheres and artemether-loaded nanorods, an increase in % parasite inhibition was observed with an increase in artemether concentration from 2 to 8 ppm. Moreover, at a lower artemether concentration, (2 ppm), nanorods showed higher % inhibition than nanospheres. While at a higher concentration (8 ppm), % inhibition of *P. berghei* schizont maturation was found to be more after incubation in nanospheres than in nanorods. Nanorods, due to their sustained drug release characteristic phenomenon, presented a slower release of artemether which could be

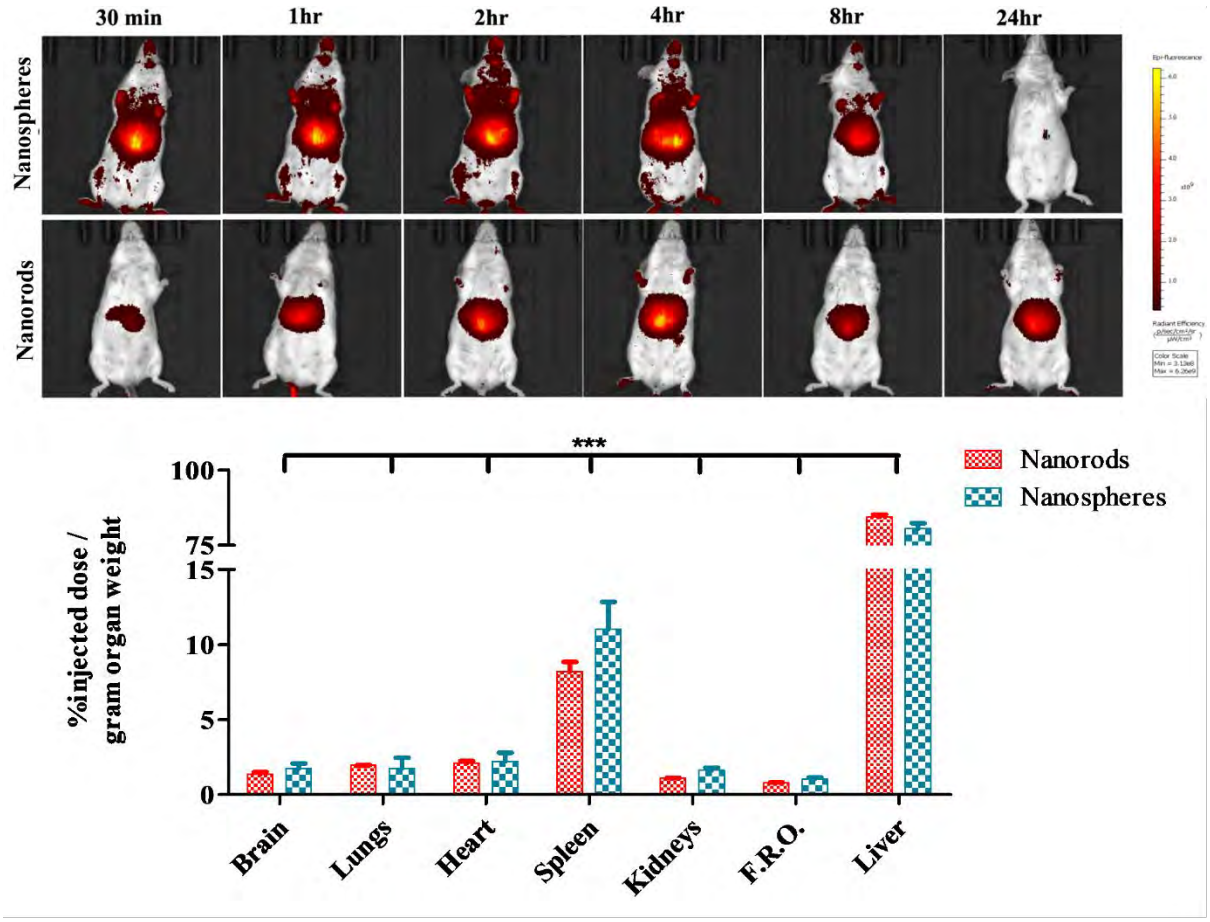

Fig. 3.8. Biodistribution study of DiR loaded nanoformulations. a) Whole-body images of BALB/c mice after intravenous administration of nanospheres and nanorods; b) comparative biodistribution profile of nanospheres and nanorods. The data was analysed using a Two-way analysis of variance. The distribution of nanospheres and nanorods was significantly different amongst different organs ($p < 0.0001$).

the possible reason for the lower % parasite inhibition of nanospheres than nanorods. The % parasite inhibition with respect to different concentrations of formulations is presented in fig. 3.9a.

3.3.10 Antimalarial efficacy of nanoformulations in *P. berghei*-infected mice

A. Suppressive activity

The infected group (no treatment) showed the highest parasitaemia, 16.75 ± 3.50 % on D7, after which all the mice died. The vehicle control-treated group (Group II) showed a growth rate similar to the infected control group with maximum parasitaemia (18.02 ± 0.76 %) on day 10 after which all mice died. The *in vivo* antimalarial efficacy of artemether-loaded nanospheres and artemether-loaded nanorods showed enhanced survival and reduction in parasitaemia as compared to infected control. The artemether-loaded nanospheres showed parasite suppression of around 78.46 % on the 5th day while 51.40 % on the 7th day thus indicating efficient chemo-suppression when compared to the infected control. On the other

hand, artemether-loaded nanorods showed increased chemo-suppression of 79.80 % and 65.01 % on day 5 and day 7 respectively. The higher chemo-suppression in case of nanorods could be a result of a sustained drug release and longer residence time of the nanorods in the circulation. However, in both cases of nanospheres and nanorods, the parasitaemia was found to be increased on 21st day which indicated the requirement for higher doses of artemether for the complete eradication of the parasite. On the other hand, artemether (free drug), showed 5.44 ± 1.46 % parasitaemia, on day 5 which increased to 27.49 ± 10.93% on day 21, which led to the death of animals due to high parasitaemia. Only one mouse survived till day 30 which also died later due to high parasitaemia. Both blank nanospheres and blank nanorods showed an increase in parasitaemia as compared to artemether-loaded nanospheres and artemether-loaded nanorods (Fig. 3.9b). The % parasitaemia at determined time points and mean survival time of the treated animals are provided in Fig. 3.9b, 3.9c.

B. Survival Analysis

Rise in parasitaemia was evident in the infected control on day 7, after which all mice died recording an MST of 7.50 ± 1.38 days. All the mice administered with the vehicle control died by day 10 highlighting no effect of the vehicle itself in clearing the rodent malaria parasite. In the Blank treated group (Nanospheres and nanorods) mortality was seen by day 21, which was statistically non-significant ($p > 0.005$) in comparison to infected control. The groups treated with Artemether alone and with the formulations (Nanospheres and nanorods) showed significant difference in survival rates when compared with infected control (Fig. 3.9c.)

3.4 Conclusion

In the present study, we reported that artemether loaded nanorods of uniform shape and narrow size distribution could be obtained using film stretching method. It was found that aspect ratio of nanorods was dictated by the film thickness, stretching extent and method of liquefaction of the particles during stretching. Drug loaded nanorods were also found to be biocompatible with THP-1 monocyte cells and RBCs. It suggested that PLGA nanorods could be used for the intravenous delivery of artemether for the treatment of cerebral malaria. Both nanospheres and nanorods were adsorbed on the surface of the rat erythrocytes, indicating the enhanced potential of artemether delivery within erythrocytes. In the case of nanorods, the higher plasma concentration and lower elimination rate of artemether as compared to nanospheres suggested the possibility of reduced dosing frequency of artemether. Nanorods also showed enhanced antimalarial efficacy in the *P. berghei* mouse model, which showed the potential to improve

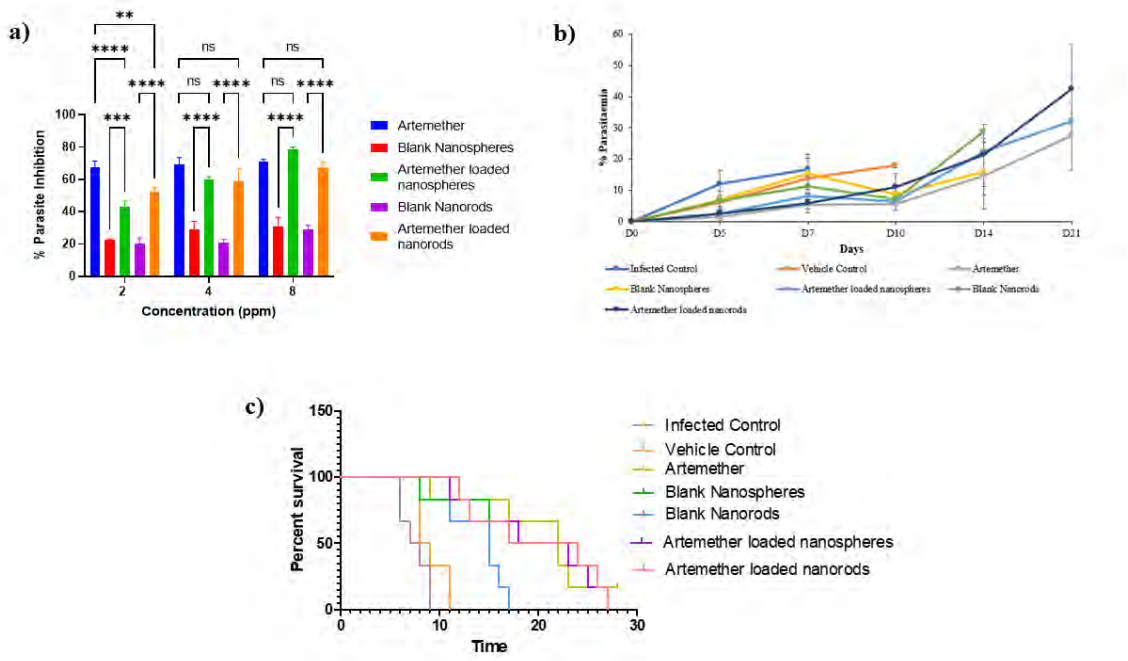

Fig. 3.9. *In vitro* and *in vivo* antimalarial efficacy studies of artemether nanospheres and artemether nanorods a) *In vitro* schizont maturation inhibition by artemether, artemether nanospheres and artemether nanorods. Results are expressed as mean ± standard deviation (S.D.) and statistically checked by a two-way analysis of variance. The p-value in comparison to artemether with other treatment groups, Blank nanospheres with artemether-loaded nanospheres and Blank nanorods with artemether-loaded rods are shown as ****p < 0.0001 to *p< 0.01 to 0.05 (significant), ns (non-significant). b) Percent parasitaemia observed in different treatment groups on different days (n = 6). c) Kaplan-Meier analysis of mice in various experimental groups in suppressive test.

the current malaria therapies. Hence, polymeric nanorods could be a promising next-generation delivery system for the treatment of malaria.

References

Almeida, A. M., Castel-Branco, M. M., & Falcão, A. C. (2002). Linear regression for calibration lines revisited: Weighting schemes for bioanalytical methods. *Journal of Chromatography B: Analytical Technologies in the Biomedical and Life Sciences*. https://doi.org/10.1016/S1570-0232(02)00244-1

Amin, N. C., Fabre, H., Blanchin, M. D., Montels, J., & Aké, M. (2013). Determination of artemether and lumefantrine in anti-malarial fixed-dose combination tablets by microemulsion electrokinetic chromatography with short-end injection procedure. *Malaria Journal*, *12*(1), 1–8. https://doi.org/10.1186/1475-2875-12-202

Aphesteguy, J. C., Kurlyandskaya, G. V., De Celis, J. P., Safronov, A. P., & Schegoleva, N. N. (2015). Magnetite nanoparticles prepared by co-precipitation method in different conditions. *Materials Chemistry and Physics*. https://doi.org/10.1016/j.matchemphys.2015.05.044

Baybay, E. K., Esposito, E., & Hauf, S. (2020). Pomegranate: 2D segmentation and 3D reconstruction for fission yeast and other radially symmetric cells. *Scientific Reports*. https://doi.org/10.1038/s41598-020-73597-w

Belew, S., Suleman, S., Duguma, M., Teshome, H., Wynendaele, E., Duchateau, L., & De Spiegeleer, B. (2020). Development of a dissolution method for lumefantrine and artemether in immediate release fixed dose artemether/lumefantrine tablets. *Malaria Journal*. https://doi.org/10.1186/s12936-020-03209-5

Bhide, A. R., Surve, D. H., Guha, S., & Jindal, A. B. (2020). A sensitive RP-HPLC method for estimation of artemether from polymeric nanoparticles after pre-column acid treatment using UV-visible detector. *Journal of Liquid Chromatography and Related Technologies*. https://doi.org/10.1080/10826076.2020.1777564

Brenner, J. S., Pan, D. C., Myerson, J. W., Marcos-Contreras, O. A., Villa, C. H., Patel, P., Hekierski, H., Chatterjee, S., Tao, J. Q., Parhiz, H., Bhamidipati, K., Uhler, T. G., Hood, E. D., Kiseleva, R. Y., Shuvaev, V. S., Shuvaeva, T., Khoshnejad, M., Johnston, I., Gregory, J. v., … Muzykantov, V. (2018). Red blood cell-hitchhiking boosts delivery of nanocarriers to chosen organs by orders of magnitude. *Nature Communications*, *9*(1). https://doi.org/10.1038/s41467-018-05079-7

Caldorera-Moore, M., Guimard, N., Shi, L., & Roy, K. (2010). Designer nanoparticles: Incorporating size, shape and triggered release into nanoscale drug carriers. In *Expert Opinion on Drug Delivery*. https://doi.org/10.1517/17425240903579971

Cao, J., Choi, J. S., Oshi, M. A., Lee, J., Hasan, N., Kim, J., & Yoo, J. W. (2019). Development of PLGA micro- and nanorods with high capacity of surface ligand conjugation for enhanced targeted delivery. *Asian Journal of Pharmaceutical Sciences*. https://doi.org/10.1016/j.ajps.2018.08.008

Castoldi, A., Empting, M., De Rossi, C., Mayr, K., Dersch, P., Hartmann, R., Müller, R., Gordon, S., & Lehr, C. M. (2019). Aspherical and Spherical InvA497-Functionalized Nanocarriers for Intracellular Delivery of Anti-Infective Agents. *Pharmaceutical Research*. https://doi.org/10.1007/s11095-018-2521-3

César, I. D. C., & Pianetti, G. A. (2009). Quantitation of artemether in pharmaceutical raw material and injections by high performance liquid chromatography. *Brazilian Journal of Pharmaceutical Sciences*, *45*(4), 737–742. https://doi.org/10.1590/S1984-82502009000400018

César, I. da C., Andrade Nogueira, F. H., & Antônio Pianetti, G. (2008). Simultaneous determination of artemether and lumefantrine in fixed dose combination tablets by HPLC with UV detection. *Journal of Pharmaceutical and Biomedical Analysis*, *48*(3), 951–954.

https://doi.org/10.1016/j.jpba.2008.05.022
Champion, J. A., Katare, Y. K., & Mitragotri, S. (2007). Making polymeric micro- and nanoparticles of complex shapes. *Proceedings of the National Academy of Sciences of the United States of America*. https://doi.org/10.1073/pnas.0705326104
Champion, J. A., & Mitragotri, S. (2009). Shape induced inhibition of phagocytosis of polymer particles. *Pharmaceutical Research*. https://doi.org/10.1007/s11095-008-9626-z
Christian, J., Shah, P., Patel, M., Patel, K., & Gandhi, T. (2017). Optimizing derivatization conditions using an experimental design and simultaneous estimation of artemether and lumefantrine by ratio first order derivative spectrophotometric method. *Journal of Taibah University for Science*, *11*, 729–740. https://doi.org/10.1016/j.jtusci.2016.08.003
Colussi, D., Parisot, C., Legay, F., & Lefèvre, G. (1999). Binding of artemether and lumefantrine to plasma proteins and erythrocytes. *European Journal of Pharmaceutical Sciences*, *9*(1), 9–16. https://doi.org/10.1016/S0928-0987(99)00037-8
da Silva-Candal, A., Brown, T., Krishnan, V., Lopez-Loureiro, I., Ávila-Gómez, P., Pusuluri, A., Pérez-Díaz, A., Correa-Paz, C., Hervella, P., Castillo, J., Mitragotri, S., & Campos, F. (2019). Shape effect in active targeting of nanoparticles to inflamed cerebral endothelium under static and flow conditions. *Journal of Controlled Release*, *309*, 94–105. https://doi.org/10.1016/j.jconrel.2019.07.026
Dasgupta, S., Auth, T., & Gompper, G. (2014). Shape and orientation matter for the cellular uptake of nonspherical particles. *Nano Letters*. https://doi.org/10.1021/nl403949h
Dendukuri, D., Tsoi, K., Hatton, T. A., & Doyle, P. S. (2005). Controlled synthesis of nonspherical microparticles using microfluidics. *Langmuir*. https://doi.org/10.1021/la047368k
Ho, C. C., Keller, A., Odell, J. A., & Ottewill, R. H. (1993). Preparation of monodisperse ellipsoidal polystyrene particles. *Colloid & Polymer Science*. https://doi.org/10.1007/BF00657391
Huang, Y., Xie, G., Zhou, Z., Sun, X., & Wang, Y. (1987). Determination of artemether in plasma and whole blood using HPLC with flow-through polarographic detection. *Biomedical Chromatography*, *2*(2), 53–56. https://doi.org/10.1002/bmc.1130020203
Idowu, O. R., Edwards, G., Ward, S. A., Orme, M. L. E., & Breckenridge, A. M. (1989). Determination of arteether in blood plasma by high-performance liquid chromatography with ultraviolet detection after hydrolysis with acid. *Journal of Chromatography B: Biomedical Sciences and Applications*, *493*(C), 125–136. https://doi.org/10.1016/S0378-4347(00)82715-2
Jefford, C. W. (1996). Six-membered Rings with no Bridgehead Heteroatom and Fused Carbocyclic Derivatives. In *Comprehensive Heterocyclic Chemistry II*.
Jindal, A. B. (2017). The effect of particle shape on cellular interaction and drug delivery applications of micro- and nanoparticles. In *International Journal of Pharmaceutics*. https://doi.org/10.1016/j.ijpharm.2017.09.028
Jindal, A. B., & Devarajan, P. V. (2015). Asymmetric lipid-polymer particles (LIPOMER) by modified nanoprecipitation: Role of non-solvent composition. *International Journal of Pharmaceutics*. https://doi.org/10.1016/j.ijpharm.2015.04.073
Jindal, A. B., Dighe, V. D., Surve, D. H., & Jirwankar, Y. B. (2020). Long-acting efavirenz and HIV-1 fusion inhibitor peptide co-loaded polymer-lipid hybrid nanoparticles: Statistical optimization, cellular uptake, and in vivo biodistribution. *Molecular Pharmaceutics*. https://doi.org/10.1021/acs.molpharmaceut.0c00773
Jurney, P., Agarwal, R., Singh, V., Choi, D., Roy, K., Sreenivasan, S. v., & Shi, L. (2017). Unique size and shape-dependent uptake behaviors of non-spherical nanoparticles by endothelial cells due to a shearing flow. *Journal of Controlled Release*.

https://doi.org/10.1016/j.jconrel.2016.11.033
Knight, D. J., & Peters. W. (1980). The antimalarial activity of N-benzyloxydihydrotriazines. I. The activity of clociguanil (BRL 50216) against rodent malaria, and studies on its mode of action. Annals of tropical medicine and parasitology, 74(4):393–404. (n.d.).
Kolhar, P., Doshi, N., & Mitragotri, S. (2011). Polymer nanoneedle-mediated intracellular drug delivery. *Small*. https://doi.org/10.1002/smll.201100497
Liu, Y., Yang, G., Jin, S., Xu, L., & Zhao, C. X. (2020). Development of High-Drug-Loading Nanoparticles. In *ChemPlusChem*. https://doi.org/10.1002/cplu.202000496
Makadia, H. K., & Siegel, S. J. (2011). Poly Lactic-co-Glycolic Acid (PLGA) as biodegradable controlled drug delivery carrier. *Polymers*. https://doi.org/10.3390/polym3031377
Mathaes, R., Winter, G., Besheer, A., & Engert, J. (2015). Non-spherical micro- and nanoparticles: Fabrication, characterization and drug delivery applications. In *Expert Opinion on Drug Delivery*. https://doi.org/10.1517/17425247.2015.963055
Mhatre, O., & Sodha, S. (2019). Pharmaceutical feasibility and flow characteristics of polymeric non-spherical particles. In *Nanomedicine: Nanotechnology, Biology, and Medicine*. https://doi.org/10.1016/j.nano.2019.03.002
Mount, D. L., Todd, G. D., & Navaratnam, V. (1995). Packed-column supercritical fluid chromatography of artemisinin (qinghaosu) with electron-capture detection. *Journal of Chromatography B: Biomedical Sciences and Applications*, *666*(1), 183–187. https://doi.org/10.1016/0378-4347(94)00560-R
https://www.fda.gov/media/75643/download
Pawar, J. N., Shete, R. T., Gangurde, A. B., Moravkar, K. K., Javeer, S. D., Jaiswar, D. R., & Amin, P. D. (2016). Development of amorphous dispersions of artemether with hydrophilic polymers via spray drying: Physicochemical and in silico studies. *Asian Journal of Pharmaceutical Sciences*, *11*(3), 385–395. https://doi.org/10.1016/j.ajps.2015.08.012
https://www.caymanchem.com/pdfs/11815.pdf
Raina, H., Kaur, S., & Jindal, A. B. (2017). Development of efavirenz loaded solid lipid nanoparticles: Risk assessment, quality-by-design (QbD) based optimisation and physicochemical characterisation. *Journal of Drug Delivery Science and Technology*, *39*, 180–191. https://doi.org/10.1016/j.jddst.2017.02.013
Resende, L. A., da Silva, P. H. R., & Fernandes, C. (2019). Quantitative determination of the antimalarials artemether and lumefantrine in biological samples: A review. *Journal of Pharmaceutical and Biomedical Analysis*, *165*, 304–314. https://doi.org/10.1016/j.jpba.2018.12.021
Rolland, J. P., Maynor, B. W., Euliss, L. E., Exner, A. E., Denison, G. M., & DeSimone, J. M. (2005). Direct fabrication and harvesting of monodisperse, shape-specific nanobiomaterials. *Journal of the American Chemical Society*. https://doi.org/10.1021/ja051977c
Sahoo, S. K., Panyam, J., Prabha, S., & Labhasetwar, V. (2002). Residual polyvinyl alcohol associated with poly (D,L-lactide-co-glycolide) nanoparticles affects their physical properties and cellular uptake. *Journal of Controlled Release*. https://doi.org/10.1016/S0168-3659(02)00127-X
Shende, P., Desai, P., Gaud, R. S., & Dhumatkar, R. (2017). Engineering of microcomplex of artemether and lumefantrine for effective drug treatment in malaria. *Artificial Cells, Nanomedicine and Biotechnology*. https://doi.org/10.1080/21691401.2016.1267012
Shukla, S., & Seal, S. (2004). Thermodynamic tetragonal phase stability in sol-gel derived nanodomains of pure zirconia. In *Journal of Physical Chemistry B*. https://doi.org/10.1021/jp037532x

Surve, D. H., & Jindal, A. B. (2019). Journal of Pharmaceutical and Biomedical Analysis Development and validation of reverse-phase high-performance liquid chromatographic (RP-HPLC) method for quantification of Efavirenz in Efavirenz-Enfuvirtide co-loaded polymer-lipid hybrid nanoparticles. *Journal of Pharmaceutical and Biomedical Analysis*, *175*, 112765. https://doi.org/10.1016/j.jpba.2019.07.013

Tayade, N. G., & Nagarsenker, M. S. (2007). Validated HPTLC method of analysis for artemether and its formulations. *Journal of Pharmaceutical and Biomedical Analysis*, *43*(3), 839–844. https://doi.org/10.1016/j.jpba.2006.08.029

Terzopoulos, D., & Fleischer, K. (1988). Modeling inelastic deformation: viscoelasticity, plasticity, fracture. *Computer Graphics (ACM)*. https://doi.org/10.1145/378456.378522

Thomas, C. G., & Ward, S. A. (1992). Selective determination , in plasma , of artemether and its major metabolite , dihydroartemisinin , by high- performance liquid chromatography with ultraviolet detection. *Journal of Chromatography*, *583*, 131–136.

Trager, W., & Jensen, J. B. (1976). Human malaria parasites in continuous culture. Science (New York, N.Y.), 193(4254), 673–675. (n.d.).

Ubale, M., & Choudhari, V. (2015). Stability-Indicating Hplc Determination of Artemether in Bulk Drug and Pharmaceutical Form. *World Journal of Pharmaceutical Research*, *5*(1), 609–625. https://doi.org/10.13140/RG.2.1.4508.7760

Validation of Analytical Procedures: Text and Methdology Q2(R1) (Vol. 1994, Issue October 1994). (2005).

Wang, L., Zhou, B., Huang, S., Qu, M., Lin, Q., Gong, T., Huang, Y., Sun, X., He, Q., Zhang, Z., & Zhang, L. (2019). Novel fibronectin-targeted nanodisk drug delivery system displayed superior efficacy against prostate cancer compared with nanospheres. *Nano Research*. https://doi.org/10.1007/s12274-019-2488-3

World Health Organization (WHO). Geneva. (2001) CTD/MAL/ 97, 20. (n.d.).

Yoo, J. W., Doshi, N., & Mitragotri, S. (2010). Endocytosis and intracellular distribution of PLGA particles in endothelial cells: Effect of particle geometry. *Macromolecular Rapid Communications*. https://doi.org/10.1002/marc.200900592

Yoo, J. W., & Mitragotri, S. (2010). Polymer particles that switch shape in response to a stimulus. *Proceedings of the National Academy of Sciences of the United States of America*. https://doi.org/10.1073/pnas.1000346107

Yu, W., & Hancock, B. C. (2008). Evaluation of dynamic image analysis for characterizing pharmaceutical excipient particles. *International Journal of Pharmaceutics*. https://doi.org/10.1016/j.ijpharm.2008.05.025

Zhang, J., Wang, J., Qiao, F., Liu, Y., Zhou, Y., Li, M., Ai, M., Yang, Y., Sui, L., & Zhou, Z. (2021). Polymeric non-spherical coarse microparticles fabricated by double emulsion-solvent evaporation for simvastatin delivery. *Colloids and Surfaces B: Biointerfaces*. https://doi.org/10.1016/j.colsurfb.2021.111560

Zhu, X., Vo, C., Taylor, M., & Smith, B. R. (2019). Non-spherical micro- and nanoparticles in nanomedicine. In Materials Horizons. https://doi.org/10.1039/c8mh01527a

Chapter 4: Development and evaluation of long-acting primaquine prodrug loaded nanorods for prolong plasma drug concentrations

4.1 Introduction

Unlike *Plasmodium falciparum* discussed in the previous chapters, *Plasmodium vivax* is the predominant species of malaria in many regions such as South and Southeast Asia, accounting for a considerable fraction of malaria infections (80% of all the malaria infections). The parasite *Plasmodium vivax* has a latent liver stage, in contrast to *Plasmodium falciparum* (Burgoine et al., 2010). *Plasmodium vivax* exhibits a stage commonly referred to as hypnozoites (or the liver stage), during which the parasite can persist in a dormant state, often undetectable, for several months (Zanghi & Vaughan, 2021). However, it still has the ability to activate further leading to relapse of the disease. This phenomenon often leads to hindrance in the therapy (Commons et al., 2020; Milligan et al., 2019). A complete therapy involves the complete eradication of the *P. vivax* parasite from the body eliminating the chances of the disease relapse (Flannery et al., 2022).

Primaquine is an antimalarial drug belonging to the class 8-aminoquinolones used widely for the treatment of malaria. It is amongst the specific drugs which have an activity against the hepatic stage of the parasite (hypnozoite) as well as the erythrocytic stage of the parasite. Additionally, it is active against the gametocytes of the Plasmodium falciparum in the blood (Baird, 2019; Carmo et al., 2017; Popovici et al., 2021). Hence it is primarily, the first choice for the radical cure of *P. vivax*. However, the drug is associated with several limitations. Due to strong dose-related hemolytic side effects in to patients with glucose-6-phosphate dehydrogenase (G6PD) deficiency, PQ's clinical applicability is limited (Wu et al., 2021). In addition, the drug (in its diphosphate salt form) needs a strict daily dose regimen in order to achieve its protective effects because of its relatively short half-life of about 4h (Andrade et al., 2023). The fluctuating plasma drug concentrations due to daily drug administration also imparts to the toxic effects of the drug (Fletcher et al., 1981; Jittamala et al., 2015). Hence, a controlled release primaquine formulation capable of reducing the systemic toxicity and increasing the drug residence time in the body is essential and the need of the hour.

Controlled release drug delivery systems are known to reduce the drug toxicity by preventing the burst release of the drug and releasing it in small amounts for extended periods thus maintaining the plasma drug concentrations for prolong durations (Weiser & Saltzman, 2014).

This improves patient compliance by reducing the dosing frequency of the treatment. Nanoformulations when administered parenterally (subcutaneously and intramuscularly) are known to form primary drug depots releasing drugs for long durations (Adepu & Ramakrishna, 2021; Jindal et al., 2023; Surve & Jindal, 2020). Additionally, non-spherical nanorods are also known to bypass macrophage uptake and form a cohesive depot due to their lower contact angle and higher surface area as compared to the nanospheres (Bhide et al., 2022; Bhide & Jindal, 2021; Champion & Mitragotri, 2009). Hence, the objective of the of the present study is development and evaluation of primaquine prodrug loaded PLGA nanorods for extended plasma drug concentration in rats after subcutaneous administration.

4.2 Materials and methods

4.2.1 Materials

N-(4-((6-methoxyquinolin-8-yl)amino)pentyl)palmitamide was synthesized using primaquine and palmitic acid. Primaquine was a gift sample from IPCA laboratories. Lumefantrine was purchased from Yarrow Chem Products (Mumbai, Maharashtra). Palmitic acid was purchased from Loba Chemie Pvt Ltd. Ethyl acetate, hexane, chloroform, dichloromethane (DCM) and ammonia solution were procured from Merck Life Science Pvt. Ltd. (Mumbai, India). Sodium sulfate (Na_2SO_4) was obtained from CDH (New Delhi, India). Silica gel 60-120, 1-ethyl-3-(3-dimethylaminopropyl) carbodiimide (EDCl), 1-Hydroxybenzotriazole (HOBt), was purchased from SRL Pvt. Ltd.- India. Poly(lactic-co-glycolic) acid (PLGA) (75:25, MW 66,000-107,000), polyvinyl alcohol (PVA, MW 9000–10,000), 3-(4,5-dimethylthiazol-2-yl)-2,5-diphenyl tetrazolium bromide (MTT) were purchased from Sigma-Aldrich Chemicals Company (Missouri, United States). Glycerol, tween 80 was obtained from S D Fine-Chem Ltd (Mumbai, India). Silicon oil was procured from Rankem^{TM} (Bangalore, India). Trehalose was acquired from Spectrochem (Mumbai, India). Water was obtained from Milli-Q system (Millipore GmbH, Germany). All other chemicals, solvents, and reagents utilized were either HPLC or analytical grade.

4.2.2 Methods

4.2.2.1 Synthesis of N-(4-((6-methoxyquinolin-8-yl)amino)pentyl)palmitamide (primaquine prodrug)

Primaquine diphosphate was converted to primaquine base as described previously with slight modifications (K. K. Singh & Vingkar, 2008). Briefly, primaquine diphosphate (200mg) was treated with ammonium hydroxide (2ml) at pH 12.0, leading to its alkalanization to form free primaquine base. The formed primaquine free base was extracted twice using chloroform

which was further washed using water followed by saturated solution of sodium chloride. Traces of water in the chloroform were removed using anhydrous sodium sulphate.

The N-(4-((6-methoxyquinolin-8-yl)amino)pentyl)palmitamide was prepared using primaquine base as previously described with slight modifications (Sloat et al., 2011). Primaquine (50 mg, 0.39 mmol), palmitic acid (121 mg, 0.42 mmol), and HOBt (57 mg, 0.42 mmol) were dissolved in 4mL of CH_2Cl_2. The solution was kept in ice bath and EDCI (89 mg, 0.46 mmol) was added into it. The reaction mixture was stirred in presence of nitrogen for a period of 12h. thereafter the reaction mixture was washed using saturated solution of sodium chloride followed by purification using by silica chromatography (3:7 EtOAc/hexane). The desired product was confirmed using ^{1}H NMR, ^{13}C NMR and mass spectrometry.

4.2.2.2 Preparation of primaquine prodrug loaded PLGA nanospheres

Primaquine prodrug nanospheres were prepared by emulsion solvent evaporation technique as reported previously with slight modifications (Prayag et al., 2021; Surve & Jindal, 2021). The primaquine prodrug (10mg) and PLGA (100mg) were initially dissolved in DCM (0.5ml) to obtain the organic phase. PVA (200mg) was dissolved in 4ml of Milli-Q water to form the aqueous phase. The aqueous phase was continuously stirred at 700rpm using a magnetic stirrer while the organic phase was added into the aqueous phase drop by drop to get a crude emulsion. The crude emulsion was then further subjected to probe sonication (Sonics & Materials, Inc., USA) at 500 watts, 25% amplitude for 3min (30 sec: ON and 10 sec: OFF). The formed nanoemulsion was further processed at reduced pressure under rotary vacuum evaporator (Heidolph, Schwabach, Germany) leading to the evaporation of DCM leaving behind the primaquine prodrug loaded polymeric nanospheres. The nanospheres were separated by centrifugation at 20,000rpm for 40min (Sorvall 150 + Micro Ultracentrifuge, Thermo Fisher Scientific, USA). The pellet obtained after centrifugation was redispersed in Milli-Q water. Further, the nanospheres obtained were characterized for particle size, polydispersity index (PDI), %entrapment efficiency, %drug loading and particle shape. The nanospheres were freeze-dried by using trehalose (10% w/v) as a cryoprotectant. Lyophilization was carried out over the course of three sequential phases, which involved freezing, primary drying, and secondary drying, lasting a combined duration of 48 hours.

4.2.2.3 Preparation of primaquine prodrug loaded PLGA nanorods

Primaquine prodrug loaded PLGA nanorods were prepared by film stretching technique as reported by our group with a few modifications (Bhide & Jindal, 2021). Primaquine prodrug loaded PLGA nanospheres were dispersed in Milli-Q water and mixed with film forming

solution. The solution was poured in a glass mould (12cm × 12cm) and left at room temperature for drying, ultimately forming a nanosphere embedded polymeric film. The film was then loaded in an *in-house* prepared film stretching instrument and immersed in preheated silicon oil (65ºC) and incubated for 15min. Post incubation, the film was stretched 4-times of its initial length at a rate of 10mm/min in one dimension. Post stretching, the film while being in stretched position, was left in the heated silicon oil for 5min for incubation. The stretched film was then removed from the assembly, dissolved in Milli-Q water and the nanorods formed in it were separated and washed by ultracentrifugation and characterized further.

4.2.2.4 Characterization of nanospheres and nanorods

A) Particle size and polydispersity index (PDI) and zeta potential

Primaquine prodrug loaded nanospheres were characterized by dynamic light scattering. Briefly, weighed quantity of primaquine prodrug loaded nanospheres were resuspended in 2mL Milli-Q water. The sample dispersion was analyzed for particle size, PDI and zeta potential using Malvern Nano ZS (Malvern Instruments Ltd. UK).

B) % Entrapment efficiency (%EE)

The primaquine prodrug loaded nanospheres were ultracentrifuged and the supernatant obtained after the process was used to analyze the %EE by the develop RP-HPLC method. %EE was calculated using the equation (1)

$$\%EE = \frac{Total\ quatity\ of\ drug\ used\ -\ Drug\ content\ in\ the\ supernatant}{Total\ quantity\ of\ drug\ used} \times 100$$

C) % Drug loading (%DL)

Drug loading is the ratio of the mass of the drug with the mass of drug loaded nanospheres. The %DL was calculated using the equation

$$\%DL = \frac{Total\ quatity\ of\ drug\ entrapped}{Total\ quantity\ of\ drug\ used + Total\ quantity\ of\ polymer\ used} \times 100$$

D) Drug content (%DC)

10mg of the primaquine prodrug loaded freeze dried formulation (nanospheres/nanorods) was dispersed in 1mL of methanol. The dispersion was sequentially exposed to vortexing (5min), sonication (30min) and centrifugation (10,000rpm; 40min). The supernatant was diluted in the mobile phase and was further analysed by the developed RP-HPLC method.

E) Field emission scanning electron microscopy

An aliquot of the aqueous dispersion of nanorods or nanospheres was spread on a coverslip, which was then allowed to dry at room temperature. The dried coverslip was attached on a metal stub using a carbon tape and the sputter coater (Quorum Technologies Q150TES, East

Sussex, England) was used to coat the sample with gold coated for 45 seconds. Following the coating, the nanoparticles were examined using an FEI scanning electron microscope (Hillsboro, Washington) operating at 20 kV high vacuum. The scale was set to 300–1000 nm, and the spot size was set at 9.0.

F) Calculation of shape descriptors of nanorods

As described in the previous chapter, shape descriptors such as Feret diameter, minor Feret diameter, AR, major axis, and minor axis were used to characterize the nanorods. Briefly the Feret diameter measures the widest span of a particle between two tangents drawn perpendicular to its two farthest ends. Minor Feret diameter, conversely, measures the closest span between two endpoints. Whereas, major axis represents the longest segment connecting the farthest points of a particle, while the minor axis indicates the shortest segment connecting the closest points. Aspect ratio is the ratio of the major axis to the minor axis of the particle. A size-frequency distribution curve was plotted using these shape descriptors by plotting percentage frequencies of various particles against particle size. The shape descriptors were determined from the SEM images of the nanorods using Fiji ImageJ software (Version 1.52p).

4.2.2.5 Release study

We used the sample and separate method to conduct the *in vitro* drug release profile of PQ-PAL from the formulation. Microcentrifuge tubes containing nanospheres and nanorods (equivalent to 100µg of PQ-PAL) dispersed in release media (1mL of 2%v/v tween-80 and 0.05%w/v sodium azide in phosphate-buffered saline pH 7.4) were prepared for each time point. The samples were kept in a water bath shaker assembly with continuous agitation at 100 rpm and at 37°C. At every time point, respective microcentrifuge tubes were taken out and centrifuged at 14000 rpm for 40min and the supernatant was withdrawn. For determining the PQ-PAL concentration, the samples were suitably diluted in acetonitrile: water (6:4), centrifuged and analysed using the developed RP-HPLC-based analytical method.

4.2.2.6 Hemolysis study

In vitro hemolysis study was carried out as reported previously by our group (Jindal et al., 2020). Fresh blood of Wistar rats was collected in microcentrifuge tubes containing Ethylenediamine tetraacetic acid (EDTA) (10% w/v). Red blood cells (RBCs) were collected after centrifugation of blood at 1000 rpm for 5 min and washed thrice with normal saline (0.9 % w/v sodium chloride). 5µL of the packed erythrocytes were treated with 95 µL of the nanospheres (PQ-PAL equivalent to 0.001, 0.01, 0.1, 1, 10, 100, and 200µg/mL) or nanorods (PQ-PAL equivalent to 0.001, 0.01, 0.1, 1, 10, 100, and 200 µg/mL). Thereafter, the samples were

centrifuged at 1000 rpm for 5 min and the supernatant was analyzed at 540 nm using an Epoch ELISA plate reader (BioTek, Winooski, United States). Normal saline and Milli-Q water were used as a negative control and positive control respectively during the study. % hemolysis was calculated using the equation

$$\%\ hemolysis = \frac{absorbance\ of\ the\ sample}{absorbance\ of\ the\ positive\ control}\ x\ 100$$

4.2.2.7 Cytotoxicity study

In a T-25 culture flask, the RAW 264.7 cell line was cultured in DMEM medium with 10% foetal bovine serum (FBS) and gentamycin (0.005%). Once the flask was confluent, the cells were trypsinized and counted, which was followed by seeding of 10,000 cells per well in a 96-well plate. For twenty-four hours, the cells were treated with PQ and PQ-PAL loaded nanospheres and PQ-PAL loaded nanorods (PQ and PQ-PAL concentrations equivalent to 0.001, 0.01, 0.1, 1, 10, 100, and 200 µg/mL). Post 24h, each well received 100 µL of 3-(4,5-dimethylthiazol-2-yl)-2,5-diphenyl tetrazolium bromide (MTT) solution (0.5 µg/mL) and was allowed to incubate for 4h. After 4h, the MTT solution was replaced with DMSO and the absorbance was recorded at 540nm using an Epoch ELISA plate reader (BioTek, Winooski, United States). % cell viability was calculated by using the following equation

$$\%\ cell\ viability = \frac{(absorbance\ of\ sample - absorbance\ of\ blank)}{(absorbance\ of\ control - absorbance\ of\ blank)}\ x\ 100$$

4.2.2.8 Pharmacokinetic studies

The formulation's ability to sustain the drug release was assessed *in vivo* using 250 ± 50g female Sprague Dawley rats. The Institutional Animal Ethics Committee of Birla Institute of Technology and Science, Pilani Campus, Pilani, accepted the protocol for the animal study (Protocol no.: IAEC/RES/33/01). There were two groups of animals (n = 4). PQ-PAL loaded polymeric nanospheres (PQ-PAL equivalent to 50mg/kg) were administered subcutaneously to animals in group I, while animals in group II received primaquine prodrug loaded polymeric nanorods (PQ-PAL equivalent to 50mg/kg). The animals were provided with normal food and water *ad libitum* prior to the commencement of the study.

Following the administration, 300µL of blood was withdrawn from the retroorbital plexus of rat at predetermined time points (1h, 3h, 6h, 12h, day 1, day 2, day 5, day 7, day 10, day 14, day 21 and day 28) and placed in a microcentrifuge tube with 20µL of 10% EDTA. The microcentrifuge tubes were centrifuged (8000 rpm; 10min) and the plasma was separated and stored (-23ºC) until further used. During analysis, initially the thawed plasma (95µL) was taken

and spiked with internal standard (10µL of 250ng/ml lumefantrine). The samples were vortex mixed for 1min. Further, the extraction of the drug and the internal standard was performed by protein precipitation by adding acetonitrile (1ml) in the samples which were vortex mixed (15min) and centrifuged (10,000rpm; 15min). The supernatant obtained after centrifugation was collected in a microcentrifuge tube, evaporated at 37ºC, reconstituted in mobile phase (100µL) and analyzed using the developed bioanalytical method on LC-MS-MS.

4.2.3 Results and discussion

4.2.3.1 Synthesis of N-(4-((6-methoxyquinolin-8-yl)amino)pentyl)palmitamide (primaquine prodrug/ PQ-PAL)

Azure-coloured solid product synthesized, 126mg, 74% yield, UV-Vis (CH_2Cl_2): λ_{max} (nm) 266; δ^1H NMR (400 MHz, Chloroform-*d*) δ 8.55 (dd, *J* = 4.2, 1.6 Hz, 1H), 7.94 (dd, *J* = 8.3, 1.6 Hz, 1H), 7.33 (dd, *J* = 8.2, 4.2 Hz, 1H), 6.36 (d, *J* = 2.5 Hz, 1H), 6.30 (d, *J* = 2.4 Hz, 1H), 6.01 (s, 1H), 5.55 (t, *J* = 5.7 Hz, 1H), 3.91 (s, 3H), 3.65 (s, 1H), 3.29 (dq, *J* = 11.5, 6.8 Hz, 2H), 2.14 – 2.08 (m, 2H), 1.74-1.64 (m, 5H), 1.59 (t, *J* = 7.4 Hz, 2H), 1.32-1.26 (m, 26H), 0.90 (t, *J* = 6.7 Hz, 3H), δ^{13}C NMR (101 MHz, $CDCl_3$) δ 173.17, 159.43, 144.90, 144.33, 135.34, 134.83, 129.92, 121.89, 96.83, 91.72, 55.22, 47.84, 39.40, 36.89, 33.99, 31.94, 29.71, 29.67, 29.64, 29.52, 29.38, 29.35, 26.34, 25.81, 22.71, 20.63, 14.15, HRMS (ESI): calculated for C31H51N3O2 $[M+H]^+$ 498.4054; found 498.4095. Fig. 4.1., 4.2., and 4.3 represents the ^{1}H NMR, ^{13}C NMR and HRMS spectrum respectively of the synthesized primaquine prodrug.

4.2.3.2 Preparation and characterization of artemether-loaded polymeric nanospheres and nanorods

PQ-PAL loaded PLGA nanospheres were prepared by the emulsion solvent evaporation. Particle size, PDI, zeta potential and % EE of nanospheres obtained after varying different parameters are presented in table 4.1. Particle size, PDI, zeta potential, and % EE were found to be affected by the ratio of organic to aqueous phase and the sonication time. There was a decrease in particle size observed when the ratio of organic to aqueous phase was increased from 1:8 to 3:8. Similarly, when the sonication time was increased from 1min to 3min, the particle size decreased from 407.10±105.68nm to 234.77±8.46nm. Moreover, an increase in the sonication time resulted in a narrow particle size distribution of with a PDI of 0.24 ± 0.03 whereas, when the ratio of organic to aqueous phase was increased alongside the sonication time, the PDI further decreased to 0.11±0.01. Of all the trials conducted, formulation PQ-E-2 was selected for subsequent studies. Fig. 4.4. Represents the particle size and zeta potential distribution curves of PQ-E-2 trial.

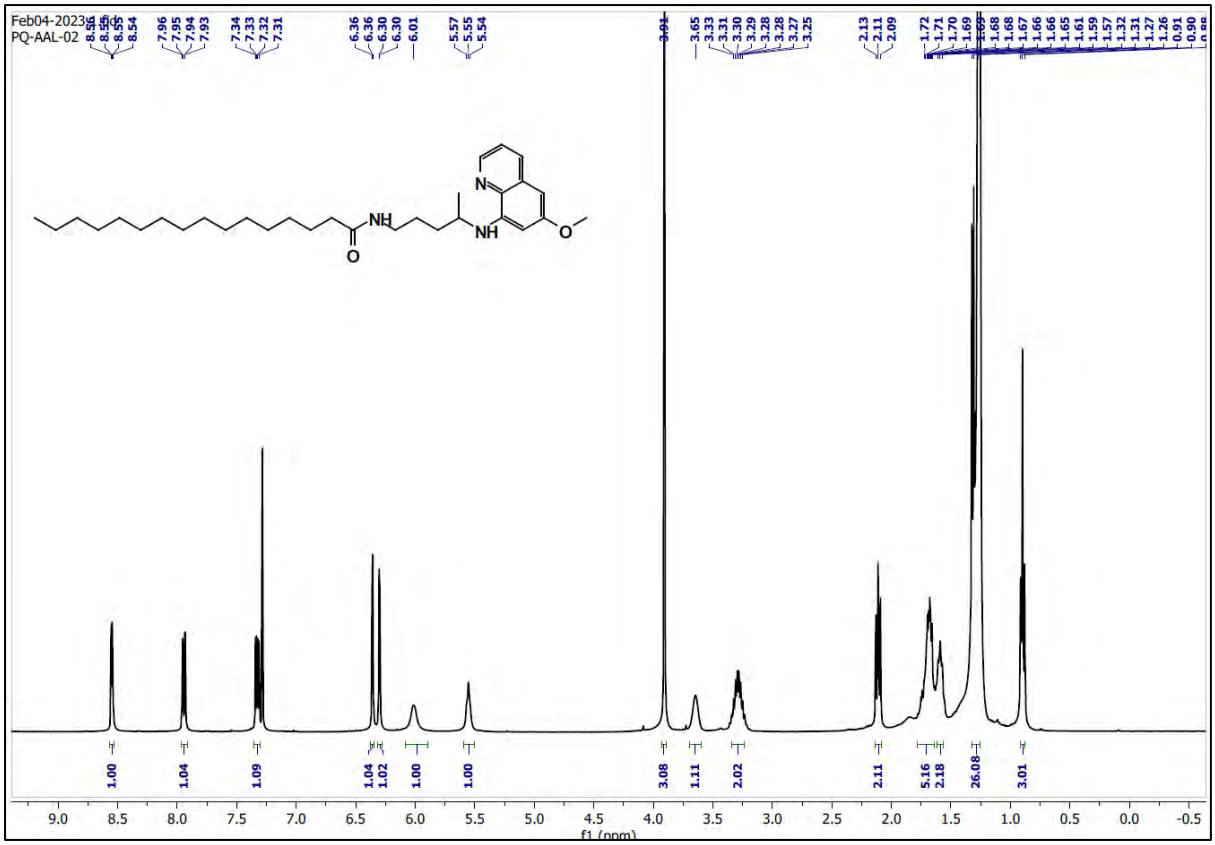

Fig. 4.1. [1]H NMR spectrum of the synthesized primaquine prodrug

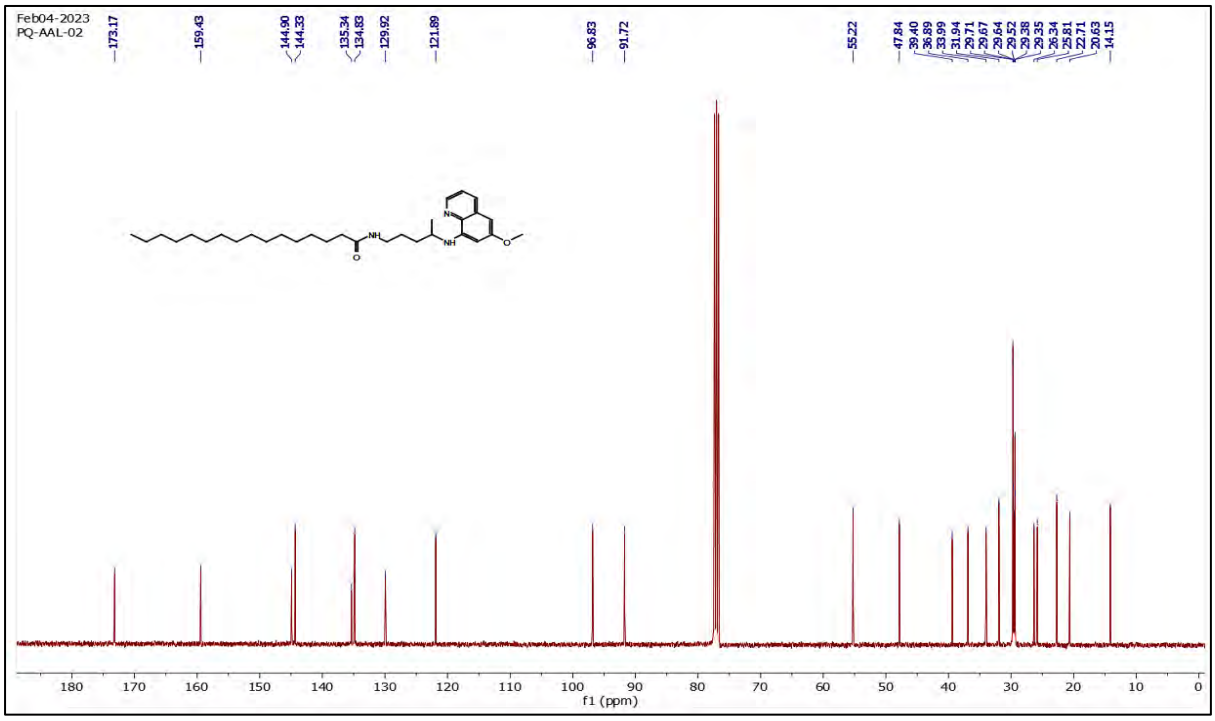

Fig. 4.2 [13]C NMR spectrum of the synthesized primaquine prodrug

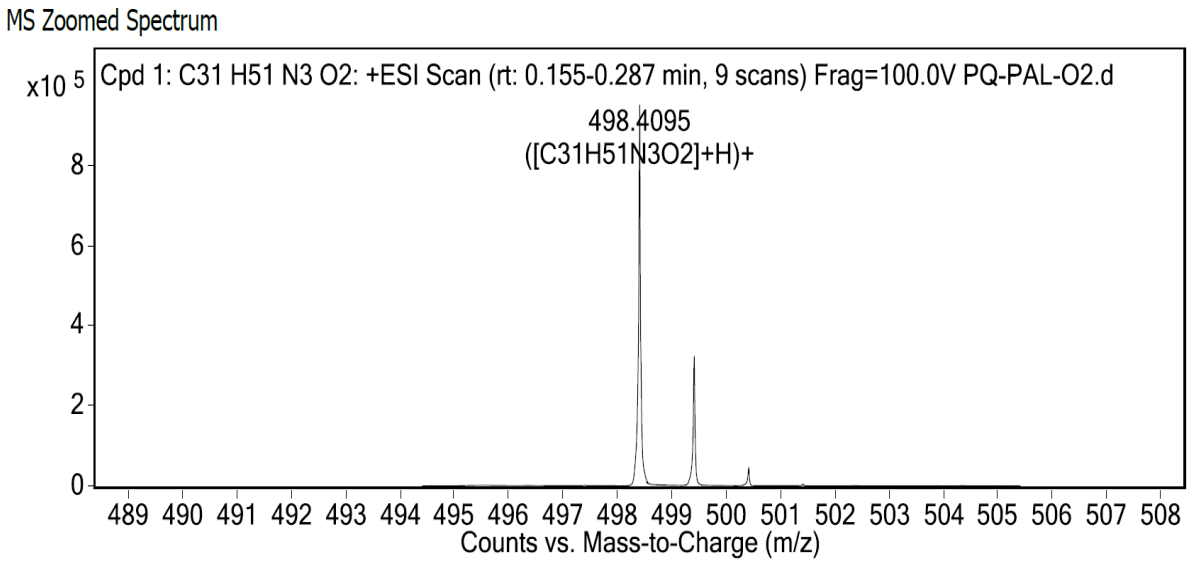

Fig. 4.3 HRMS spectrum of the synthesized primaquine prodrug

PLGA nanorods loaded with PQ-PAL were prepared by mechanically stretching PQ-PAL loaded PLGA nanospheres using an *in-house* fabricated film stretching apparatus. During stretching, the nanospheres experienced stress, potentially surpassing the cohesive forces within the polymer, thus resulting in the stretching of spherical nanoparticles into elongated nanorods (Bhide & Jindal, 2021). The nanorods were characterized for drug content, major axis, minor axis, major Feret's diameter, minor Feret's diameter, and aspect ratio which are presented in table 4.2. The formulated nanorods did not have significant difference between their major and minor axes and their respective Feret's diameters thus indicating symmetry of the shape of the formulated nanorods. (D90 major = 2300nm and D90 minor = 280 nm, D50 major = 1400 nm and D50 minor = 220 nm, and D10 major = 1100 nm and D10 minor = 130 nm). D90, D50, and D10 of the nanorods suggested uniformity in size, affirming that the nanorods produced from stretching nanospheres were consistent in dimensions. Fig. 4.5. presents the size frequency distribution curves of major and minor axis of nanorods and SEM images of nanospheres and nanorods.

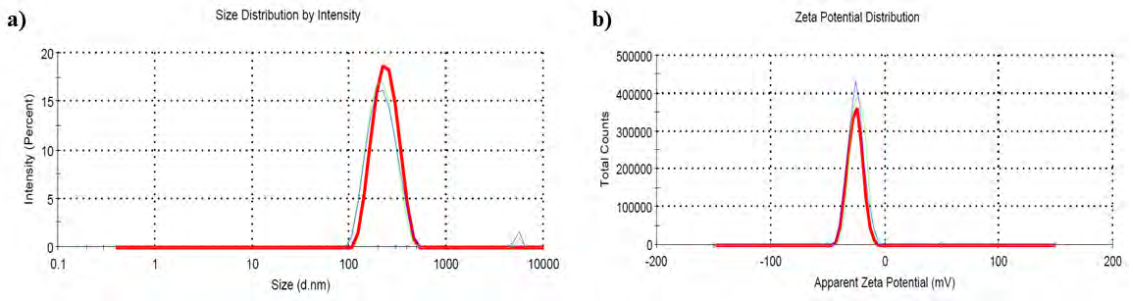

Fig. 4.4. Characterization of PQ-PAL loaded PLGA nanospheres a) Particle size distribution b) zeta potential

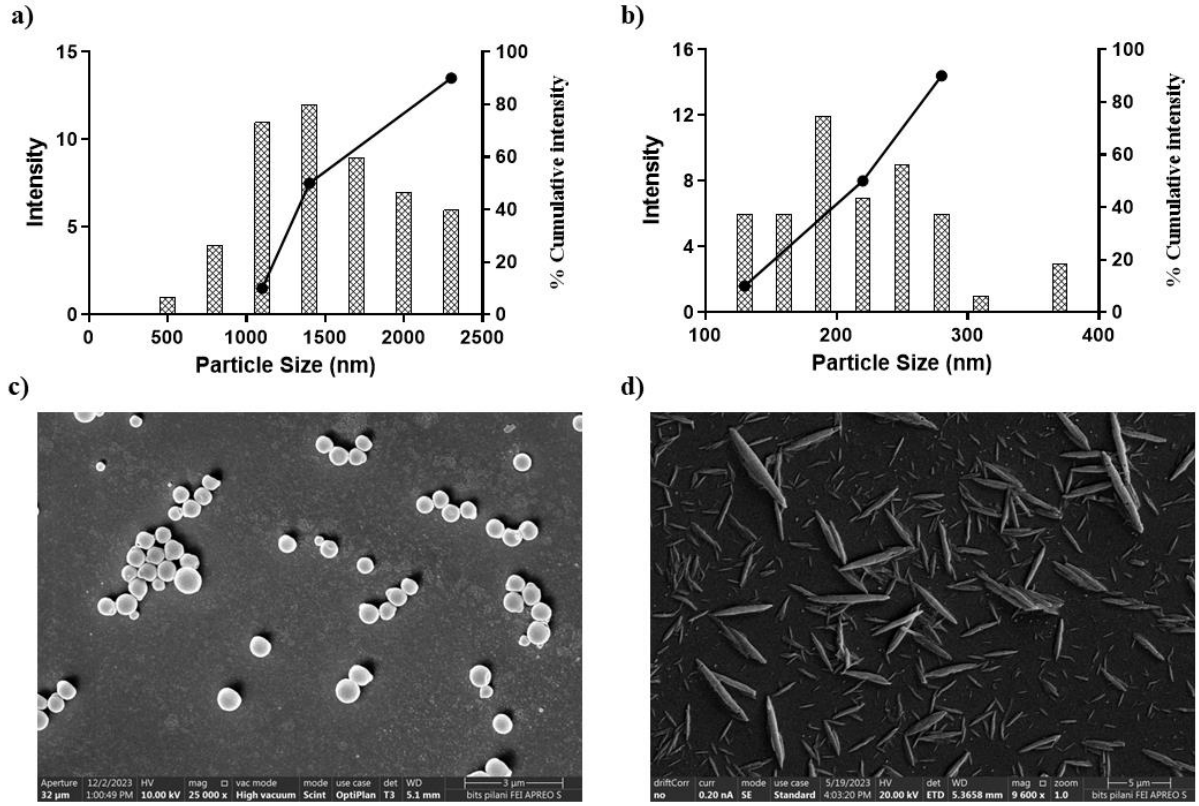

Fig. 4.5. Size-frequency distribution
curves of major axis (a), minor axis (b) of nanorods; SEM images of nanospheres (c) and nanorods (d)

4.2.3.3 Release study

Fig. 4.6. represents the *in vitro* release profile of PQ-PAL-loaded nanospheres and nanorods. Both nanospheres and nanorods showed a sustained PQ-PAL release. At all time points, nanorods exhibited significantly slower PQ-PAL release ($p < 0.0001$) compared to nanospheres. By the end of the 7^{th} day, almost 45% and 23% of PQ-PAL was released from the nanospheres and nanorods respectively. Nanorods are reported to exhibit cohesive nature and tendency to align under flow conditions (margination) due to their distinct shape and surface area. Furthermore, the particle orientation within the dissolution medium might have influenced the available surface area for drug release. The sustained PQ-PAL release from nanorods, as compared to nanospheres, can be attributed to their specific orientation hindering efficient drug release under turbulent conditions and leading to the formation of a stagnant layer around the particles.

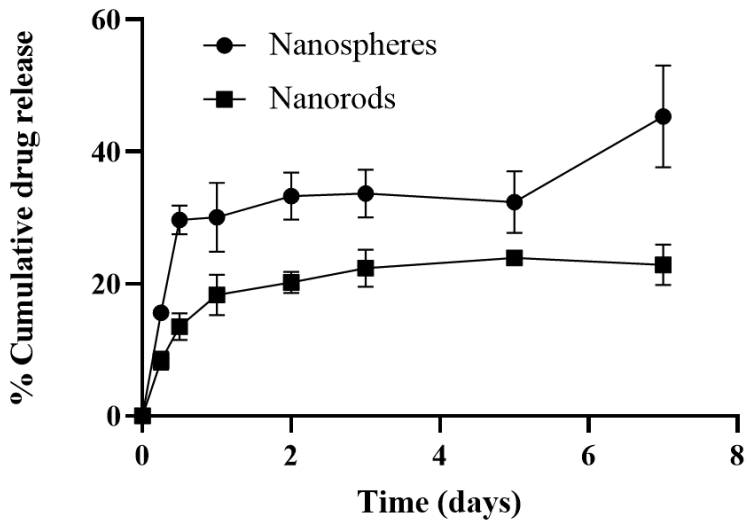

Fig. 4.6. *In vitro* drug release profile of PQ-PAL loaded nanospheres and nanorods

4.2.3.4 Hemolysis study

The haemolytic potential of nanospheres and nanorods was evaluated *in vitro* using rat blood-derived erythrocytes. Across all PQ-PAL concentrations, nanorods and nanospheres exhibited lower red blood cell (RBC) haemolysis compared to free PQ-PAL (Fig. 4.7.). Primaquine diphosphate also found to be non-haemolytic at all the evaluated concentrations. Nonetheless, both nanospheres and nanorods displayed less than 10% haemolysis across all concentrations thus rendering their safety towards the erythrocytes.

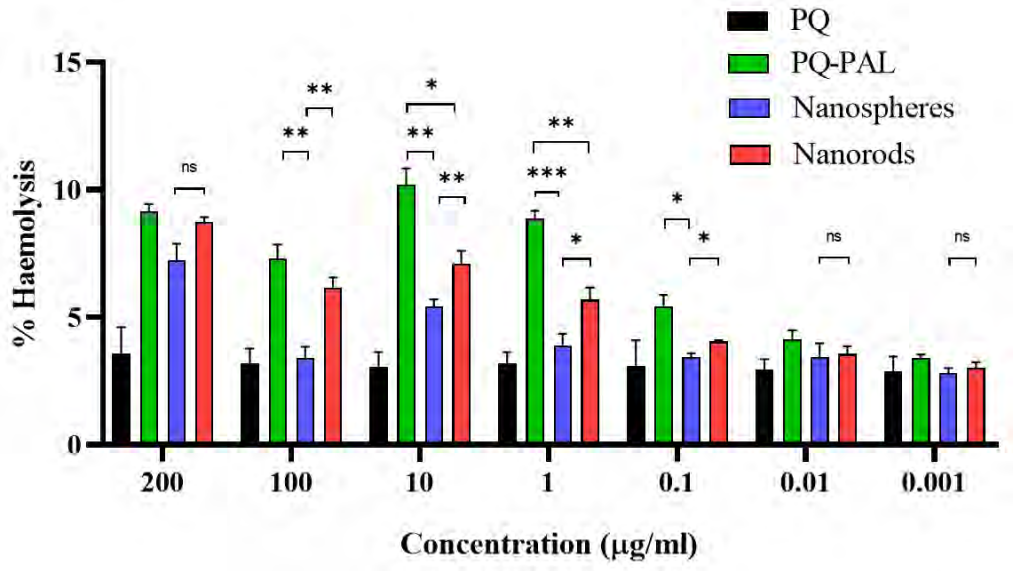

Fig. 4.7. %Haemolysis of rat blood derived RBC by PQ, PQ-PAL, & PQ-PAL loaded nanospheres and nanorods

Table 4.1. Formulation and characterization of PQ-PAL loaded PLGA nanospheres

	Composition						Parameters					
Formulation code.	**Drug (mg)**	**PLGA (mg)**	**PVA (mg)**	**DCM (ml)**	**Water (ml)**	**Sonication time (min)**	**Particle size (nm)**	**PDI**	**Zeta potential**	**%EE**	**%DL**	**DC (µg/mg)**
PQ-E-1	10	100	200	0.5	4	1	407.10 ± 105.68	0.55 ± 0.03	-7.86 ± 0.38	N.D.	N.D.	N.D.
PQ-E-2	10	100	200	1.5	4	3	162.47 ± 2.40	0.11 ± 0.01	-17.83 ± 0.55	N.D.	N.D.	N.D.
PQ-E-3	10	100	200	0.5	4	3	234.77 ± 8.46	0.24 ± 0.03	-25.03 ± 1.29	88.99 ± 1.56	8.09 ± 0.14	28.8

Each value presented as mean ± SD, n = 3; N.D. – Not determined

Table 4.2. Characterization of PQ-PAL loaded PLGA nanorods

Nanoformulation	**DC (µg/mg)**	**Major axis (nm)**	**Minor axis (nm)**	**Major Feret's diameter (nm)**	**Minor Feret's diameter (nm)**	**Aspect ratio**
Nanorods	12.95	1380.69 ± 545.32	203.65 ± 62.37	1348.48 ± 544.16	237.77 ± 67.41	6.73 ± 1.46

Each value presented as mean ± SD, n = 50

4.2.3.5 Cytotoxicity study

In vitro cytotoxicity of PQ free drug and PQ-PAL loaded nanospheres and nanorods were studied at different concentrations of PQ-PAL using RAW 264.7cell line. Almost 90% cell viability was found when RAW 264.7cells were treated with PQ (0.001 to 0.1µg/mL) and nanospheres, and nanorods equivalent to 0.001 to 0.1µg/mL of PQ-PAL (Fig. 4.8). There was no significant difference with % cell viability when cells when treated with PQ-PAL loaded nanospheres, PQ-PAL loaded nanorods and PQ at a concentration range of 0.001 to 10µg/mL. Furthermore, at higher PQ and PQ-PAL concentrations (100 and 200µg/mL), a significant decrease in % cell viability was observed in case of free PQ. However, at those concentrations, PQ-PAL loaded nanospheres and nanorods showed significantly higher % cell viability as compared to PQ free drug. Thus, the prepared nanospheres and nanorods showed a better safety profile against PQ free drug in RAW 264.7cells.

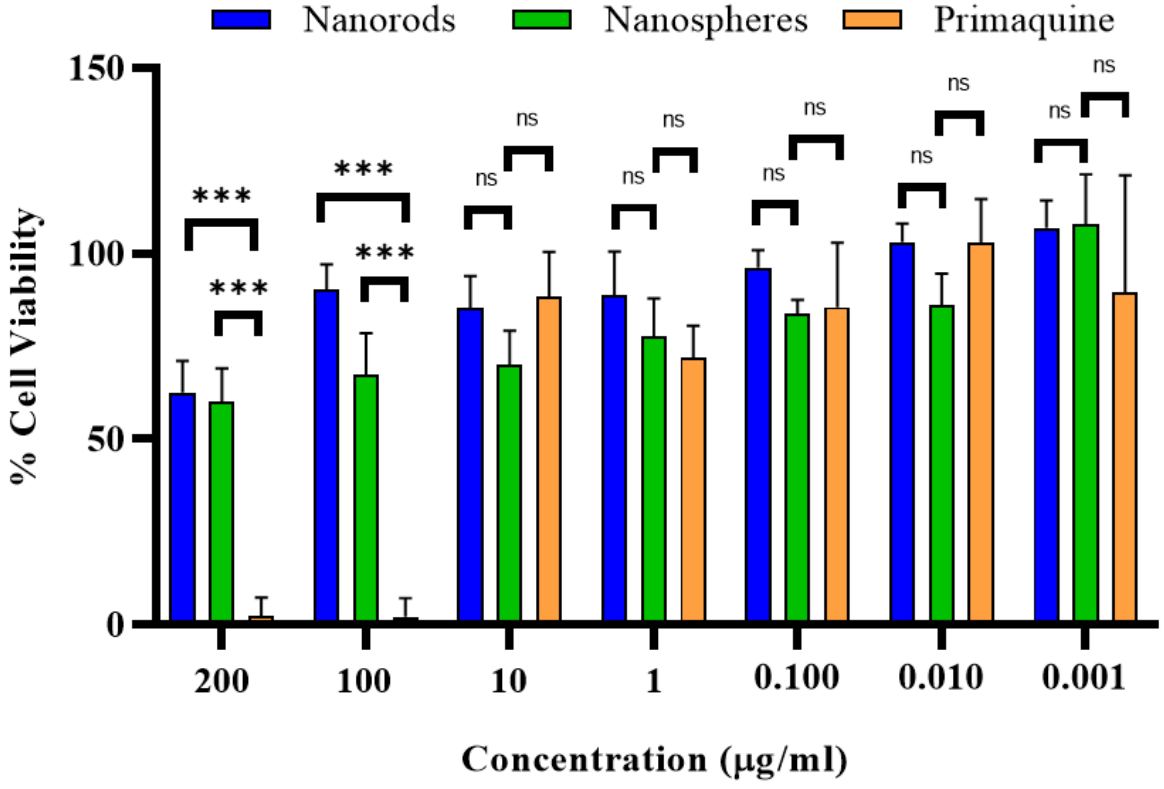

Fig. 4.8 *In vitro* cytotoxicity of PQ free drug, nanospheres and nanorods

4.2.3.6 Pharmacokinetic study

The pharmacokinetic parameters that were determined by non-compartmental analysis of the data are presented in table 4.3. In addition, the plasma conc. vs. time profile of the formulation and the free drug following subcutaneous delivery is shown in Fig. 4.9.

In case of PQ-PAL loaded PLGA nanospheres, the C_{max} value reached 115.28ng/ml at 9.12

hours. Furthermore, PQ-PAL was detected in the plasma upto 28 days ($MRT_{0-\infty}$ - 7.2 days; half-life – 5.12 days) thus demonstrating the long-acting potential of nanospheres. The $AUC_{0-\infty}$ for the nanospheres was found to be 2.16-folds that of the nanorods.

Whereas in case of PQ-PAL loaded PLGA nanorods, the C_{max} value reached 84.06ng/ml at 12.48 hours. In this case, the plasma PQ-PAL concentrations were also observed upto 28 days ($MRT_{0-\infty}$ - 8.9 days; half-life – 5.6 days). Unlike nanospheres, nanorods have a unique shape and hence are expected to behave in a different manner *in vitro* and *in vivo*.

Nanospheres have been known to form a primary depot at the site of injection, whereas create a secondary depot in the macrophages and the T cells (Surve & Jindal, 2020). These primary and secondary depots could be responsible for the sustained drug release from the PQ-PAL loaded nanospheres. Whereas the greater residence time of the nanorods in the animals could be due to a stronger cohesive primary depot formed at the site of injection. It is well known that the nanorods have a higher surface area and contact angle as compared to the spheres, thereby has an ability to form as cohesive depot which could contribute significantly prolong plasma drug concentration. Furthermore, it has been reported that the macrophage uptake of the nanorods is limited due to its shape which further reduces the chance of they getting cleared off, eventually resulting in a sustained drug release. As observed from the pharmacokinetic parameters, the $AUC_{0-\infty}$ for the nanospheres was found to be 2.16-folds that of the nanorods. However, the $MRT_{0-\infty}$ and t_{max} in case of nanorods was 1.25-folds and 1.4-folds greater than that of nanorods. Whereas the C_{max} for nanospheres was 1.4-folds that of nanorods which could have been probably due to the initial burst drug release from the nanospheres.

This study highlighted the significance of the nanoparticle shape, which could enhance its retention at the injection site, thereby facilitating the development of a more robust depot capable of prolonged drug release.

Table 4.3. The plasma non-compartmental PK parameters obtained after SC administration of PQ-PAL loaded PLGA nanospheres and nanorods in Sprague Dawley rats using Phoenix WiNonlin software (version 6.3)

Parameter	Result	
	Nanospheres	**Nanorods**
$t_{1/2}$ (days)	5.12 ± 0.8	5.64 ± 0.48
C_{max} (ng/ml)	115.28 ± 57.03	84.06 ± 25.43
$AUC_{0-\infty}$	386.39 ± 109.35	178.79 ± 33.24
Vz/F (L/Kg)	259842.25 ± 104890.40	585099 ± 129029.4
Cl/F	34434.44 ± 9987.73	71649.4 ± 12557.17
$MRT_{0-\infty}$ (days)	7.20 ± 1.60	8.99 ± 1.46

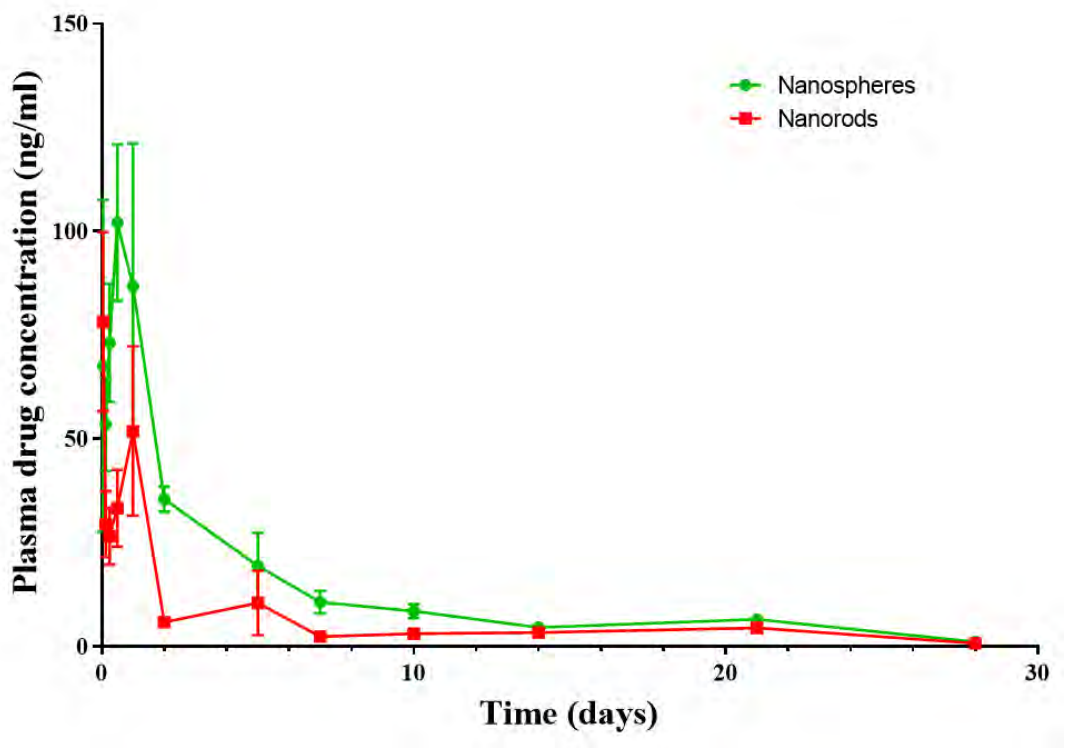

Fig. 4.9. Pharmacokinetic profile of nanospheres (green) and nanorods (red) after subcutaneous administration of PQ-PAL-loaded nanospheres and PQ-PAL-loaded nanorods

4.3 Conclusion

In the current chapter, hydrophilic primaquine was converted to a hydrophobic prodrug which could be efficiently loaded on the nanocarriers. Further, it was demonstrated that the prodrug loaded nanospheres can be fabricated into nanorods of uniform shape, narrow size distribution and high aspect ratio. The nanorods were also found to be non-toxic towards the RAW 264.7 cells and rat erythrocytes thus demonstrating their safety for the *in vivo* administration. Furthermore, these nanorods in the *in vitro* as well as *in vivo* study demonstrated their ability to sustain the drug release which is highly desirable for the treatment of *P. vivax* infection where the treatment regimen continues for a long duration. Thus, it can be concluded that the polymeric nanorods could be a promising next-generation delivery system for the treatment of malaria.

References

Adepu, S., & Ramakrishna, S. (2021). Controlled Drug Delivery Systems: Current Status and Future Directions. *Molecules*, *26*(19), 5905. https://doi.org/10.3390/molecules26195905

Andrade, A. O., Santos, N. A. C., Bastos, A. S., Pontual, J. D. C., Araújo, J. E., Silva, A. M. V., Martinez, L. N., Lima, A. A., Aguiar, A. C. C., G. Teles, C. B., Medeiros, J. F., Pereira, D. B., Vinetz, J. M., Gazzinelli, R. T., & Araújo, M. S. (2023). Transmission-blocking activity of antimalarials for Plasmodium vivax malaria in Anopheles darlingi. *PLOS Neglected Tropical Diseases*, *17*(6), e0011425. https://doi.org/10.1371/journal.pntd.0011425

Baird, J. K. (2019). 8-Aminoquinoline Therapy for Latent Malaria. *Clinical Microbiology Reviews*, *32*(4). https://doi.org/10.1128/CMR.00011-19

Baird, J. K., & Hoffman, S. L. (2004). Primaquine Therapy for Malaria. *Clinical Infectious Diseases*, *39*(9), 1336–1345. https://doi.org/10.1086/424663

Bhide, A. R., & Jindal, A. B. (2021). Fabrication and evaluation of artemether loaded polymeric nanorods obtained by mechanical stretching of nanospheres. *International Journal of Pharmaceutics*, *605*(June), 120820. https://doi.org/10.1016/j.ijpharm.2021.120820

Bhide, A. R., Suri, M., Katnoria, S., Kaur, S., Jirwankar, Y. B., Dighe, V. D., & Jindal, A. B. (2022). *Evaluation of Pharmacokinetics, Biodistribution, and Antimalarial Efficacy of Artemether-Loaded Polymeric Nanorods*. https://doi.org/10.1021/acs.molpharmaceut.2c00507

Burgoine, K. L., Bancone, G., & Nosten, F. (2010). The reality of using primaquine. *Malaria Journal*, *9*(1), 376. https://doi.org/10.1186/1475-2875-9-376

Carmo, A. P. B. do, Borborema, M., Ribeiro, S., De-Oliveira, A. C. X., Paumgartten, F. J. R., & Moreira, D. de L. (2017). A newly validated high-performance liquid chromatography method with diode array ultraviolet detection for analysis of the antimalarial drug primaquine in the blood plasma. *Revista Da Sociedade Brasileira de Medicina Tropical*, *50*(4), 499–505. https://doi.org/10.1590/0037-8682-0023-2017

Champion, J. A., & Mitragotri, S. (2009). Shape induced inhibition of phagocytosis of polymer particles. *Pharmaceutical Research*. https://doi.org/10.1007/s11095-008-9626-z

Commons, R. J., Simpson, J. A., Watson, J., White, N. J., & Price, R. N. (2020). Estimating the Proportion of Plasmodium vivax Recurrences Caused by Relapse: A Systematic Review and Meta-Analysis. *The American Journal of Tropical Medicine and Hygiene*, *103*(3), 1094–1099. https://doi.org/10.4269/ajtmh.20-0186

Flannery, E. L., Kangwanrangsan, N., Chuenchob, V., Roobsoong, W., Fishbaugher, M., Zhou, K., Billman, Z. P., Martinson, T., Olsen, T. M., Schäfer, C., Campo, B., Murphy, S. C., Mikolajczak, S. A., Kappe, S. H. I., & Sattabongkot, J. (2022). Plasmodium vivax latent liver infection is characterized by persistent hypnozoites, hypnozoite-derived schizonts, and time-dependent efficacy of primaquine. *Molecular Therapy - Methods & Clinical Development*, *26*, 427–440. https://doi.org/10.1016/j.omtm.2022.07.016

Fletcher, K. A., Evans, D. A., Gilles, H. M., Greaves, J., Bunnag, D., & Harinasuta, T. (1981). Studies on the pharmacokinetics of primaquine. *Bulletin of the World Health Organization*, *59*(3), 407–412.

Jindal, A. B., Bhide, A. R., Salave, S., Rana, D., & Benival, D. (2023). Long-acting parenteral drug delivery systems for the treatment of chronic diseases. *Advanced Drug Delivery Reviews*, *198*, 114862. https://doi.org/10.1016/j.addr.2023.114862

Jindal, A. B., Dighe, V. D., Surve, D. H., & Jirwankar, Y. B. (2020). Long-acting efavirenz and HIV-1 fusion inhibitor peptide co-loaded polymer-lipid hybrid nanoparticles:

Statistical optimization, cellular uptake, and in vivo biodistribution. *Molecular Pharmaceutics*. https://doi.org/10.1021/acs.molpharmaceut.0c00773

Jittamala, P., Pukrittayakamee, S., Ashley, E. A., Nosten, F., Hanboonkunupakarn, B., Lee, S. J., Thana, P., Chairat, K., Blessborn, D., Panapipat, S., White, N. J., Day, N. P. J., & Tarningb, J. (2015). Pharmacokinetic interactions between primaquine and pyronaridine-artesunate in healthy adult Thai subjects. *Antimicrobial Agents and Chemotherapy*, *59*(1), 505–513. https://doi.org/10.1128/AAC.03829-14

Milligan, R., Daher, A., & Graves, P. M. (2019). Primaquine at alternative dosing schedules for preventing relapse in people with *Plasmodium vivax* malaria. *Cochrane Database of Systematic Reviews*. https://doi.org/10.1002/14651858.CD012656.pub2

Popovici, J., Tebben, K., Witkowski, B., & Serre, D. (2021). Primaquine for Plasmodium vivax radical cure: What we do not know and why it matters. *International Journal for Parasitology: Drugs and Drug Resistance*, *15*, 36–42. https://doi.org/10.1016/j.ijpddr.2020.12.004

Prayag, K. S., Paul, A. T., Ghorui, S. K., & Jindal, A. B. (2021). Preparation and Evaluation of Quinapyramine Sulphate-Docusate Sodium Ionic Complex Loaded Lipidic Nanoparticles and Its Scale Up Using Geometric Similarity Principle. *Journal of Pharmaceutical Sciences*, *110*(5), 2241–2249. https://doi.org/10.1016/j.xphs.2021.01.033

Singh, K. K., & Vingkar, S. K. (2008). Formulation, antimalarial activity and biodistribution of oral lipid nanoemulsion of primaquine. *International Journal of Pharmaceutics*, *347*(1–2), 136–143. https://doi.org/10.1016/j.ijpharm.2007.06.035

Sloat, B. R., Sandoval, M. A., Li, D., Chung, W.-G., Lansakara-P, D. S. P., Proteau, P. J., Kiguchi, K., DiGiovanni, J., & Cui, Z. (2011). In vitro and in vivo anti-tumor activities of a gemcitabine derivative carried by nanoparticles. *International Journal of Pharmaceutics*, *409*(1–2), 278–288. https://doi.org/10.1016/j.ijpharm.2011.02.037

Surve, D. H., & Jindal, A. B. (2020). Recent advances in long-acting nanoformulations for delivery of antiretroviral drugs. *Journal of Controlled Release*, *324*, 379–404. https://doi.org/10.1016/j.jconrel.2020.05.022

Surve, D. H., & Jindal, A. B. (2021). Development of Cationic Isometamidium Chloride loaded Long-Acting Lipid Nanoformulation: Optimization, Cellular Uptake, Pharmacokinetics, Biodistribution, and Immunohistochemical Evaluation. *European Journal of Pharmaceutical Sciences*, *167*(May), 106024. https://doi.org/10.1016/j.ejps.2021.106024

Weiser, J. R., & Saltzman, W. M. (2014). Controlled release for local delivery of drugs: barriers and models. *Journal of Controlled Release*, *190*, 664–673. https://doi.org/10.1016/j.jconrel.2014.04.048

Wu, K. W., Sweeney, C., Dudhipala, N., Lakhani, P., Chaurasiya, N. D., Tekwani, B. L., & Majumdar, S. (2021). Primaquine Loaded Solid Lipid Nanoparticles (SLN), Nanostructured Lipid Carriers (NLC), and Nanoemulsion (NE): Effect of Lipid Matrix and Surfactant on Drug Entrapment, in vitro Release, and ex vivo Hemolysis. *AAPS PharmSciTech*, *22*(7), 1–12. https://doi.org/10.1208/s12249-021-02108-5

Zanghi, G., & Vaughan, A. M. (2021). Plasmodium vivax pre-erythrocytic stages and the latent hypnozoite. *Parasitology International*, *85*, 102447. https://doi.org/10.1016/j.parint.2021.102447

Chapter 5: Development and evaluation of long-acting polymeric nanoparticles loaded biodegradable implant for prolong plasma drug concentration of primaquine prodrug

5.1 Introduction

Malaria, an infectious disease resulting from *Plasmodium species* transmitted through the bite of female Anopheles mosquitoes, requires preventive measures encompassing anti-vectorial measures as well as chemoprophylaxis (Sato, 2021; Schlagenhauf & Petersen, 2008). Plasmodium vivax relapse is a major challenge in the complete eradication of malaria. After the treatment of *P. vivax* infection, hypnozoites remains in the body for several months with no symptoms of malaria which can transport the parasite to new areas. Primaquine phosphate is indicated for the radical cure (prevention of relapse) of vivax malaria. A 14-day course is found to be effective for the prevention of vivax malaria relapse (Castelli et al., 2010; Rodrigues et al., 2012). Patients suffering from an attack of vivax malaria or having parasitized red blood cells should receive a course of chloroquine phosphate, which quickly destroys the erythrocytic parasites and terminates the paroxysm. Primaquine phosphate should be administered concurrently in order to eradicate the exoerythrocytic parasites in a dosage of 1 tablet (equivalent to 15 mg base) daily for 14 days (Kevin Baird et al., 2003).

Adherence to the 14-day regimen of primaquine is a major challenge for the prevention of relapse which was varied from 25-85% (Brown, 1993; Mazier et al., 2009). Although direct observation of dosing intake has improved the adherence to the therapy, it is practically difficult and time-consuming. To meet the WHO mission of 90% reduction of malaria cases by 2030, there is an urgent need for either a new antimalarial drug that can remain in the blood in the therapeutic range for weeks after single-dose administration or an innovative drug delivery strategy that could enable long-acting release of antimalarial drugs for few days and plasma concentration of the drug can be maintained within the therapeutic range. The discovery of the new antimalarial drug is a time-consuming process and demands huge investments. On the other hand, exploration of new drug delivery technology which could meet the requirements of maintenance of plasma concentration of the drug for a few days after single-dose administration is a significantly fast process and can be completed by low investment than the amount required for the discovery of a new drug.

The peak plasma concentrations of primaquine are achieved after 2-3h after its administration, whereas, the drug has a short half-life of about 4h thus requiring its repetitive administration

(Fletcher et al., 1981; Jittamala et al., 2015). Additionally, the drug possesses dose dependent adverse effects thus often leading to poor adherence to the therapy (Ashley et al., 2014; Fernando et al., 2011). Therefore, there is a significant need for a formulation that can effectively sustain the plasma drug concentration of primaquine within the therapeutic range for extended periods. This sustained presence within the optimal therapeutic window is essential for ensuring the drug's effectiveness over time, thus enhancing its therapeutic impact. Solid implants have been extensively investigated for their potential in drug delivery, functioning as sustained-release depots over prolonged periods (Maturavongsadit, Paravyan, et al., 2021; Maturavongsadit, Shrivastava, et al., 2021). However, their size necessitates surgical procedures for implantation (Santos et al., 2014). In contrast, technologies such as AtrigelTM offer a different approach, as they are administered parenterally and solidify into implants, gradually releasing the drug over weeks or months (Ivaturi et al., 2017; Southard et al., 1998). Nevertheless, AtrigelTM is not without its limitations. It relies on synthetic polymers as the structural matrix for implant formation, presenting challenges in handling, particularly when compared to standard aqueous solutions, due to the high viscosity of the formulations. Additionally, the viscosity impedes the filtration of the formulation, necessitating sterilization through gamma irradiation (Southard et al., 1998).

We utilized albumin in the preparation of a long-acting injectable implant. Albumin, being the most abundant circulating protein, is considered highly biocompatible for drug delivery purposes (Moman et al., 2023). Moreover, it already serves as a natural drug transporter within the body. The structure of albumin consists of amino acids arranged into three recurring homologous domains, each comprising two distinct sub-domains labeled A and B, interconnected by interchain disulfide bridges (Mohan et al., 2018). When in a dissolved state, these disulfide bridges are enclosed within the protein structure and remain shielded from the surrounding solvent (Borzova et al., 2016). However, it is noteworthy that albumin can undergo conformational isomerization when exposed to specific chemicals and physiological stress. Upon exposure to stress agents, albumin undergoes conformational isomerization, leading to the exposure of hydrophobic regions to the solvent (McClellan & Franses, 2003). This exposure of hydrophobic regions results in the formation of insoluble aggregates, giving the albumin solution a gel-like nature.

In our process, we have developed a long-acting injectable implant using albumin. The initial step involves exposing the albumin solution to an ethanol solution, triggering the formation of insoluble aggregates within a specified timeframe, dependent on the quantity of ethanol used.

These insoluble aggregates contribute to the viscosity of the solution mixture. The addition of ethanol to the albumin solution induces conformational changes in the native α-helices of the protein to β-sheets which have the capacity to trap water molecules thus attributing gel like structure to the formulation. Consequently, when administered parenterally, this solution serves as a depot for sustained drug release. Unlike in situ forming depots, the formation of this depot is not contingent on the physiological conditions of the injection site but is solely determined by the quantity of ethanol employed to induce albumin denaturation. Therefore, the objective of the present study was the development of a long-acting drug-loaded implant that is both biodegradable and undergoes formation within a specific timeframe, independent of the physiological environment at the injection site.

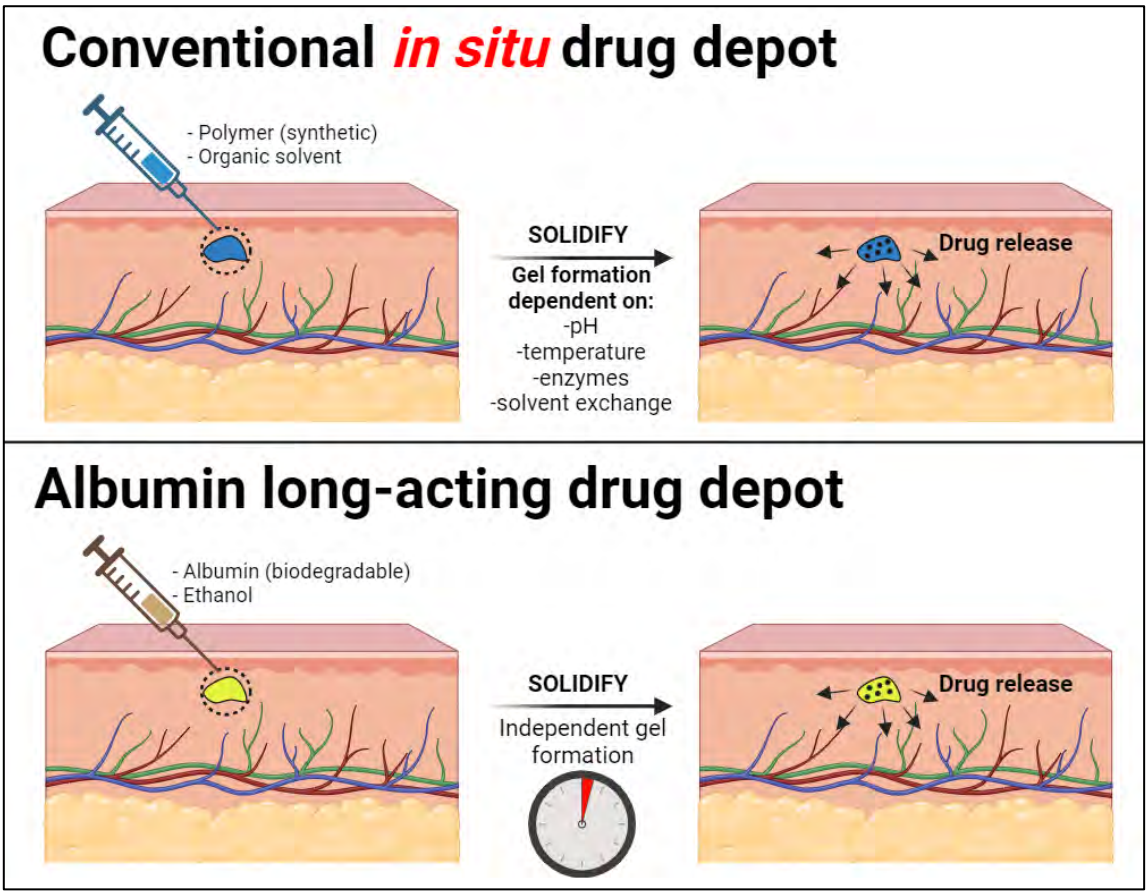

Fig 5.1. Pictorial depiction of in situ gel formation and albumin biodegradable long-acting gel

5.2 Materials and methods

5.2.1 Materials

N-(4-((6-methoxyquinolin-8-yl)amino)pentyl)palmitamide was synthesized using primaquine and palmitic acid. Primaquine was a gift sample from IPCA laboratories. Lumefantrine was purchased from Yarrow Chem Products (Mumbai, Maharashtra). Palmitic acid was purchased

from Loba Chemie Pvt Ltd. The organic solvent, ethyl acetate, hexane, chloroform, dichloromethane (DCM) and ammonia solution were procured from Merck Life Science Pvt. Ltd. (Mumbai, India). Sodium sulfate (Na_2SO_4) was obtained from CDH (New Delhi, India). Silica gel 60-120, 1-ethyl-3-(3-dimethylaminopropyl) carbodiimide (EDCl), 1-Hydroxybenzotriazole (HOBt), albumin was purchased from SRL Pvt. Ltd.- India. Poly(lactic-co-glycolic) acid (PLGA) (75:25, MW 66,000-107,000), polyvinyl alcohol (PVA, MW 9000–10,000) were purchased from Sigma-Aldrich Chemicals Company (Missouri, United States). Glycerol, tween 80 was obtained from S D Fine-Chem Ltd (Mumbai, India). Silicon oil was procured from Rankem^{TM} (Bangalore, India). Trehalose was acquired from Spectrochem (Mumbai, India). Water was obtained from Milli-Q system (Millipore GmbH, Germany). All other chemicals, solvents, and reagents utilized were either HPLC or analytical grade.

5.2.2 Methods

5.2.2.1 Preparation of primaquine prodrug loaded PLGA nanospheres

Primaquine prodrug nanospheres were prepared by emulsion solvent evaporation technique as reported previously with slight modifications (Prayag et al., 2021; Surve & Jindal, 2021). The primaquine prodrug (10mg) and PLGA (100mg) were initially dissolved in DCM (0.5ml) to obtain the organic phase. PVA (200mg) was dissolved in 4ml of Milli-Q water to form the aqueous phase. The aqueous phase was continuously stirred at 700rpm using a magnetic stirrer while the organic phase was added into the aqueous phase drop by drop to get a crude emulsion. The crude emulsion was then further subjected to probe sonication (Sonics & Materials, Inc., USA) at 500 watts, 25% amplitude for 3min (30 sec: ON and 10 sec: OFF). The formed nanoemulsion was further processed at reduced pressure under rotary vacuum evaporator (Heidolph, Schwabach, Germany) leading to the evaporation of DCM leaving behind the primaquine prodrug loaded polymeric nanospheres. The nanospheres were separated by centrifugation at 20,000rpm for 40min (Sorvall 150 + Micro Ultracentrifuge, Thermo Fisher Scientific, USA). The pellet obtained after centrifugation was redispersed in Milli-Q water. Further, the nanospheres obtained were characterized for particle size, polydispersity index (PDI), %entrapment efficiency, %drug loading and particle shape. The nanospheres were freeze-dried by using trehalose (10% w/v) as a cryoprotectant. Lyophilization was carried out over the course of three sequential phases, which involved freezing, primary drying, and secondary drying, lasting a combined duration of 48 hours.

5.2.2.2 Characterization of prodrug loaded PLGA nanospheres

A. Particle size and polydispersity index (PDI) and zeta potential

2.2.2.1 Particle size and polydispersity index (PDI) and zeta potential of primaquine prodrug loaded nanospheres were characterized by dynamic light scattering. Briefly, weighed quantity of primaquine prodrug loaded nanospheres were resuspended in 2mL Milli-Q water and analyzed using Malvern Nano ZS (Malvern Instruments Ltd. UK).

B. % Entrapment efficiency (%EE)

The primaquine prodrug loaded nanospheres were ultracentrifuged and the supernatant obtained after centrifugation and aliquot was withdrawn from supernatant obtained from centrifugation. %EE was determined after using RP-HPLC based analytical method after appropriate dilution. %EE was calculated using the equation (4.1)

$$\%EE = \frac{Total\ quatity\ of\ drug\ used\ -\ Drug\ content\ in\ the\ supernatant}{Total\ quantity\ of\ drug\ used} \times 100 \ldots\ldots\ldots(4.1)$$

C. % Drug loading (%DL)

Drug loading is the ratio of the mass of the drug with the mass of drug loaded nanospheres. The %DL was calculated using the equation

$$\%DL = \frac{Total\ quatity\ of\ drug\ entrapped}{Total\ quantity\ of\ drug\ used + Total\ quantity\ of\ polymer\ used} \times 100 \ldots\ldots\ldots(4.2)$$

D. Drug content

A quantity of 10mg of the primaquine prodrug-loaded freeze-dried nanospheres was added into 1mL of methanol. The resulting mixture underwent vortex mixing for 5 minutes and subsequent sonication to facilitate the dissolution of the drug. Following this, centrifugation was used at 10000rpm for a duration of 40 minutes to separate insoluble materials, and an aliquot derived from the supernatant was subjected to analysis using the RP-HPLC method.

E. Field emission scanning electron microscopy

On a coverslip, an aliquot of the aqueous dispersion of nanords or nanospheres was spread, and it was left to dry at room temperature. Using carbon tape, the dried coverslip was attached to a metal stub. The sample was then coated with gold for 45 seconds using a sputter coater (Quorum Technologies Q150TES, East Sussex, England). After coating, the nanoparticles were amalysed in a 20 kV high vacuum using an FEI scanning electron microscope (Hillsboro, Washington). The spot size was set at 9.0 and the scale was set between 300 and 1000 nm (Bhide et al., 2022; Bhide & Jindal, 2021).

5.2.2.3 Preparation and optimization of long-acting formulation composition

The long-acting formulation comprised two distinct compositions, denoted as composition 1 and composition 2. Composition 1 was prepared by dissolving varying amounts of albumin in

water through sonication. In parallel, composition 2 consisted of different quantities of ethanol, serving as a pharmaceutically acceptable organic solvent. Subsequently, composition 2 was introduced to composition 1, and the resulting mixture was vigorously shaken. Following the mixing phase, the mixture underwent incubation at 37ºC for a specified period, leading to the formation of a viscous gel or solid implant. The diverse amounts of albumin or ethanol utilized in the preparation of the long-acting formulation are detailed in Table 5.1.

For the preparation of a long-acting formulation containing free drug, the drug was initially dissolved in ethanol and subjected to the aforementioned process. On the other hand, in the preparation of a long-acting formulation loaded with polymeric nanoparticles, the nanoparticles were dispersed in the albumin solution and processed as described above. Subsequently, the long-acting formulation underwent characterization for viscosity and in vitro drug release.

5.2.2.4 Characterization of long-acting formulation

A. Time of gel formation

The impact of the concentration of composition 1 and the volume of composition 2 on the time required for the formation of a viscous gel was assessed. In glass vials, distinct quantities of albumin were dissolved in water and combined with varying volumes of ethanol, as outlined in Table 5.1. The resulting mixture was then subjected to incubation at 37ºC in a water bath. At 1-minute intervals, the solution was examined to ascertain the time required for gel formation.

B. Rheology studies

Determining viscosity was an important aspect as it indicated the strength of the gel as well as correlated with the conformational change of albumin. Viscosity of different gel compositions were calculated using MCR 92, Modular Compact Rheometer (Anton Paar GmbH). Briefly, the sample gel was placed between the Parallel plate (PP25) and the Peltier temperature device (P-PTD 200). The samples were equilibrated before and during the experiment at 37ºC. The measurements of viscosity and shear strength were carried out as a function of shear rate ranging from 0.1 to 100sec^{-1} with a total of 21 measurements. Three different formulations with low (100mg), intermediate (200mg) and high (250mg) concentration of albumin were selected to compare the rheological parameters of the formulations. Viscosity and shear strength values were the primary parameters used for the comparison.

5.2.2.5 Release studies

In vitro release of PQ loaded gel implant, PQ-PAL loaded gel implant and PQ-PAL

nanoparticle loaded gel implant (PQ-PAL – 4mg, albumin – 200mg, water - 400µL, organic solvent - 350µL) was carried out by suspending the solid implant (obtained after mixing composition 1 and composition 2) in the release media. Briefly, the optimized long-acting gel formulation was immersed in 20ml release media (10mM phosphate buffer pH 7.4 with 2%w/v polysorbate 80 along with 0.05% w/v sodium azide under constant agitation (200rpm) at 37ºC in a bath shaker. At predetermined time points (2h, 6h, 12h, day 1, day 2, day 3, day 5 and day 7), 1ml of the release media was withdrawn and replaced with equal amount of fresh release media. The release samples were analyzed for PQ and PQ-PAL with the developed RP-HPLC method. PQ was quantified using Shimadzu HPLC system (Kyoto, Japan) equipped with a binary pump (LC-20AD), autosampler (SIL-20AC HT) and UV-visible detector (SPD-20A). The column utilized for the analysis was Zodiac (C18 column, 250 mm x 4.6 mm, 5 µm). Mobile phase system consisted of reservoir A (acetonitrile) and reservoir B [Phosphate buffer solution (PBS), 10mM; pH 3.5] with a ratio of 30:70 (%A: %B) with a flow rate of 1ml/min. The injection volume was set to 20µL with a column temperature of 30°C with a total run time of 7min at a wavelength of 259nm. The study was performed in triplicate (n = 3).

5.2.2.6 Pharmacokinetic studies

The ability of long-acting gel formulation of sustaining the drug release was evaluated *in vivo* in the female Sprague Dawley rats (250 ± 50g). The protocol for the animal study was approved by the Institutional Animal Ethics Committee of Birla Institute of Technology and Science, Pilani Campus, Pilani (Protocol no.: IAEC/RES/33/01). Animals were divided into two groups (n = 4). Animals from group I were subcutaneously administered with primaquine prodrug (50mg/kg) loaded long-acting gel formulation while animals in group II were subcutaneously administered with primaquine prodrug loaded polymeric nanospheres (primaquine prodrug equivalent to 50mg/kg) loaded in long-acting gel formulation. Before starting the study, the animals were fed with regular food and water *ad libitum*. Post administration, 300µL of blood was withdrawn from the retro-orbital plexus of the rat at 1h, 3h, 6h, 12h, day 1, day 2, day 5, day 7, day 10, day 14, day 21, day 28, day 35, day 42, day 49 and day 56 in a microcentrifuge tube containing 20µL of 10% EDTA. The microcentrifuge tubes were centrifuged at 8000rpm for 10min and the obtained plasma was separated and stored at -23ºC till further analysis. For the analysis of primaquine prodrug in plasma, plasma (95µL) was taken in a microcentrifuge tube and spiked with internal standard (10µL of 250ng/ml lumefantrine). The drug and the internal standard were extracted by protein precipitation method using acetonitrile (1mL). After addition of acetonitrile, the samples were vortex mixed (15min), centrifuged (10,000rpm;

15min) and the supernatant was evaporated at 37ºC. Finally, the samples were reconstituted in acetonitrile: water (80:20) and analyzed using the developed LC-MS-MS method.

5.3 Results and discussion

5.3.1 Preparation and characterization of PQ-PAL loaded polymeric nanospheres

The particle size distribution and zeta potential of nanospheres are shown in Fig. 5.3a. and Fig. 5.3b. respectively. Fig. 5.3c. represents the SEM images of the nanospheres. The preparation of PQ-PAL nanospheres was carried out using the standard emulsion solvent evaporation process. Table 5.2. reports the particle size, PDI, zeta potential, % entrapment efficiency, % drug loading and drug content of the PQ-PAL loaded nanospheres.

5.3.2 Preparation of long-acting gel formulation

The long-acting gel formulation loaded with PQ-PAL was formed through the mixing and subsequent incubation of composition 1 and composition 2. A schematic depiction of the preparation process for the long-acting gel formulation is illustrated in Fig. 5.2. Table 5.1 provides detailed information on the influence of albumin concentration and ethanol volume on the time necessary for gel formation.

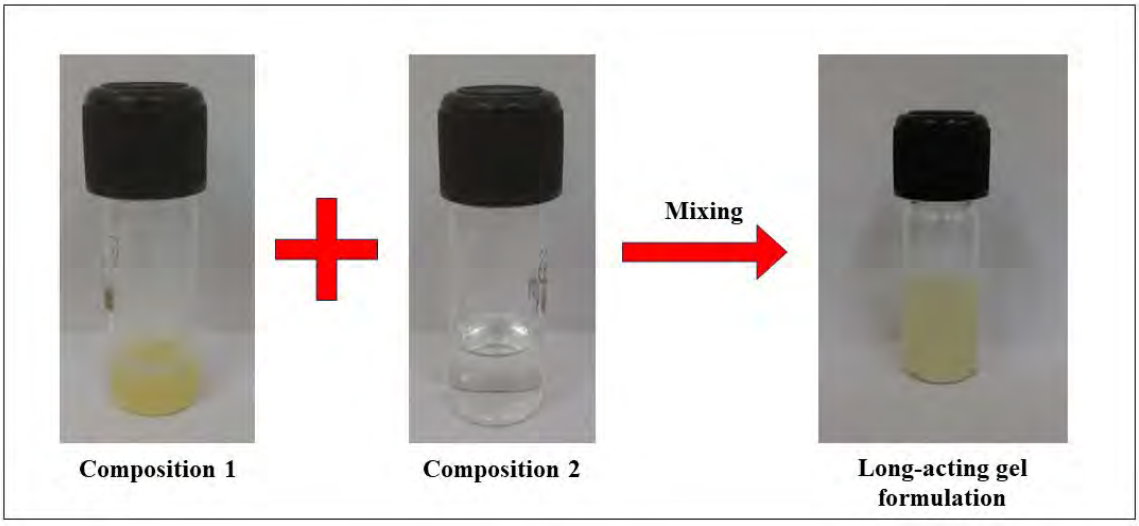

Fig. 5.2 Long-acting gel formulation

The observed time for gel formation exhibited dependency on two key factors: 1) the concentration of albumin in water, and 2) the amount of ethanol. Elevating the concentration of albumin in the aqueous phase corresponded to a reduction in the time required for the gel formation. Conversely, an increase in the volume of the organic solvent in the formulation also contributed to a decrease in the time needed for gel formation.

The introduction of ethanol induced the denaturation of albumin, prompting conformational changes and imparting a gel-like structure to the formulation.

It is evident that augmenting the volume of organic solvent volume expedites the process, thereby reducing the time required for gel formation. Conversely, an increase in the concentration of albumin in the formulation results in a higher quantity of denatured proteins, subsequently enhancing the viscosity of the formulation. Fig. 5.4 represents the relationship between the organic solvent, water, and the quantity of albumin concerning the time required for gel formation.

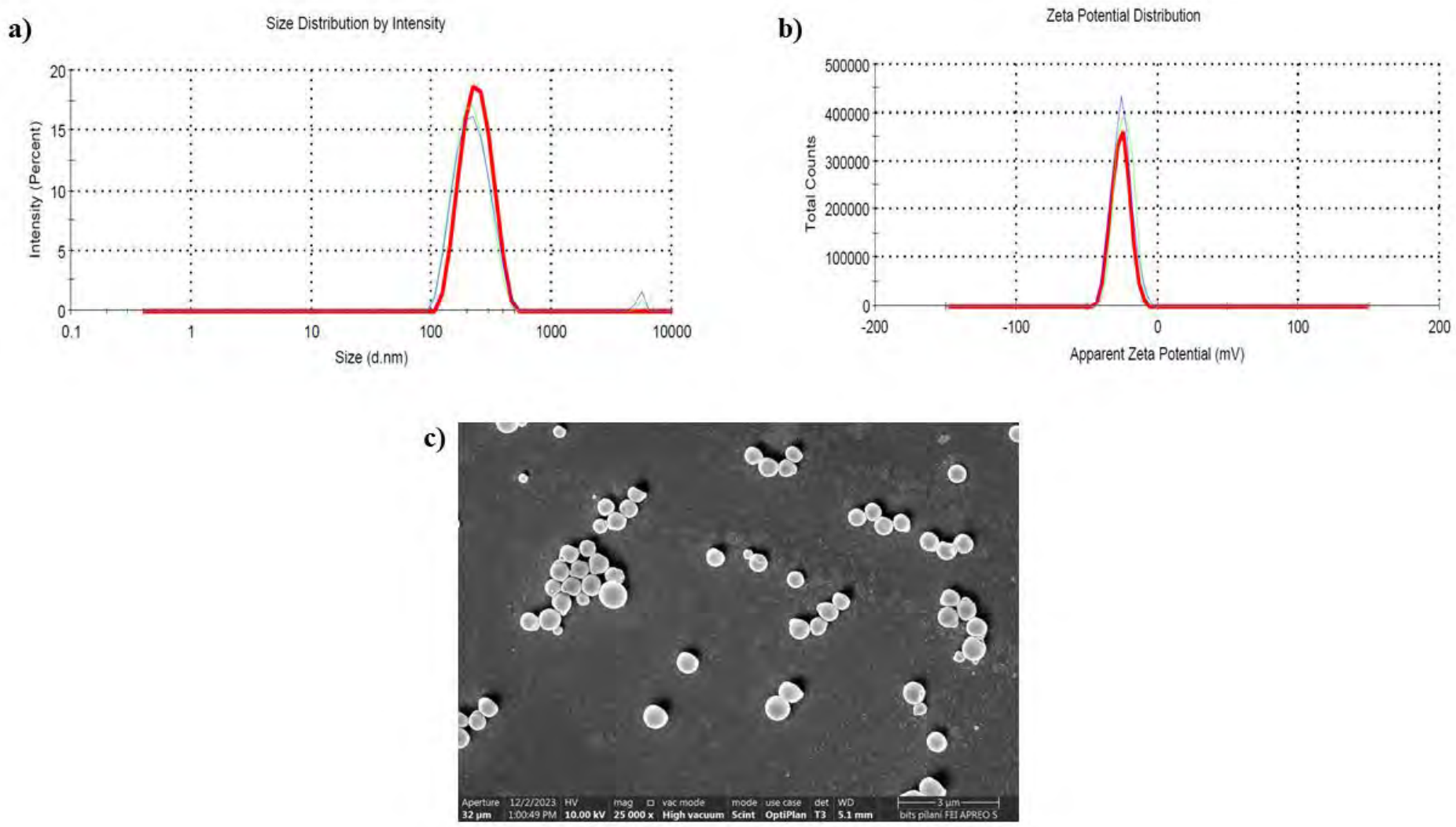

Fig. 5.3 Characterization of PQ-PAL loaded PLGA nanospheres a) Particle size distribution b) zeta potential; and c) SEM image

Table 5.1. Trials for the determining the effect of albumin concentration and organic solvent volume on time required for the formation of albumin gel

Trial. No.	Albumin (mg)	Water (µL)	Organic solvent (µL)	Time for gel formation (min)	Sr. No.	Albumin (mg)	Water (µL)	Organic solvent (µL)	Time for gel formation (min)
G1	100	200	100	4	G25	150	500	370	4
G2	100	200	150	3	G26	150	500	400	2
G3	100	200	200	1	G27	150	500	350	5
G4	100	300	100	32	G28	150	600	450	7
G5	100	300	200	5	G29	200	500	300	15
G6	100	300	300	1	G30	200	500	350	6
G7	100	400	200	32	G31	200	500	400	3
G8	100	400	250	13	G32	200	600	380	9
G9	100	400	300	5	G33	200	600	400	7
G10	100	500	300	32	G34	200	700	450	20
G11	100	500	400	5	G35	200	700	500	8
G12	100	600	450	13	G36	200	800	550	10
G13	100	600	500	4	G37	200	800	520	15
G14	100	500	350	7	G38	200	800	600	1
G15	100	500	370	4	G39	250	600	400	8
G16	100	600	470	4	G40	250	700	400	15
G17	100	600	460	16	G41	250	700	500	5
G18	150	300	100	32	G42	250	600	450	4
G19	150	300	200	1	G43	250	700	450	9
G20	150	300	300	1	G44	250	600	420	3

G21	150	400	100	32	G45	250	700	470	8
G22	150	400	200	20	G46	250	800	500	14
G23	150	400	300	1	G47	250	800	550	3
G24	150	500	300	17	G48	250	800	530	10

Table 5.2. Characterization of PQ-PAL loaded PLGA nanospheres

	Composition						Parameters					
Formulation code.	**Drug (mg)**	**PLGA (mg)**	**PVA (mg)**	**DCM (ml)**	**Water (ml)**	**Sonication time (min)**	**Particle size (nm)**	**PDI**	**Zeta potential (nV)**	**%EE**	**%DL**	**DC (µg/mg)**
PQ-E-1	10	100	200	0.5	4	1	407.10 ± 105.68	0.55 ± 0.03	-7.86 ± 0.38	N.D.	N.D.	N.D.
PQ-E-2	10	100	200	1.5	4	3	162.47 ± 2.40	0.11 ± 0.01	-17.83 ± 0.55	N.D.	N.D.	N.D.
PQ-E-3	10	100	200	0.5	4	3	234.77 ± 8.46	0.24 ± 0.03	-25.03 ± 1.29	88.99 ± 1.56	8.09 ± 0.14	28.8

N.D. – Not determined

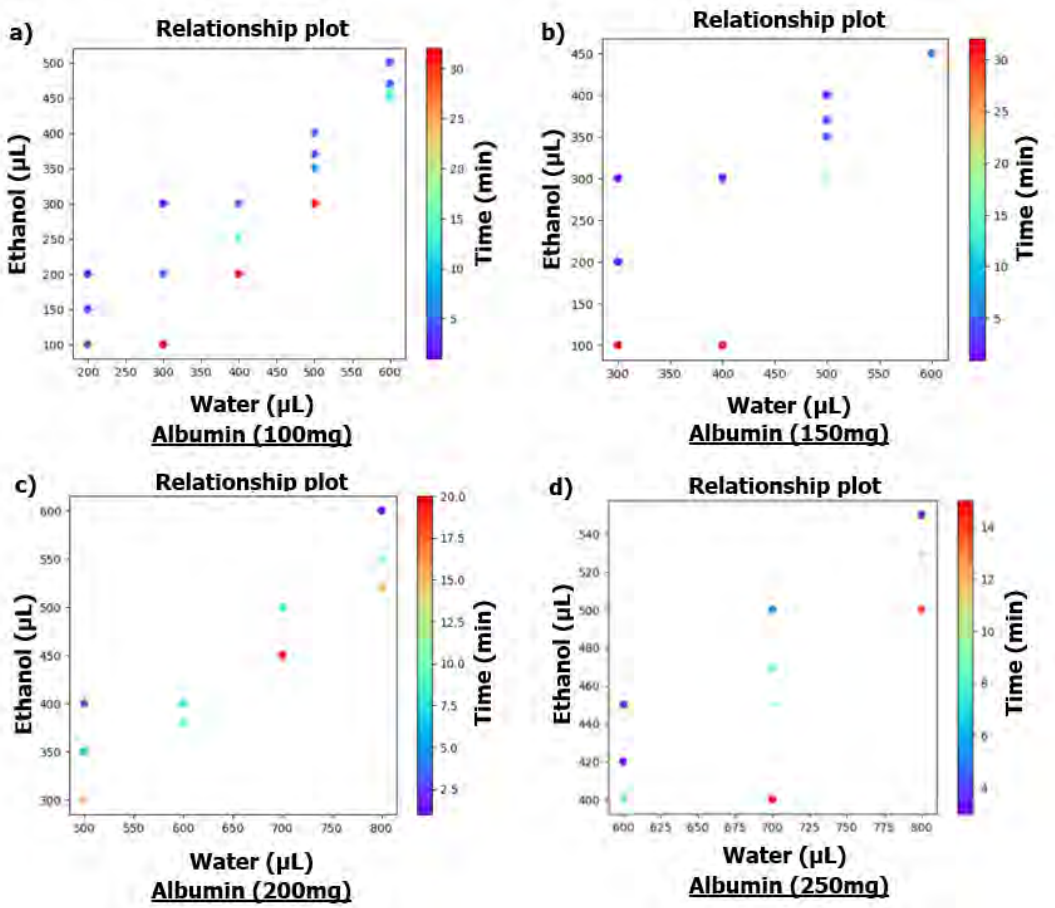

Fig. 5.4 Relation between the organic solvent, water and quantity of albumin on time required for gel formation

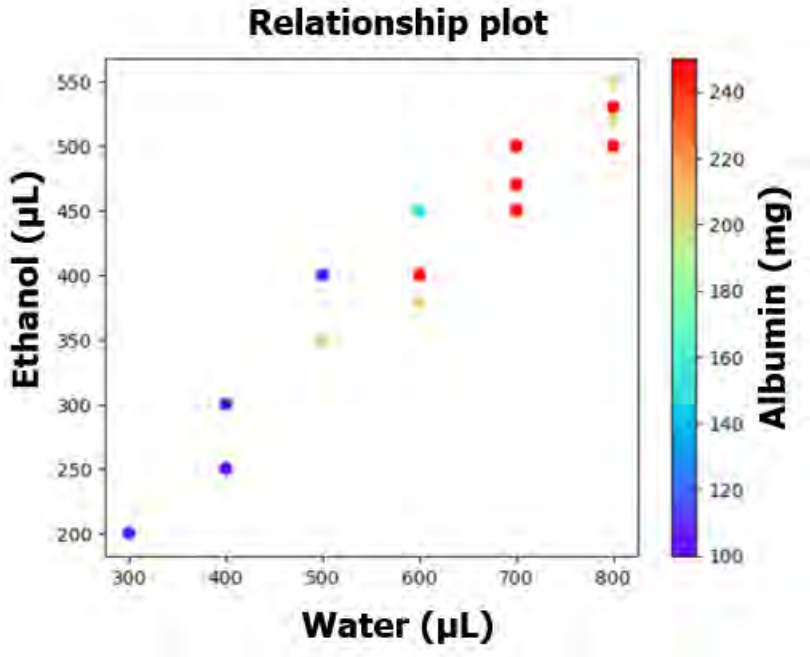

Fig. 5.5 Correlation between albumin concentration and organic solvent volume for the albumin gel formation

The formulations that exhibited gel formation within the time range of 5 to 15 minutes were selected out for further analysis. In case of selected composition, correlation between albumin concentration and the volume of the organic phase, as depicted in Fig. 5.5.

Analysis of rheological parameters for the formulations indicated a notable increase in both viscosity and shear stress with the increase of albumin concentration.

The concentration of albumin demonstrated a direct correlation with both shear rate and viscosity in the formulated long-acting gel. Following exposure to ethanol, the denaturation of albumin occurred, attributed to the unfolding of its hydrophobic regions (Nikolaidis et al., 2017). The conformational changes in denatured proteins have the potential to generate cage-like structures that effectively trap water molecules. These alterations lead to the formation of viscous gels, significantly augmenting the viscosity of the solution (Arabi et al., 2018). In formulations featuring higher concentrations of albumin, it is plausible that the denaturation of a larger albumin quantity resulted in a more restricted entrapment of water molecules, consequently amplifying viscosity and shear stress. The viscosity of injectable depots is typically fine-tuned to facilitate prolonged drug delivery. A higher viscosity in depots is generally associated with a longer duration of action (Southard et al., 1998). Therefore, in this case, gels prepared with the higher albumin concentrations could be explored for the sustained delivery of drugs over extended periods. Fig. 5.6 presents relationship between shear rate, shear stress, and viscosity across three distinct albumin concentrations.

5.3.3 Release studies

The PQ-PAL loaded long-acting gel formulation was immersed in a release medium to assess the drug release behavior of the gel. Fig 5.7 represents the release profile of the PQ-PAL loaded long-acting gel formulation.

In case of primaquine diphosphate 8% of the drug was found to be released by the end of day 1 while only 9.41% drug was found to be released by the end of 7^{th} day. Whereas both the prodrug loaded gel formulation and prodrug nanoparticles loaded gel formulation showed a drug release of less than 2% by the end of 7 days. Remarkably, the gel structure remained intact during entire 7 days. The gradual release of the drug can be attributed to the rigid and intact structure of the gel, wherein the drug is embedded in its matrix. Additionally, it has been reported that the fatty acid chains are known to interact with the amino acid side chains of albumin. This interaction may also have contributed to the retarded release of the prodrug from the gel. The study clearly indicates that the albumin based long-acting gel formulation has an ability to sustain the drug release.

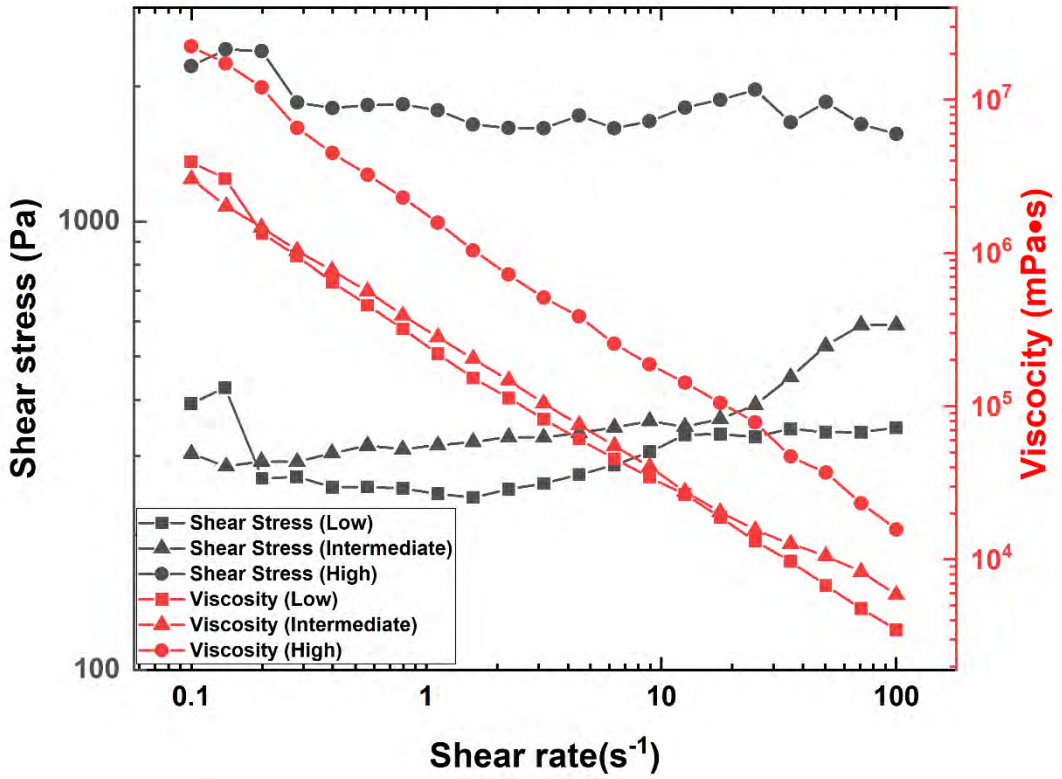

Fig. 5.6 Rheological behavior of different compositions of long-acting gel formulation

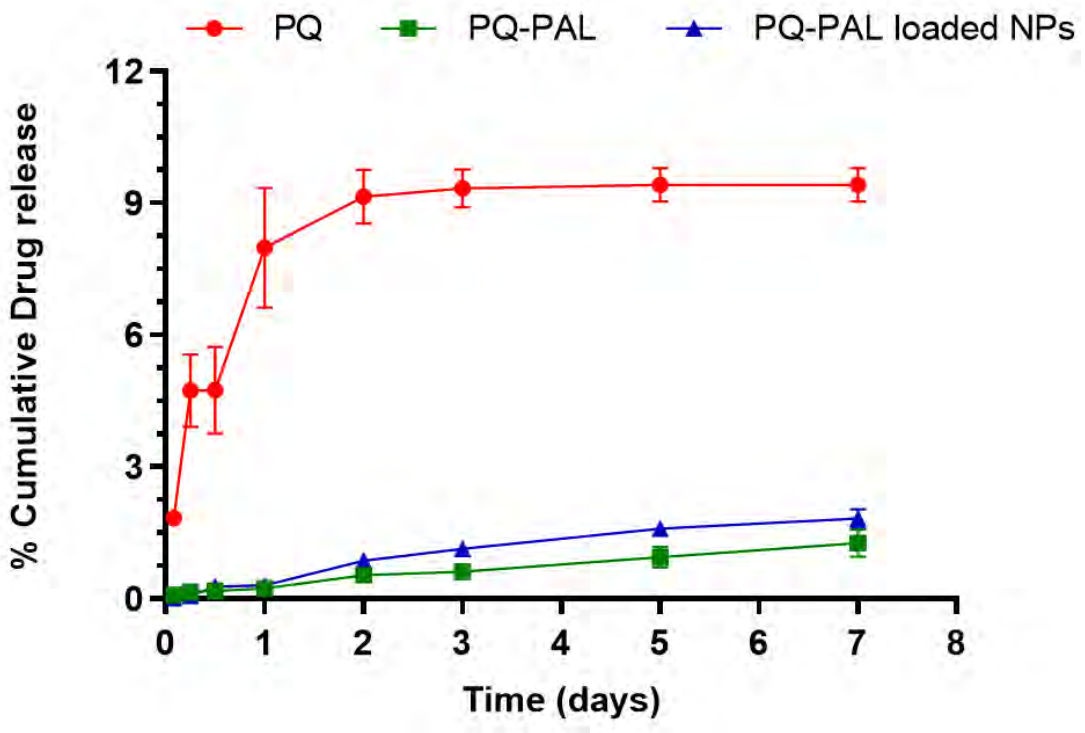

Fig. 5.7. *In vitro* drug release profile of long-acting gel formulation

5.3.4 Pharmacokinetic study

The pharmacokinetic parameters, derived through non-compartmental analysis of the data, are

presented in Table 5.3. In addition, the plasma concentration vs. time profile of the formulation and the free drug subsequent to subcutaneous administration is presented in Fig. 5.8.

Table 5.3. Plasma non-compartmental PK parameters obtained after SC administration of Long-acting drug loaded gel formulation and Long-acting nanoparticles loaded gel formulation in Sprague Dawley rats using Phoenix WiNonlin software (version 6.3)

Parameter	Result	
	Long-acting drug loaded gel formulation	Long-acting nanoparticles loaded gel formulation
$t_{1/2}$ (h)	11.31 ± 2.58	12.29 ± 2.05
C_{max} (ng/ml)	176.55 ± 140.94	20.19 ± 8.18
$AUC_{0-\infty}$	540.08 ± 363.41	162.25 ± 34.18
Vz/F (L/Kg)	530662.29 ± 404501.70	1376661.91 ± 109351.53
Cl/F	33713.01 ± 24743.42	79780.50 ± 17571.63
$MRT_{0-\infty}$ (h)	16.34 ± 2.11	19.52 ± 1.68

In the case of the free PQ-PAL loaded long-acting gel formulation, the C_{max} value reached 176.54 ng/ml at 17.28 hours. In contrast, for the PQ-PAL nanoparticle loaded long-acting gel formulation, the C_{max} was 20.9 ng/ml at 31.92 hours. The higher C_{max} observed in the free prodrug formulation may be attributed to the faster drug release from the depot, leading to increased plasma drug concentrations. However, the subsequent steady decline followed by sustained drug release over 56 days could be attributed to the slower diffusion of the drug from the gel formed at the injection site. The drug release kinetics may be influenced by inherent dual barriers of the formulation. The primary barrier to drug release could be the nanoparticle matrix where the drug release could be dependent on the time required for the diffusion of the drug from the nanoparticle matrix and/or the time required for the degradation of the polymer from the nanoparticles. Meanwhile, the secondary barrier could be the drug's diffusion through the gel matrix. Thus, the nanoparticles may have retarded the drug release, resulting in a flat curve with a lower C_{max} concentration. The mean residence time ($MRT_{0-\infty}$) and half-life for the free drug-loaded formulation were 16.34 days and 11.30 days, respectively. For the nanoparticle-loaded gel, $MRT_{0-\infty}$ and half-life were 19.52 days and 12.29 days, respectively. The longer mean residence time and half-life of the nanoparticle-loaded gel suggested a steady release of the drug from the depot. This prolonged release could be attributed to the dual retardation mechanism of the formulation, where the matrix of the nanospheres acts as the primary barrier for protracted drug release. Additionally, the gel matrix of the formulation serves as a secondary barrier, further slowing down the release of the drug. This results in a

non-fluctuated plasma drug concentration, leading to an extended drug residence time in the body.

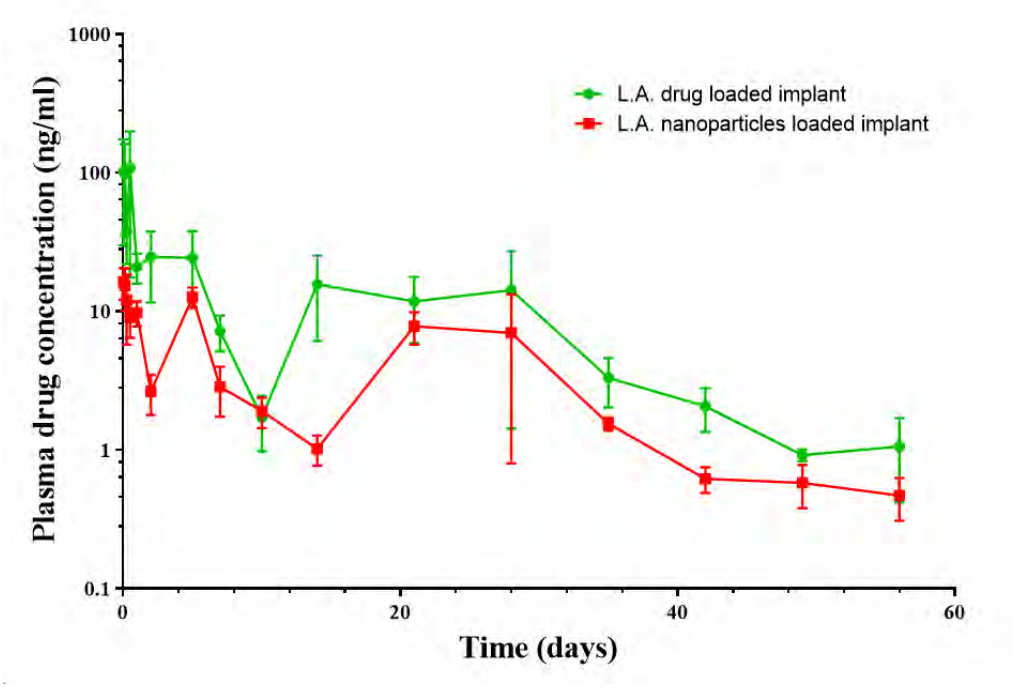

Fig. 5.8 Plasma concentration vs. time profile of the L.A. drug loaded implant and the L.A. nanoparticles loaded implant following their subcutaneous delivery in S.D. rats

5.4 Conclusion

The long-acting gel formulation presents a promising strategy to enhance the in vivo residence time of the drug. Our approach involves a formulation that avoids complex preparation steps, making it more straightforward. Additionally, the components utilized in its preparation are biodegradable and known to be safe. The viscosity of the formulation is adaptable, allowing customization by adjusting the concentration of the hydrophilic excipient, albumin. Importantly, the pharmacokinetic study demonstrated the capability of the formulation for sustained drug release, and the nanoformulation-loaded gel further enhanced the release kinetics. Our findings underscore the potential of a cost-effective preparation method with a simple process, making it a viable technology for a long-acting injectable formulation. This approach holds promise for improving patient compliance and therapeutic outcome.

References

Arabi, S. H., Aghelnejad, B., Schwieger, C., Meister, A., Kerth, A., & Hinderberger, D. (2018). Serum albumin hydrogels in broad pH and temperature ranges: characterization of their self-assembled structures and nanoscopic and macroscopic properties. *Biomaterials* Science, 6(3), 478–492. https://doi.org/10.1039/C7BM00820A

Ashley, E. A., Recht, J., & White, N. J. (2014). Primaquine: the risks and the benefits. *Malaria Journal*, *13*(1), 418. https://doi.org/10.1186/1475-2875-13-418

Bhide, A. R., & Jindal, A. B. (2021). Fabrication and evaluation of artemether loaded polymeric nanorods obtained by mechanical stretching of nanospheres. *International Journal of Pharmaceutics*, *605*(June), 120820. https://doi.org/10.1016/j.ijpharm.2021.120820

Bhide, A. R., Suri, M., Katnoria, S., Kaur, S., Jirwankar, Y. B., Dighe, V. D., & Jindal, A. B. (2022). *Evaluation of Pharmacokinetics, Biodistribution, and Antimalarial Efficacy of Artemether-Loaded Polymeric Nanorods*. https://doi.org/10.1021/acs.molpharmaceut.2c00507

Borzova, V. A., Markossian, K. A., Chebotareva, N. A., Kleymenov, S. Yu., Poliansky, N. B., Muranov, K. O., Stein-Margolina, V. A., Shubin, V. V., Markov, D. I., & Kurganov, B. I. (2016). Kinetics of Thermal Denaturation and Aggregation of Bovine Serum Albumin. *PLOS ONE*, 11(4), e0153495. https://doi.org/10.1371/journal.pone.0153495

Brown, G. V. (1993). Chemoprophylaxis of malaria. *Medical Journal of Australia*, *159*(3), 187–196. https://doi.org/10.5694/j.1326-5377.1993.tb137787.x

Castelli, F., Odolini, S., Autino, B., Foca, E., & Russo, R. (2010). Malaria Prophylaxis: A Comprehensive Review. *Pharmaceuticals*, *3*(10), 3212–3239. https://doi.org/10.3390/ph3103212

Fernando, D., Rodrigo, C., & Rajapakse, S. (2011). Primaquine in vivax malaria: an update and review on management issues. *Malaria Journal*, *10*(1), 351. https://doi.org/10.1186/1475-2875-10-351

Fletcher, K. A., Evans, D. A., Gilles, H. M., Greaves, J., Bunnag, D., & Harinasuta, T. (1981). Studies on the pharmacokinetics of primaquine. *Bulletin of the World Health Organization*, *59*(3), 407–412.

Ivaturi, V., Gopalakrishnan, M., Gobburu, J. V. S., Zhang, W., Liu, Y., Heidbreder, C., & Laffont, C. M. (2017). Exposure-response analysis after subcutaneous administration of RBP-7000, a once-a-month long-acting Atrigel formulation of risperidone. *British Journal of Clinical Pharmacology*, *83*(7), 1476–1498. https://doi.org/10.1111/bcp.13246

Jittamala, P., Pukrittayakamee, S., Ashley, E. A., Nosten, F., Hanboonkunupakarn, B., Lee, S. J., Thana, P., Chairat, K., Blessborn, D., Panapipat, S., White, N. J., Day, N. P. J., & Tarningb, J. (2015). Pharmacokinetic interactions between primaquine and pyronaridine-artesunate in healthy adult Thai subjects. *Antimicrobial Agents and Chemotherapy*, *59*(1), 505–513. https://doi.org/10.1128/AAC.03829-14

Kevin Baird, J., Fryauff, D. J., & Hoffman, S. L. (2003). Primaquine for Prevention of Malaria in Travelers. *Clinical Infectious Diseases*, *37*(12), 1659–1667. https://doi.org/10.1086/379714

Mazier, D., Rénia, L., & Snounou, G. (2009). A pre-emptive strike against malaria's stealthy hepatic forms. *Nature Reviews Drug Discovery*, 8(11), 854–864. https://doi.org/10.1038/nrd2960

Maturavongsadit, P., Paravyan, G., Kovarova, M., Garcia, J. V., & Benhabbour, S. R. (2021). A new engineering process of biodegradable polymeric solid implants for ultra-long-acting drug delivery. *International Journal of Pharmaceutics: X*, *3*, 100068. https://doi.org/10.1016/j.ijpx.2020.100068

Maturavongsadit, P., Shrivastava, R., Sykes, C., Cottrell, M. L., Montgomery, S. A., Kashuba,

A. D. M., & Rahima Benhabbour, S. (2021). Biodegradable polymeric solid implants for ultra-long-acting delivery of single or multiple antiretroviral drugs. *International Journal of Pharmaceutics*, *605*, 120844. https://doi.org/10.1016/j.ijpharm.2021.120844

Mazier, D., Rénia, L., & Snounou, G. (2009). A pre-emptive strike against malaria's stealthy hepatic forms. *Nature Reviews Drug Discovery*, *8*(11), 854–864. https://doi.org/10.1038/nrd2960

McClellan, S. J., & Franses, E. I. (2003). Effect of concentration and denaturation on adsorption and surface tension of bovine serum albumin. *Colloids and Surfaces B: Biointerfaces*, *28*(1), 63–75. https://doi.org/10.1016/S0927-7765(02)00131-5

Mohan, V., Sengupta, B., Acharyya, A., Yadav, R., Das, N., & Sen, P. (2018). Region-Specific Double Denaturation of Human Serum Albumin: Combined Effects of Temperature and GnHCl on Structural and Dynamical Responses. *ACS Omega*, *3*(8), 10406–10417. https://doi.org/10.1021/acsomega.8b00967

Moman, R. N., Gupta, N., & Varacallo, M. (2023). *Physiology, Albumin*.

Nikolaidis, A., Andreadis, M., & Moschakis, T. (2017). Effect of heat, pH, ultrasonication and ethanol on the denaturation of whey protein isolate using a newly developed approach in the analysis of difference-UV spectra. *Food Chemistry*, *232*, 425–433. https://doi.org/10.1016/j.foodchem.2017.04.022

Prayag, K. S., Paul, A. T., Ghorui, S. K., & Jindal, A. B. (2021). Preparation and Evaluation of Quinapyramine Sulphate-Docusate Sodium Ionic Complex Loaded Lipidic Nanoparticles and Its Scale Up Using Geometric Similarity Principle. *Journal of Pharmaceutical Sciences*, *110*(5), 2241–2249. https://doi.org/10.1016/j.xphs.2021.01.033

Rodrigues, T., Prudêncio, M., Moreira, R., Mota, M. M., & Lopes, F. (2012). Targeting the Liver Stage of Malaria Parasites: A Yet Unmet Goal. *Journal of Medicinal Chemistry*, *55*(3), 995–1012. https://doi.org/10.1021/jm201095h

Santos, A., Sinn Aw, M., Bariana, M., Kumeria, T., Wang, Y., & Losic, D. (2014). Drug-releasing implants: current progress, challenges and perspectives. *J. Mater. Chem. B*, *2*(37), 6157–6182. https://doi.org/10.1039/C4TB00548A

Sato, S. (2021). Plasmodium—a brief introduction to the parasites causing human malaria and their basic biology. *Journal of Physiological Anthropology*, *40*(1), 1. https://doi.org/10.1186/s40101-020-00251-9

Schlagenhauf, P., & Petersen, E. (2008). Malaria Chemoprophylaxis: Strategies for Risk Groups. *Clinical Microbiology Reviews*, *21*(3), 466–472. https://doi.org/10.1128/CMR.00059-07

Singh, K. K., & Vingkar, S. K. (2008). Formulation, antimalarial activity and biodistribution of oral lipid nanoemulsion of primaquine. *International Journal of Pharmaceutics*, *347*(1–2), 136–143. https://doi.org/10.1016/j.ijpharm.2007.06.035

Southard, G., Dunn, R., & Garrett, S. (1998). The drug delivery and biomaterial attributes of the ATRIGEL®technology in the treatment of periodontal disease. *Expert Opinion on Investigational Drugs*, *7*(9), 1483–1491. https://doi.org/10.1517/13543784.7.9.1483

Surve, D. H., & Jindal, A. B. (2021). Development of Cationic Isometamidium Chloride loaded Long-Acting Lipid Nanoformulation: Optimization, Cellular Uptake, Pharmacokinetics, Biodistribution, and Immunohistochemical Evaluation. European Journal of Pharmaceutical Sciences, 167(May), 106024. https://doi.org/10.1016/j.ejps.2021.106024

Chapter 6: Summary and conclusion

Malaria is an infectious disease caused by the parasite *Plasmodium* and is transmitted by the bite of female Anopheles mosquito vector. The disease is prevalent in Africa and Asia where in 2018, 93% of the total cases of malaria were from Africa whereas, 3.4% of the cases were from WHO South-East Asia Region. Due to the absence of any anti-malarial vaccine, the treatment burden lies on the available chemotherapeutic agents. The treatment regimen for malaria relies on the type of infection. For instance, in case of *P. falciparum* infection, the treatment is focused on the elimination of the erythrocytic stage of the parasite. In such case, chloroquine is generally preferred. However, nowadays, various strains of *Plasmodium* have reportedly been resistant to chloroquine. In such instances Coartem® oral therapy (artemether ad lumefantrine) is recommended and is the primary choice for the treatment of *P. falciparum*. In case of severe infections, intravenous artesunate is often administered until the patient is conscious to continue with the for oral therapy. On the other hand, in case of *P. vivax* infection, for the elimination of the erythrocytic stage of the parasite, chloroquine is recommended. However, in order to treat the hepatic stage of the parasite, primaquine therapy is recommended. Primaquine is amongst the only available drug which is able to treat the hypnozoite stage of the parasite. However, these available drugs have their own limitations. In case of Coartem®, for adult patients weighing 35 kg or more are advised a 3-day treatment plan comprising 6 doses: Four tablets initially, followed by another 4 tablets after 8 hours, and then 4 tablets twice daily (morning and evening) over the subsequent 2 days, totaling 24 tablets for the entire course. Whereas, primaquine should be taken preemptively, starting one or two days before visiting a region prone to the disease, continued daily during the stay, and extended for seven days upon returning to the home country. For preventive measures against relapse, primaquine is administered for 14-day following departure from an endemic area. In both the cases, the therapy involves a long duration and high pill burden which often leads to poor adherence to the therapy. Additionally, primaquine is also associated with dose dependent side effects. Therefore, the therapy unequivocally necessitates interventions involving formulations that require less frequent dosing and exhibit reduced toxicity.

In this dissertation, we initially studied about effect of particle shape on the efficacy of the formulation. We prepared artemether loaded PLGA nanospheres using nanoprecitation. These nanospheres were immobilized in a hydrophilic film and stretched to alter their shape using an *in-house* prepared film stretching assembly. The stretched particles were retrieved and characterized for their shape using scanning electron microscopy on the basis of shape

descriptors like major and minor axis of the nanorods, major and minor Feret's diameter of the nanorods and the aspect ratio. The effect of film thickness, hydrophobicity of polymer, extent of stretching, method of liquification on the final shape of nanorods were studied. Subsequently, an analytical and a bioanalytical method for the quantification of artemether was developed using RP-HPLC and LC-MS-MS. In the release study, the nanorods were fond to release the drug in more sustained manner as compared to the nanospheres. The nanospheres and the nanorods both were found to be hemocompatible and non-cytotoxic. The erythrocyte interaction study showed that the nanorods are capable to interact with the erythrocytes due to their greater contact angle and surface area. Following intravenous administration in rats, artemether nanorods demonstrated increased plasma concentration and reduced elimination rate compared to nanospheres. Biodistribution studies in BALB/c mice revealed higher liver concentration of DiR-loaded nanospheres than DiR-loaded nanorods at 30 minutes post intravenous administration. *In vitro* schizont inhibition studies indicated concentration-dependent parasitic inhibition by both nanorods and nanospheres. Nanorods displayed superior effectiveness at lower concentrations (2ppm), whereas nanospheres showed higher effectiveness at higher concentrations. Additionally, nanorods exhibited heightened chemosuppression on day 5 and day 7 compared to nanospheres and free artemether using the *Plasmodium berghei* mouse model. Treatment with artemether nanoformulations also increased the survival rate of *P. berghei* infected mice compared to free artemether.

Primaquine diphosphate being a hydrophilic drug was difficult to load on a nanocarrier. Hence, a hydrophobic prodrug of primaquine (PQ-PAL) was prepared using palmitic acid. The synthesized prodrug was confirmed using ^{1}H NMR, ^{13}C NMR and HRMS. PQ-PAL loaded PLGA nanospheres were prepared and characterized using emulsion solvent evaporation technique. PQ-PAL loaded nanospheres were immobilized in a PVA film and stretched in warm oil. The obtained nanorods were characterized using SEM. The *in vitro* release study revealed that the nanorods had significantly sustained release of the drug than the nanospheres. Whereas, both the nanoformulation were found to be non-hemolytic. Finally, in the pharmacokinetic study, it was observed that the nanorods released drug slowly as compared to the nanospheres whereas, they had a higher residence time and half-life as compared to the nanospheres.

PQ-PAL loaded long-acting biodegradable gel formulation was prepared with an intent to serve as a prophylactic parenteral formulation. It involved preparation of 2 compositions, one consisting of albumin dissolved in water whereas another consisting of ethanol. The mixing of

the compositions would result into formation of the gel. In case of preparation of drug loaded gel, the drug had to be dissolved in the organic phase and mixed further. Whereas, in case for the preparation of nanoparticle loaded gel, the nanoparticles were dispersed in the aqueous phase before mixing of the compositions. Various trials were conducted in order to optimize the quantities of formulation components which led to the formation of gel in desired time. Further, the effect of gel composition on its viscosity and shear stress was monitored. It was followed by an *in vitro* release study in which the gel presented a sustained drug release. Finally in the pharmacokinetic study, the drug loaded long-acting gel formulation showed an initial burst release followed by sustained drug release upto 56days, whereas in case of nanoparticles loaded long-acting gel formulation, the formulation showed a protracted drug release with lower C_{max} and higher mean residence time than the free drug loaded long-acting formulation. Hence, the ability of the biodegradable gel of being a long-acting implant capable of sustaining the drug release was evaluated.

This research primarily addresses the key challenges posed by existing antimalarial treatments. Polymeric nanoformulations, in particular, have exhibited heightened drug concentrations over an extended duration, possibly reducing the necessary dosing frequency for complete parasite elimination and mitigating dose-related adverse effects. The three formulations developed were identified as non-toxic and proficient in maintaining drug release within the body, highlighting their potential as promising antimalarial formulations.

APPENDICES

Thesis related Publications

Bhide, A. R., & Jindal, A. B. (2021). Fabrication and evaluation of artemether loaded polymeric nanorods obtained by mechanical stretching of nanospheres. **International Journal of Pharmaceutics**, 605, 120820. https://doi.org/10.1016/j.ijpharm.2021.120820 **(IF-5.8)**

Bhide, A. R., Suri, M., Katnoria, S., Kaur, S., Jirwankar, Y. B., Dighe, V. D., & Jindal, A. B. (2023). Evaluation of Pharmacokinetics, Biodistribution, and Antimalarial Efficacy of Artemether-Loaded Polymeric Nanorods. **Molecular Pharmaceutics**, 20(1), 118–127. https://doi.org/10.1021/acs.molpharmaceut.2c00507 **(IF-4.9)**

Bhide, A. R., Surve, D. H., & Jindal, A. B. (2023). Nanocarrier based active targeting strategies against erythrocytic stage of malaria. **Journal of Controlled Release**: Official Journal of the Controlled Release Society, 362, 297–308. https://doi.org/10.1016/j.jconrel.2023.08.043 **(IF-10.8)**

Jindal, A. B., Bhide, A. R., Salave, S., Rana, D., & Benival, D. (2023). Long-acting parenteral drug delivery systems for the treatment of chronic diseases. **Advanced drug delivery reviews**, 198, 114862. https://doi.org/10.1016/j.addr.2023.114862 **(IF-16.1)**

Bhide, A. R., Surve, D. H., Guha, S., & Jindal, A. B. (2020). A sensitive RP-HPLC method for estimation of artemether from polymeric nanoparticles after pre-column acid treatment using UV-visible detector. **Journal of Liquid Chromatography & Related Technologies**, 43(15-16), 624-632. https://doi.org/10.1080/10826076.2020.1777564 **(IF-1.3)**

Patent

Jindal Anil Brijbhushan, **Bhide Atharva Rajendra**, 'Gelling composition for sustained release of an active ingredient and method of preparing the same', Date of filing: 6th Oct' 2023. **(Application no - 202311067467)**

Book chapters

Surve, D. H., **Bhide, A**., Jindal, A. B., & Devarajan, P. V. (2023). Nanomedicines for the Treatment of Veterinary Parasitic Infections. In Nanomedicines for the Prevention and Treatment of Infectious Diseases (pp. 149-196). Cham: Springer International Publishing.

Conference presentations

Atharva R. Bhide, Anil B. Jindal, Evaluation of artemether loaded polymeric nanorods prepared by mechanical stretching of nanospheres in **3rd National Biomedical Research Competition** dated 6-10th Dec. 2021. (NBRCOM 2021, SYBS, India)

Atharva R. Bhide, Anil B. Jindal, Pharmacokinetics and red blood cell interaction of artemether-loaded polymeric nanorods prepared by mechanical stretching in **21st International Symposium on Advances in Technology and Business Potential of New Drug Delivery Systems** dated 24-25th Feb. 2023. (CRS India Local Chapter, NMIMS, Mumbai)

Atharva R. Bhide, Anil B. Jindal, Fabrication and evaluation of long-acting primaquine prodrug loaded polymeric nanorods prepared by mechanical stretching in **22nd International Symposium on Advances in Technology and Business Potential of New Drug Delivery Systems** dated 29th Feb-1st Mar. 2024. (CRS India Local Chapter, Mumbai).

Awards

Awarded '**Best Oral Presentation**' at 3rd National Biomedical Research Competition, 2021, organized by Society of Young Biomedical Scientists, India.

Awarded '**Best Poster Award**' on Research Scholar's Day at BITS Pilani, Pilani Campus on 5th January 2024.

Supervisor's Biography

Dr. Anil Jindal is an Associate Professor at the Department of Pharmacy BITS Pilani and has over a decade of experience in drug delivery technology and nanomedicine. His primary research focus revolves around the development of nanoformulations for efficient drug delivery in both human and animal infectious diseases. He obtained his PhD from ICT, Mumbai, M. Pharm from Bombay College of Pharmacy, Mumbai, and B.Pharm from the University of Rajasthan. Dr. Jindal has also gained valuable industry experience with well-known pharmaceutical companies such as Pfizer and IPCA before joining BITS Pilani. He has published more than 30 research and review papers in high-impact factor journals and 15 book chapters, covering a diverse range of topics in drug delivery, nanomedicine, and pharmaceutical sciences. Notably, his publications have achieved a remarkable impact factor, reaching as high as 16.06. His outstanding achievements have earned him international recognition, with Stanford University listing him among the top 2% of scientists worldwide for two consecutive years (2022 and 2023). Throughout his career, Dr. Jindal has been the recipient of several prestigious research awards, including the Prof. ML Khorana Memorial Award, Eudragit Award, and SERB Early Career Research Award, all of which highlight his significant contributions to the field. Demonstrating his expertise as an editor, he has successfully edited/co-edited two significant books in the domain of drug delivery: "Pharmaceutical Process Engineering and Scale-up Principles" and "Nanomedicine for the Prevention and Treatment of Infectious Diseases," both of which were published by Springer in 2023. Dr. Jindal's laboratory has been generously funded, receiving over 90 lakhs from government and industry sources over the last five years. This funding has translated into successful product commercialization, with the development of the product "BEAUTISAN" through an industry- sponsored project, now available for purchase in the US market. Dr. Jindal has been invited to deliver talks at prestigious forums, including Nirma University, AICTE-sponsored Faculty Development Programmes and an international event organized by CRS Inc., involving South Africa, India, and Turkey. Additionally, Dr. Jindal has been serving as a Managing Theme Editor for the esteemed journal Advanced Drug Delivery Reviews (Impact Factor 16.01 in 2023) since July 2022. Dr. Jindal's expertise as an expert reviewer is highly sought after, with invitations to review grant applications for government funding agencies such as DBT and SERB. Furthermore, he has lent his expertise as a reviewer for reputed journals in the field, including Advanced Drug Delivery Reviews, Journal of Drug Delivery Science and Technology, AAPS

PharmSciTech, Molecular Pharmaceutics, and PLOS ONE, among many others.

Candidate's Biography

Atharva Rajendra Bhide is currently a Ph.D. research scholar in Department of Pharmacy, BITS-Pilani. He has obtained his Bachelor of Pharmacy degree from Gurunanak college of Pharmacy, Nagpur, and Master of Pharmacy in Pharmaceutics from School of Pharmacy and Technology Management, NMIMS, Mumbai. He secured AIR- 1798 in GPAT-2017. During his Master's degree he completed his major project at FDC Ltd, Mumbai for 6 months. He has worked as a JRF under the supervision of Prof. Anil B. Jindal on the project, 'Rod-shaped polymeric nanoparticles for targeted delivery of artemisinin-derivatives to plasmodium-infected erythrocytes for improved intravenous therapy of cerebral malaria' funded by DST-SERB from June 2019 to March 2022. Since his admission in BITS-Pilani, he has been working on the development and characterization of nonspherical polymeric nanoformulations against infectious disease Malaria. His proficiency in the field of research is evident by his publications in Scopus indexed journals and books (2-review publications, 1-book chapters, 3-research publication, and 1-patent filed). He was also awarded for 'Best Oral Presentation' at 3rd National Biomedical Research Competition, 2021, organized by Society of Young Biomedical Scientists, India and 'Best Poster Award' on Research Scholar's Day at BITS Pilani, Pilani Campus.